



universität
wien

DISSERTATION

Titel der Dissertation

„Putting the brakes on mammary tumorigenesis:
Loss of STAT1 predisposes to intraepithelial neoplasias“

Verfasserin

Mag.rer.nat. Christine Schneckenleithner

angestrebter akademischer Grad

Doktorin der Naturwissenschaften (Dr.rer.nat.)

Wien, 2012

Studienkennzahl lt. Studienblatt: A 091 441

Dissertationsgebiet lt. Studienblatt: Dr.-Studium der Naturwissenschaften Genetik – Mikrobiologie (Stzw)

Betreuerin: Univ.-Prof. Dr. Veronika Sexl

I would like to express my deepest gratitude to Prof. Veronika Sexl for her excellent guidance during my whole PhD. Thanks for all the support and motivation, the constructive discussions and for providing me with such excellent working conditions!

Special thanks goes also to Zsuzsanna Horvath for sharing her huge knowledge about breast cancer with me. She was a great help and a real catalyzer for my work. Many thanks as well to Helmut Dolznig who introduced me into the field of 3D-culturs and confocal microscopy. I would also like to mention Kay-Uwe Wagner, who often supported me with constructive ideas and helped to set up the manuscript.

Of course I am also very grateful to all members of the SFB-28, Richard Morrigl, Dagmar Stoiber, Thomas Decker, Mathias Müller and Brigit Strobl for all their helpful advices and productive discussions during our numerous internal meetings.

Further, I would like to mention especially Karoline Kollmann, Wolfgang Warsch, Ruth Scheicher, Eva Eckelhart and Eva Grundschober who always supported me, both emotionally and technically throughout my whole PhD life. Thanks for all the valuable scientific discussions and the great times we spent together!

Thanks as well to Dagmar Gotthard, Eva-Maria Putz, Andrea Hölbl, Angelika Berger, Sabine Fajmann and Philipp Jodl for the nice working atmosphere!

Finally, a big respect and gratitude goes to my family and friends who were always there for me when I was in need. Thanks for giving me stability and balance in life.



TABLE OF CONTENTS

| | |
|---|------------|
| Introductory word | III |
| Summary | V |
| Zusammenfassung | VII |
| 1. Introduction | 1 |
| 1.1 The JAK-STAT signaling pathway | 1 |
| Canonical JAK-STAT signaling | 1 |
| Characteristic features of JAKs and STATs | 3 |
| Achieving specificity in JAK-STAT signaling | 6 |
| Negative regulation of the JAK-STAT signaling pathway | 7 |
| Non-canonical JAK-STAT signaling | 8 |
| The biology of STAT1 | 9 |
| STAT1 – an essential mediator of IFN signaling | 10 |
| IFN-independent functions of STAT1 | 12 |
| Influences of STAT1 on the hematopoietic system | 12 |
| STAT1 as tumor suppressor | 13 |
| 1.2 STATs in mammary gland development and tumorigenesis | 14 |
| STATs in mammary gland development | 14 |
| STATs in mammary tumorigenesis | 16 |
| STAT1 in breast cancer | 17 |
| IRF1 – a downstream factor of STAT1 | 19 |
| 1.3 Breast cancer | 20 |
| Facts and statistics | 20 |
| Risk factors | 20 |
| Types of breast cancer and classification | 22 |
| Current therapy and treatment methods | 24 |
| 1.4 References | 26 |
| 2. Aim of the thesis | 37 |

| | |
|---|------------|
| 3. Results (manuscripts) | 39 |
| 3.1 Putting the brakes on mammary tumorigenesis – Loss of STAT1 predisposes to intraepithelial neoplasias | 40 |
| 3.2 Lipoxygenase mediates invasion of intrametastatic lymphatic vessels and propagates lymph node metastasis of human mammary carcinoma xenografts in mouse | 61 |
| 3.3 Conditional STAT1 ablation reveals the importance of interferon signaling for immunity to <i>Listeria monocytogenes</i> infection | 77 |
| 3.4 A new kinase-independent function of CDK6 links the cell cycle to tumour angiogenesis | 93 |
| 4. Discussion | 139 |
| 5. Abbreviations | 153 |
| 6. Curriculum Vitae | 155 |

INTRODUCTORY WORD

During the 4 years of my doctoral thesis, I was very lucky to work in an excellent established, efficient and well-respected laboratory which allowed me to learn a huge variety of scientific techniques and to exceedingly improve my knowledge about cancer research and immune biology in every way. The focus of my laboratory lies on the JAK-STAT signaling pathway and its impact on the immune system and tumor biology. My specific goal for the doctoral thesis was to elucidate the function of the transcription factor STAT1 in the development of breast cancer using a murine model system (see section 3.1). Previous studies and reports in mice and human had already indicated that it is worth investigating STAT1 in this context. I contributed as well to studies of several collaboration partners who worked either on STAT1 or on mammary cancer, thereby fitting perfectly into my field of interest (see section 3.2 and 3.3). In addition, I was intensively involved in the work of one of my lab-colleges working on the cell cycle kinase CDK6 (see section 3.4). However, as it would be too extensive to discuss all studies in detail, here in this work I will focus on my main project dealing with the impact of STAT1 in mammary tumorigenesis. All additional work will be presented in form of published or submitted manuscripts and the part of my contribution will be delineated. I hope that the following pages can convince you, that I did my best to honestly achieve my doctoral degree.

SUMMARY

Interferons are important signaling molecules of the immune system that allow cells of an organism to react specifically to pathogens such as viruses, parasites, bacteria but also tumor cells. The transcription factor STAT1 (signal transducer and activator of transcription 1) is an essential mediator of interferon signaling and therefore a prerequisite for a fully functional immune system. STAT1 is also required for the efficient cytotoxic activity of T cells (CTLs) and natural killer (NK) cells. Functional deficiency or mutation of STAT1 leads to hypersensitivity to viral and bacterial infections in both mice and men. Besides being a key factor in immune regulation, STAT1 is also considered as an important tumor suppressor. A breast cancer study correlated a high expression and activation of STAT1 positively with an overall longer and relapse-free survival of cancer patients. In mouse models of ErbB2-induced breast cancer the complete but also the tissue specific deletion of STAT1 results in a decreased latency of tumor formation. These observations indicate STAT1 as important safeguard in mammary cancer development. However, the exact role of STAT1 in the mammary gland tissue and the mechanism how STAT1 confers mammary tumor suppression had not yet been clarified.

During my PhD thesis I revealed that loss of STAT1 suffices to promote mammary tumor formation in mice. *Stat1*^{-/-} mice developed spontaneous pregnancy-induced mammary tumors with an overall higher incidence and shorter latency when compared to *Stat1*^{+/+} controls. The importance of STAT1 in tumor suppression was further confirmed as STAT1-positive tumors of the control group showed a mosaic expression and partially down-regulation of STAT1 protein. *Stat1*^{-/-} tumors displayed a heterogeneous histopathology and did not show a particular pattern of expression of the estrogen receptor (ER) or human epidermal growth factor receptor 2 (HER2). This identifies STAT1 as a global mammary tumor suppressor that acts independent of a distinct oncogenic driver. The transplantation of *Stat1*^{-/-} mammary tissue into wild type mice and vice versa linked the tumor suppressing role of STAT1 to both, the immune system AND the mammary tissue. Cytotoxic T cells were defined as the main executors of mammary tumor surveillance, whereas NK cells play only a marginal role. I further demonstrated that STAT1 is responsible for maintaining growth control in the mammary epithelium - an effect which is

mediated by IRF1, a downstream-factor of STAT1. Both transformed and primary *Stat1*^{-/-} mammary epithelial cells displayed increased growth rates compared to wild type controls. Further, STAT1- and IRF1-deficiency resulted in the formation of unstructured mammospheres in 3D cultures. Consistently, *Stat1*^{-/-} mice developed mammary intraepithelial neoplasias (MINs) with high frequency. MINs are characterized by abnormal growth of mammary epithelial cells and represent a potential pre-carcinogenic stage as they have a high potential to develop into invasive breast cancer.

In summary I unequivocally conclude from my data, that STAT1 controls mammary tumor formation in a dual way: On the one hand by sustaining efficient cytotoxic T cell surveillance and on the other hand by maintaining growth control of mammary epithelial cells. The growth inhibitory effect of STAT1 might be exerted via the transcription factor IRF1.

ZUSAMMENFASSUNG

Interferone sind wichtige Signalmoleküle des Immunsystems die es den Zellen eines Organismus ermöglichen zielgerecht auf Pathogene wie Viren, Parasiten, Bakterien aber auch Tumorzellen zu reagieren. Der Transkriptionsfaktor STAT1 (signaltransducer and activator of transcription 1) spielt eine zentrale Rolle in der Signalübertragung durch Interferone und ist daher Voraussetzung für ein voll funktionstüchtiges Immunsystem. STAT1 wird ebenfalls für die effiziente zytotoxische Aktivität von T Zellen (CTLs) sowie natürliche Killerzellen (NK Zellen) benötigt. Funktionelle Deletionen oder Mutationen des STAT1 Genes in Mäusen aber auch Menschen äußern sich in einer Hypersensibilität gegenüber viralen und bakteriellen Infektionen. Abgesehen von seiner Schlüsselfunktion im Immunsystem wird STAT1 aber auch eine wichtige Rolle als Tumor-Suppressor zugeschrieben. Eine Brustkrebsstudie an Frauen konnte eine hohe Expression und Aktivität von STAT1 mit einem längeren und rezidivfreien Überleben der Patientinnen positiv korrelieren. Mausmodelle mit ErbB2-induzierten Brusttumoren zeigten außerdem, dass die totale oder die gewebsspezifische Deletion von STAT1 zu einer verkürzten Latenz der Tumorentstehung führt. Diese Erkenntnisse weisen darauf hin, dass STAT1 eine wichtige Rolle in der Brustkrebsentstehung besitzt. Die genaue Funktion von STAT1 im Brustgewebe und der Mechanismus, wie STAT1 die Brustkrebsentstehung unterdrückt, konnten bislang jedoch noch nicht aufgeklärt werden.

Im Rahmen meiner Dissertation konnte ich anhand von Mausmodellen zeigen, dass der Verlust von STAT1 ausreicht, um Brustkrebs auszulösen. *Stat1*^{-/-} Mäuse entwickelten spontane schwangerschaftsvermittelte Brusttumore mit einer generell höheren Inzidenz und verkürzten Latenz als *Stat1*^{+/+} Kontrolltiere. Die Wichtigkeit von STAT1 in der Tumorentstehung wurde auch dadurch bestätigt, da STAT1-positive Brusttumore der Kontrollgruppe eine mosaikartige Expression und einen teilweisen Verlust des STAT1 Proteins aufwiesen. *Stat1*^{-/-} Tumore zeigten eine heterogene Histopathologie und kein einheitliches Expressionsmuster des Estrogenrezeptors (ER) oder des humanen epithelialen Wachstumsfaktors 2 (HER2). Dies bedeutet, dass sich die tumorsuppressive Funktion von STAT1 nicht auf einen bestimmten onkogenen Treiber beschränkt, sondern dass STAT1 als globaler Brusttumorsuppressor wirkt. Die

Transplantation von *Stat1*^{-/-} Brustgewebe in *Stat1*^{+/+} Mäuse und vice versa zeigte, dass STAT1 im Immunsystem UND im Brustgewebe wichtig für die Unterdrückung der Krebsentstehung ist. Zytotoxische T Zellen wurden als Hauptmediatoren in der Überwachung von Brusttumoren identifiziert; NK Zellen spielen hierbei nur eine untergeordnete Rolle. Zusätzlich konnte ich zeigen, dass STAT1 im Brustepithel für die Aufrechterhaltung der Wachstumskontrolle zuständig ist - ein Effekt der über IRF1, einen Downstream-Faktor von STAT1 vermittelt wird. Sowohl transformierte als auch primäre Zellen des Brustepithels wiesen eine erhöhte Teilungsrate im Vergleich zu Wildtyp-Kontrollen auf. In 3D Kulturen bildeten *Stat1*^{-/-} und *Irf1*^{-/-} Brustepithelzellen unstrukturierte Mammosphären. Übereinstimmend damit fanden sich auffällig häufig sogenannte "mammary intraepithelial neoplasias" (MINs) in den *Stat1*^{-/-} Mäusen. MINs zeichnen sich durch abnormes Zellwachstum aus und stellen ein präkarzinogenes Stadium dar, welches das Potential besitzt sich in invasiven Brustkrebs weiterzuentwickeln.

Zusammenfassend kam ich durch meine Forschungsergebnisse zu dem eindeutigen Schluss, dass der Transkriptionsfaktor STAT1 die Brustkrebsentstehung über zwei unabhängige Mechanismen unterdrückt: Einerseits durch die Aufrechterhaltung einer effizienten Tumorüberwachung mittels zytotoxischer T Zellen, und andererseits durch die Wachstumskontrolle von Zellen des Brustepithels, welche über den Transkriptionsfaktor IRF1 vermittelt wird.

INTRODUCTION

1.1 The JAK-STAT signaling pathway

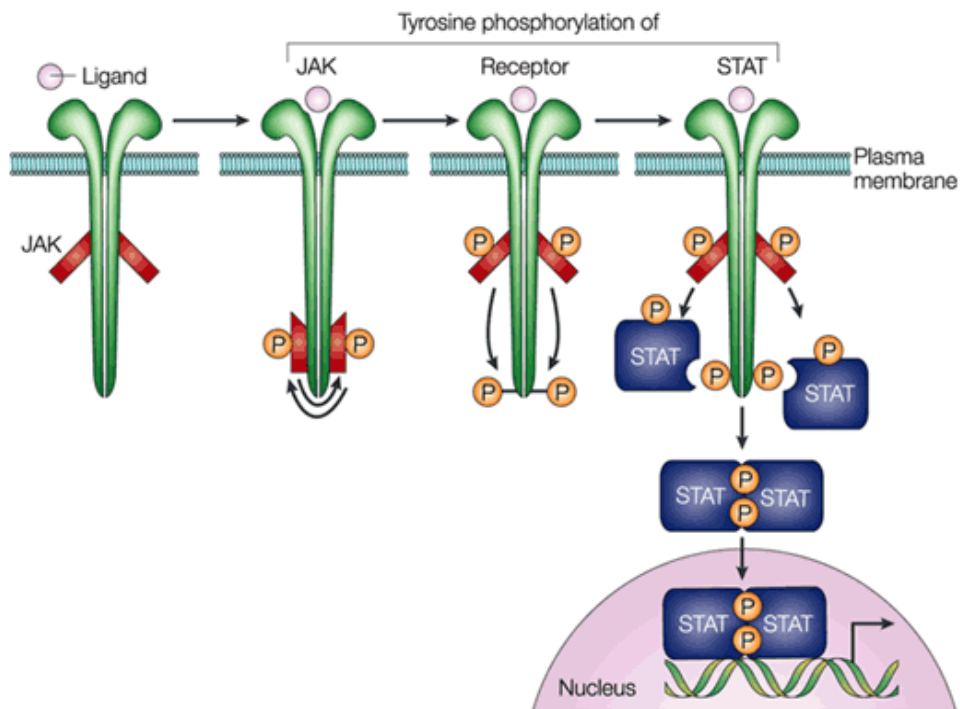
Canonical JAK-STAT signaling

The history of Janus kinase (JAK)-signal transducer and activator of transcription (STAT) signaling started in 1957 with the discovery of interferons (IFNs) by Alick Isaacs and Jean Lindenmann. These small proteins were found to be secreted by cells after virus infection and to confer protective effects towards noninfected cells^{1,2}. Intense biochemical and genetically studies on interferons lead to the identification of the tyrosine kinases JAKs and DNA-binding proteins STATs and uncovered a complex intercellular communication system^{3,4}. Today it is well described, that the JAK-STAT signaling pathway displays a fast track to transmit extracellular signals from cell surface receptors into the cell nucleus where it activates the transcription of specific target genes. Thereby, many important cellular functions such as growth and development, survival and apoptosis, homeostasis as well as immune responses are tightly regulated. Consequentially, dysregulation of the JAK-STAT pathway has severe impact on crucial cellular properties and is associated with a broad range of diseases, cancer development or immune disorders⁵⁻⁷. Persistent STAT activation - particularly of STAT3 or STAT5 (but also STAT1) - has been described in various types of human cancers (a short selection is listed in **Table I**)⁸. Gene mutations in all different components of the JAK-STAT signaling pathway have been associated with all kinds of human diseases⁹. Therefore, the various modules of the JAK-STAT pathway gained attention as they provide attractive potential targets for drug development and cancer therapy and are of great interest for basic but also translational research.

Table I. Activation of STATs in human cancers. (Taken from Yu and Jove, 2004 in Nat. Rev. Cancer ⁸)
 Constitutive STAT activation is often found in different cancer entities. Epstein Barr-Virus (EBV), human T-lymphotrophic virus-1 (HTLV-1).

| Tumour type | Activated STAT |
|---|-----------------------|
| Blood tumours | |
| Multiple myeloma | STAT1, STAT3 |
| Leukaemias: | |
| HTLV-I-dependent | STAT3, STAT5 |
| Erythroleukaemia | STAT1, STAT5 |
| Acute myelogenous leukaemia (AML) | STAT1, STAT3, STAT5 |
| Chronic myelogenous leukaemia (CML) | STAT5 |
| Large granular lymphocyte leukaemia (LGL) | STAT3 |
| Lymphomas: | |
| EBV-related/Burkitt's | STAT3 |
| Mycosis fungoides | STAT3 |
| Cutaneous T-cell lymphoma | STAT3 |
| Non-Hodgkins lymphoma (NHL) | STAT3 |
| Anaplastic large-cell lymphoma (ALCL) | STAT3 |
| Solid tumours | |
| Breast cancer | STAT1, STAT3, STAT5 |
| Head and neck cancer | STAT1, STAT3, STAT5 |
| Melanoma | STAT3 |
| Ovarian cancer | STAT3 |
| Lung cancer | STAT3 |
| Pancreatic cancer | STAT3 |
| Prostate cancer | STAT3 |

In the canonical mode of JAK-STAT signaling the signal transduction from the cell surface into the nucleus is mediated by a series of tyrosine-phosphorylations carried out by the JAK proteins (**Fig1.**). Activation of the JAK-STAT pathway happens through the binding of cytokines, growth factors or other small peptides to cell-surface receptors. This results in receptor dimerization and subsequent trans-phosphorylation of receptor-associated JAKs on tyrosine residues. Activated JAKs further tyrosine-phosphorylate the cytoplasmic domains of the receptors, thereby creating docking sites for the Src-homology-2 (SH2) domains of the STAT proteins. The STAT proteins are then recruited to the JAK proteins where they get tyrosine-phosphorylated. Phosphorylated STAT proteins dimerize and translocate into the nucleus where they activate target gene transcription ^{6,7}.



Nature Reviews | Molecular Cell Biology

Figure 1. Canonical JAK-STAT pathway. (Taken from Levy and Darnell, 2002 in *Nat. Rev. Mol. Cell Biol.* ⁷) The classical activation of the JAK-STAT pathway is mediated by ligand binding to their cognate receptors. Dimerization of receptors then initiates a number of activating phosphorylation-steps: trans-phosphorylation of receptor-associated JAKs, phosphorylation of receptor's tyrosine-residues which creates docking sites for the SH2-domains of the STAT proteins, and finally phosphorylation of STATs. Activated STATs form dimers, translocate into the nucleus and switch on target gene transcription.

Characteristic features of JAKs and STATs

The JAKs belong to the family of protein tyrosine kinases (PTKs) and are associated with membrane bound cytokine receptors that lack intrinsic catalytic activities. The task of the JAKs is to transmit phosphate groups to tyrosine residues, thereby inducing activation. The four mammalian JAK proteins JAK1, JAK2, JAK3 and tyrosine kinase 2 (Tyk2) share a very similar protein structure (**Fig2.**): The carboxyl-terminus consists of a conserved kinase domain followed by a catalytic inactive pseudo-kinase domain. Due to these two domains, the proteins were called "Janus kinases", based on the two-faced Roman god Janus, god of doorways, beginnings, and transitions (one apocryphal story is that the discoverer A.F. Wilks initially termed them

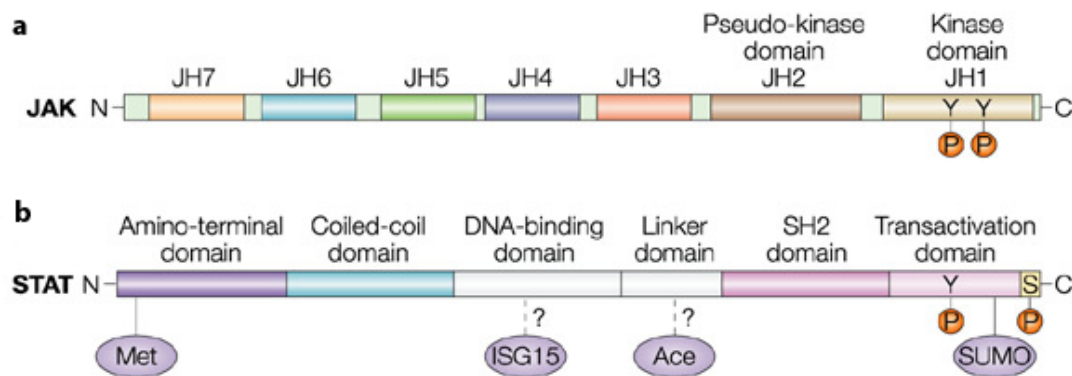
“Just-Another-Kinase”) ¹⁰. The amino-terminal domains JH3-JH7 also show sequence similarities between the different JAKs and mediate selective binding to cytokine receptors ⁷. JAK1, JAK2 and Tyk2 are ubiquitously expressed, whereas JAK3 is primarily restricted to hematopoietic cells ¹¹.

All JAKs have been deleted in mice; gene-targeted mice confirmed their essential role in the signaling of various cytokine receptors. Further, the removal of different JAKs in mice uncovered severe defects in hematopoiesis, leading to perinatal death in JAK1-deficient mice ¹², embryonic lethality in JAK2-deficient mice ^{13,14} and a severe combined immunodeficiency disease (SCID) in JAK3 deficient-mice ¹⁵. Tyk2-deficiency exhibits the weakest effects with defective clearance of certain viruses ¹⁶.

The STATs comprise seven mammalian members: STAT1, STAT2, STAT3, STAT4, STAT5a, STAT5b and STAT6. The dual function of the STATs can already be deduced from their name: they transmit extracellular signals into the nucleus, where they activate transcription of specific target genes. Unphosphorylated STAT proteins are latently present in the cytoplasm. After phosphorylation, STAT proteins form homo- or heterodimers, depending on the STAT protein and are shuttled into the nucleus. Also STAT proteins share a common structure (**Fig5.**): They consist of a N-terminal domain which is implicated in the regulation of STAT activity such as tetramer formation and protein-protein interactions ⁶, an adjacent coiled-coil domain which is involved in interactions with regulatory proteins, a STAT-specific DNA-binding domain and a SH2-domain that mediates binding to phospho-tyrosines and therefore activation and dimerization of STATs. The C-terminal transactivation domain is involved in interactions with other transcription factors and co-activators and contains the phosphorylation sites necessary for STAT activation.

Equal to the JAKs, all STATs have been deleted in mice. This defined essential, non-redundant roles for each of the STAT proteins ¹⁷. Animals deficient for STAT1 or STAT2 are highly susceptible to viral infections as they yield an impaired interferon signaling ¹⁸⁻²⁰ (in a later section the characteristics of STAT1-deficient mice will be described in more detail). STAT4 ablation leads to defective T_H1-cell development due to impaired responses to IL-12 signals ²¹, in contrast to STAT6 deficiency which leads to impaired T_H2-cell differentiation caused by a lack of IL-4-receptor signaling ²². The highly homologous STAT5a and STAT5b proteins (96% identity) own distinct roles in development, especially in hematopoiesis. STAT5a/b double-knockout mice are in >99% perinatal lethal but analysis of fetuses at embryonic day 18 revealed defective B and T cell development, absence of natural killer cells as well as severe anemia ^{23,24}. Moreover, STAT5a is essential for prolactin and growth-hormone receptor signaling, thus STAT5a deficient

mice display impaired mammary gland development and lactogenesis²⁵. STAT3 displays a crucial role in normal development as STAT3 ablation leads to early embryonic lethality²⁶. Studies on conditional STAT3-knockout mice uncovered its role in mammary gland involution and several, also contradictory roles in cellular proliferation, survival, apoptosis and differentiation^{27,28}.



Nature Reviews | Immunology

Figure 2. The domain structures of JAKs and STATs. (Taken from Shuai and Liu, 2003 in Nat. Rev. Immunol.⁶)

a) JAKs share 7 highly homologous domains (JH1-JH7). JH1 encodes the active kinase domain. It contains tyrosine sites that are phosphorylated after ligand stimulation and mediate JAK activation. The adjacent pseudo-kinase domain JH2 lacks kinase activity and is implicated in the regulation of JH1. Domains JH3-JH7 are involved in receptor binding. **b)** Also STAT proteins share conserved domains. The transactivation domain (TAD) contains the phosphorylation sites necessary for STAT activation. The TADs of individual STATs do not share sequence similarities but function. STATs further share a conserved SH2 domain, a linker domain, a DNA-binding domain, a coiled-coil domain and an amino-terminal domain. STAT activity can also be regulated by protein modifications such as methylation (Met), ISGylation (ISG15), acetylation (Ace) and sumoylation (SUMO).

Despite their functions in mice, defects in the JAK-STAT signaling pathway have frequently been associated with a broad range of human malignancies. Very often the human disease reflects the phenotype of its knockout mouse model: JAK3 mutations in people have been associated with the SCID syndrome characterized by the absence of T cells and functionally defective B cells^{29,30}. Similarly, the STAT1 knockout mouse model recapitulates the human situation, as several reports of patients with germline STAT1 mutations or complete STAT1-deficiency revealed severe immunodeficiencies, especially susceptibility to mycobacterial and viral infections³¹⁻

³⁵. The proven pivotal role of JAKs and STATs in human malignancies makes them not only interesting for basic but also translational research and offers a promising target for drug development.

Achieving specificity in JAK-STAT signaling

As we now know, there is only a limited panel of JAKs and STATs however the number of upstream cytokines is relatively large. The question remains how cytokines achieve their specificity. One answer is that each cell type and tissue expresses distinct receptor combinations which allow a fine-tuned response to cytokines released by the microenvironment or the whole organism. One cell is therefore able to combine the signals mediated by multiple receptors ¹⁷. Further, cell type and tissue specificity also determines the activation of only distinct sets of target genes. Besides the JAK-STAT pathway, several other signaling cascades exist (e.g. PI3-kinase/Akt, Ras/MAPK pathway), each being activated by a distinct set of signaling molecules. As the components of the JAK-STAT pathway also cross-talk with components of other signaling cascades, one stimulus can activate an orchestra of signaling molecules that communicate with each other and ultimately lead to the appropriate cellular answer.

On the other side, cytokine receptors are very restricted to their associated Janus kinases and use mainly only one JAK or JAK combination to transmit their received signals. For example, the IFN γ receptor uses only JAK1 and JAK2 whereas IFN α/β receptors use only JAK1 and Tyk2 (**Fig3.**).

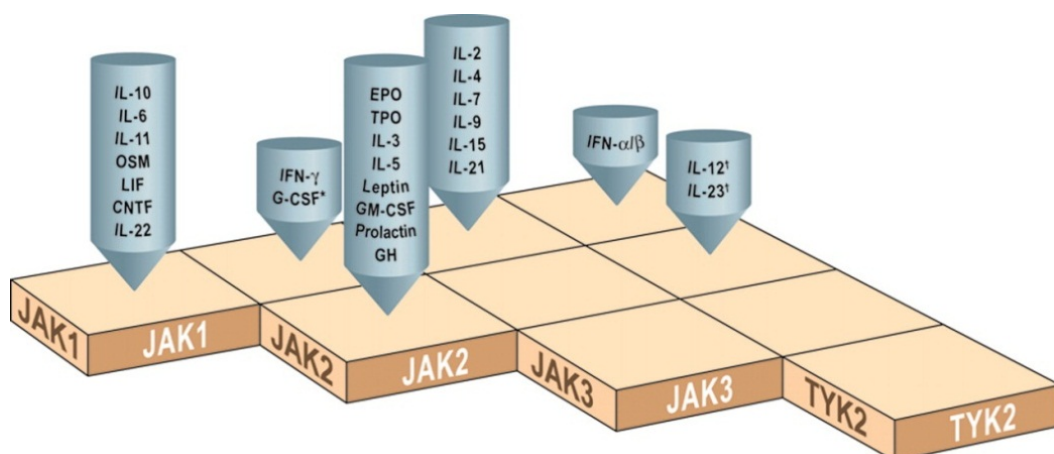


Figure 3. Cytokine receptor specificity. (Taken from Murray, 2007 in J Immunol. ¹⁷)

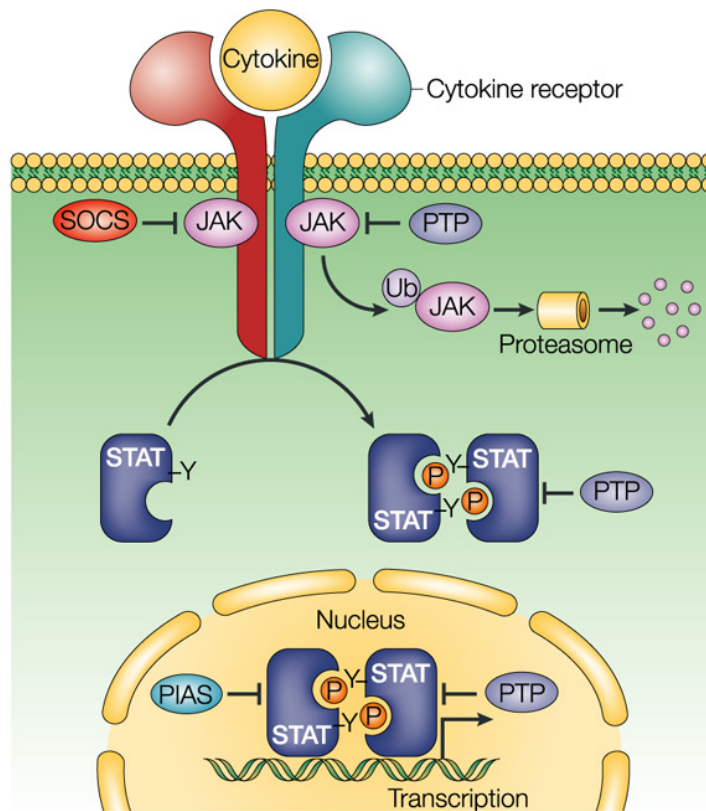
Most cytokine receptors signal through three JAK combinations: JAK1 alone, JAK2 alone or JAK1 and JAK3. The IFN α/β receptors use JAK1 and Tyk2, whereas the IFN γ receptor requires JAK1 and JAK2. No receptors that use JAK2 and JAK3, JAK3 alone, Tyk2 alone or JAK3 and Tyk2 have been described yet.

Negative regulation of the JAK-STAT signaling pathway

Upon activation, STAT proteins increase the transcription of distinct and cell specific target genes within minutes. However the time and extend of an active signal transduction has to be tightly controlled to avoid imbalances but also disease development. Therefore, the JAK-STAT signaling cascade may be interrupted at various stages (**Fig4.**)^{6,7}. The main mediators of negative JAK-STAT regulation are the suppressor of cytokine signaling (SOCS) proteins, protein tyrosine phosphatases (PTPs) and protein inhibitors of activated STATs (PIAS).

Suppressor of cytokine signaling (SOCS) proteins are the best studied regulators of JAK-STAT signaling. They are constantly present at low levels in unstimulated cells but become rapidly induced upon cytokine activation, thereby creating a negative feedback loop. SOCS proteins contain a SH2 domain which binds to tyrosine-phosphorylated JAKs and inhibit further signal transduction. Other members of the SOCS family termed CIS proteins bind directly to the receptor docking sites where they compete with STAT proteins. Moreover, SOCS proteins are also involved in the ubiquitin-proteasome pathway mediating the degradation of JAKs and other proteins. The protein tyrosine phosphatases (PTPs) regulate JAK-STAT signaling by dephosphorylating cytokine receptors, JAK or STAT proteins. In the nucleus, protein inhibitors of activated STATs (PIAS) block DNA-binding of STAT dimers.

Further, naturally occurring C-terminally truncated forms of the STAT proteins (β -isoforms) function as dominant negative regulators by DNA binding without activating transcription. Finally, distinct modifications such as ubiquitylation or ISGylation and the crosstalk between different cytokine-signaling pathways add another level of complexity to control this signaling circuit.



Nature Reviews | Immunology

Figure 4. Negative regulation of the JAK-STAT pathway. (Taken from Shuai and Liu, 2003 in Nat. Rev. Immunol. ⁶)

The JAK-STAT pathway can be regulated at various stages. SH2-domain-containing suppressor of cytokine signaling (SOCS) proteins can inhibit signal transduction through binding to phosphorylated tyrosines of JAKs or receptors. They are further involved in the ubiquitin-mediated degradation of JAKs and other proteins. Protein tyrosine phosphatases (PTPs) interfere by dephosphorylating JAKs, STATs or cytokine receptors. Protein inhibitor of activated STAT (PIAS) block the DNA-binding of activated STAT-dimers. In addition, C-terminally truncated forms of the STAT proteins can act as dominant-negative regulators.

Non-canonical JAK-STAT signaling

In addition to the classical JAK-STAT signaling described above (canonical pathway), a non-canonical mode has been recently uncovered in drosophila. Unphosphorylated STAT (U-STAT) proteins are located in the nucleus and physically interact with heterochromatin protein 1 (HP1) to promote heterochromatin stability ³⁶. Phosphorylation of STAT proteins causes their dispersal from heterochromatin and leads to HP1 displacement and heterochromatin destabilization. Importantly, for this process the induction of STAT transcriptional target genes is not required. This finding indicates that the JAK-STAT pathway is involved in chromatin remodeling and

possesses the ability to control the cellular epigenetic status ³⁷. In line, unphosphorylated STAT proteins have been found to shuttle constitutively between nucleus and cytoplasm ³⁸. Further, there is evidence that JAK1 and JAK2 are present in the nucleus ^{11,39}.

Additional functions of U-STATs have been described. They can also act as transcription factors thereby regulating genes distinct from their tyrosine-phosphorylated forms. For example, U-STAT1 can confer prolonged resistance to virus infections. After the initial response to IFN γ , the tyrosine-phosphorylation of STAT1 is down-regulated rapidly. However, elevated levels of U-STAT1 still persist in the nucleus and activate the expression of several immune regulatory and antiviral genes ⁴⁰.

The biology of STAT1

The STAT1 α protein - the first STAT to be discovered - is 750 amino acids in size and has a molecular weight of 91 kDa ⁴. It consists of 25 exons and is located on mouse chromosome 1 or human chromosome 2. STAT1 α possesses two phosphorylation sites in its C-terminal transactivation domain: tyrosine 701 (T701) and serine 727 (S727). Activation of STAT1 α depends on T701 phosphorylation, whereas S727 phosphorylation is required for maximal transcriptional activity ⁴¹. The naturally occurring spliced form STAT1 β lacks the serine 727 site and acts as dominant-negative regulator against the full length STAT1 α (Fig5.) ⁴².

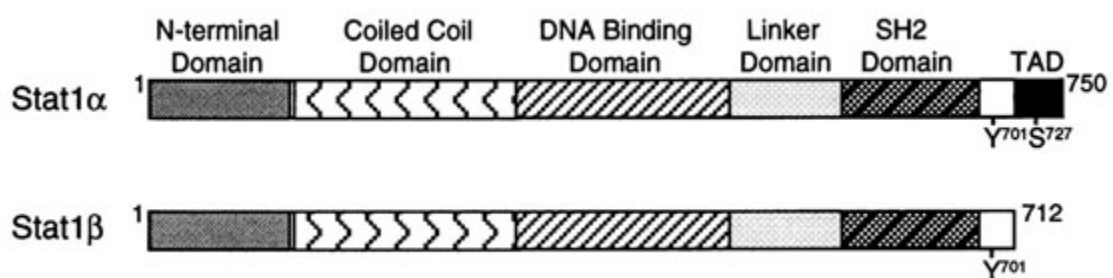


Figure 5. Schematic overview of STAT1 α and STAT1 β . (Adapted from Zhang *et al.*, 1998 in The EMBO Journal. ⁴³)

The two isoforms of STAT1 are generated by alternative splicing. Full length STAT1 α contains two phosphorylation sites at Y701 and S727, whereas the C-terminally truncated STAT1 β lacks the S727 site. It is postulated that STAT1 β can act as dominant negative regulator against STAT1 α . Transcription activation domain (TAD).

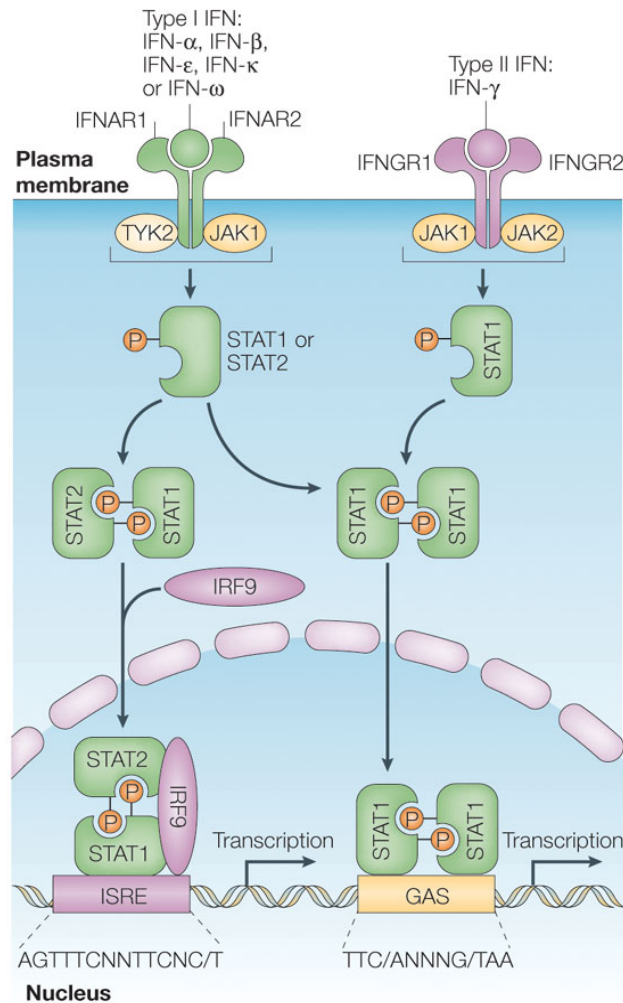
STAT1 - an essential mediator of IFN signaling

Interferons (IFNs) are cytokines that mediate antiviral, antiproliferative, proapoptotic and immunomodulatory effects. They play an essential role in the defense against viral infections and are crucial for the immunosurveillance of malignant cells⁴⁴. STAT1 is a central mediator of both type I IFNs (IFN- α/β) as well as type II IFN (IFN- γ) responses and has been identified as major effector of IFN- γ signaling (**Fig6.**)^{18,19}. In response to IFN- γ stimulation, STAT1 forms homodimeres which bind to gamma-activated sequence (GAS)-sites in the promoter regions of target genes, thereby activating transcription. In contrast, IFN- α/β stimulates heterodimeric interactions between STAT1 and STAT2. STAT1-STAT2 heterodimers associate with a third component, p48 (IRF9), thus forming the IFN-stimulated gene factor 3 (ISGF3) transcription factor complex which binds to IFN α -stimulated gene response element (ISRE)-sequences in the nucleus. IFN- α stimulation can also induce STAT1 homo- or STAT1-STAT3 heterodimerization leading to activation of the GAS sequence⁴⁵.

The generation and characterization of mice with a targeted disruption of the STAT1 gene has further highlighted the crucial role of STAT1 in IFN signaling. STAT1-deficient mice display no abnormalities in reproduction, tissue and organ development, but their cells fail to respond to either IFN α or IFN γ . The consequences are severe defects in the ability to resist microbial and viral infections^{18,19}. In contrast, the response to growth hormone, epidermal growth factor (EGF) and interleukin (IL)-10, which have been shown to activate STAT1 *in vitro* functions properly⁴⁶. In line, several reports of humans with homo- or heterozygote STAT1 mutations describe increased susceptibility to mycobacterial diseases and multiple viral infections, often with a lethal outcome in young years³¹⁻³⁵.

STAT1 plays also a crucial role in promoting cell death via apoptotic but also necrotic and autophagic pathways⁴⁵. The expression of several death-modulating genes is transcriptionally regulated by STAT1 including several caspases⁴⁷, death receptors and their ligands (e.g. Fas/FasL, TRAIL/TRAIL-R)⁴⁸, inducible nitric oxide synthase (iNOs) and the pro-survival gene Bcl-xL⁴⁹. Further, STAT1 is implicated in ROS-mediated necrosis and autophagy⁴⁵. The C-terminal domain of STAT1 interacts with the tumor suppressor p53 and acts as a coactivator, thereby regulating apoptosis through transcription-independent mechanisms. In response to DNA damage, the expression of p53 is reduced in STAT1 deficient cells, thereby weakening the p53-activated apoptotic pathway⁵⁰. In addition, STAT1 acts as negative regulator of the p53 inhibitor Mdm2⁵¹. In cardiac myocytes, overexpression of STAT1 is able to induce apoptotic cell death

which is dependent on S727 but independent of Y701 phosphorylation⁴⁸. Considering the role of STAT1 in apoptosis, it is not surprising that cells deficient for STAT1 are more resistant to apoptosis-inducing agents. Accordingly, mice lacking STAT1 show an increased incidence of spontaneous, chemically induced tumors compared to wild type mice⁵¹.



Nature Reviews | Immunology

Figure 6. Activation of STAT1 by type I and type II interferons (IFNs). Taken from Plataniias, 2005 in Nat. Rev. Immunol.⁴⁴⁾

STAT1 can be activated either by type I IFNs (IFN α , β , ϵ , κ or ω) or type II IFNs (IFN γ). Type I IFNs bind to a common type I IFN receptor that is composed of the two subunits IFNAR1 and IFNAR2. IFNAR1 is associated with Tyk2, IFNAR2 with JAK1. Activation of type I IFN receptors result in the formation of STAT1-STAT2 dimers. Together with the interferon regulatory factor 9 (IRF9) they form the IFN-stimulated gene factor 3 (ISGF3) complex that translocates into the nucleus, binds to IFN-stimulated response elements (ISRE) and activates target gene transcription. In contrast, the type II IFN receptor is a heterodimeric receptor consisting of the two subunits IFNGR1 and IFNGR2 which associate with JAK1 and JAK2, respectively. Its activation results in the formation of STAT1-STAT1 homodimers that bind to interferon gamma-activated sites (GAS) in the proximity of IFN-stimulated genes (ISGs) and activate their transcription. Interferon alpha receptor (IFNAR), interferon gamma receptor (IFNGR).

In addition to mediating cell-death, STAT1 also has the ability to negatively regulate cell cycle progression. STAT1 directly interacts with cyclin D1 and the cell cycle kinase CDK4 thereby mediating cell cycle arrest⁵². Further, STAT1 induces the transcription of the cell cycle inhibitor p21^{WAF1/cip1} by specifically binding to its promoter region⁵³.

IFN-independent functions of STAT1

Most anti-tumor activities of STAT1 depend on its property to act downstream of interferon signaling. However, also IFN-independent mechanisms of STAT1 are described. One example is the ability of STAT1 to act as inhibitor of Ras-mediated transformation and tumorigenesis by up-regulating the expression of the cell cycle inhibitor p27^{Kip1} (encoded by the *Cdkn1b* gene)^{54,55}. The regulation of p27^{Kip1} occurs via two different mechanisms: On the one hand, STAT1 together with STAT3 specifically binds to the *Cdkn1b* promoter and activates the transcription of p27^{Kip1}. Interestingly, this is dependent of STAT1 phosphorylation on Y701 and active STAT3 but is independent of STAT1 phosphorylation on S727⁵⁴. On the other hand, STAT1 binds to the promoter and decreases the expression of the S-phase kinase-associated protein 2 (Skp2), a protein with the ability to induce degradation of several antiproliferative and tumor-suppressive proteins such as p27^{Kip1}. Of note, down-regulation of Skp2 in Ras-transformed cells cannot be detected in response to IFN treatment⁵⁵. Further evidence that STAT1 acts as a key regulator of Ras-mediated transformation is given as STAT1 acts as inhibitor of Ras-MAPK signaling, suppressor of Rho small GTPase expression and regulates the transcriptional activity of STAT3 and STAT5. Thereby STAT1 can fundamentally influence gene expression in Ras-transformed cells⁵⁶. Another effect of STAT1 that is at least partly independent of IFN-signaling is its impact on lymphocyte survival and proliferation. STAT1-deficient T cells (but also Abelson virus-transformed pre-B cells) display enhanced proliferation and decreased apoptosis compared to wild type controls. IFNs are known to confer antiproliferative activities; however the effects of IFN γ -deficiency on lymphoid cells are by far less pronounced than those mediated by STAT1-deficiency. This suggests an additional mechanism of STAT1 which is not mediated by IFNs⁵⁷.

Influences of STAT1 on the hematopoietic system

The detailed analysis of *Stat1*^{-/-} mice revealed several defects in hematopoietic compartments. NK cells of STAT1-deficient mice display highly impaired cytolytic activities as shown by *in vitro*

and *in vivo* experiments⁵⁸. The reason lies most likely in an “educational” defect of *Stat1*^{-/-} NK cells as *Stat1*^{-/-} mice comprise normal NK cell-numbers and an intact lytic machinery but the NK cells show reduced expression-levels of the maturation marker KLRG1 and a shift from the mature CD11b⁺/CD27⁻ fraction towards the immature fractions CD11b⁺/CD27⁺ and CD11b⁻/CD27⁺^{58,59}. Further, STAT1 deficiency abolishes and mutation of the S727 phosphorylation site reduces cytotoxic T cell activity. This stems also partly from activation defects of *Stat1*^{-/-} dendritic cells (DCs) which are incapable to stimulate the expansion of Ag-specific CD8⁺ T cells due to reduced MHC I expression^{60,61}. As already mentioned, *Stat1*^{-/-} T cells show reduced apoptosis and increased proliferation capacities. This leads to an enhanced incidence of carcinogen-induced thymic tumors in *Stat1*^{-/-} mice^{57,60}. Concerning the erythroid cell compartment, deletion of STAT1 affects the distribution of erythroid progenitors and leads to a block in differentiation⁶². A recent paper also described STAT1 to be involved in the development of JAK2V617F-caused myeloproliferative disorders (MPDs)⁶³. The JAK2 mutation V617F results in a constitutive active form of JAK2 and can lead to two phenotypic distinct diseases: polycythemia vera (PV) and thrombocytopenia (ET). The cause of the different disease outcomes of JAK2V617F was unknown until Chen *et al.* revealed that an increased activity of STAT1 results in the ET-like phenotype, whereas reduced activity of STAT1 leads to the PV-like phenotype⁶³.

STAT1 as tumor suppressor

Based on the observations described above, STAT1 has generally achieved the reputation to act as tumor suppressor. Several reports on mice and human strengthen this view. As already mentioned, the presence of STAT1 protects mice from developing carcinogen-induced tumors. When treated with the chemical methylcholanthrene (MCA), both STAT1-single knockout mice and STAT1/p53-double knockout mice develop tumors more rapidly and with a greater frequency than wild type or p53-single knockout mice⁵¹. *N*-nitroso-*N*-methylurea (NMU)-challenged *Stat1*^{-/-} mice develop thymic tumors earlier and more frequently than wild type controls⁵⁷. STAT1-deficient MMTV-neu mice have been shown to be more susceptible to develop spontaneous ovarian teratomas than wild type controls⁶⁴. Further, STAT1 has been shown to act as suppressor of ErbB2-mediated mammary tumor development: in the presence of the ErbB2/neu-oncogene, *Stat1*^{-/-} mice develop mammary carcinomas with decreased latency than controls animals^{65,66}. A breast cancer study correlated a high expression and activation of STAT1 positively with an overall longer and relapse-free survival of cancer patients and indicates

a prognostic value of STAT1⁶⁷. However, under several circumstances STAT1 can also function as tumor-promoter. In the case of v-abl- and TEL/JAK2-induced leukemia, *Stat1*^{-/-} mice are partially protected from disease development by down-regulating MHC class I levels on tumor cells, thereby enabling efficient NK cell lysis⁶⁸. Further, human studies connected STAT1 activation with apoptotic resistance of Wilms' tumor cells or resistance to docetaxel-treatment in prostate cancer cells^{69,70}. Therefore, even though STAT1 signaling exhibits an attractive target for therapeutic drugs, one should carefully consider its character in different cell or tumor types.

1.2 STATs in mammary gland development and tumorigenesis

STATs in mammary gland development

STAT proteins play distinct roles in mammary gland development. STAT5a was originally described in lactating mammary glands of sheep and rats, which exhibited very high levels of this protein. Therefore STAT5a was initially named mammary gland factor (MGF) or milk protein binding factor (MPBF) as it was shown to bind to promoter sequences of milk protein genes and to activate their transcription⁷¹. Further investigations revealed that all known STAT proteins (except STAT2) are expressed and act during distinct stages of mammary gland development, albeit at various levels (**Fig7.**). STAT1 and STAT3 are constitutively expressed but show a reciprocal pattern of tyrosine-phosphorylation: activated STAT1 is found only in virgin glands, early pregnancy and late involution, whereas STAT3 activation is restricted to the day of birth and involution. STAT5 expression rises during pregnancy when alveolar epithelial cells begin to appear. Reciprocal to STAT5, STAT4 is only expressed in virgin glands and during early pregnancy and is predominately activated in the stroma⁷. STAT6 can be detected throughout adult mammary gland development with a peak during pregnancy⁷².

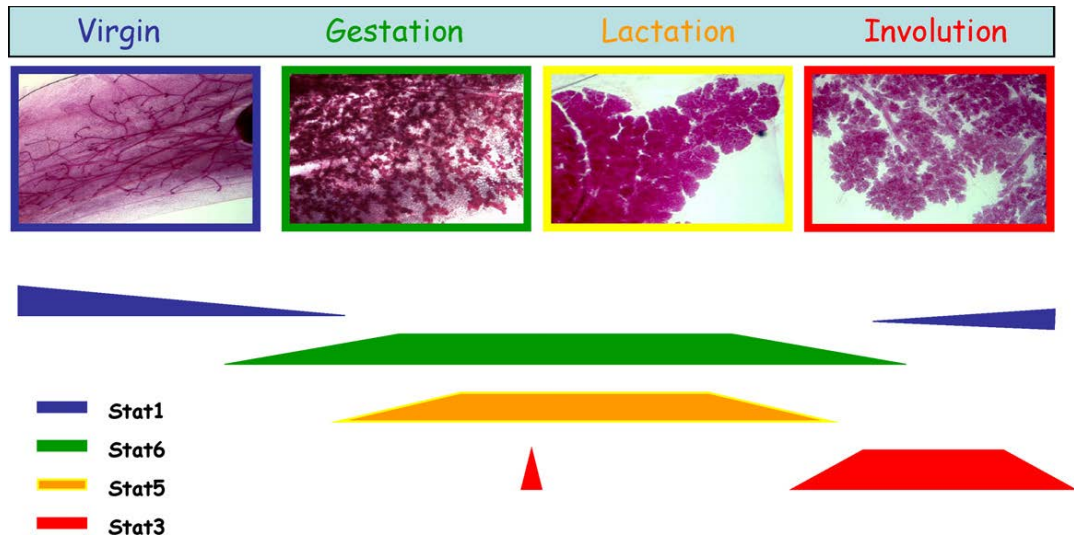


Figure 7. STAT activity during mammary gland development. (Taken from Watson and Neoh, 2008 in *Semin Cell Dev Biol.* ⁷³)

Tyrosine phosphorylation of STAT proteins was assessed throughout the different phases of mammary gland development. The requirements for each individual STAT was determined by gene deletion studies and overlap with the depicted pattern of activity. STAT1 is active in the virgin mammary gland and during late involution. Phosphorylated STAT6 can be detected throughout the whole developmental cycle. STAT5 activity is essential for complete alveolar development and lactation, whilst STAT3 plays a crucial role during involution.

For some of the STAT proteins, distinct roles in the mammary gland were delineated. STAT5a has an essential role in mammary gland development, as STAT5a-knockout mice display impaired lobulalveolar development and fail to lactate after the first pregnancy ^{25,74}. This stems from defective prolactin-signaling, a hormone that plays a central role in the promotion of mammapoiesis and lactogenesis. During late pregnancy and lactation, elevated levels of prolactin trigger the phosphorylation of STAT5a and STAT5b in a JAK2 dependent manner. This leads to the expansion and differentiation of milk-producing alveolar cells ⁷⁵. Mice heterozygous for the prolactin receptor (PRLR) as well as mice with a mammary specific deletion of JAK2 essentially recapitulate the phenotype of STAT5a-deficient mice and also display impaired alveologenesis ^{76,77}. Interestingly, STAT5b-deficiency does not result in developmental defects of the mammary gland, likely because STAT5b is only present at low levels in the mammary tissue and cedes the key role to STAT5a. ⁷⁸ However, multiple gestation cycles of STAT5a-knockout mice lead to an up-regulation of STAT5b protein expression, coinciding with a partial restored mammary differentiation and normal lactation in the absence of STAT5a. Therefore, under a persistent lactogenic stimuli STAT5b can partly compensate for the loss of STAT5a ⁷⁹. Of note,

conditional deletion of both STAT5 genes results in the complete absence of alveolar cells⁸⁰. Further, STAT5a/b-double deficient mammary glands comprise a severe reduction of CD61⁺ luminal progenitor cells and re-expression of STAT5a is able to restore normal luminal progenitor populations and rescue alveologenesis⁸¹. The second STAT protein with a distinct function in the mammary gland is STAT3. Mice with a conditional deletion of STAT3 show a drastic decrease in apoptosis of mammary epithelial cells and a delay in involution after weaning. This might be due to reduced levels of the Insulin-like growth factor-binding protein 5 (IGFBP-5), a direct or indirect target of STAT3. Of note, precocious activation of STAT1 and elevated levels of p21^{WAF1/cip1} and p53 were noted in STAT3-deficient mammary glands and were described as compensatory mechanism to initiate delayed apoptosis²⁷.

Until now, the exact function of STAT1 in the mammary gland is still unclear. The phosphorylation pattern of STAT1 - elevated in virgin glands, low throughout gestation and lactation, rising again at late involution - is unique, which points to a discrete function of STAT1 within the mammary tissue⁷³. Further, STAT1 is expressed in the epithelial compartment of the mammary gland, suggesting that it plays a distinct role in breast epithelial cells⁷².

STATs in mammary tumorigenesis

As STAT proteins are activated and their expression is tightly regulated during all different stages of mammary gland development, it is not surprising that dysregulation of the JAK-STAT signaling pathway is implicated in mammary tumorigenesis. Activation especially of STAT1, STAT3 and STAT5 has been described in breast cancer patients (**Table I**)^{8,82,83}. Several independent studies revealed high expression and activation of STAT5 in human breast tumors by employing immunohistochemistry, microarrays and western blotting techniques^{82,84,85}. Of note, high STAT5 activation was associated with good prognosis. Further, the level of STAT5 activity correlated with the grade of differentiation of breast tumor cells; STAT5 activity was gradually lost during cancer progression and metastasis formation^{84,85}. This could be explained since STAT5 up-regulates the expression of the invasion-suppressive adhesion molecule E-cadherin⁸⁶. In contrast to the human situation, in WAP-TAg transgenic mouse models (expression of the Simian Virus 40 T antigen (TAg) under the control of the whey acidic protein (WAP) promoter induces formation of mammary adenocarcinoma after at least one round of pregnancy) the loss of one STAT5a allele resulted in a reduced incidence of mammary tumor formation⁸⁷. Therefore, STAT5 might have a dual role in breast cancer: on the one hand it might serve as initiator of

tumorigenesis, but on the other hand also promotes the differentiation of already established tumors⁸⁸. Similarly, constitutive STAT3 activation was detected in the majority of primary breast cancers (50-60%)⁸⁰. In several human breast cancer cell lines the pharmacological inhibition of STAT3 as well as the introduction of the dominant negative form STAT3-Y705F resulted in reduced proliferative capacities and cell death^{89,90}. In mouse models, the growth of the murine breast cancer cell line 4T1 was abrogated by introduction of STAT3-Y705F; 50% of the challenged mice remained tumor free and 90% did not develop metastasis⁹¹. Further, in the presence of a constitutive active form of STAT3, MMTV/neu-induced tumors developed faster and with increased metastasis potential⁹². Inhibiting STAT3 activity in tumor cells has been associated with the induction of proinflammatory cytokines and chemokines and may therefore shape the immunogenicity of tumor cells by provoking efficient immune responses⁹¹. Thus, targeting STAT3 signaling in breast tumor cells displays an attractive target for immunotherapy.

STAT1 in breast cancer

STAT1 has been characterized as critical factor modulating tumorigenesis^{51,64,68}. Several studies also investigated STAT1 in the context of mammary cancer development. Similar to STAT3 and STAT5, elevated levels of active STAT1 were described in human breast tumor tissue⁸³. Analysis of breast cancer patients correlated high activity of STAT1 with an overall longer and relapse-free survival and revealed an independent prognostic significance of STAT1 in breast cancer⁶⁷. Studies on mouse models further supported STAT1's tumor suppressive role in mammary cancer: In two independent reports, Klover *et al.* and Raven *et al.* investigated the contribution of STAT1 in ErbB2/neu-induced mammary tumor development. Both studies reached the conclusion, that loss of STAT1 drastically decreases the latency of tumor formation^{65,66}. Of note, in the study of Klover *et al.*, mammary gland-specific deletion of STAT1 was sufficient to accelerate tumor development as demonstrated by *Stat1^{f/f}* x *MMTV-neu-IRES-cre* animals⁶⁵. This implies tumor suppressive functions of STAT1 within the mammary epithelium. Raven and coworkers showed that active ErbB2 expression is associated with accelerated phosphorylation of STAT1 on Y701 which can be blocked by pharmacological inhibition of ErbB2⁶⁶. This up-regulation of STAT1 activity might represent an internal safeguard to counteract transformation. Further, when using *p53^{-/-}/Stat1^{-/-}* MEFs, Neu-mediated cell transformation was inhibited by STAT1 as demonstrated by *in vivo* transplantation studies. Interestingly, in the experiments done by Raven *et al.*, tumor growth was reduced in the presence of STAT1 but also the

phosphorylation mutants STAT1S-727F and STAT1-Y701A. This indicates a tumor suppressive function of STAT1 that is independent of its phosphorylation. However, in a recent study published by Chan *et al.*, the tumor suppressive function of STAT1 relied on phosphorylation of Y701. Their experiments were performed in *Stat1*^{-/-} mammary tumor cell lines; the different cellular systems of Raven *et al.* and Chan *et al.* may explain their different outcomes. As the study of Chan *et al.* was released shortly after the publication of my own results, the data will not be described in detail in this introductory section but will be extensively reviewed in the discussion (see section 4). In brief, similar to my observations Chan *et al.* also described the development of spontaneous mammary tumors in *Stat1*^{-/-} animals and confirmed some of my results quite nicely⁹³. A further study by Zhang *et al.* showed that also Tyk2 - one of the kinases necessary to activate STAT1 in response to IFN α and IFN β - regulates breast cancer growth. *Tyk2*^{-/-} mice comprise highly effective myeloid-derived suppressor cells that inhibit T cell responses and therefore enable accelerated growth and metastasis of breast cancer cells⁹⁴.

Recently, it has been postulated that STAT1 activation potentiates the cytotoxic effects of chemotherapeutic agents such as norcatharidin and doxorubicin in human breast cancer cell lines^{95,96}. On the other hand, genes of the IFN-signaling pathway and here especially STAT1 were reported to be highly overexpressed in radioresistant breast cancer cells^{97,98}. In summary, the effect of STAT1 in modulating cytotoxic effects of chemotherapeutic treatment still remains controversial and requires deeper investigations.

Another interesting fact is that the C-terminal transactivation domain of STAT1 physically interacts with the well-described breast cancer gene BRCA1 (Breast Cancer 1)⁹⁹. Inherited mutations of BRCA1 confer a high risk to develop breast cancer but also ovarian cancer and a few other tumor types. The tumor suppressive role of BRCA1 is attributed to its role in regulating DNA damage response, cell cycle progression, apoptosis, genome integrity and transcription. BRCA1 itself is not a sequence-specific DNA binding transcription factor, however by binding to various transcription factors it functions as coregulator of transcription. It was shown to regulate expression of p21^{WAF1/cip1}, p27^{Kip1}, p53 and ER α . Together with STAT1, BRCA1 acts in concert to induce a subset of IFN γ responsive genes (such as p21^{WAF1/cip1}) and potentiates IFN γ mediated growth inhibition and apoptosis. Of note, mutations of STAT1's S727 site result in poor binding to BRCA1 which underlines the importance of S727 in the recruitment of transcriptional coactivators^{99,100}. This connection to the prominent breast cancer susceptibility gene BRCA1

makes STAT1 an even more interesting and promising candidate in the field of breast cancer research.

IRF1 – a downstream factor of STAT1

Interferon regulatory factor 1 (IRF1) is a transcription factor of the IFN γ signaling pathway and is activated by STAT1. It is ubiquitously expressed at low basal levels and acts as a weak transcriptional activator. IRF1 possesses several serine/threonine phosphorylation sites, although it is not verified whether the activity of IRF1 is regulated in a phosphorylation-dependent manner¹⁰¹. IRF1 activates the promoter of its close homologue IRF2 which binds to the same DNA consensus sequence and thereby antagonizes the transcriptional activation of IRF1¹⁰². As IRF1 is a mediator of IFN-induced signals, it confers (similar to STAT1) the induction of typical IFN functions such as antiviral state, tumor surveillance and immune regulation. The tumor suppressive functions of IRF1 stem at least partly from its involvement in cell cycle regulation and apoptosis. IRF1 acts as a negative regulator of cell proliferation and the overexpression of IRF1 in various mammalian cells mediates growth inhibition^{103–105}. IRF1 can transcriptionally induce expression of several caspases, FasL and other pro-apoptotic genes. Moreover, IRF1 regulates expression of the anti-proliferative genes p27^{Kip1} and p21^{Waf/Cip1}^{106,107}. Several studies strongly point towards a cooperation of IRF1 with the tumor suppressor p53 to prevent DNA-damage accumulation by activating distinct cell cycle components^{22,108}. Gene deletion studies in mice surprisingly revealed that IRF1-deficiency does not change the expression of type I IFNs and does not result in an increased susceptibility to viral infections¹⁰⁹. However, in response to IFN γ or lipopolysaccharide (LPS) treatment, *Irf1*^{-/-} macrophages produce no or very little nitric oxide (NO) which plays a crucial role in macrophage cytotoxicity. Therefore, *Irf1*^{-/-} mice are more sensitive to *Mycobacterium bovis* infection than wild type mice¹¹⁰. Further, *Irf1*^{-/-} mice display altered T cell development with a reduction of CD4⁺/CD8⁺ thymic cells^{109,111} and a reduced cytotoxic activity of NK cells¹¹².

It is not a big surprise that - similar to STAT1 - IRF1 has gained the reputation to act as tumor suppressor. Mutations, rearrangements or loss of IRF1 have been described in several cancers, including hematopoietic¹¹³, gastric¹¹⁴ and breast cancer¹¹⁵. Tissue arrays of breast cancer patients revealed a significant negative correlation between IRF1 expression and tumor grade. High-grad ductal carcinomas in situ as well as invasive forms of breast cancer are more likely to

express lower levels of IRF1 than untransformed tissue ^{116,117}. Moreover, overexpression of IRF1 in the human breast cancer cell line MCF7 revealed tumor suppressive activities via induction of apoptosis ¹¹⁸.

1.3 Breast cancer

Facts and statistics

Breast cancer is the worldwide most frequently diagnosed cancer and the leading cause of cancer death among women. Accounting to the GLOBOCAN 2008 estimates, about 384.155.000 breast cancer cases and 850.000 deaths have been documented worldwide in 2008 ¹¹⁹. The Statistics Austria counted 4611 breast cancer cases and 1531 deaths in 2007, making it as well in Austria the most prominent female cancer type (**Fig8.**). Even though men can develop breast cancer, it's a relatively rare condition accounting for only about 1% of all cases. Over the last decades, breast cancer incidence has continuously increased, however mortality has slightly decreased (**Fig9.**). The reason for the constantly rising cancer statistic stems from population aging and the adoption of pro-cancer lifestyle. Increased screening intensities further boost the number of detected cancer cases. On the positive side, early detection through regular health screenings as well as new and improved treatment methods could significantly limit breast cancer death rates.

Risk factors

Apart from being a woman, numerous factors play a potential role for the development of breast cancer. Only about 5% to 10% of the cases are considered to be hereditary and the result of inherited gene defects. The by far most powerful breast cancer predictor is an inherited mutation in the tumor-suppressor genes BRCA1 or BRCA2 (Breast Cancer 1/2). People carrying germline mutations in one of these genes have a risk as high as 40-80% for developing breast cancer ¹²⁰. Further gene mutations associated with inherited breast cancer have been defined in the ATM, TP53, CHEK2, PTEN, CDH1 and STK11 genes, albeit at low frequency ^{121,122}. Overall, white Caucasian women are slightly more likely to develop breast cancer when compared to

African-American women. Other factors which are known to increase the risk to develop breast cancer are age, a late first pregnancy, late menopause, oral contraceptives, hormone replacement therapy, obesity and alcohol consumption. Especially, synthetic progesterone derivatives (progestins) which are used for hormone replacement therapies and contraceptives have been associated with an increased risk to develop breast cancer^{123,124}. A very recent study revealed, that progestins trigger the massive induction of RANKL (receptor activator of NF- κ B ligand) in mammary epithelial cells¹²⁵. The crucial role for RANKL in breast cancer development was underlined by genetic inactivation or deletion of RANKL's receptor RANK (receptor activator of NF- κ B) from the mammary epithelium which significantly reduced progestin induced tumor development.

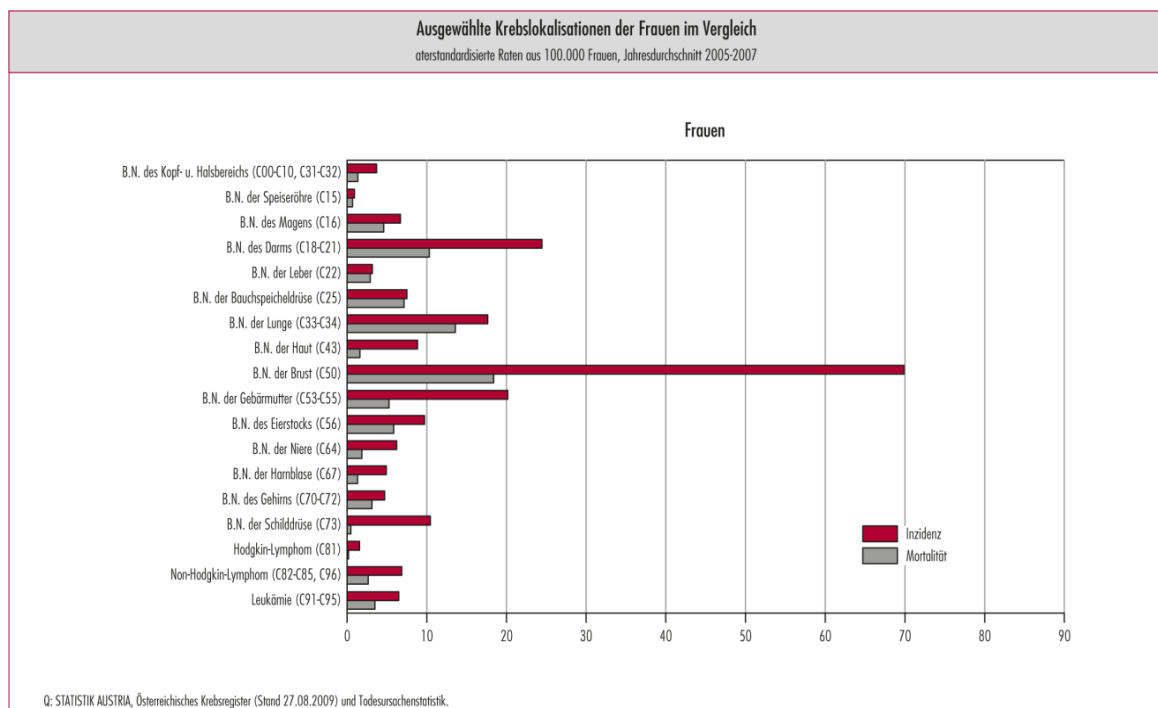


Figure 8. Incidence and mortality of selected cancer cases in women. (Taken from Statistik Austria¹²⁶)
 The evaluation covers all cancer cases registered between 2005-2007 in Austrian femals of all ages. Breast cancer is by far the most common form of cancer among women, considering incidence as well as mortality.

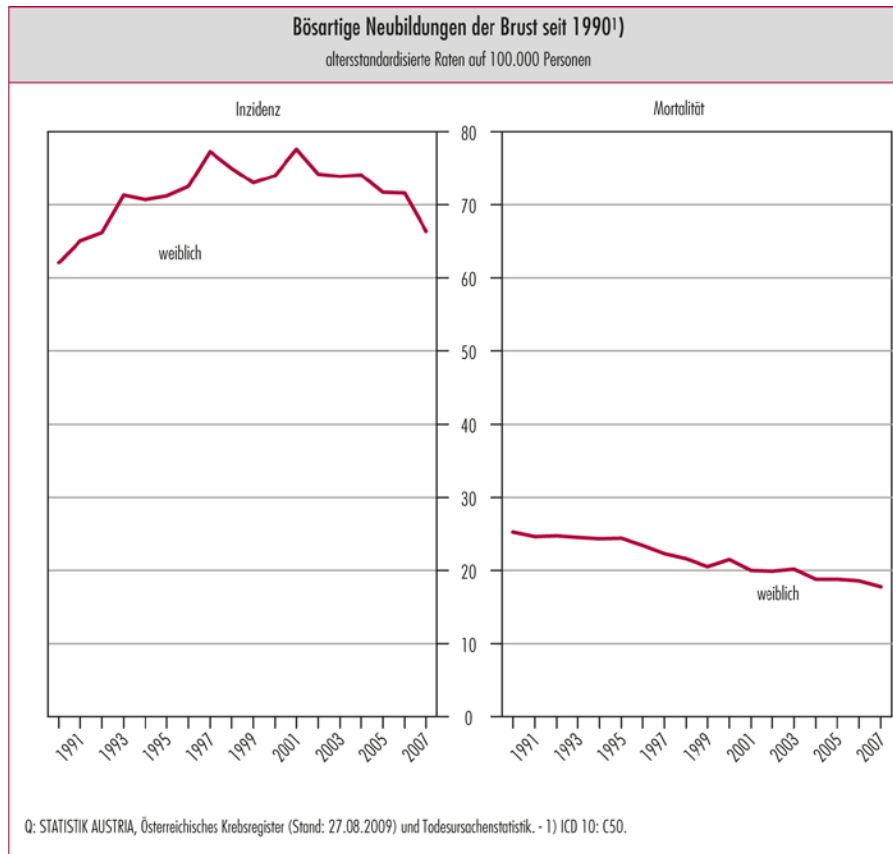


Figure 9. Breast cancer incidence and mortality trends in Austria (1990-2007). (Taken from Statistik Austria ¹²⁶)

Depicted are the numbers of newly diagnosed breast cancer cases per year. Rates are per 100.000 women. Since 1990, the incidence of newly diagnosed breast cancer cases has increased, whilst mortality has decreased. In 2007, around 66 of 100.000 females were diagnosed with breast cancer, 18 out of 100.000 died.

Types of breast cancer and classification

The primary role of the female mammary glands is to provide nutrition for the offspring. Mammary glands consist of lobules which are the milk producing glands and ducts that drain the milk to the nipple. Breast cancer may occur in all different areas of the breast - the ducts, the lobules, or less commonly also the stromal tissue in between. In both ductal and lobular carcinomas, one differentiates between in situ ("in its original place") and invasive carcinomas. The in situ carcinoma is a non-invasive form of breast cancer, characterized by the malignant proliferation of epithelial cells which have not crossed the basement membrane of the milk duct or the lobule (**Fig10.**). It is still under debate whether in situ carcinomas represent a direct precursor of invasive breast cancer. However, the risk of developing invasive cancer after

diagnosis of an in situ carcinoma is relatively high, and there is the general consensus that an in situ carcinoma exhibits an intermediate step between normal breast tissue and invasive breast cancer ¹²⁷. In the case of invasive cancer, malignant cells have already broken through the basement membrane and have begun to spread within the surrounding breast tissue and subsequently also into other areas of the body, developing metastasis. Bone, lungs, regional lymph nodes, liver and brain are the main targets for metastatic breast cancer, with the most common site being the bone. Metastasis represents an additional burden for breast cancer patients, as metastatic cancer cells frequently differ from the preceding primary breast cancer. They may display a different receptor status and have often developed resistance to previously used treatments. For this reason, the prognosis for metastatic breast cancer is poor and it accounts for approximately 90% of all breast cancer deaths.

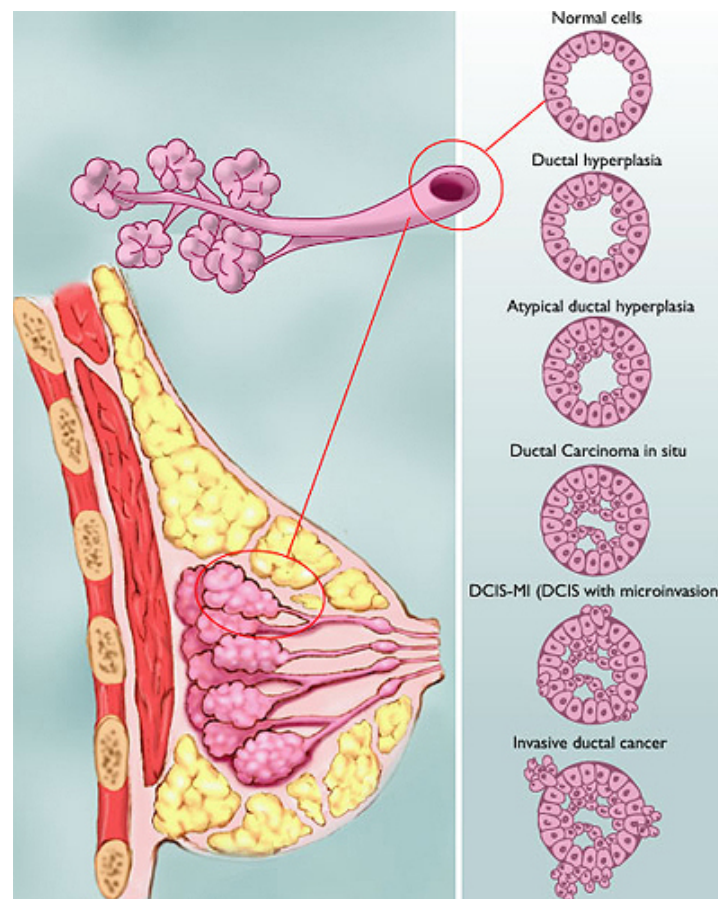


Figure 10. Range of ductal carcinoma in situ. (Taken from BreastCancer.org ¹²⁸)

Normal breast ducts are lined by a single layer of epithelial cells. Depending on the grade of abnormal cell growth and morphology, one can differentiate between ductal hyperplasia, atypically ductal hyperplasia, ductal carcinoma in situ or ductal carcinoma in situ with microinvasion. These abnormal forms are not cancerous yet, however they might harbor the risk to develop into an invasive form of cancer (invasive ductal cancer).

A successful therapy design and treatment depends on reliable predictive and prognostic factors. Therefore, breast cancer patients are rated by a combination of classical time-dependent variables (called “staging”) including tumor size, the involvement of lymph nodes and extent of tumor spread, as well as biological variables including morphologic variables like tumor grade (how different do the tumor cells look from normal cells) and molecular markers such as hormone receptors (estrogen receptor, ER and progesterone receptor, PR) and human epidermal growth factor receptor 2 (HER2) status. In addition to this classical tumor classification, gene expression profiling using microarray-based methods has further improved our understanding of breast cancer biology in the past decade¹²⁹. This novel technology could associate numerous gene signatures with prognosis and response to systemic therapies. However, their use in routine clinical decision-making could not replace but complement the classical classification system.

Current therapy and treatment methods

Early detection of breast cancer is crucial for successful treatment. To detect a tumor in its early phase before it has begun to metastasize prevents painful and often ineffective therapies. Preventive screening tests imply regular breast-palpation for any suspicious lumps or alterations, and with increasing age also yearly screening mammograms. Once substantial suspicion for breast cancer occurs, different diagnostic tests such as ultrasound, breast MRI (magnetic resonance imaging) and biopsy follow to gather more information about the cancer type to guide decisions about treatment. Every breast tumor has to be excised, however prior to surgery very often neoadjuvant therapies are applied. The aim of neoadjuvant therapies is to reduce the size or at least the extent of the cancer, thus making treatment easier and more likely to succeed. Adjuvant therapy is applied after tumor surgery to reduce the risk of future breast cancer recurrence or metastasis development. Both neoadjuvant and adjuvant therapies include treatments such as chemotherapy, hormone therapy or targeted therapy as well as radiation therapy. Chemotherapy is the use of different cytostatic drugs alone or in combination to inhibit tumor cell growth. However, since they act systemic and affect all cells of the body, they are associated with heavy side effects. Targeted therapy includes substances that specifically interfere with target molecules involved in tumor growth to inhibit further proliferation and progression of the tumor. Thereafter, it is less harmful for normal cells. The monoclonal antibody herceptin (trade name: Trastuzumab) specifically binds to the human epidermal growth factor receptor 2 (HER2) and is therefore applied to HER2-overexpressing breast tumors.

Another monoclonal antibody called Avastin (trade name: Bevacizumab) inhibits vascular endothelial growth factor A (VEGF-A), an important stimulator of blood vessel formation (angiogenesis). Avastin was the first commercially available angiogenesis-inhibitor, and was recommended in combination with standard chemotherapy for the treatment of metastatic breast cancer. However in 2011, the U.S. Food and Drug Administration revoked its approval of the breast cancer indication for Avastin, as it was not proven to be safe and effective for that use¹³⁰. Avastin showed only a small effect on tumor growth and no evidence to prolong life or improve its quality compared to the use of standard chemotherapy alone. Therefore the use of Avastin cannot justify its severe side effects such as high blood pressure, heart attack or heart failure, bleeding, hemorrhaging or the appearance of perforations of the stomach or the intestine¹³⁰. Besides antibody targeted therapy also includes small molecular weight inhibitors targeting kinases. The tyrosine-kinase inhibitor Lapatinib (trade name: Tykerb/Tyverb) binds to the ATP-binding pocket of both the epidermal growth factor receptor (EGFR) and HER2 protein kinase domain and prevents activation of the signal transduction cascade. It is approved for the treatment of advanced or metastatic HER2 positive breast cancer. Hormonal therapy is generally a very effective way to treat breast cancer, however with the limitation that it can only be applied for hormone receptor positive (ER⁺, PR⁺) cancers. Blocking the estrogen receptor or lowering the amount of estrogen in the body is an effective way to inhibit the growth of ER⁺ receptor positive tumor cells. One well known example for an estrogen-receptor antagonist is tamoxifen. As hormone ER⁺ cancers have an easily accessible point of action, they are generally regarded to have a good prognosis.

Although the treatment methods for breast cancer are constantly improving, there is still need for novel therapeutics, molecular targets and of course also for reliable prognostic and predictive markers to forecast drug responses, disease development and outcome. My study on the transcription factor STAT1 may hopefully improve the general knowledge about mechanisms involved in breast cancer development and provide potential starting-points for novel treatment methods.

1.4 References

1. Isaacs, A. & Lindenmann, J. Virus interference. I. The interferon. *Proceedings of the Royal Society of London. Series B, Containing papers of a Biological character. Royal Society (Great Britain)* **147**, 258–67 (1957).
2. Isaacs, A., Lindenmann, J. & Valentine, R. C. Virus interference. II. Some properties of interferon. *Proceedings of the Royal Society of London. Series B, Containing papers of a Biological character. Royal Society (Great Britain)* **147**, 268–73 (1957).
3. Wilks, A. F. *et al.* Two novel protein-tyrosine kinases, each with a second phosphotransferase-related catalytic domain, define a new class of protein kinase. *Molecular and cellular biology* **11**, 2057–65 (1991).
4. Shuai, K., Schindler, C., Prezioso, V. R. & Darnell, J. E. Activation of transcription by IFN-gamma: tyrosine phosphorylation of a 91-kD DNA binding protein. *Science (New York, N.Y.)* **258**, 1808–12 (1992).
5. Calò, V. *et al.* STAT proteins: from normal control of cellular events to tumorigenesis. *Journal of cellular physiology* **197**, 157–68 (2003).
6. Shuai, K. & Liu, B. Regulation of JAK-STAT signalling in the immune system. *Nature reviews. Immunology* **3**, 900–11 (2003).
7. Levy, D. E. & Darnell, J. E. Stats: transcriptional control and biological impact. *Nature reviews. Molecular cell biology* **3**, 651–62 (2002).
8. Yu, H. & Jove, R. The STATs of cancer--new molecular targets come of age. *Nature reviews. Cancer* **4**, 97–105 (2004).
9. Bowman, T., Garcia, R., Turkson, J. & Jove, R. STATs in oncogenesis. *Oncogene* **19**, 2474–88 (2000).
10. Wilks, A. F. The JAK kinases: not just another kinase drug discovery target. *Seminars in cell & developmental biology* **19**, 319–28 (2008).
11. Zouein, F. a, Duhé, R. J. & Booz, G. W. JAKs go nuclear: emerging role of nuclear JAK1 and JAK2 in gene expression and cell growth. *Growth factors (Chur, Switzerland)* **29**, 245–52 (2011).
12. Rodig, S. J. *et al.* Disruption of the Jak1 Gene Demonstrates Obligatory and Nonredundant Roles of the Jaks in Cytokine-Induced Biologic Responses. *Cell* **93**, 373–383 (1998).
13. Parganas, E. Jak2 Is Essential for Signaling through a Variety of Cytokine Receptors. *Cell* **93**, 385–395 (1998).
14. Neubauer, H. *et al.* Jak2 Deficiency Defines an Essential Developmental Checkpoint in Definitive Hematopoiesis. *Cell* **93**, 397–409 (1998).

-
15. Nosaka, T. *et al.* Defective Lymphoid Development in Mice Lacking Jak3. *Science* **270**, 800–802 (1995).
 16. Karaghiosoff, M. *et al.* Partial Impairment of Cytokine Responses in Tyk2-Deficient Mice. *Immunity* **13**, 549–560 (2000).
 17. Murray, P. J. The JAK-STAT signaling pathway: input and output integration. *Journal of immunology (Baltimore, Md. : 1950)* **178**, 2623–9 (2007).
 18. Meraz, M. A. *et al.* Targeted disruption of the Stat1 gene in mice reveals unexpected physiologic specificity in the JAK-STAT signaling pathway. *Cell* **84**, 431–42 (1996).
 19. Durbin, J. E., Hackenmiller, R., Simon, M. C. & Levy, D. E. Targeted disruption of the mouse Stat1 gene results in compromised innate immunity to viral disease. *Cell* **84**, 443–50 (1996).
 20. Park, C., Li, S., Cha, E. & Schindler, C. Immune response in Stat2 knockout mice. *Immunity* **13**, 795–804 (2000).
 21. Kaplan, M. H., Sun, Y. L., Hoey, T. & Grusby, M. J. Impaired IL-12 responses and enhanced development of Th2 cells in Stat4-deficient mice. *Nature* **382**, 174–7 (1996).
 22. Takeda, K. *et al.* Essential role of Stat6 in IL-4 signalling. *Nature* **380**, 627–30 (1996).
 23. Yao, Z. *et al.* Stat5a/b are essential for normal lymphoid development and differentiation. *Proceedings of the National Academy of Sciences of the United States of America* **103**, 1000–5 (2006).
 24. Cui, Y. *et al.* Inactivation of Stat5 in mouse mammary epithelium during pregnancy reveals distinct functions in cell proliferation, survival, and differentiation. *Molecular and cellular biology* **24**, 8037–47 (2004).
 25. Liu, X. *et al.* Stat5a is mandatory for adult mammary gland development and lactogenesis. *Genes & development* **11**, 179–86 (1997).
 26. Takeda, K. *et al.* Targeted disruption of the mouse Stat3 gene leads to early embryonic lethality. *Proceedings of the National Academy of Sciences of the United States of America* **94**, 3801–4 (1997).
 27. Chapman, R. S. *et al.* Suppression of epithelial apoptosis and delayed mammary gland involution in mice with a conditional knockout of Stat3. *Genes & development* **13**, 2604–16 (1999).
 28. Levy, D. E. & Lee, C. What does Stat3 do? *The Journal of clinical investigation* **109**, 1143–8 (2002).
 29. Notarangelo, L. D. *et al.* Mutations in severe combined immune deficiency (SCID) due to JAK3 deficiency. *Human Mutation* **18**, 255–263 (2001).

-
30. Macchi, P. *et al.* Mutations of Jak-3 gene in patients with autosomal severe combined immune deficiency (SCID). *Nature* **377**, 65–8 (1995).
 31. Tsumura, M. *et al.* Dominant-negative STAT1 SH2 domain mutations in unrelated patients with Mendelian susceptibility to mycobacterial disease. *Human mutation* (2012).doi:10.1002/humu.22113
 32. Kong, X.-F. *et al.* A novel form of human STAT1 deficiency impairing early but not late responses to interferons. *Blood* **116**, 5895–906 (2010).
 33. Averbuch, D., Chapgier, A., Boisson-Dupuis, S., Casanova, J.-L. & Engelhard, D. The clinical spectrum of patients with deficiency of Signal Transducer and Activator of Transcription-1. *The Pediatric infectious disease journal* **30**, 352–5 (2011).
 34. Kristensen, I. A., Veirum, J. E., Møller, B. K. & Christiansen, M. Novel STAT1 alleles in a patient with impaired resistance to mycobacteria. *Journal of clinical immunology* **31**, 265–71 (2011).
 35. Vairo, D. *et al.* Severe impairment of IFN- γ and IFN- α responses in cells of a patient with a novel STAT1 splicing mutation. *Blood* **118**, 1806–17 (2011).
 36. Shi, S. *et al.* Drosophila STAT is required for directly maintaining HP1 localization and heterochromatin stability. *Nature cell biology* **10**, 489–96 (2008).
 37. Li, W. X. Canonical and non-canonical JAK-STAT signaling. *Trends in cell biology* **18**, 545–51 (2008).
 38. Reich, N. C. & Liu, L. Tracking STAT nuclear traffic. *Nature reviews. Immunology* **6**, 602–12 (2006).
 39. Lobie, P. E. Constitutive nuclear localization of Janus kinases 1 and 2. *Endocrinology* **137**, 4037–4045 (1996).
 40. Cheon, H. & Stark, G. R. Unphosphorylated STAT1 prolongs the expression of interferon-induced immune regulatory genes. *Proceedings of the National Academy of Sciences of the United States of America* **106**, 9373–8 (2009).
 41. Wen, Z., Zhong, Z. & Darnell, J. E. Maximal activation of transcription by Stat1 and Stat3 requires both tyrosine and serine phosphorylation. *Cell* **82**, 241–50 (1995).
 42. O’Shea, J. J., Gadina, M. & Schreiber, R. D. Cytokine signaling in 2002: new surprises in the Jak/Stat pathway. *Cell* **109 Suppl**, S121–31 (2002).
 43. Zhang, J. J. *et al.* Ser727-dependent recruitment of MCM5 by Stat1 α in IFN- γ -induced transcriptional activation. *The EMBO journal* **17**, 6963–71 (1998).
 44. Plataniias, L. C. Mechanisms of type-I- and type-II-interferon-mediated signalling. *Nature reviews. Immunology* **5**, 375–86 (2005).

-
45. Kim, H. S. & Lee, M.-S. STAT1 as a key modulator of cell death. *Cellular signalling* **19**, 454–65 (2007).
 46. Stark, G. R., Kerr, I. M., Williams, B. R., Silverman, R. H. & Schreiber, R. D. How cells respond to interferons. *Annual review of biochemistry* **67**, 227–64 (1998).
 47. Stephanou, A. *et al.* Ischemia-induced STAT-1 expression and activation play a critical role in cardiomyocyte apoptosis. *The Journal of biological chemistry* **275**, 10002–8 (2000).
 48. Stephanou, A. *et al.* Induction of apoptosis and Fas receptor/Fas ligand expression by ischemia/reperfusion in cardiac myocytes requires serine 727 of the STAT-1 transcription factor but not tyrosine 701. *The Journal of biological chemistry* **276**, 28340–7 (2001).
 49. Stephanou, A., Brar, B. K., Knight, R. A. & Latchman, D. S. Opposing actions of STAT-1 and STAT-3 on the Bcl-2 and Bcl-x promoters. *Cell death and differentiation* **7**, 329–30 (2000).
 50. Townsend, P. A. *et al.* STAT-1 interacts with p53 to enhance DNA damage-induced apoptosis. *The Journal of biological chemistry* **279**, 5811–20 (2004).
 51. Kaplan, D. H. *et al.* Demonstration of an interferon gamma-dependent tumor surveillance system in immunocompetent mice. *Proceedings of the National Academy of Sciences of the United States of America* **95**, 7556–61 (1998).
 52. Dimco, G., Knight, R. A., Latchman, D. S. & Stephanou, A. STAT1 interacts directly with cyclin D1/Cdk4 and mediates cell cycle arrest. *Cell cycle (Georgetown, Tex.)* **9**, 4638–49 (2010).
 53. Chin, Y. E. *et al.* Cell growth arrest and induction of cyclin-dependent kinase inhibitor p21 WAF1/CIP1 mediated by STAT1. *Science (New York, N.Y.)* **272**, 719–22 (1996).
 54. Wang, S., Raven, J. F., Durbin, J. E. & Koromilas, A. E. Stat1 phosphorylation determines Ras oncogenicity by regulating p27 kip1. *PloS one* **3**, e3476 (2008).
 55. Wang, S., Raven, J. F. & Koromilas, A. E. STAT1 represses Skp2 gene transcription to promote p27Kip1 stabilization in Ras-transformed cells. *Molecular cancer research : MCR* **8**, 798–805 (2010).
 56. Wang, S. & Koromilas, A. E. Stat1 is an inhibitor of Ras-MAPK signaling and Rho small GTPase expression with implications in the transcriptional signature of Ras transformed cells. *Cell cycle (Georgetown, Tex.)* **8**, 2070–9 (2009).
 57. Lee, C. K., Smith, E., Gimeno, R., Gertner, R. & Levy, D. E. STAT1 affects lymphocyte survival and proliferation partially independent of its role downstream of IFN-gamma. *Journal of immunology (Baltimore, Md. : 1950)* **164**, 1286–92 (2000).
 58. Lee, C. K. *et al.* Distinct requirements for IFNs and STAT1 in NK cell function. *Journal of immunology (Baltimore, Md. : 1950)* **165**, 3571–7 (2000).

-
59. Robbins, S. H., Tessmer, M. S., Van Kaer, L. & Brossay, L. Direct effects of T-bet and MHC class I expression, but not STAT1, on peripheral NK cell maturation. *European journal of immunology* **35**, 757–65 (2005).
 60. Pilz, A. *et al.* Dendritic cells require STAT-1 phosphorylated at its transactivating domain for the induction of peptide-specific CTL. *Journal of immunology (Baltimore, Md. : 1950)* **183**, 2286–93 (2009).
 61. Fallarino, F. & Gajewski, T. F. Cutting edge: differentiation of antitumor CTL in vivo requires host expression of Stat1. *Journal of immunology (Baltimore, Md. : 1950)* **163**, 4109–13 (1999).
 62. Halupa, A. *et al.* A novel role for STAT1 in regulating murine erythropoiesis: deletion of STAT1 results in overall reduction of erythroid progenitors and alters their distribution. *Blood* **105**, 552–61 (2005).
 63. Chen, E. *et al.* Distinct clinical phenotypes associated with JAK2V617F reflect differential STAT1 signaling. *Cancer cell* **18**, 524–35 (2010).
 64. Hannesdóttir, L. *et al.* MMTV-neu mice deficient in STAT1 are susceptible to develop ovarian teratomas. *The International journal of developmental biology* **56**, 279–83 (2012).
 65. Klover, P. J. *et al.* Loss of STAT1 from mouse mammary epithelium results in an increased Neu-induced tumor burden. *Neoplasia (New York, N.Y.)* **12**, 899–905 (2010).
 66. Raven, J. F. *et al.* Stat1 is a suppressor of ErbB2/Neu-mediated cellular transformation and mouse mammary gland tumor formation. *Cell cycle (Georgetown, Tex.)* **10**, 794–804 (2011).
 67. Widschwendter, A. *et al.* Prognostic significance of signal transducer and activator of transcription 1 activation in breast cancer. *Clinical cancer research : an official journal of the American Association for Cancer Research* **8**, 3065–74 (2002).
 68. Kovacic, B. *et al.* STAT1 acts as a tumor promoter for leukemia development. *Cancer cell* **10**, 77–87 (2006).
 69. Timofeeva, O. A. *et al.* Serine-phosphorylated STAT1 is a prosurvival factor in Wilms' tumor pathogenesis. *Oncogene* **25**, 7555–64 (2006).
 70. Patterson, S. G. *et al.* Novel role of Stat1 in the development of docetaxel resistance in prostate tumor cells. *Oncogene* **25**, 6113–22 (2006).
 71. Watson, C. J., Gordon, K. E., Robertson, M. & Clark, A. J. Interaction of DNA-binding proteins with a milk protein gene promoter in vitro: identification of a mammary gland-specific factor. *Nucleic acids research* **19**, 6603–10 (1991).
 72. Philp, J. A., Burdon, T. G. & Watson, C. J. Differential activation of STATs 3 and 5 during mammary gland development. *FEBS letters* **396**, 77–80 (1996).

-
73. Watson, C. J. & Neoh, K. The Stat family of transcription factors have diverse roles in mammary gland development. *Seminars in cell & developmental biology* **19**, 401–6 (2008).
 74. Liu, X., Robinson, G. W. & Hennighausen, L. Activation of Stat5a and Stat5b by tyrosine phosphorylation is tightly linked to mammary gland differentiation. *Molecular endocrinology (Baltimore, Md.)* **10**, 1496–506 (1996).
 75. Wagner, K.-U. & Rui, H. Jak2/Stat5 signaling in mammaryogenesis, breast cancer initiation and progression. *Journal of mammary gland biology and neoplasia* **13**, 93–103 (2008).
 76. Ormandy, C. J. *et al.* Null mutation of the prolactin receptor gene produces multiple reproductive defects in the mouse. *Genes & development* **11**, 167–78 (1997).
 77. Wagner, K.-U. *et al.* Impaired alveologenesi and maintenance of secretory mammary epithelial cells in Jak2 conditional knockout mice. *Molecular and cellular biology* **24**, 5510–20 (2004).
 78. Teglund, S. *et al.* Stat5a and Stat5b Proteins Have Essential and Nonessential, or Redundant, Roles in Cytokine Responses. *Cell* **93**, 841–850 (1998).
 79. Liu, X., Gallego, M. I., Smith, G. H., Robinson, G. W. & Hennighausen, L. Functional rescue of Stat5a-null mammary tissue through the activation of compensating signals including Stat5b. *Cell growth & differentiation : the molecular biology journal of the American Association for Cancer Research* **9**, 795–803 (1998).
 80. Wagner, K.-U. & Schmidt, J. W. The two faces of Janus kinases and their respective STATs in mammary gland development and cancer. *Journal of carcinogenesis* **10**, 32 (2011).
 81. Yamaji, D. *et al.* Development of mammary luminal progenitor cells is controlled by the transcription factor STAT5A. *Genes & development* **23**, 2382–7 (2009).
 82. Cotarla, I. *et al.* Stat5a is tyrosine phosphorylated and nuclear localized in a high proportion of human breast cancers. *International journal of cancer. Journal international du cancer* **108**, 665–71 (2004).
 83. Watson, C. J. & Miller, W. R. Elevated levels of members of the STAT family of transcription factors in breast carcinoma nuclear extracts. *British journal of cancer* **71**, 840–4 (1995).
 84. Yamashita, H. *et al.* Stat5 expression predicts response to endocrine therapy and improves survival in estrogen receptor-positive breast cancer. *Endocrine-related cancer* **13**, 885–93 (2006).
 85. Nevalainen, M. T. *et al.* Signal transducer and activator of transcription-5 activation and breast cancer prognosis. *Journal of clinical oncology : official journal of the American Society of Clinical Oncology* **22**, 2053–60 (2004).

-
86. Sultan, A. S. *et al.* Stat5 promotes homotypic adhesion and inhibits invasive characteristics of human breast cancer cells. *Oncogene* **24**, 746–60 (2005).
 87. Ren, S., Cai, H. R., Li, M. & Furth, P. A. Loss of Stat5a delays mammary cancer progression in a mouse model. *Oncogene* **21**, 4335–9 (2002).
 88. Koptyra, M., Gupta, S., Talati, P. & Nevalainen, M. T. Signal transducer and activator of transcription 5a/b: biomarker and therapeutic target in prostate and breast cancer. *The international journal of biochemistry & cell biology* **43**, 1417–21 (2011).
 89. Garcia, R. *et al.* Constitutive activation of Stat3 by the Src and JAK tyrosine kinases participates in growth regulation of human breast carcinoma cells. *Oncogene* **20**, 2499–513 (2001).
 90. Garcia, R. *et al.* Constitutive activation of Stat3 in fibroblasts transformed by diverse oncoproteins and in breast carcinoma cells. *Cell growth & differentiation : the molecular biology journal of the American Association for Cancer Research* **8**, 1267–76 (1997).
 91. Tkach, M. *et al.* Targeting Stat3 Induces Senescence in Tumor Cells and Elicits Prophylactic and Therapeutic Immune Responses against Breast Cancer Growth Mediated by NK Cells and CD4+ T Cells. *Journal of immunology (Baltimore, Md. : 1950)* **189**, 1162–72 (2012).
 92. Barbieri, I. *et al.* Constitutively active Stat3 enhances neu-mediated migration and metastasis in mammary tumors via upregulation of Cten. *Cancer research* **70**, 2558–67 (2010).
 93. Chan, S. R. *et al.* STAT1-deficient mice spontaneously develop estrogen receptor alpha-positive luminal mammary carcinomas. *Breast cancer research : BCR* **14**, R16 (2012).
 94. Zhang, Q. *et al.* The role of Tyk2 in regulation of breast cancer growth. *Journal of interferon & cytokine research : the official journal of the International Society for Interferon and Cytokine Research* **31**, 671–7 (2011).
 95. Thomas, M. *et al.* STAT1: a modulator of chemotherapy-induced apoptosis. *Cancer research* **64**, 8357–64 (2004).
 96. Yang, P.-Y. *et al.* Norcantharidin induces apoptosis of breast cancer cells: involvement of activities of mitogen activated protein kinases and signal transducers and activators of transcription. *Toxicology in vitro : an international journal published in association with BIBRA* **25**, 699–707 (2011).
 97. Zhan, J.-F. *et al.* STAT1 promotes radioresistance of CD44(+)/CD24(-/low) cells in breast cancer. *Experimental biology and medicine (Maywood, N.J.)* **236**, 418–22 (2011).
 98. Khodarev, N. N. *et al.* STAT1 is overexpressed in tumors selected for radioresistance and confers protection from radiation in transduced sensitive cells. *Proceedings of the National Academy of Sciences of the United States of America* **101**, 1714–9 (2004).

-
99. Ouchi, T., Lee, S. W., Ouchi, M., Aaronson, S. A. & Horvath, C. M. Collaboration of signal transducer and activator of transcription 1 (STAT1) and BRCA1 in differential regulation of IFN-gamma target genes. *Proceedings of the National Academy of Sciences of the United States of America* **97**, 5208–13 (2000).
 100. Rosen, E. M., Fan, S. & Ma, Y. BRCA1 regulation of transcription. *Cancer letters* **236**, 175–85 (2006).
 101. Kröger, A., Köster, M., Schroeder, K., Hauser, H. & Mueller, P. P. Activities of IRF-1. *Journal of interferon & cytokine research : the official journal of the International Society for Interferon and Cytokine Research* **22**, 5–14 (2002).
 102. Harada, H. *et al.* Structurally similar but functionally distinct factors, IRF-1 and IRF-2, bind to the same regulatory elements of IFN and IFN-inducible genes. *Cell* **58**, 729–39 (1989).
 103. Romeo, G. *et al.* IRF-1 as a negative regulator of cell proliferation. *Journal of interferon & cytokine research : the official journal of the International Society for Interferon and Cytokine Research* **22**, 39–47 (2002).
 104. Kirchhoff, S., Schaper, F. & Hauser, H. Interferon regulatory factor 1 (IRF-1) mediates cell growth inhibition by transactivation of downstream target genes. *Nucleic acids research* **21**, 2881–9 (1993).
 105. Harada, H. *et al.* Anti-oncogenic and oncogenic potentials of interferon regulatory factors-1 and -2. *Science (New York, N.Y.)* **259**, 971–4 (1993).
 106. Moro, A., Santos, A., Araña, M. J. & Perea, S. E. Activation of the human p27(Kip1) promoter by IFNalpha 2b. *Biochemical and biophysical research communications* **269**, 31–4 (2000).
 107. Tanaka, N. *et al.* Cooperation of the tumour suppressors IRF-1 and p53 in response to DNA damage. *Nature* **382**, 816–8 (1996).
 108. Tanaka, N. *et al.* Cellular commitment to oncogene-induced transformation or apoptosis is dependent on the transcription factor IRF-1. *Cell* **77**, 829–39 (1994).
 109. Reis, L. F., Ruffner, H., Stark, G., Aguet, M. & Weissmann, C. Mice devoid of interferon regulatory factor 1 (IRF-1) show normal expression of type I interferon genes. *The EMBO journal* **13**, 4798–806 (1994).
 110. Kamijo, R. *et al.* Requirement for transcription factor IRF-1 in NO synthase induction in macrophages. *Science (New York, N.Y.)* **263**, 1612–5 (1994).
 111. Matsuyama, T. *et al.* Targeted disruption of IRF-1 or IRF-2 results in abnormal type I IFN gene induction and aberrant lymphocyte development. *Cell* **75**, 83–97 (1993).
 112. Duncan, G. S., Mittrücker, H. W., Kägi, D., Matsuyama, T. & Mak, T. W. The transcription factor interferon regulatory factor-1 is essential for natural killer cell function in vivo. *The Journal of experimental medicine* **184**, 2043–8 (1996).

-
113. Willman, C. L. *et al.* Deletion of IRF-1, mapping to chromosome 5q31.1, in human leukemia and preleukemic myelodysplasia. *Science (New York, N.Y.)* **259**, 968–71 (1993).
 114. Nozawa, H. *et al.* Functionally inactivating point mutation in the tumor-suppressor IRF-1 gene identified in human gastric cancer. *International journal of cancer. Journal international du cancer* **77**, 522–7 (1998).
 115. Cavalli, L. R., Riggins, R. B., Wang, A., Clarke, R. & Haddad, B. R. Frequent loss of heterozygosity at the interferon regulatory factor-1 gene locus in breast cancer. *Breast cancer research and treatment* **121**, 227–31 (2010).
 116. Connett, J. M., Badri, L., Giordano, T. J., Connett, W. C. & Doherty, G. M. Interferon regulatory factor 1 (IRF-1) and IRF-2 expression in breast cancer tissue microarrays. *Journal of interferon & cytokine research : the official journal of the International Society for Interferon and Cytokine Research* **25**, 587–94 (2005).
 117. Doherty, G. M., Boucher, L., Sorenson, K. & Lowney, J. Interferon regulatory factor expression in human breast cancer. *Annals of surgery* **233**, 623–9 (2001).
 118. Bouker, K. B. *et al.* Interferon regulatory factor-1 (IRF-1) exhibits tumor suppressor activities in breast cancer associated with caspase activation and induction of apoptosis. *Carcinogenesis* **26**, 1527–35 (2005).
 119. Jemal, A. *et al.* Global cancer statistics. *CA: a cancer journal for clinicians* **61**, 69–90 (2011).
 120. Fackenthal, J. D. & Olopade, O. I. Breast cancer risk associated with BRCA1 and BRCA2 in diverse populations. *Nature reviews. Cancer* **7**, 937–48 (2007).
 121. van der Groep, P., van der Wall, E. & van Diest, P. J. Pathology of hereditary breast cancer. *Cellular oncology (Dordrecht)* **34**, 71–88 (2011).
 122. Ripperger, T., Gadzicki, D., Meindl, A. & Schlegelberger, B. Breast cancer susceptibility: current knowledge and implications for genetic counselling. *European journal of human genetics : EJHG* **17**, 722–31 (2009).
 123. Collaborators, M. W. S. Breast cancer and hormone-replacement therapy in the Million Women Study. *The Lancet* **362**, 419–427 (2003).
 124. Risks and Benefits of Estrogen Plus Progestin in Healthy Postmenopausal Women: Principal Results From the Women’s Health Initiative Randomized Controlled Trial. *JAMA: The Journal of the American Medical Association* **288**, 321–333 (2002).
 125. Schramek, D. *et al.* Osteoclast differentiation factor RANKL controls development of progestin-driven mammary cancer. *Nature* **468**, 98–102 (2010).
 126. Statistik Austria. at <<http://www.statistik.at/>>

-
127. Virnig, B. A., Tuttle, T. M., Shamliyan, T. & Kane, R. L. Ductal carcinoma in situ of the breast: a systematic review of incidence, treatment, and outcomes. *Journal of the National Cancer Institute* **102**, 170–8 (2010).
 128. BreastCancer.org. at <<http://www.breastcancer.org/>>
 129. Colombo, P.-E., Milanezi, F., Weigelt, B. & Reis-Filho, J. S. Microarrays in the 2010s: the contribution of microarray-based gene expression profiling to breast cancer classification, prognostication and prediction. *Breast cancer research : BCR* **13**, 212 (2011).
 130. Press Announcements - FDA Commissioner announces Avastin decision. at <<http://www.fda.gov/NewsEvents/Newsroom/PressAnnouncements/ucm280536.htm>>

AIM OF THE THESIS

The importance of STAT1 for tumor surveillance is well described since several years. STAT1 is a central mediator of interferon signaling and plays an essential role in innate as well as adaptive immunity. STAT1 deficiency manifests in impaired NK and T cell function and in a reduced capacity to induce apoptosis, therefore providing tumor promoting conditions. Regarding mammary cancer, several studies in mice and men already delineated STAT1 to act in a tumor suppressive way. In ErbB2-induced mammary tumor models complete but also tissue specific deletion of STAT1 results in accelerated mammary tumor formation. This indicates that STAT1 plays a certain cell-autonomous tumor-suppressive role within the mammary gland. The exact mechanism how loss of STAT1 promotes mammary tumor development has not been elucidated until now, neither in the immune system nor cell-intrinsically.

We observed the frequent occurrence of spontaneous mammary tumor formation in multiparous STAT1-deficient mice. As it is a novel finding that loss of STAT1 suffices to promote mammary tumor development, the aim of my thesis was to characterize this phenomenon in detail. A further goal was to deepen our understanding of STAT1's immune-modulatory and cell autonomous contributions in mammary tumor formation. To dissect these two factors, reciprocal mammary gland transplantation experiments were performed (*Stat1*^{-/-} mammary glands in *Stat1*^{+/+} immunological surrounding, and vice versa). All developing mammary tumors were analyzed and classified to find tumor patterns that correlate with STAT1 deficiency. I further investigated how loss of STAT1 affects immune control and which of the impaired immune cells (NK and/or T cells) are essential for mammary tumor surveillance. Therefore, I performed orthotopic transplantations of mammary tumor cell lines in mice lacking either NK cells and/or T cells. Finally, I analyzed the cell-specific function of STAT1 in mammary epithelial cells using a 3D culture system.

RESULTS

This section consists of 4 manuscripts. The results of the main project of my doctoral thesis are described in section 3.1. I additionally contributed to several other manuscripts and the results from these projects are described in section 3.2, 3.3 and 3.4. In each section, my contribution to the manuscript will be outlined briefly.

3.1 Putting the brakes on mammary tumorigenesis – Loss of STAT1 predisposes to intraepithelial neoplasias.

Manuscript published in Oncotarget. 2011 Dec;2(12):1043-54.

Schneckenleithner C, Bago-Horvath Z, Dolznig H, Neugebauer N, Kollmann K, Kolbe T, Decker T, Kerjaschki D, Wagner KU, Müller M, Stoiber D, Sexl V.

3.2 Lipoxigenase mediates invasion of intrametastatic lymphatic vessels and propagates lymph node metastasis of human mammary carcinoma xenografts in mouse.

Manuscript published in J Clin Invest. 2011 May;121(5):2000-12. doi: 10.1172/JCI44751. Epub 2011 Apr 11.

Kerjaschki D, Bago-Horvath Z, Rudas M, Sexl V, **Schneckenleithner C**, Wolbank S, Bartel G, Krieger S, Kalt R, Hantusch B, Keller T, Nagy-Bojarszky K, Huttary N, Raab I, Lackner K, Krautgasser K, Schachner H, Kaserer K, Rezar S, Madlener S, Vonach C, Davidovits A, Nosaka H, Hämmerle M, Viola K, Dolznig H, Schreiber M, Nader A, Mikulits W, Gnant M, Hirakawa S, Detmar M, Alitalo K, Nijman S, Offner F, Maier TJ, Steinhilber D, Krupitza G.

3.3 Conditional STAT1 ablation reveals the importance of interferon signaling for immunity to Listeria monocytogenes infection.

Manuscript published in PLoS Pathog. 2012 Jun;8(6):e1002763. Epub 2012 Jun 14.

Kernbauer E, Maier V, Stoiber D, Strobl B, **Schneckenleithner C**, Sexl V, Reichert U., Reizis B, Kalinke U, Jamieson A, Müller M, Decker T.

3.4 A new kinase-independent function of CDK6 links the cell cycle to tumour angiogenesis.

Manuscript under review in Nature Cell Biology.

Kollmann K, Heller G*, Schneckenleithner C*, Warsch W*, Scheicher R, Ott R G, Schäfer M, Fajmann S, Schiefer AI, Reichert U, Mayerhofer M, Hoeller C, Zochbauer-Mueller S, Kerjaschki D, Kenner L, Hoefler G, Freissmuth M, Moriggl R, Busslinger M, Malumbres M, Sexl V.

3.1 Putting the brakes on mammary tumorigenesis – Loss of STAT1 predisposes to intraepithelial neoplasias.

Manuscript published in Oncotarget. 2011 Dec;2(12):1043-54.

Christine Schneckenleithner¹, Zsuzsanna Bago-Horvath², Helmut Dolznig³, Nina Neugebauer¹, Karoline Kollmann¹, Thomas Kolbe⁴, Thomas Decker⁵, Donscho Kerjaschki², Kay-Uwe Wagner⁶, Mathias Müller⁷, Dagmar Stoiber^{8,9}, and Veronika Sexl¹

¹ Institute of Pharmacology and Toxicology, University of Veterinary Medicine, Vienna, Austria, ² Clinical Institute of Pathology, Medical University of Vienna, Austria, ³ Institute of Medical Genetics, Medical University of Vienna, Austria, ⁴ Biomodels Austria, University of Veterinary Medicine, Vienna and Biotechnology in Animal Production, IFA-Tulln, University of Natural Resources and Applied Life Sciences, Vienna, ⁵ Max F. Perutz Laboratories, Department of Genetics, Microbiology and Immunobiology, University of Vienna, Austria, ⁶ Eppley Institute for Research in Cancer and Allied Diseases, University of Nebraska Medical Center, Omaha, Nebraska, ⁷ Institute of Animal Breeding and Genetics and Biomodels Austria, University of Veterinary Medicine, Vienna, Austria, ⁸ Ludwig Boltzmann Institute for Cancer Research, Vienna, Austria, ⁹ Institute of Pharmacology, Medical University of Vienna, Austria

My contribution: Designed research, performed experiments, analyzed data, wrote paper.

Putting the brakes on mammary tumorigenesis: Loss of STAT1 predisposes to intraepithelial neoplasias

Christine Schneckenleithner¹, Zsuzsanna Bago-Horvath², Helmut Dolznig³, Nina Neugebauer¹, Karoline Kollmann¹, Thomas Kolbe⁴, Thomas Decker⁵, Donscho Kerjaschki², Kay-Uwe Wagner⁶, Mathias Müller⁷, Dagmar Stoiber^{8,9} and Veronika Sexl¹

¹ Institute of Pharmacology and Toxicology, University of Veterinary Medicine, Vienna, Austria

² Clinical Institute of Pathology, Medical University of Vienna, Austria

³ Institute of Medical Genetics, Medical University of Vienna, Austria

⁴ Biomodels Austria, University of Veterinary Medicine, Vienna and Biotechnology in Animal Production, IFA-Tulln, University of Natural Resources and Applied Life Sciences, Vienna

⁵ Max F. Perutz Laboratories, Department of Genetics, Microbiology and Immunobiology, University of Vienna, Austria

⁶ Eppley Institute for Research in Cancer and Allied Diseases, University of Nebraska Medical Center, Omaha, Nebraska

⁷ Institute of Animal Breeding and Genetics and Biomodels Austria, University of Veterinary Medicine, Vienna, Austria

⁸ Ludwig Boltzmann Institute for Cancer Research, Vienna, Austria

⁹ Institute of Pharmacology, Medical University of Vienna, Austria

Correspondence to: Veronika Sexl, email: veronika.sexl@vetmeduni.ac.at

Keywords: Stat1, MIN, IRF1, mammary cancer, tumorsurveillance

Received: December 1, 2011,

Accepted: December 2, 2011,

Published: December 19, 2011

Copyright: © Schneckenleithner et al. This is an open-access article distributed under the terms of the Creative Commons Attribution License, which permits unrestricted use, distribution, and reproduction in any medium, provided the original author and source are credited.

ABSTRACT:

Multiparous *Stat1*^{-/-} mice spontaneously develop mammary tumors with increased incidence: at an average age of 12 months, 55% of the animals suffer from mammary cancer, although the histopathology is heterogeneous. We consistently observed mosaic expression or down-regulation of STAT1 protein in wild-type mammary cancer evolving in the control group. Transplantation experiments show that tumorigenesis in *Stat1*^{-/-} mice is partially influenced by impaired CTL mediated tumor surveillance. Additionally, STAT1 exerts an intrinsic tumor suppressing role by controlling and blocking proliferation of the mammary epithelium. Loss of STAT1 in epithelial cells enhances cell growth in both transformed and primary cells. The increased proliferative capacity leads to the loss of structured acini formation in 3D-cultures. Analogous effects were observed when *Irf1*^{-/-} epithelial cells were used. Accordingly, the rate of mammary intraepithelial neoplasias (MINs) is increased in *Stat1*^{-/-} animals: MINs represent the first step towards mammary tumors. The experiments characterize STAT1/IRF1 as a key growth inhibitory and tumor suppressive signaling pathway that prevents mammary cancer formation by maintaining growth control. Furthermore, they define the loss of STAT1 as a predisposing event via enhanced MIN formation.

INTRODUCTION

The signal transducers and activators of transcription (STATs) are an intensely studied family of transcription factors that have been recognized as critical mediators of cytokine and growth factor receptor signaling, required for cell proliferation, survival and differentiation [1, 2].

Activation of STATs is frequently observed in different cancer entities and it has been postulated that deregulation of these factors may be involved in tumorigenesis. STAT1 is constitutively expressed throughout the entire development of the mammary gland. Its phosphorylation pattern – elevated in virgin glands, low throughout gestation and lactation, rising again at late involution –

is unique, although the exact function of phosphorylation is unclear [3]. STAT1 is expressed in the epithelial compartment of the mammary gland, suggesting it has an active role in epithelial cells [4]. STAT1 is of particular interest in mammary cancer as it is known to possess an independent prognostic significance in human breast cancer: high activation of STAT1 has been reported to correlate with an overall longer and relapse-free survival [5, 6]. Furthermore, treatment of human mammary tumor cells with cytostatic drugs has been shown to induce STAT1 activation, resulting in enhanced apoptosis [7, 8]. Recent work in mouse models of neu/ERBB2-induced breast cancer has underlined STAT1's tumor suppressive role [9, 10]. By crossing *Stat1^{fl/fl}* mice with *MMTV-neu-ires-cre* mice, Klover *et al.* showed that tumor onset is significantly accelerated in *Stat1^{fl/fl} x MMTV-neu-ires-cre* mice compared to STAT1-expressing wild-type controls. This conclusion suggests that STAT1 has an autonomous role in neu/ERBB2-induced mammary tumor formation. The second report did not discriminate between the intrinsic and the immunological contribution of STAT1-deficiency but came nevertheless to the conclusion that *Stat1^{-/-} x ERBB2/neu* mice develop mammary tumors significantly faster than control mice. Together, the studies unequivocally defined STAT1 as a tumor suppressor in mammary cancer.

STAT1's tumor suppressing properties may be related to cell-intrinsic effects as STAT1 has been shown to block proliferation and to be involved in the induction of apoptosis [11-15]. Furthermore, *Stat1^{-/-}* mice have a severely compromised immune system due to their lack of IFN-signaling [16, 17] as well as to an impaired cytotoxic NK-cell and CTL capacity [18, 19]. The contributions of these different components to mammary tumor surveillance are to date poorly understood. Moreover, all previous studies have been based on oncogene-driven mammary tumor formation in the absence of STAT1.

We now report for the first time that loss of STAT1 alone is sufficient to cause pregnancy-associated mammary cancer in BALB/c mice, independent of any other transgenic oncogene. By transplanting *Stat1^{-/-}* mammary glands into wild type recipient mice and vice versa we reveal that STAT1 contributes to the formation of mammary tumors through cell-intrinsic as well as immunological activities. *Stat1^{-/-}* mammary epithelial cells exhibit enhanced proliferation, which might facilitate the development of mammary intraepithelial neoplasias (MINs) and subsequently also invasive mammary tumors. We suggest that STAT1/IRF1 acts in a linear axis to block growth. It is known that cytotoxic T-cells are impaired in *Stat1^{-/-}* mice and we also characterize cytotoxic T-cells as major mediators of mammary tumor surveillance.

RESULTS

STAT1 deficiency is sufficient to cause mammary cancer

BALB/c mice are predisposed to develop mammary tumors and are therefore suitable to study spontaneous mammary tumorigenesis [11]. To evaluate the role of STAT1 in the spontaneous development of mammary tumors we crossed *Stat1^{-/-}* mice into the BALB/c genetic background. Groups of wild-type BALB/c and *Stat1^{-/-}* female mice were kept under breeding conditions and regularly controlled by palpation for mammary tumor formation. Within an average of one year, 55% of the multiparous *Stat1^{-/-}* mice had developed mammary tumors. In the control group, only 10% had mammary tumors and disease onset was significantly later (*Stat1^{-/-}*: 394.5 days \pm 13.52 and *Stat1^{+/+}*: 479.3 days \pm 11.46; $^{**}P = 0.0089$; values represent mean \pm SEM) (Fig. 1A and 1B). No mammary tumors were detected in wild-type or *Stat1^{-/-}* nulliparous animals over a period of 20 months. Interestingly, all tumors that evolved in wild-type mice showed a mosaic expression and partial down-regulation of STAT1 protein (Fig. 1C). Loss or down-regulation of STAT1 was restricted to tumor cells and was not observed in the normal mammary tissue surrounding the cancer.

Mammary epithelial transplantation uncovers a mammary gland cell-intrinsic and an immunological contribution of STAT1 to the development of mammary tumors

To test whether these results stemmed from an intrinsic action of STAT1 within the mammary epithelium rather than simply being related to tumor-promoting changes triggered by the impaired immune system of the *Stat1^{-/-}* animals, we transplanted *Stat1^{-/-}* mammary epithelial tissue into the cleared fat pad of the 4th mammary gland of *Stat1^{+/+}* mice, and vice versa (see scheme in Fig. 1D). To control for tumor onset provoked by the transplantation procedure itself, we additionally transplanted *Stat1^{+/+}* mammary tissue into *Stat1^{+/+}* mice. Moreover, a group of *Stat1^{-/-}* mice was maintained under identical conditions in a non-transplanted setting. All animals were bred constantly to accelerate mammary tumor development. Animals were sacrificed when any evolving mammary tumor reached a diameter of one centimeter or earlier if there were signs of disease such as weight loss, scrubby fur or reduced mobility. All transplanted mammary glands – irrespective of whether a visible tumor had evolved – were subjected to histological analysis to assess the

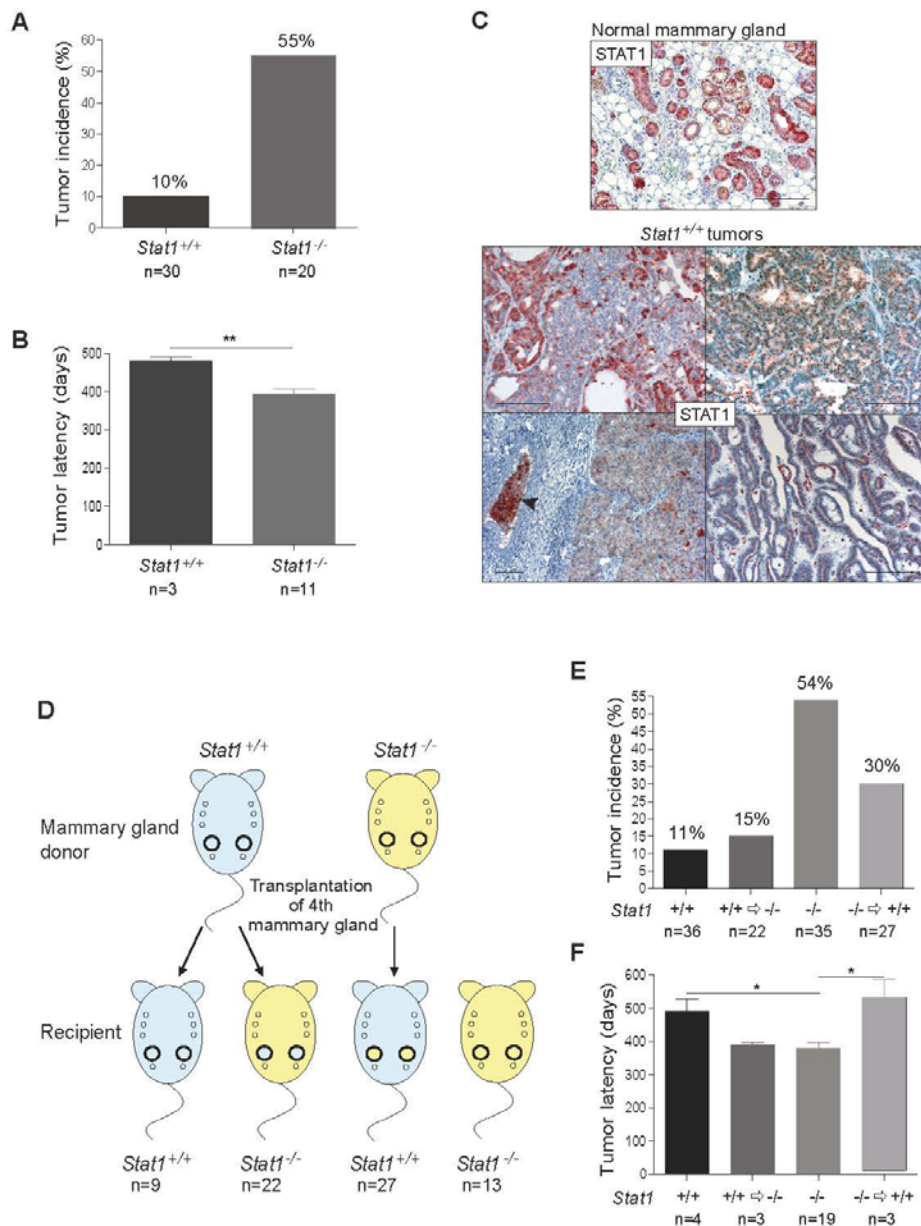


Figure 1: (A-C) Loss of STAT1 increases incidence and decreases latency of mammary tumors. (A) Incidence and (B) latency of spontaneously occurring, parity-induced mammary tumors in *Stat1*^{+/+} (n=30) and *Stat1*^{-/-} (n=20) mice. Tumor development was monitored for up to 20 months. (C) STAT1-stained histological sections of a normal mammary gland from a multiparous wild type mouse after involution (upper panel) and of *Stat1*^{+/+} mammary tumors (bottom panel). *Stat1*^{+/+} tumors display mosaic expression and partial downregulation of STAT1 protein. The arrow indicates a vascular invasion. Scale bars: 100 μ m. **(D-F) Absence of STAT1 in the immune system and also in the mammary gland tissue influences mammary tumor formation.** (D) Experimental setup of mammary gland transplantation experiment. Mammary gland tissue of *Stat1*^{-/-} mice was transplanted into the cleared fat pad of the 4th mammary gland of *Stat1*^{+/+} mice (n=27), or *Stat1*^{+/+} mammary glands were transplanted into *Stat1*^{-/-} animals (n=22). Control groups: *Stat1*^{+/+} tissue transplanted into *Stat1*^{+/+} animals (n=9), non-transplanted *Stat1*^{-/-} animals (n=13). Mice were bred constantly and checked for mammary tumor growth for up to 20 months. On average, each animal had 7 litters. (E) Incidence and (F) latency of spontaneously occurring, parity-induced mammary tumors in all mice in the transplantation experiment. Tumors were classified into four groups: *Stat1*^{+/+} tumors in *Stat1*^{+/+} mice, *Stat1*^{+/+} tumors in *Stat1*^{-/-} mice, *Stat1*^{-/-} tumors in *Stat1*^{-/-} mice and *Stat1*^{-/-} tumors in *Stat1*^{+/+} mice.

success of the transplantation procedure and to study spontaneous tumorigenesis.

Immunohistochemical staining for STAT1 revealed a successful outgrowth in 36% of *Stat1*^{-/-} donor tissue in *Stat1*^{+/+} recipient mice upon transplantation, whereas in the *Stat1*^{+/+} => *Stat1*^{+/+} setting the take rate reached 90% (Fig. S1A and S1B). FACS analysis did not show any significant differences in mammary stem cell populations between wild type and *Stat1*^{-/-} animals, eliminating the possibility that this cell compartment contributed to the repopulation frequency (Fig. S2A). The analysis of freshly transplanted mammary glands uncovered a dense infiltration with CD3⁺ T-lymphoid cells and NKp46⁺ NK-cells, irrespective of the genotype (Fig. S2B). Although we used syngenic mice in the experiment – all animals were back-crossed to BALB/c – an inflammatory infiltrate is unavoidable due to tissue damage during the transplantation procedure. We assumed that *Stat1*^{-/-} mice accepted the transplanted tissue better due to their partially impaired immune system.

Spontaneous tumor development was monitored over a period of 20 months in our cohort of transplanted animals. STAT1 expression was surveyed by immunohistochemical staining and PCR-analysis. Non-transplanted mammary glands were analyzed for tumor development and served as an internal control. The observed tumor incidence and latency are summarized in Figs 1E and 1F. Spontaneous tumors developed within 20 months from non-transplanted tissue in 19/35 (54%) of the *Stat1*^{-/-} mice and in 4/36 (11%) of the *Stat1*^{+/+} mice. During this time, 3/22 (14%) of the *Stat1*^{-/-} animals displayed tumors that originated from the transplanted *Stat1*^{+/+} mammary glands. Even when adjusted for the success rate of transplantation (90%), the tumor incidence did not exceed 15% in this group. In the reverse experiment, 3/27 *Stat1*^{-/-} tumors evolved in *Stat1*^{+/+} mice, translating into a 30% tumor incidence after adjustment for the significantly lower transplantation success rate.

In summary, our observations enable us to conclude that STAT1 suppresses tumor formation in the mammary epithelial cells themselves. Tumor incidence increases upon transplantation of *Stat1*^{-/-} mammary glands into *Stat1*^{+/+} recipients compared to a *Stat1*^{+/+} => *Stat1*^{+/+} scenario (30% versus 11%). We also deduce that the STAT1-deficient immune system contributes to and accelerates carcinogenesis. *Stat1*^{+/+} as well as *Stat1*^{-/-} mammary tumors occurred with an increased incidence in a *Stat1*^{-/-} environment compared to in *Stat1*^{+/+} surroundings (15% versus 11% for *Stat1*^{+/+} tumors; 54% versus 30% for *Stat1*^{-/-} tumors). Consistently, tumor development occurred with a significantly shorter latency in a *Stat1*^{-/-} environment, irrespective of whether spontaneous tumor development or carcinomas evolving after transplantation are compared (Fig. 1F).

Loss of STAT1 favors mammary intraepithelial neoplasias (MINs)

An overview of the histopathological and immunohistochemical features of the tumors that arose in our animal cohort is provided in Table I. Fig. 2A depicts representative panels of the immunohistochemical characterization of two *Stat1*^{+/+} and two *Stat1*^{-/-} tumors. The tumors were characterized either as neoplasias *in situ* (mammary intraepithelial neoplasia, MIN) or as invasive ductal carcinomas. No lobular carcinomas were diagnosed. Grading was performed according to Elston and Ellis [20]. Invasive features were present in 62% of all *Stat1*^{-/-} and in 80% of all *Stat1*^{+/+} tumors. We did not detect any genotype-related pattern with regard to grading of tubule formation, nuclear polymorphism or mitotic count. However, we found a high incidence of MIN (8/13) in *Stat1*^{-/-} tumors: 4 of low grade and 4 of high grade (Table I). In contrast, 2/5 *Stat1*^{+/+} tumors displayed only low-grade MINs and no high-grade MIN could be detected. Importantly, the two cases of MIN detected in *Stat1*^{+/+} mice had largely lost STAT1 protein expression (Fig. 2B). These observations revealed an increased incidence of MIN upon loss of STAT1.

The STAT1/IRF1 axis is implicated as having an important role in MIN formation, regulating the proliferation of mammary epithelial cells

Loss of the STAT1 downstream transcription factor IRF1 has been reported in MIN cases of human breast cancer [21]. Moreover, the loss of heterozygosity at the IRF1 gene locus has been found to be a frequent event in human breast cancer [22]. It thus seems possible that STAT1 and IRF1 act in a common axis to suppress MIN and subsequently mammary tumor formation [23, 24]. Initial evidence for this hypothesis was provided by the analysis of STAT1 and IRF1 protein expression in primary mouse mammary tumor tissue: the levels of IRF1 protein correlated with the expression levels of STAT1. Furthermore, IRF1 expression in *Stat1*^{-/-} tumors was shown to be low (Fig. 3A). To evaluate whether both *Stat1*^{-/-} and *Irf1*^{-/-} mice are predisposed to develop mammary tumors, whole mounts of mammary glands were analyzed. It was noteworthy that already at the virgin state *Stat1*^{-/-} and *Irf1*^{-/-} mice displayed an increased amount of ductal structure compared to wild-type controls (Fig. 3B and S3), although MIN could not be detected at that age in these *Stat1*^{-/-} and *Irf1*^{-/-} mice.

To investigate the role of STAT1 and IRF1 in MIN formation, we employed an *in vitro* three-dimensional culture system, which allowed us to monitor the formation of polarized acini from single mammary epithelial cells [25]. Mammary epithelial cells were prepared from glands of 6- to 8- week-old virgin wild-type, *Stat1*^{-/-}

and *Irf1*^{-/-} mice and analyzed in this 3D culture system. Acini developed irrespective of the genotype and with no significant difference in total volumes of the spheres (Fig. S4). Remarkably, *Stat1*^{-/-} and *Irf1*^{-/-} acini displayed a significantly higher cellularity at all time points compared to wild-type controls (Figs 3C, top panel and 3D). Whereas mammospheres of wild-type controls were formed by a single monolayer, immunofluorescent staining showed a less organized cell array and partial epithelial bi-layering in *Stat1*^{-/-} and *Irf1*^{-/-} spheres (Fig. 3C, bottom panel and Videos S1A, B and C). The increased cellularity could not be attributed to decreased apoptosis as there were no detectable signs of cleaved caspase-3 activity, even

at early time points (day 2) when the lumen of the acini starts to evolve (Fig. S5). This finding is in line with the observations made by Jechlinger [25], who described that lumina form without epithelial cells undergoing apoptosis. The polarity of the *Stat1*^{-/-} and *Irf1*^{-/-} acini was unaltered as staining for the basal marker Integrin $\alpha 6$ did not reveal any major changes. Furthermore, we failed to detect any changes in the formation of tight junctions by staining for Zona Occludens-1 (ZO1), a protein that binds directly to occludins and is a bona fide marker for tight junctions (Fig. 3C, bottom panel). However, examining BrdU incorporation revealed a significantly increased proliferation rate in *Stat1*^{-/-} and *Irf1*^{-/-} spheres

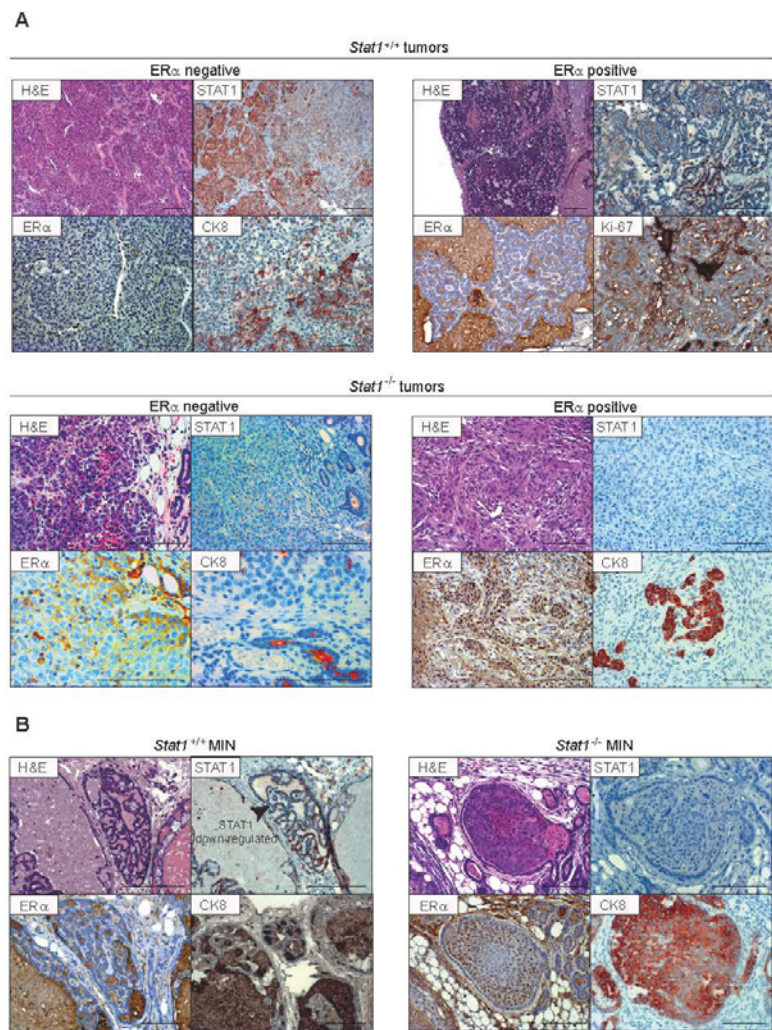


Figure 2: (A) Both, *Stat1*^{+/+} and *Stat1*^{-/-} mammary tumors are heterogeneous. Representative pictures of immunohistochemical characterization of two *Stat1*^{+/+} (top panel) and two *Stat1*^{-/-} mammary tumors (bottom panel). Scale bars: 100 μ m. **(B) Loss of STAT1 correlates with MIN formation.** Representative pictures of immunohistochemical characterization of one low-grade *Stat1*^{+/+} (left panel) and one high-grade *Stat1*^{-/-} MIN (right panel). *Stat1*^{+/+} MINs display down-regulation of STAT1 protein, as indicated by the arrow. Scale bars: 100 μ m; ER α : estrogen receptor alpha; CK8: cytokeratin 8.

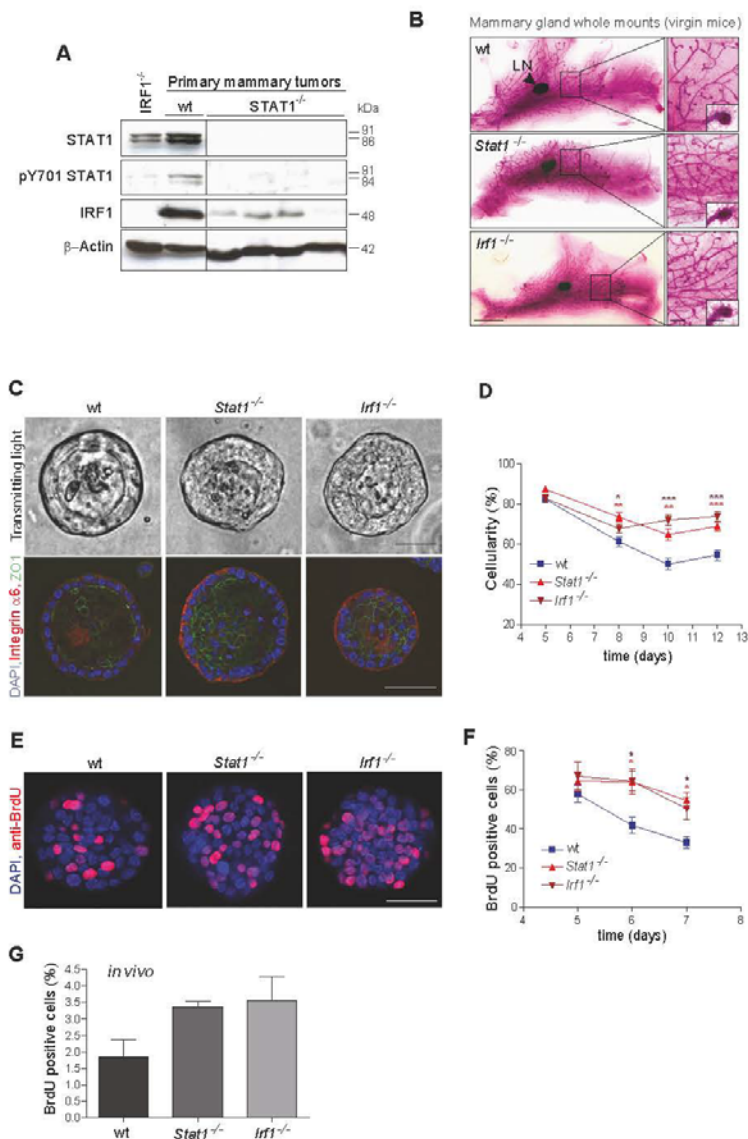


Figure 3: (A, B) Loss of STAT1 might cause mammary tumor formation by down-regulating IRF1. (A) Western blotting of mammary tumor samples. Low expression of IRF1 protein correlates with STAT1 expression. (B) Representative pictures of whole mounts of mammary glands from 50 day-old virgin wild-type (wt), *Stat1*^{-/-} and *Irf1*^{-/-} mice. *Stat1*^{-/-} and *Irf1*^{-/-} glands show an increased density of ductal structures but no differences in end duct formation. Scale bars: 0.5 cm, 500 μm, 100 μm. LN: lymph node. **(C-F) Mammary epithelial cells of *Stat1*^{-/-} and *Irf1*^{-/-} mice show enhanced proliferation.** (C+D) In a 3D culture assay, primary mammary epithelial cells derived from *Stat1*^{-/-} and *Irf1*^{-/-} mice formed spheres with increased cellularity compared to wild-type controls. (C) Representative bright-field microscopy pictures (top panel) and fluorescence microscopy pictures (bottom panel) from 8 day-old spheres of different genotypes. (Blue) DAPI; (red) Integrin α6; (green) ZO1. Scale bars: 50 μm. (D) Cellularity of spheres was measured at different time points. For details of calculations see SI Materials and Methods. n ≥ 33 per genotype. (E+F) To measure proliferation, spheres were exposed to BrdU for 24h, before fixation. (E) Representative fluorescence microscopy pictures of 6 day-old spheres derived from wt, *Stat1*^{-/-} and *Irf1*^{-/-} epithelial cells. (Blue) DAPI; (red) anti-BrdU. Scale bars: 50 μm. (F) Percentage of BrdU-positive cells was calculated at different times of growth. n ≥ 18; 1 n = 1 sphere. (D+F) Statistical analysis: asterisks represent significances to the wild type. No significant differences could be detected between any *Stat1*^{-/-}/*Irf1*^{-/-} pair. Data are representative of three independent experiments. (G) To measure proliferation *in vivo*, BrdU was injected intraperitoneally into mice. Mammary gland cells were isolated and percentages of BrdU-positive mammary gland cells after 3 days of BrdU administration were measured using the BD FACS-Canto II FACS device with the BD FACS Diva software (Beckton Dickinson). n = 3 per genotype.

compared to wild type controls *in vitro* (Fig. 3E and 3F). This was confirmed by analysis of mammary epithelial proliferation *in vivo*. For this purpose, BrdU was injected intraperitoneally into mice for a period of 3 days. Isolated mammary glands were digested and cells in single-cell suspensions were stained with anti-BrdU antibody. Quantification of BrdU-positive cells by flow cytometry confirmed the enhanced proliferation of *Stat1^{-/-}* and *Ifi1^{-/-}* mammary epithelial cells (Fig. 3G).

Mammary tumor formation is under the control of cytotoxic T-lymphocytes (CTLs)

Our transplantation studies revealed that the absence of STAT1 from the immune system significantly enhances

tumor incidence and shortens the latency of mammary tumor formation. STAT1 is believed to have an essential role in CTL- and NK-cell cytotoxicity; both lymphoid lineages are important mediators of tumor surveillance. Immunohistochemical staining for CD3 and NKp46 verified a dense infiltration of all mammary tumors with cytotoxic T-cells, whereas in all tumors NK-cells were rare and not consistently detectable (Fig. 4A). To clarify the contribution of NK and/or cytotoxic T cells to tumor surveillance, we generated mammary tumor cell lines. Four cell lines (#1, #2: *Stat1^{-/-}*; #3, #4: *Stat1^{+/+}*) were established during the course of our study, all of which displayed an epithelial-like phenotype (Fig. 4B). Of note, cell lines lacking STAT1 had a proliferative advantage *in vitro* and *in vivo* over *Stat1^{+/+}* lines (Fig. 4C and S6A-C). 5x10⁵ cells were orthotopically injected into the mammary

Table I: Histopathological and immunohistochemical analysis and classification of mammary tumors. Histological sections of all available mammary tumors were analyzed and mouse mammary tumors characterized according to a standard nomenclature used to classify human breast carcinomas. Invasive carcinomas were graded according to Elson and Ellis [20]. 1: well-differentiated breast cells, cells generally appear normal and do not grow rapidly, cancer arranged in small tubules; 2: moderately-differentiated breast cells, have characteristics between Grade 1 and Grade 3 tumors; 3: poorly differentiated breast cells, cells do not appear normal and tend to grow and spread more aggressively. Tubule formation (% of carcinoma composed of tubular structures) – 1: > 75%; 2: 10-75%; 3: less than 10%. Nuclear pleomorphism – 1: small, uniform cells; 2: moderate increase in size and variation; 3: marked variation. Mitosis count – 1: up to 7; 2: 8 to 14; 3: 15 or more. Mammary intraepithelial neoplasia (MIN) – -: not detected; low grade; moderate grade; high grade. Estrogen receptor alpha (ERα) – Reiner score [36], i.e. 0-2: negative; 3: low positive; 4-5: moderate positive; 6-7: strong positive. Human epidermal growth factor receptor 2 (HER2) – 0-1: negative; 2: low positive; 3: strong positive.

| Number | Genotype Tumor | Genotype Mouse | Histological Classification | Invasiveness | | | | MIN | ERα | HER2 |
|--------|----------------------------|----------------------------|----------------------------------|------------------|----------------------|---------------|---------|------------|----------|------|
| | | | | Tubule formation | Nuclear pleomorphism | Mitosis count | Grading | | | |
| 1 | <i>Stat1^{-/-}</i> | <i>Stat1^{-/-}</i> | ductal/with medullary features | 3 | 3 | 3 | 3 | - | 0 | 0 |
| 2 | <i>Stat1^{-/-}</i> | <i>Stat1^{-/-}</i> | ductal | 2 | 2 | 1 | 1 | - | 0 | 0 |
| 3 | <i>Stat1^{-/-}</i> | <i>Stat1^{-/-}</i> | ductal | 3 | 3 | 3 | 3 | - | 0 | 0 |
| 4 | <i>Stat1^{-/-}</i> | <i>Stat1^{-/-}</i> | ductal | 2 | 3 | 3 | 3 | high grade | 4(60%/2) | 1 |
| 5 | <i>Stat1^{-/-}</i> | <i>Stat1^{-/-}</i> | ductal | 3 | 3 | 3 | 3 | high grade | 3(30%/1) | 0 |
| 6 | <i>Stat1^{-/-}</i> | <i>Stat1^{-/-}</i> | ductal/with metaplastic features | 3 | 3 | 2 | 3 | high grade | 3(20%/1) | 0 |
| 7 | <i>Stat1^{-/-}</i> | <i>Stat1^{-/-}</i> | intraductal with microinvasion | | | | | low grade | 0 | 1-2 |
| 8 | <i>Stat1^{-/-}</i> | <i>Stat1^{-/-}</i> | intraductal-papillary | | | | | low grade | 3(10%/1) | 0 |
| 9 | <i>Stat1^{-/-}</i> | <i>Stat1^{-/-}</i> | intraductal with microinvasion | | | | | low grade | 3(50%/1) | 0 |
| 10 | <i>Stat1^{-/-}</i> | <i>Stat1^{-/-}</i> | Intraductal-papillary | | | | | low grade | 0 | 0 |
| 11 | <i>Stat1^{-/-}</i> | <i>Stat1^{+/+}</i> | ductal | 2 | 2 | 1 | 1 | - | 0 | 1 |
| 12 | <i>Stat1^{-/-}</i> | <i>Stat1^{+/+}</i> | ductal | 3 | 3 | 2 | 3 | - | 4(60%/2) | 0 |
| 13 | <i>Stat1^{-/-}</i> | <i>Stat1^{+/+}</i> | intraductal | | | | | high grade | 4(60%/2) | 1 |
| 14 | <i>Stat1^{+/+}</i> | <i>Stat1^{-/-}</i> | ductal/with metaplastic features | 3 | 3 | 2 | 3 | - | 0(<10%) | 0 |
| 15 | <i>Stat1^{+/+}</i> | <i>Stat1^{+/+}</i> | ductal | 1 | 1 | 1 | 1 | - | 5(50%/3) | 2 |
| 16 | <i>Stat1^{+/+}</i> | <i>Stat1^{+/+}</i> | ductal | 2 | 2 | 3 | 2 | - | 0 | 1 |
| 17 | <i>Stat1^{+/+}</i> | <i>Stat1^{+/+}</i> | ductal | 1 | 1 | 1 | 1 | low grade | 0(<10%) | 0 |
| 18 | <i>Stat1^{+/+}</i> | <i>Stat1^{+/+}</i> | intraductal with microinvasion | | | | | low grade | 0 | n.a. |

glands of wild type, *Stat1*^{-/-}, *Rag2*^{-/-} or *Stat1*^{-/-}*Rag2*^{-/-} mice. As *Rag2*^{-/-} animals lack T cells and rely on NK cells for tumor surveillance, this experiment allowed us to determine the individual contribution of T and NK cells to tumor surveillance. The experiment was terminated and tumor weights determined when the first tumors reached approximately 1 cm in diameter. The *Stat1*^{-/-} cell line #2 failed to induce tumors in wild-type mice and tumor formation was restricted to immuno-compromised animals. This observation is consistent with previous findings that tumors evolving in immunodeficient hosts (such as *Stat1*^{-/-}) are more immunogenic and not immuno-edited and may be rejected in immuno-competent surroundings [26].

Fig. 4D summarizes the data from orthotopic tumor injections. We found a consistently and significantly enhanced tumor growth in *Stat1*^{-/-} mice compared to

wild-type controls, irrespective of the cell line injected. Compared to *Rag2*^{-/-} animals, tumor growth in *Stat1*^{-/-} or *Stat1*^{-/-}*Rag2*^{-/-} hosts was not significantly accelerated, indicating that the NK-cell compartment played at most a minor part in restricting proliferation of the transplanted tumor cells. Support for this conclusion came from a comparison of wild-type recipients with *Rag2*^{-/-} mice. Although *Rag2*^{-/-} mice contain functionally competent NK-cells, tumor growth in these mice was significantly increased, indicating that the NK cell compartment was not capable of significantly limiting tumor expansion. In summary, the data indicate a dominant role for cytotoxic T cells in tumor surveillance in spontaneously occurring, parity-induced mammary tumors.

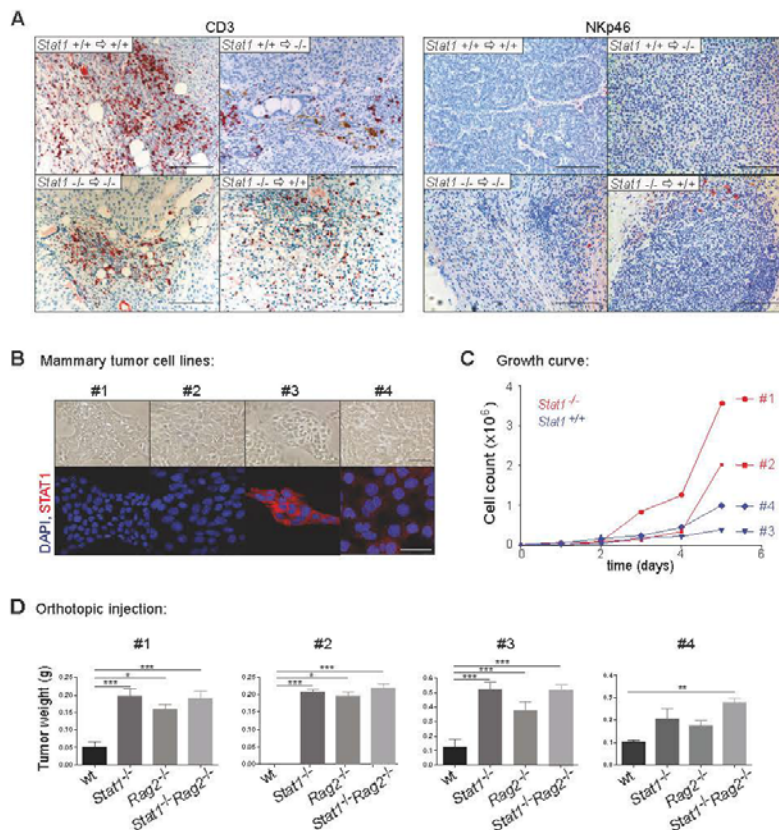


Figure 4: Mammary tumor growth is mainly controlled by cytotoxic T-cells and only to a minor extent by NK-cells. (A) Histological sections of spontaneously occurring mammary tumors of the transplant experiment were stained with CD3 and NKp46 antibodies. Tumors are listed in four groups: *Stat1*^{+/+} tumors in *Stat1*^{+/+} mice, *Stat1*^{+/+} tumors in *Stat1*^{-/-} mice, *Stat1*^{-/-} tumors in *Stat1*^{-/-} mice and *Stat1*^{-/-} tumors in *Stat1*^{+/+} mice. Scale bars: 100 μ m. (B) Bright-field (top panel) and fluorescence (bottom panel) microscopy pictures of tumor cell lines derived from two *Stat1*^{-/-} (#1, #2) and two *Stat1*^{+/+} (#3, #4) spontaneous mammary tumors. (Blue) DAPI; (red) STAT1. Scale bars: 50 μ m. (C) Growth curve of mammary tumor cell lines. (D) Mammary tumor cell lines were orthotopically injected into wt, *Stat1*^{-/-}, *Rag2*^{-/-} and *Stat1*^{-/-}*Rag2*^{-/-} animals. Tumor weights of different groups were compared. n \geq 5 per genotype. All data are representative of two independent experiments.

DISCUSSION

We show that the transcription factor STAT1 has a tumor-suppressing function against the formation of parity-induced, spontaneous mammary tumors. We show that STAT1 deficiency significantly increases tumor incidence in BALB/c mice as well as decreasing disease latency. STAT1 acts in a dual manner. It sustains proper CTL activity and thus ensures tumor surveillance, while also exerting growth inhibitory and tumor suppressing effects via its downstream regulator IRF1.

Our findings are in line with recent reports on the role of STAT1 in the context of ERBB2/neu/HER2 induced mammary cancer development [9, 10]. Using different mouse models, both groups concluded that STAT1 suppresses ERBB2/neu/HER2 tumor formation. In our cohort of mice we characterized tumors that evolved spontaneously in the absence of a driving oncogene. The fact that only 2/13 of the mammary cancers expressed ERBB2/neu/HER2 indicates that STAT1's tumor-suppressing effect is not limited to ERBB2/neu/HER2-induced tumorigenesis. The effect of STAT1 loss is also not restricted to tumors that display a particular pattern of expression of the estrogen receptor (ER): 7/13 of the spontaneously evolving *Stat1*^{-/-} mammary cancers were ER⁺, while the remaining cases did not express detectable levels of the ER protein. These findings show conclusively that STAT1 is a global tumor suppressor that acts independently of a distinct oncogenic driver.

The importance of STAT1 as a tumor suppressor was underlined by the finding that all *Stat1*^{+/+} mammary cancers had partially lost or down-regulated STAT1 protein expression. Similar observations were reported in human patients, where low levels of STAT1 activation have been linked to a poor prognosis [5, 27]. The selection pressure to down-regulate or lose STAT1 in tumor cells may have more than one cause as the loss of STAT1 has several important consequences: the tumor cells lose responsiveness towards interferon-mediated growth inhibition (interferons are important players in tumor surveillance). Moreover, STAT1 is the key regulator of MHC class I expression. By losing STAT1 the cells may down-regulate MHCI and thus escape CTL-mediated tumor surveillance [28, 29]. As NK cells play a negligible part in tumor surveillance, MHCI loss represents a clear-cut advantage. CTLs dominated the immune infiltrate in the tumor sections and their importance was further verified in transplant studies. In the absence of the adaptive immune system, tumor development occurred rapidly and was significantly accelerated, whereas the presence of NK cells did not interfere with tumor onset. Hence, mammary tumors are partially able to escape immune control by down-regulating STAT1. In *Stat1*^{-/-} animals, the selective pressure to escape immune control is less important as the mice have several defects that limit their capability to exert effective tumor surveillance. As a

consequence, mammary cancer formation is increased in a *Stat1*^{-/-} micro-environment, irrespective of whether the epithelial cells themselves express STAT1. The finding underlines the role of the immune system in spontaneously evolving mammary cancer. Although a pro-inflammatory environment and T-cell infiltration may exert a tumor promoting effect, our orthotopic injection experiments unequivocally show that there is a tumor suppressing function that opposes the tumor promoting effect of the immune infiltrate.

Loss or down-regulation of STAT1 confers an additional advantage, i.e. accelerated cell proliferation. Under normal conditions, STAT1 puts the brakes on cell proliferation in mammary epithelial cells, presumably via the transcription factor IRF1. Two lines of evidence support this assumption. First, whole mounts of *Stat1*^{-/-} as well as of *Irf1*^{-/-} mammary glands display increased amounts of ductal structures compared to wild type controls, even in the virgin state. Secondly, BrdU incorporation studies *in vitro* and *in vivo* confirm an increased DNA synthesis and thus enhanced growth in mammary epithelial cells of both *Stat1*^{-/-} and *Irf1*^{-/-} mice.

As a consequence of enhanced cell proliferation, MIN formation was frequently found in *Stat1*^{-/-} mice. This finding was also reflected in 3D-culture experiments, in which the cell composition of *Stat1*^{-/-} and *Irf1*^{-/-} acini was less organized. The original report describing the 3D system used the two oncogenes *MYC* and *Kras*^{G12D} to characterize the occurrence of highly proliferative depolarized spheres resembling MIN. As expected, the alterations observed in *Stat1*^{-/-} and *Irf1*^{-/-}-derived spheres are less pronounced than those occurring in the presence of *MYC* and *Kras*^{G12D}. In the absence of STAT1 and IRF1, polarity of the spheres is preserved and a lumen – albeit smaller – is maintained in most cases. Therefore, additional alterations are required to allow mammary tumor formation. These additional alterations are most probably triggered by hormonal stimulation and changes occurring during lactation in the breast tissue, as we failed to detect spontaneous tumorigenesis in nulliparous mice. Our conclusion that STAT1/IRF1 act in a linear axis to block growth is in perfect accordance with reports by others that attribute a negative regulatory role of IRF1 on cell growth: enforced expression of IRF1 in mammalian cell lines slows or even halts proliferation [30-32].

Cancer formation is a multi-level process during which a cell successively acquires several genetic or epigenetic alterations that ultimately cooperate to allow the development of a malignant tumor. One of the alterations required to initiate the process is loss of growth control. Our findings support a model in which STAT1 represents a critical safeguard that preserves growth control in mammary epithelial cells. The absence of STAT1 facilitates cell proliferation and therefore MIN

formation, which represents the first step on the road from normal breast tissue towards invasive breast cancer [33].

The exact characterization of the early alterations has a significant potential for use in preventative therapy of invasive breast cancer and might lead to the development of novel immune-modulatory strategies to combat the disease. The critical effect of STAT1 is not restricted to any distinct tumor type but is of global relevance.

MATERIAL AND METHODS

Mice

All animals were maintained in spf quality at the University of Veterinary Medicine, Vienna. C.Cg-Stat1^{tm1} (*Stat1*^{-/-}) [16], C.Cg-Irf1^{tm1Mak} (*Irf1*^{-/-}) [34] and C.129S6-Rag2^{tm1Fwa} (*Rag2*^{-/-}) [35] mice have been described previously. C.Cg-Stat1^{tm1}-Rag2^{tm1Fwa} (*Stat1*^{-/-}*Rag2*^{-/-}) mice were crossed at the University of Veterinary Medicine, Vienna. Animal experiments were discussed and approved by the institutional ethics committee and undertaken in conformance with Austrian laws.

Orthotopic injection of mammary tumor cell lines

Mammary tumor cell lines #1-#4 were derived from spontaneous mammary tumors. For orthotopic injection of mammary tumor cell lines, mice were anaesthetized and depilated on the belly. 5x10⁶ cells were injected via the nipple into the fat pad of the 4th and 5th mammary gland of wild type, *Stat1*^{-/-}, *Rag2*^{-/-} and *Stat1*^{-/-}*Rag2*^{-/-} mice. The mice were sacrificed when the tumors reached one centimeter in diameter.

Histology and immunohistochemistry

The following antibodies were used for immunostaining in accordance with to the manufacturers' protocol: STAT1 (Santa Cruz, #sc-592), CD3 (Neomarkers, RM9107), NKp46 (BioLegend, #137601), ER α (Santa Cruz, #sc-542), CK8 (Developmental Studies Hybridoma Bank, TROMA-I) and Ki67 (Novocastra, NCL-Ki67). Nuclear counterstaining was performed with hematoxylin. Pictures were taken on a Zeiss AxioImager Z1 microscope system with a CCD camera using the software PixelNK Capture 3.0.

Immunofluorescence

For immunofluorescent staining, cells or 3D cultures were incubated with primary antibodies against STAT1 (Santa Cruz, #sc-592), integrin α 6 (Millipore, #MA1378) or ZO1 (Zymed Laboratories, #33-9100), followed by

incubation with Alexa546-conjugated or Alexa488-conjugated goat antibodies against rat or mouse IgG (Molecular Probes, #A11081 and #A11001). Incubation times were prolonged for 3D cultures to ensure complete staining. Cells were counterstained with DAPI and imaged using a confocal laser-scanning microscope (Carl Zeiss LSM 700, Occlulare 10x, 40x Oil) using the software ZEN 2009 LE.

Statistics

All statistical analysis was performed using GraphPad Prism 4. Differences were assessed for statistical significance by One-way ANOVA using the Tukey's Multiple Comparison Test. For Figure 1B only, the unpaired t-test was used. Error bars represent mean \pm SD. *P* values are considered as follows: <0.05: *; <0.01: **; <0.001: ***.

ACKNOWLEDGEMENTS

We thank M. Gröger for help and support with confocal microscopy and S. Fajmann and M. Schlederer for technical assistance with histo-pathology. We are indebted to S. Gratzl and the team of the Institute of Animal Breeding and Genetics and Biomodels Austria (BIAT) for taking excellent care of the mice. We are grateful to R. Moriggl, A. Jamieson, B. Strobl and all members of the SFB 28 for helpful discussions.

This work was supported by the Austrian Science Fund (FWF) by a grant to VS, TD and MM (SFB F28) and to DS (19534), the Austrian Federal Ministry of Science and Research by grant BM_WFa GZ200.112/1-VI/1/2004, GZ BMWF-200.191/1-II/1a/2008 to MM and the BM WFa program GEN-AU II and III project Austromouse to MM. K.-U. Wagner is supported by a Public Health Service Grant (CA117930) from the National Cancer Institute. HD is supported by the Herzfelder Family Foundation and Life Science Krems.

REFERENCES

1. Yu H, Pardoll D, Jove R. STATs in cancer inflammation and immunity: a leading role for STAT3. *Nature reviews*. 2009; 9:798-809.
2. Catlett-Falcone R, Dalton WS, Jove R. STAT proteins as novel targets for cancer therapy. *Signal transducer and activator of transcription*. *Current opinion in oncology*. 1999; 11:490-496.
3. Watson CJ, Neoh K. The Stat family of transcription factors have diverse roles in mammary gland development. *Semin Cell Dev Biol*. 2008; 19:401-406.
4. Philp JA, Burdon TG, Watson CJ. Differential activation of STATs 3 and 5 during mammary gland development.

- FEBS Lett. 1996; 396:77-80.
5. Widschwendter A, Tonko-Geymayer S, Welte T, Daxenbichler G, Marth C, Doppler W. Prognostic significance of signal transducer and activator of transcription 1 activation in breast cancer. *Clin Cancer Res.* 2002; 8:3065-3074.
 6. Yau C, Esserman L, Moore DH, Waldman F, Sninsky J, Benz CC. A multigene predictor of metastatic outcome in early stage hormone receptor-negative and triple-negative breast cancer. *Breast Cancer Res.* 2010; 12:R85.
 7. Thomas M, Finnegan CE, Rogers KM, Purcell JW, Trimble A, Johnston PG, Boland MP. STAT1: a modulator of chemotherapy-induced apoptosis. *Cancer Res.* 2004; 64:8357-8364.
 8. Yang PY, Chen MF, Kao YH, Hu DN, Chang FR, Wu YC. Norcantharidin induces apoptosis of breast cancer cells: Involvement of activities of mitogen activated protein kinases and signal transducers and activators of transcription. *Toxicol In Vitro.* 2011.
 9. Klover PJ, Muller WJ, Robinson GW, Pfeiffer RM, Yamaji D, Hennighausen L. Loss of STAT1 from mouse mammary epithelium results in an increased neu-induced tumor burden. *Neoplasia.* 2010; 12:899-905.
 10. Raven JF, Williams V, Wang S, Tremblay ML, Muller WJ, Durbin JE, Koromilas AE. Stat1 is a suppressor of ErbB2/ Neu-mediated cellular transformation and mouse mammary gland tumor formation. *Cell Cycle.* 2011; 10:794-804
 11. Koch JG, Gu X, Han Y, El-Naggar AK, Olson MV, Medina D, Jerry DJ, Blackburn AC, Peltz G, Amos CI, Lozano G. Mammary tumor modifiers in BALB/cJ mice heterozygous for p53. *Mamm Genome.* 2007; 18:300-309.
 12. Townsend PA, Scarabelli TM, Davidson SM, Knight RA, Latchman DS, Stephanou A. STAT-1 interacts with p53 to enhance DNA damage-induced apoptosis. *J Biol Chem.* 2004; 279:5811-5820.
 13. Lee CK, Smith E, Gimeno R, Gertner R, Levy DE. STAT1 affects lymphocyte survival and proliferation partially independent of its role downstream of IFN-gamma. *J Immunol.* 2000; 164:1286-1292.
 14. Stephanou A, Scarabelli TM, Brar BK, Nakanishi Y, Matsumura M, Knight RA, Latchman DS. Induction of apoptosis and Fas receptor/Fas ligand expression by ischemia/reperfusion in cardiac myocytes requires serine 727 of the STAT-1 transcription factor but not tyrosine 701. *J Biol Chem.* 2001; 276:28340-28347.
 15. Kim HS, Lee MS. STAT1 as a key modulator of cell death. *Cellular signalling.* 2007; 19:454-465.
 16. Durbin JE, Hackenmiller R, Simon MC, Levy DE. Targeted disruption of the mouse Stat1 gene results in compromised innate immunity to viral disease. *Cell.* 1996; 84:443-450.
 17. Meraz MA, White JM, Sheehan KC, Bach EA, Rodig SJ, Dighe AS, Kaplan DH, Riley JK, Greenlund AC, Campbell D, Carver-Moore K, DuBois RN, Clark R, Aguet M, Schreiber RD. Targeted disruption of the Stat1 gene in mice reveals unexpected physiologic specificity in the JAK-STAT signaling pathway. *Cell.* 1996; 84:431-442.
 18. Pilz A, Kratky W, Stockinger S, Simma O, Kalinke U, Lingnau K, von Gabain A, Stoiber D, Sexl V, Kolbe T, Rulicke T, Muller M, Decker T. Dendritic cells require STAT-1 phosphorylated at its transactivating domain for the induction of peptide-specific CTL. *J Immunol.* 2009; 183:2286-2293.
 19. Lee CK, Rao DT, Gertner R, Gimeno R, Frey AB, Levy DE. Distinct requirements for IFNs and STAT1 in NK cell function. *J Immunol.* 2000; 165:3571-3577.
 20. Elston CW, Ellis IO. Pathological prognostic factors in breast cancer. I. The value of histological grade in breast cancer: experience from a large study with long-term follow-up. *Histopathology.* 1991; 19:403-410.
 21. Doherty GM, Boucher L, Sorenson K, Lowney J. Interferon regulatory factor expression in human breast cancer. *Ann Surg.* 2001; 233:623-629.
 22. Cavalli LR, Riggins RB, Wang A, Clarke R, Haddad BR. Frequent loss of heterozygosity at the interferon regulatory factor-1 gene locus in breast cancer. *Breast Cancer Res Treat.* 2009; 121:227-231.
 23. Kim PK, Armstrong M, Liu Y, Yan P, Bucher B, Zuckerbraun BS, Gambotto A, Billiar TR, Yim JH. IRF-1 expression induces apoptosis and inhibits tumor growth in mouse mammary cancer cells in vitro and in vivo. *Oncogene.* 2004; 23:1125-1135.
 24. Bouker KB, Skaar TC, Riggins RB, Harburger DS, Fernandez DR, Zwart A, Wang A, Clarke R. Interferon regulatory factor-1 (IRF-1) exhibits tumor suppressor activities in breast cancer associated with caspase activation and induction of apoptosis. *Carcinogenesis.* 2005; 26:1527-1535.
 25. Jechlinger M, Podsypanina K, Varmus H. Regulation of transgenes in three-dimensional cultures of primary mouse mammary cells demonstrates oncogene dependence and identifies cells that survive deinduction. *Genes Dev.* 2009; 23:1677-1688.
 26. Shankaran V, Ikeda H, Bruce AT, White JM, Swanson PE, Old LJ, Schreiber RD. IFN-gamma and lymphocytes prevent primary tumour development and shape tumour immunogenicity. *Nature.* 2001; 410:1107-1111.
 27. Charpin C, Secq V, Giusiano S, Carpentier S, Andrac L, Lavaut MN, Allasia C, Bonnier P, Garcia S. A signature predictive of disease outcome in breast carcinomas, identified by quantitative immunocytochemical assays. *International journal of cancer.* 2009; 124:2124-2134.
 28. Ward PL, Schreiber H. MHC class I restricted T cells and immune surveillance against transplanted ultraviolet light-induced tumors. *Seminars in cancer biology.* 1991; 2:321-328.
 29. Philipps C, Stauss HJ, Wortzel RD, Schreiber H. A novel MHC class I molecule as a tumour-specific antigen. Correlation between the antibody-defined and the CTL-

-
- defined target structure. *Journal of immunogenetics*. 1986; 13:93-99.
30. Kirchhoff S, Schaper F, Hauser H. Interferon regulatory factor 1 (IRF-1) mediates cell growth inhibition by transactivation of downstream target genes. *Nucleic Acids Res*. 1993; 21:2881-2889.
 31. Romeo G, Fiorucci G, Chiantore MV, Percario ZA, Vannucchi S, Affabris E. IRF-1 as a negative regulator of cell proliferation. *J Interferon Cytokine Res*. 2002; 22:39-47.
 32. Taniguchi T, Harada H, Lamphier M. Regulation of the interferon system and cell growth by the IRF transcription factors. *Journal of cancer research and clinical oncology*. 1995; 121:516-520.
 33. Virnig BA, Tuttle TM, Shamliyan T, Kane RL. Ductal carcinoma in situ of the breast: a systematic review of incidence, treatment, and outcomes. *J Natl Cancer Inst*. 2010; 102:170-178.
 34. Matsuyama T, Kimura T, Kitagawa M, Pfeffer K, Kawakami T, Watanabe N, Kundig TM, Amakawa R, Kishihara K, Wakeham A, et al. Targeted disruption of IRF-1 or IRF-2 results in abnormal type I IFN gene induction and aberrant lymphocyte development. *Cell*. 1993; 75:83-97.
 35. Shinkai Y, Rathbun G, Lam KP, Oltz EM, Stewart V, Mendelsohn M, Charron J, Datta M, Young F, Stall AM, et al. RAG-2-deficient mice lack mature lymphocytes owing to inability to initiate V(D)J rearrangement. *Cell*. 1992; 68:855-867.
 36. Regitnig P, Reiner A, Dinges HP, Hofler G, Muller-Holzner E, Lax SF, Obrist P, Rudas M, Quehenberger F. Quality assurance for detection of estrogen and progesterone receptors by immunohistochemistry in Austrian pathology laboratories. *Virchows Arch*. 2002; 441:328-334.

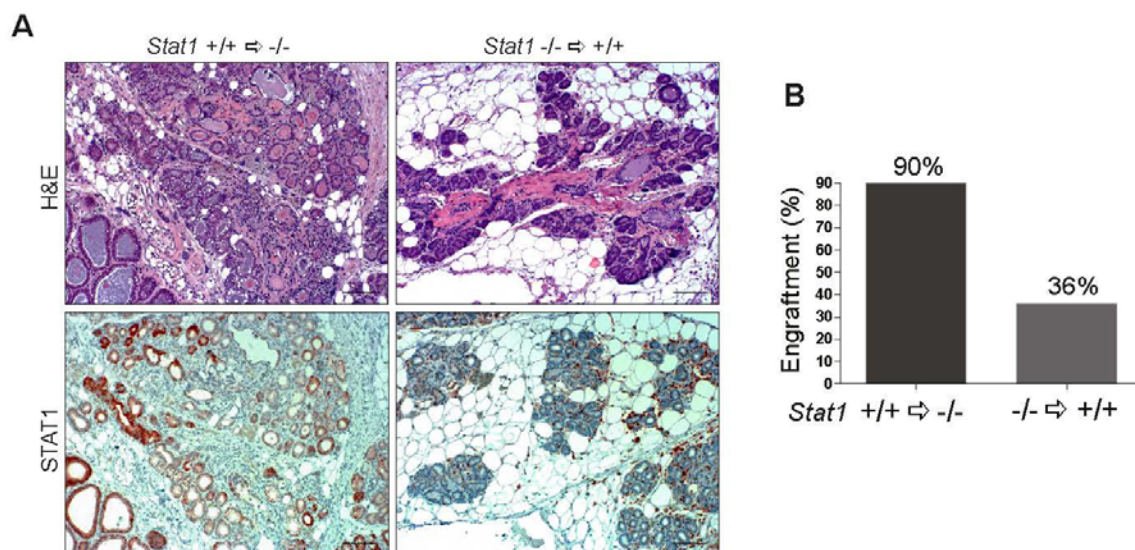


Fig. S1. Verification of successful engraftment of transplanted mammary gland tissue. (A) Histological sections of transplanted mammary glands were stained for H&E and STAT1 to verify successful engraftment of transplants. Left panel: *Stat1*^{+/+} mammary gland tissue was transplanted into a *Stat1*^{-/-} mouse; right panel: *Stat1*^{-/-} mammary gland tissue was transplanted into a *Stat1*^{+/+} mouse. Scale bars: 100 μ m. (B) Rate of successful engraftment of transplanted mammary gland tissue in *Stat1*^{+/+} and *Stat1*^{-/-} animals. Transplant groups: *Stat1*^{+/+} tissue in *Stat1*^{-/-} mice, *Stat1*^{-/-} tissue in *Stat1*^{+/+} mice.

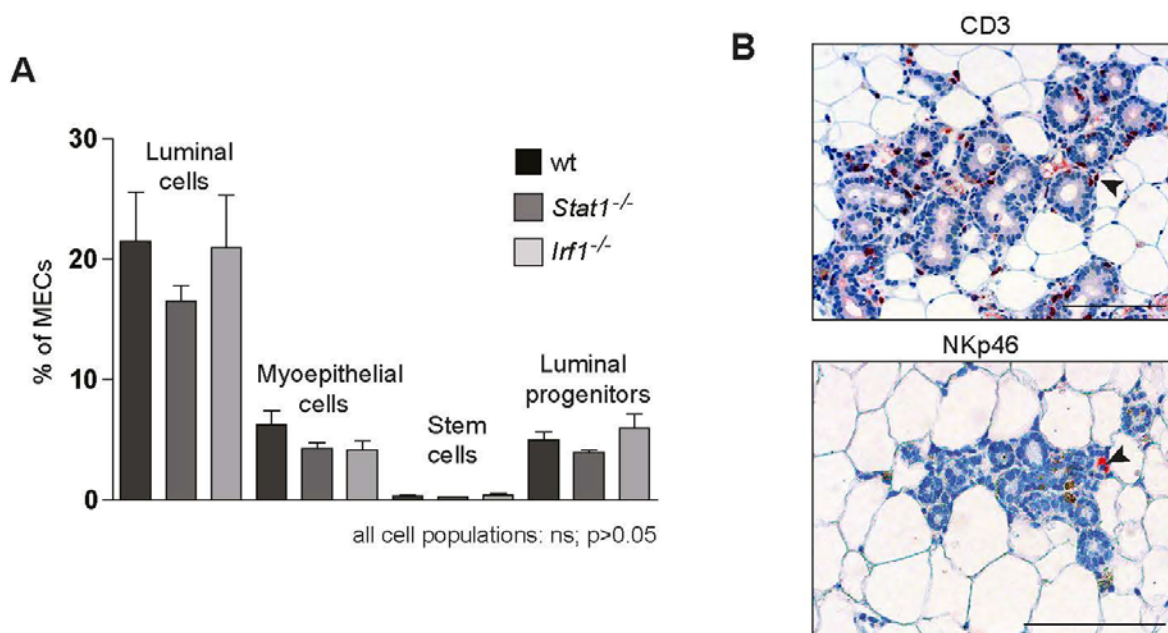


Fig. S2. Successful engraftment of transplanted mammary gland tissue is influenced by CTLs and NK-cells but not by differences in mammary stem cell populations. (A) Flow cytometric analysis of mammary cells from wt, *Stat1*^{-/-} and *Irf1*^{-/-} mice. Luminal cells: CD24^{hi}CD49f^{lo}, myoepithelial cells: CD24^{lo}CD49f^{hi}, stem cells: CD24^{mid}CD49f^{hi}, Luminal progenitors: CD24^{hi}CD49f^{lo}CD61⁺. (B) CD3- and NKp46-stained histological sections of transplanted mammary glands show infiltration with CTLs and NK-cells. Scale bars: 100 μ m.

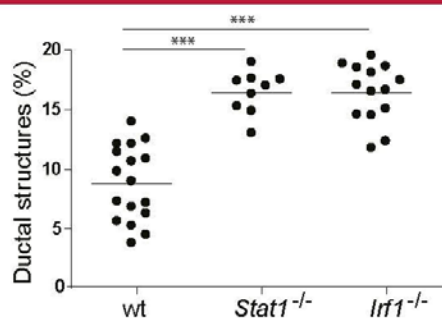
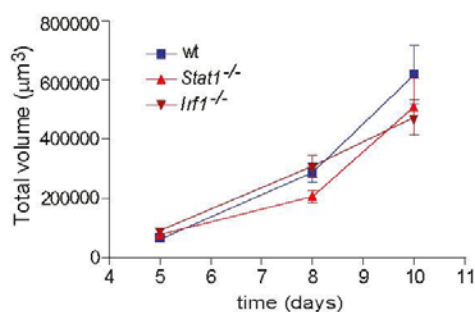


Fig. S3. Quantitative analysis of ductal density from mammary gland whole mounts. Pictures of 2.5x magnification were taken and analyzed using ImageJ 1.37a software. $n \geq 9$.



all time points: ns; $p > 0.05$

Fig. S4. Total volume of 3D-cultured spheres derived from wt, *Stat1*^{-/-} and *lrf1*^{-/-} mammary epithelial cells at different time points of growth. Total volume (V_T) was calculated by means of the formula $V_T = 4/3 * r_T^3$.

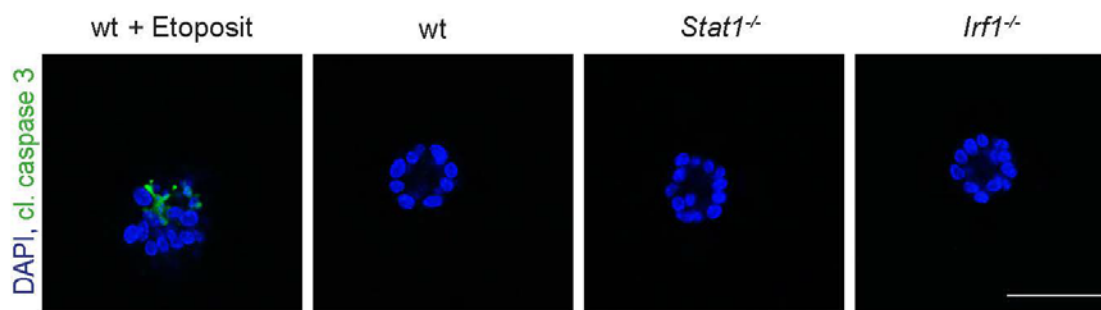


Fig. S5. Mammospheres for lumen without involvement of apoptotic mechanisms. Fluorescence microscopy pictures from 2 day-old spheres of different genotypes. To ensure a positive cleaved caspase 3 staining, wildtype mammospheres were treated with 50 μm Etoposit for 24h. (Blue) DAPI; (green) Cleaved caspase 3. Scale bar: 50 μm .

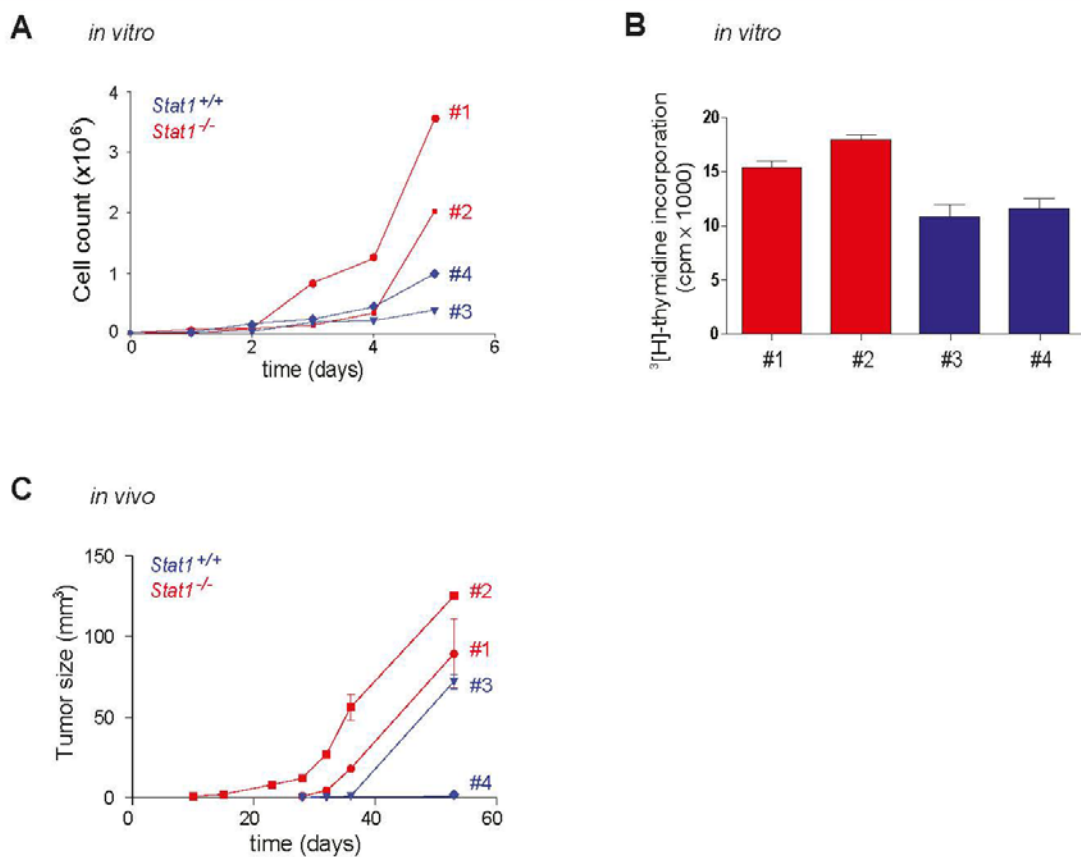


Fig. S6. *Stat1*^{-/-} mammary tumor cell lines show increased proliferation *in vitro* and *in vivo*. (A) Growth curve of mammary tumor cell lines #1-#4. (B) [³H]-thymidine incorporation of mammary tumor cell lines #1-#4. (C) *In vivo* proliferation of mammary tumor cell lines #1-#4. 2×10^5 cells of each cell line were orthotopically injected into *Stat1*^{-/-} mice. Tumor growth was measured at different time points with tumor size calculated by means of the formula $V = 3/4 \times \pi \times L \times W \times H$. $n \geq 4$ per cell line.

Supporting Information:

Materials and Methods

Mammary epithelial transplant procedure. Procedures for transplantation of tissues into cleared mammary fat pads have been described recently [1]. In brief, small pieces (1-2 mm³) of mammary epithelium from the 4th mammary gland were taken from 3-month-old virgin females and implanted into the cleared fat pad of the 4th mammary gland of 3-week-old female recipient mice. Eight weeks after surgery, transplant recipients were housed with males for impregnation and monitored regularly for mammary tumor growth by palpation. A mouse was sacrificed when any evolving mammary tumor reached one centimeter in diameter or earlier if there were signs of disease.

3D-cultures of primary mouse mammary epithelial cells. 3D culture assays of primary mammary epithelial cells were performed as described previously [2] with minor alterations. The tissue from two mammary glands was placed in 5 ml digestion medium (DMEM with L-glutamine supplemented with 1 M HEPES-Buffer to a final concentration of 25 mM, 150 U/ml Collagenase type 3 (Worthington, #LS004182) and 20 µg/ml Liberase (Roche applied science, #05401119001)) and digested for 6 h at 37°C. Following 40 min of treatment with 0.25% Trypsin-EDTA, cells were seeded onto collagen-coated plates. One day after plating, cells were harvested and counted. 10,000 cells were resuspended in 50 µl of “Cultrex 3D Culture Matrix™ Basement Membrane Extract” (TREVIGEN, #3445-005-01) and carefully dispensed onto 4-well chamber slides (Millipore, #PEZGS0416). After solidification at 37°C, gels were supplemented with Mammary Epithelial Cell Medium (BulletKit, Lonza, #CC-3150) and maintained at 37°C in a CO₂ incubator until analysis.

Calculating the cellularity of mammospheres: Spheres were assumed to be round. Circles were drawn around the entire sphere and at the borders of the lumen; total volume (V_T) and lumen volume (V_L) were calculated by means of the formula $V_{TL} = 4/3 * r_{TL}^3$, so cellularity was $C = V_T - V_L$. Pictures were taken on an Olympus iX5 using the cell[^]F software.

BrdU incorporation assay. The APC BrdU Flow Kit (BD Pharmingen™) was used to determine proliferation. For *in vitro* experiments, 3D cultures were incubated with 10 ng/ml BrdU for 24 hours and fixed and processed according to the manufacturer's instructions with minor changes. Incorporated BrdU was detected by APC-conjugated anti-BrdU antibody and cell nuclei were counterstained with DAPI. The stainings were visualized under a confocal laser scanning microscope (Carl Zeiss LSM 700, Occulare 10x, 40x Oil). Spheres in random microscopic fields were taken to determine the percentage of cells with nuclear BrdU incorporation from the total cell number within one sphere. For *in vivo* experiments, mice were injected intraperitoneally with 4 mg BrdU solution. After 3 days the mice were sacrificed and mammary glands were dissected and digested as described above. Cells were fixed and processed according to the manufacturer's instructions. APC-conjugated anti-BrdU-stained cells were analyzed by flow cytometry using the BD FACS-Canto II FACS device and BD FACS Diva software (Beckton Dickinson). Epithelial cells not exposed to BrdU but stained with anti-BrdU antibody were used as appropriate negative control to avoid counting background signals as false positive.

-
1. Young LJT: The cleared mammary fat pad and the transplantation of mammary gland morphological structures and cells. In: *Methods in mammary gland biology and breast cancer research*. Edited by Ip MM, Asch BB. Heidelberg: Springer 2000: 67-74.
 2. Jechlinger M, Podsypanina K, Varmus H. Regulation of transgenes in three-dimensional cultures of primary mouse mammary cells demonstrates oncogene dependence and identifies cells that survive deinduction. *Genes Dev.* 2009; 23:1677-1688.

3.2 Lipoxigenase mediates invasion of intrametastatic lymphatic vessels and propagates lymph node metastasis of human mammary carcinoma xenografts in mouse.

Manuscript published in J Clin Invest. 2011 May;121(5):2000-12. doi: 10.1172/JCI44751. Epub 2011 Apr 11.

Dontscho Kerjaschki^{1,2}, Zsuzsanna Bago-Horvath^{1,2,3}, Margaretha Rudas^{1,2,3}, Veronika Sexl⁴, **Christine Schneckenleithner**⁴, Susanne Wolbank⁵, Gregor Bartel¹, Sigurd Krieger¹, Romana Kalt¹, Brigitte Hantusch^{1,2}, Thomas Keller¹, Katalin Nagy-Bojarszky¹, Nicole Huttary¹, Ingrid Raab¹, Karin Lackner¹, Katharina Krautgasser¹, Helga Schachner¹, Klaus Kaserer¹, Sandra Rezar¹, Sybille Madlener¹, Caroline Vonach¹, Agnes Davidovits¹, Hitonari Nosaka¹, Monika Hämmerle¹, Katharina Viola¹, Helmut Dolznig¹, Martin Schreiber⁶, Alexander Nader⁷, Wolfgang Mikulits^{2,8}, Michael Gnant^{2,3,9}, Satoshi Hirakawa¹⁰, Michael Detmar¹¹, Kari Alitalo¹², Sebastian Nijman¹³, Felix Offner¹⁴, Thorsten J. Maier¹⁵, Dieter Steinhilber¹⁵, and Georg Krupitza^{1,2}

¹Clinical Institute of Pathology, ²Comprehensive Cancer Center, ³Austrian Breast and Colorectal Cancer Study Group (ABCSCG), and ⁴Institute of Pharmacology, Medical University of Vienna, Vienna, Austria. ⁵Ludwig Boltzmann Institute for Experimental and Clinical Traumatology, Vienna, Austria. ⁶Department of Gynaecology, Medical University of Vienna, Vienna, Austria. ⁷Pathology Institute, Hanusch Hospital, Vienna, Austria. ⁸Institute of Cancer Research and ⁹Department of Surgery, Medical University of Vienna, Vienna, Austria. ¹⁰Department of Dermatology, Ehime University Graduate School of Medicine, Ehime, Japan. ¹¹Department of Pharmacogenomics, Swiss Federal Institute of Technology ETH-Zurich, Zurich, Switzerland. ¹²Molecular/Cancer Biology Laboratory, Biomedicum Helsinki, University of Helsinki, Helsinki, Finland. ¹³Ce-M-M-Research Center for Molecular Medicine of the Austrian Academy of Sciences, Vienna, Austria. ¹⁴Institute for Pathology, LKH Feldkirch, Austria. ¹⁵Institute of Pharmaceutical Chemistry/ZAFES, Frankfurt/Main, Germany.

My contribution: Performed all *in vivo* experiments and analyzed data.

I performed the xenograft experiment to monitor metastasis formation of the human breast cancer cell line MCF7 *in vivo* (Fig6. and page 2004-2005). The purpose of the experiment was to validate whether ALOX15 is required for formation of lymph node metastasis by enabling the entry of tumor cells into intrametastatic lymphatic vessels. Therefore, MCF7/VEGF-C cells harbouring either a shRNA construct targeting ALOX15 or a non-coding shRNA construct were orthotopically injected in the mammary glands of female SCID mice. As MCF7 cells grow hormone-dependent, 2 days before orthotopic injection, slow-release estrogen-pellets were subcutaneously implanted in the mice. The presence of a luciferase reporter construct allowed us to monitor cell growth. Tumor growth and lymph node metastasis formation was measured at 10-day intervals by non-invasive bioluminescence imaging. At termination of the experiment, primary tumors and lymph nodes were taken and further used for immunohistochemical analysis.



Lipoxygenase mediates invasion of intrametastatic lymphatic vessels and propagates lymph node metastasis of human mammary carcinoma xenografts in mouse

Dontscho Kerjaschki,^{1,2} Zsuzsanna Bago-Horvath,^{1,2,3} Margaretha Rudas,^{1,2,3} Veronika Sexl,⁴ Christine Schneckenleithner,⁴ Susanne Wolbank,⁵ Gregor Bartel,¹ Sigurd Krieger,¹ Romana Kalt,¹ Brigitte Hantusch,^{1,2} Thomas Keller,¹ Katalin Nagy-Bojarszky,¹ Nicole Huttary,¹ Ingrid Raab,¹ Karin Lackner,¹ Katharina Krautgasser,¹ Helga Schachner,¹ Klaus Kaserer,¹ Sandra Rezar,¹ Sybille Madlener,¹ Caroline Vonach,¹ Agnes Davidovits,¹ Hitonari Nosaka,¹ Monika Hämmerle,¹ Katharina Viola,¹ Helmut Dolznig,¹ Martin Schreiber,⁶ Alexander Nader,⁷ Wolfgang Mikulits,^{2,8} Michael Gnant,^{2,3,9} Satoshi Hirakawa,¹⁰ Michael Detmar,¹¹ Kari Alitalo,¹² Sebastian Nijman,¹³ Felix Offner,¹⁴ Thorsten J. Maier,¹⁵ Dieter Steinhilber,¹⁵ and Georg Krupitza^{1,2}

¹Clinical Institute of Pathology, ²Comprehensive Cancer Center, ³Austrian Breast and Colorectal Cancer Study Group (ABCSCG), and ⁴Institute of Pharmacology, Medical University of Vienna, Vienna, Austria. ⁵Ludwig Boltzmann Institute for Experimental and Clinical Traumatology, Vienna, Austria. ⁶Department of Gynaecology, Medical University of Vienna, Vienna, Austria. ⁷Pathology Institute, Hanusch Hospital, Vienna, Austria. ⁸Institute of Cancer Research and ⁹Department of Surgery, Medical University of Vienna, Vienna, Austria. ¹⁰Department of Dermatology, Ehime University Graduate School of Medicine, Ehime, Japan. ¹¹Department of Pharmacogenomics, Swiss Federal Institute of Technology ETH-Zurich, Zurich, Switzerland. ¹²Molecular/Cancer Biology Laboratory, Biomedicum Helsinki, University of Helsinki, Helsinki, Finland. ¹³Ce-M-M-Research Center for Molecular Medicine of the Austrian Academy of Sciences, Vienna, Austria. ¹⁴Institute for Pathology, LKH Feldkirch, Austria. ¹⁵Institute of Pharmaceutical Chemistry/ZAFES, Frankfurt/Main, Germany.

In individuals with mammary carcinoma, the most relevant prognostic predictor of distant organ metastasis and clinical outcome is the status of axillary lymph node metastasis. Metastases form initially in axillary sentinel lymph nodes and progress via connecting lymphatic vessels into postsentinel lymph nodes. However, the mechanisms of consecutive lymph node colonization are unknown. Through the analysis of human mammary carcinomas and their matching axillary lymph nodes, we show here that intrametastatic lymphatic vessels and bulk tumor cell invasion into these vessels highly correlate with formation of postsentinel metastasis. In an *in vitro* model of tumor bulk invasion, human mammary carcinoma cells caused circular defects in lymphatic endothelial monolayers. These circular defects were highly reminiscent of defects of the lymphovascular walls at sites of tumor invasion *in vivo* and were primarily generated by the tumor-derived arachidonic acid metabolite 12S-HETE following 15-lipoxygenase-1 (ALOX15) catalysis. Accordingly, pharmacological inhibition and shRNA knockdown of ALOX15 each repressed formation of circular defects *in vitro*. Importantly, ALOX15 knockdown antagonized formation of lymph node metastasis in xenografted tumors. Furthermore, expression of lipoxygenase in human sentinel lymph node metastases correlated inversely with metastasis-free survival. These results provide evidence that lipoxygenase serves as a mediator of tumor cell invasion into lymphatic vessels and formation of lymph node metastasis in ductal mammary carcinomas.

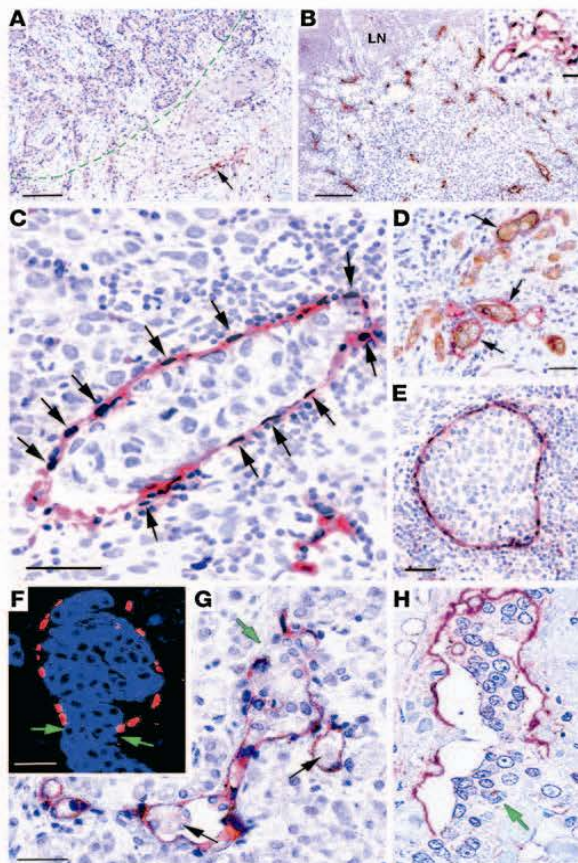
Introduction

A tumor's metastatic potential is determined by complex and specific genetic gains and/or losses of function that enable tumor cells to emigrate from their primary site to access the blood or lymphatic vasculature and to form premetastatic niches in target organs that provide the essential "soil" for "seeding" of incoming tumor cells (1). Despite the obvious clinical relevance of these events, relatively little is currently known about the underlying mechanisms. For example, only some aspects of niche formation in distant organs have been identified; these include local accumulation of bone marrow-derived cells, fibronectin deposition (2), and interactions between tumor cells and thrombocytes (3).

Whether tumors metastasize initially into lymph nodes or are distributed by hematogenous dissemination into distant organs remains a matter for debate, and there is experimental evidence for each hypothesis (4–6). One view holds that metastatic tumor cells colonize distant organs via the blood stream either from lymph nodes ("metastasis from metastasis") (7) or by cross seeding from the primary tumor by recirculation (8). Alternatively, clonogenic tumor cells, presumably with stem cell-like characteristics, could disseminate simultaneously at an early time point from primary tumors into both the blood and lymphatic vasculature and then develop metastases asynchronously in both compartments (9). Although currently evidence is accumulating in favor of the latter hypothesis (5), it falls short of explaining why the number of regional lymph nodes affected by metastases most accurately predicts the general extent of metastatic spreading and overall clinical outcome, for

Conflict of interest: The authors have declared that no conflict of interest exists.

Citation for this article: *J Clin Invest*. 2011;121(5):2000–2012. doi:10.1172/JCI44751.

**Figure 1**

Intrametastatic lymphangiogenesis and tumor cell invasion into lymphatic vessels in sentinel lymph nodes of human ductal mammary carcinomas with postsentinel metastasis. Lymphatic endothelial cells are localized by double labeling for podoplanin (red) and PROX1 (black) in **A–C** and **E**. **(A)** In a primary ductal carcinoma, lymphatic vessels are localized in the peritumoral stroma (arrow). The tumor border is marked by a green line. **(B)** Sentinel lymph node metastasis of the same carcinoma as in part **A**, with dense intrametastatic lymphatic vascularization. LN, residual lymph node parenchyma. Insert, FLT4 (red) in an intrametastatic lymphatic vessel (PROX1, black). **(C)** High-power view of an intrametastatic lymphatic vessel with podoplanin+ lymphatic endothelial cells and PROX1-expressing nuclei (arrows). The vessel contains a tumor embolus and is surrounded by mononuclear inflammatory or tumor cells. **(D)** Keratin+ tumor cell emboli (brown) within intrametastatic lymphatic vessels with podoplanin+ endothelial cells (red). **(E)** Large tumor embolus completely filling the lumen of an intrametastatic lymphatic vessel. **(F)** Aggregate of keratin+ carcinoma cells disrupts an intrametastatic lymphatic vessel that is outlined by a single line of PROX1+ nuclei (red). The margins of the vessel's rupture are indicated by green arrows. **(G** and **H)** Embolic tumor cell clusters (black arrows) within a branched intrametastatic lymphatic vessel, and a focal disruption of the lymphatic vascular wall by a bulk of aggregated tumor cells (green arrow). The lymphatic vessel's walls are composed of a single endothelial layer. Scale bars: 100 μm ; 25 μm (insert).

example, in mammary carcinomas. This well-established fact is reflected in clinically validated and diagnostically indispensable consensus systems used in routine histopathological mammary tumor staging (10, 11). Testing these hypotheses, which are not mutually exclusive, depends on better understanding of the so-far elusive molecular mechanisms that determine the initial tumor cells' specific preference for invasion of blood or lymphatic vessels to reach their respective target organs.

Here we have systematically analyzed the lymphometastatic properties of human mammary carcinomas. These have distinct advantages for such studies, including the anatomically conserved lymphatic draining patterns of the human breast (12) and their repetitive pattern of metastatic spreading. Thus, most mammary carcinomas form their initial metastasis in up to 3 axillary lymph node or nodes that receive afferent lymph from the tumor and peritumoral tissue and are designated as "sentinel lymph nodes." Further metastatic progression occurs by successive colonization of the postsentinel lymph nodes in the axillary basin. Previous work has shown that lymphangiogenesis in sentinel lymph node metastases correlates with postsentinel tumor spreading (13). In this study, we have addressed the mechanisms underlying this process, using immunohistochemistry with selective lymphatic endothelial markers (podoplanin, LYVE1, and PROX1) (14–16), *in vitro* models, and xenograft tumors. The findings are compatible with a context-specific reaction of lymphatic

endothelial cells with tumor-derived products of lipoxygenases that is critical for tumor cell entry into the lymphatic vessel and metastatic spreading from the sentinel to postsentinel lymph nodes. The results also shed light on the fact that different tumor types use different means to invade intrametastatic lymphatics.

Results

Intrametastatic lymphatic carcinosis. We localized lymphatic endothelial cells in 104 precisely matched primary ductal and lobular mammary carcinomas (stages pT1c, N0, or N1a, or pooled stages N2 and N3; ref. 11 and Supplemental Table 1; supplemental material available online with this article; doi:10.1172/JCI44751DS1) and in their corresponding sentinel and postsentinel axillary lymph nodes (Figure 1). Lymphatic vessels were restricted to the peritumoral stroma (17) in all the primary carcinomas. In contrast, the sentinel lymph node metastases of these tumors were often endowed with lymphatic vessels connected to those in the residual sentinel lymph node's parenchyma (Supplemental Figure 1). Their endothelial cells expressed the major lymphatic markers FLT4 (VEGFR3), podoplanin, PROX1, and, with some variability, also LYVE1, as reported (18). The density of intrametastatic lymphatics and their endothelial mitotic rate were more than 2-fold higher than those in residual lymph nodes (Supplemental Figure 2). The metastatic tumor cells were a major source of the lymphangiogenic factors



Table 1
Characterization of tumors and patients' outcome

| pN Stage | Primary tumor stage pT1c diameter | Peritumoral carcinoma primary tumor | Grading | Grading (%) | Intrametastatic carcinoma | Local recurrence | Distant organ metastasis | Death | Follow-up period (months) |
|--------------------------|-----------------------------------|-------------------------------------|----------------|--------------------------------|---------------------------|------------------|--------------------------|---------|---------------------------|
| Ductal carcinoma | | | | | | | | | |
| pN1a (n = 39) | 1.8 ± 0.4 cm | 19 (49%) | G1 G2 G3 | 2 (5%) 22 (56%) 15 (39%) | 0 of 39 (0%) | 0 | 5 (13%) | 3 (8%) | 54 |
| pN2/3 (n = 20) | 1.9 ± 0.3 cm | 16 (65%) | G1 G2 G3 | 3 (15%) 8 (40%) 9 (45%) | 20 of 20 (100%) | 2 (10%) | 5 (25%) | 5 (25%) | 56 |
| Lobular carcinoma | | | | | | | | | |
| pN1a (n = 17) | 1.9 ± 0.35 cm | 4 (24%) | G1 G2 G3 | 0 (0%) 14 (82%) 3 (18%) | 0 (0%) | 0 | 0 | 0 | 55 |
| pN2/3 (n = 12) | 1.8 ± 0.6 cm | 5 (42%) | G1 G2 G3 | 0 (0%) 10 (83%) 2 (17%) | 6 of 12 (50%) | 1 (8%) | 3 (25%) | 3 (25%) | 57 |

Mean age, 56.9 ± 12.8 years. pT1c, primary tumors with diameters between 1–2 cm; pN1a, metastasis in 1–3 axillary lymph node(s), at least 4 larger than 2 mm in greatest diameter; pN2/3, metastases in more than 4 (ipsilateral) lymph nodes, at least 1 larger than 2 mm in greatest diameter. Data applies to all 3 tumor grades.

VEGFC and VEGFA (19), and their expression in the metastasis frequently exceeded that of the corresponding primary tumors (Supplemental Figure 3) and that of mononuclear cells (20) in the adjacent residual lymph node parenchyma or in naive lymph nodes (data not shown). These results suggest that metastatic tumor colonies provide lymphangiogenic factors and coopt the sentinel lymph node's premetastatic lymphatics and extend them by intrametastatic lymphangiogenesis.

We identified carcinoma cell emboli of various sizes within the intrametastatic lymphatic vessels of sentinel lymph nodes (Figure 1). Emboli were present in 100% (20 of 20) of ductal carcinomas with postsentinel lymph node involvement (Table 1), similar to our recent findings in extramammary Paget carcinomas (21). Strikingly, intrametastatic carcinosis was also present in all postsentinel lymph node metastases from individuals with advanced disease (data not shown). In contrast, lymphatic carcinosis was not detected in any of the 56 individuals in whom metastatic tumors were restricted to the sentinel lymph node (Table 1). After mean follow-up of 4.5 years, distant organ metastasis and death were more frequent in the patient group with (25%, 5 of 20 patients) than without intrametastatic lymphatic carcinosis (8%, 3 of 39 patients). The primary tumor's peritumoral lymphatic carcinosis was (statistically nonsignificantly) increased with the incidence of intrametastatic tumor emboli (Table 1). No further correlation of intrametastatic lymphatic carcinosis with luminal, basal, or ERBB2-overexpressing carcinoma subtypes (22) was observed. However, in contrast to ductal carcinomas, we found intrametastatic lymphatic carcinosis only in 50% (6 of 12) of lobular carcinomas with postsentinel lymph node involvement (Table 1). This is in line with previous results showing that the global gene expression of ductal and lobular subtypes differs significantly (23).

Using oligonucleotide arrays, we identified several gene products (DUSP1, RGS1, CYR61, CXCR4, and VEGFC) that were overexpressed in tumor cells of the metastasis compared with primary tumors, and the same discriminatory "markers" were also differentially expressed in intrametastatic lymphatic tumor emboli (Supplemental Figure 4). This indicates that tumor emboli originate from the surrounding metastasis rather than from the primary tumor directly via lymphatics in the premetastatic lymph node.

Bulk invasion of tumor cells into intrametastatic lymphatics. Due to the high density of intrametastatic lymphatics, we frequently observed that tumor cells aggregated into clusters and penetrated in bulk through large discontinuities of the intrametastatic lymphatic's walls (Figure 1). Tumor cell aggregates are located within the vascular lumen, and the vascular walls that border the discontinuity consist of a single endothelial cell layer. This is documented by localization of PROX1 that forms a single "rosary"-like cover around the tumor cells (Figure 1). These histological features are not compatible with surrounding and engulfment of the tumor cell clusters by newly formed lymphatic vessels that would result in a double layer of endothelial cells. Our results favor the interpretation of a direct penetration of the tumor cell aggregates through ruptures in the vascular wall that is also in line with the recent *ex vivo* observation obtained by video microscopy (24).

An *in vitro* model of lymphatic invasion. We used an *in vitro* coculture system to analyze the mechanisms of tumor cell-mediated disruption of lymphatic vessels. This employed spheroids (25, 26) of MCF7 mammary carcinoma cells to reproduce the clusters of cells seen in tumor emboli *in vivo*. MCF7 cell spheroids remained stable



Table 2
Overexpression of genes in MCF-7 spheroids versus monolayers

| Description | Gene | Spheroid/monolayer | P value |
|--|----------------|--------------------|---------|
| Gain | | | |
| CD44 (Indian blood group) | <i>CD44</i> | 3.45 | 0.0039 |
| Intercellular adhesion molecule 1 (CD54) | <i>ICAM1</i> | 2.67 | 0.0012 |
| Vascular endothelial growth factor (VEGFA) | <i>VEGFA</i> | 2.73 | 0.0100 |
| Selectin L (lymphocyte adhesion molecule 1) | <i>SELL</i> | 2.45 | 0.0055 |
| Thrombospondin 2 | <i>THBS2</i> | 2.30 | 0.0125 |
| Arachidonate 15-lipoxygenase | <i>ALOX15</i> | 1.89 ^A | 0.0397 |
| Cadherin 1 type 1, E-cadherin (epithelial) | <i>CDH1</i> | 1.80 | 0.0139 |
| Integrin alpha 5 (fibronectin receptor) | <i>ITGA5</i> | 1.76 | 0.0370 |
| Loss | | | |
| Laminin beta 1 | <i>LAMB1</i> | -3.87 | 0.0133 |
| Collagen type XII, alpha 1 | <i>COL12A1</i> | -4.21 | 0.0016 |
| Platelet/endothelial cell adhesion molecule (CD31) | <i>PECAM1</i> | -1.95 | 0.0041 |
| Thrombospondin 1 | <i>THBS1</i> | -1.91 | 0.0008 |
| Vascular endothelial growth factor C (VEGFC) | <i>VEGFC</i> | -1.81 | 0.0295 |
| Vitronectin | <i>VTN</i> | -1.45 | 0.0559 |

MCF7 cells were grown as spheroids or as monolayers, and lysed to extract and reverse transcribe RNA for low density arrays (Human Extracellular Matrix and Adhesion Molecules PCR Array; SABiosciences). Genes were identified that are differentially induced or repressed by MCF7 cell spheroid formation and could be related to bulk-like invasion through the lymphatic vasculature. ^ACorresponding gene products were studied in more detail.

for more than 6 hours. When aggregated into spheroids, MCF7 cells changed their gene expression patterns when compared with monolayers and increased their expression of CD44, ICAM1, and VEGFA; they also reduced their expression of matrix components (Table 2). Confluent monolayers of freshly isolated or telomerase “immortalized” (27) human dermal lymphatic endothelial cells were used as surrogates for intrametastatic lymphatics. We found no difference between intra- and extratumoral dermal lymphatics for the expression of several proteins (podoplanin, PROX1, FLT4, biglycan, endoglin, VE-cadherin, variably CD34, and LYVE1) (Supplemental Figure 4), justifying their use for the *in vitro* studies.

MCF7 spheroids were placed on top of lymphatic endothelial monolayers (Figure 2), which resulted in the highly reproducible formation of circular discontinuities that we designated as circular chemorepellent-induced defects (CCID) in monolayers precisely underneath the MCF7 spheroids. They were highly reminiscent of the defects seen in the lymphovascular walls at sites of tumor cell invasion *in vivo*. Lymphatic endothelial cells were more than 5 times more sensitive to MCF7 spheroid-induced CCID formation than blood vessel endothelia. CCID formation was not seen using spheroids of the nontumorigenic mammary gland epithelial cell line MCF-10A or human lung fibroblasts (HLFs) (Figure 2).

CCIDs form by migration of lymphatic endothelial cells. Time-lapse videos revealed centrifugal migration of lymphatic endothelial cells strictly beneath the MCF7 spheroids (Figure 2 and Supplemental Video). This correlated also with rearrangement and fragmentation of VE-cadherin in lymphatic endothelial cell junctions at the border of MCF7 spheroid-induced CCIDs (Figure 2). The migratory phenotype of the lymphatic endothelia was confirmed by the localization of the cell movement-associated activated protein phosphatase 1 regulatory inhibitor subunit 12 A (PPP1R12A, MYPT1) (ref. 28 and Figure 2). We discounted a role for apoptosis of lymphatic endothelial cells in the formation of CCIDs by TUNEL and Hoechst 33258 staining both *in vitro* and *in vivo* in human sentinel metastases (Supplemental Figure 5).

12(S)-HETE induces CCIDs in lymphatic endothelial cell monolayers. Oligonucleotide array analyses revealed the specific induction of several genes in MCF7 cell spheroids when compared with monolayers, including the hypoxia inducible (29) enzyme 15-lipoxygenase-1 (ALOX15) (Table 2), which metabolizes arachidonic acid to 12[S]-hydroxy-eicosatetraenoic acid (12[S]-HETE) and 15(S)-hydroxyeicosatetraenoic acid (15[S]-HETE). In humans, 12(S)-HETE is produced by ALOX15 and ALOX12, which are the respective products of the *ALOX15* and *ALOX12* genes (30). We have found that MCF7 cells only express *ALOX15* (Table 2), and it was shown previously that they lack *ALOX15B* (31). 12(S)-HETE was identified as a tumor cell-derived retraction factor for blood vessel endothelial cells (32). In lymphatic endothelial monolayers, 12(S)-HETE also transiently reduced VE-cadherin expression (Figure 2). These results fostered the speculation that 12(S)-HETE might be involved in MCF7-induced CCID formation.

We inhibited the enzymatic activity of ALOX15 in MCF7 cells by pharmacologic inhibition with the pan-LOX inhibitor nordihydroguaiaretic acid (33), which resulted in a significant and dose-dependent reduction of MCF7 spheroid-induced CCID areas in lymphatic endothelial cell monolayers (Supplemental Table 2). This result was confirmed with the LOX inhibitor baicalin (34) at nontoxic concentrations (Figure 3 and Supplemental Figure 6), which reduced CCID formation by 90% after 2 hours, and by 40% to 60% after 6 hours of coincubation as determined in pilot experiments (26).

Direct proof for the hypothesis that 12(S)-HETE triggered CCIDs was obtained by placing fibroblast spheroids soaked with synthetic 12(S)-HETE onto lymphatic endothelial cell monolayers. This resulted in CCID formation similar to that induced by MCF7 spheroids, whereas fibroblast spheroids imbibed with 15(S)-HETE or solvent were ineffective (Figure 3). Conversely, blocking 12(S)-HETE with a specific polyclonal antibody (35) inhibited the formation of MCF7 spheroid-induced CCIDs (Figure 3).

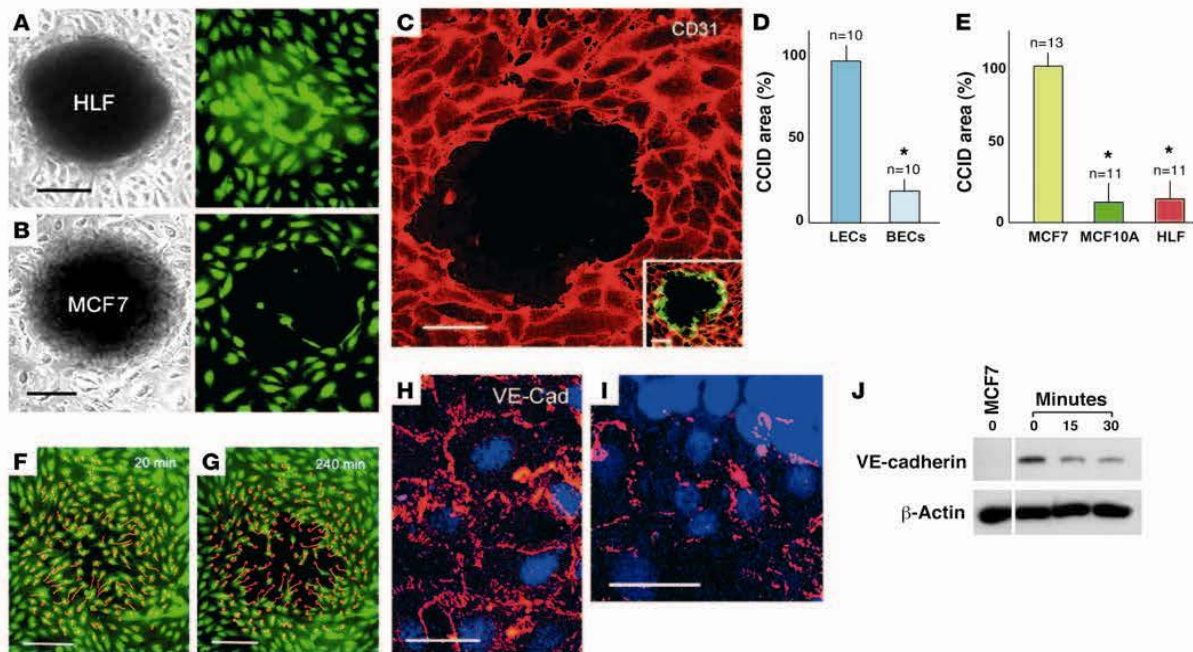


Figure 2

MCF7 cell spheroids induce CCIDs in lymphatic endothelial cell monolayers and disrupt VE-cadherin at the CCIDs. (A) Spheroid of HLFs fails to induce any defects in a monolayer of human lymphatic endothelial cells (LECs, Cytotracker tagged in green) after 4 hours of cocultivation. (B) MCF7 spheroids induce circular CCIDs. (C) A MCF7 spheroid-induced CCID is outlined when the LEC borders are stained for CD31 (red, confocal image). Inset, LECs (demarcated with CD31 in red) at the margin of the CCIDs show expression of PPP1R12A (MYPT1) (green) indicating cell mobility (confocal image). (D) MCF7 spheroids induce CCIDs preferentially in LEC monolayers (left bar), but significantly less (14.3% of lymphatics; $*P = 0.0047$) in monolayers of microvascular blood endothelial cells (BECs, right bar). (E) When compared with spheroids of MCF7 cells (left bar, 100%), CCID formation in lymphatic monolayers is marginally induced by nonmalignant human breast epithelial cells MCF-10A (9.6% of MCF7 spheroids), and HLFs (11.3%). Data are presented as mean \pm SEM. $*P < 0.0001$. (F and G) Tracings of LEC migration (red lines; starting positions are marked by circles) beneath a spheroid during a 4-hour cocultivation. (H) Confocal image shows continuous LEC junctions of VE-cadherin (VE Cad) at distance from a spheroid. (I) At the spheroid's margin, the VE-cadherin pattern is disrupted. (J) Confluent LECs were incubated with $1 \mu\text{M}$ 12(S)-HETE for 15 and 30 minutes or with solvent (0), and cell lysates were immunoblotted with antibodies to VE-cadherin or β -actin. As controls, VE-cadherin⁻ MCF7 cells were used. Lanes were run on the same gel but are noncontiguous. Scale bars: 100 μm (A, B, F, and G); 25 μm (C); 50 μm (H and I).

These results indicated that CCIDs were induced by MCF7 cell spheroids, which were placed onto the upper side of the lymphatic endothelial monolayer that presumably corresponds to the luminal endothelial aspect in vivo. Here we show that CCIDs were also generated when the MCF7 spheroids were placed onto the basolateral aspects of lymphatic endothelial cells in Transwell chambers (Figure 4).

CCIDs were also obtained with spheroids of tumor lines other than MCF7 cells. This was found for human mammary carcinoma cells (HCC1419, HCC1443, and MDA-MB231) and colon cancer (LS174CoCa, HT29, HTC116), melanoma (CRL1675), and pancreatic adenocarcinoma (PANC1) (Figure 3).

Pharmacological inhibition of cognate mechanisms of tumor invasion and metastasis revealed a minor contribution of metalloproteinases since the pan-matrix-metalloprotease inhibitor GM6001 (36, 37), and specific inhibition of MMP9, TIMP2, and MMP2 reduced CCID formation only by approximately 25%. Reactive oxygen species and cyclooxygenases and their products were not involved (Supplemental Table 2).

Inhibition of 15LOX reduces CCID formation in lymphatic monolayers. Further evidence for the central role of *ALOX15* in CCID formation was obtained by shRNA-mediated knockdown in MCF7 cells (MCF7/*ALOX15*⁻ cells), which resulted in stable reduction of over 80% of *ALOX15* mRNA as well as 12(S)-HETE and 15(S)-HETE production (Figure 5). Nonmalignant human MCF-10A cells or fibroblasts failed to induce CCIDs, to express *ALOX15* and *ALOX12* genes, and to synthesize 12(S)-HETE (Figure 5). Spheroids of MCF7/*ALOX15*⁻ cells induced small CCIDs that were similar to baicalein-treated MCF7 spheroids, whereas controls (scrambled shRNA or empty vector-transfected MCF7 cells) were similar to unmodified MCF7 cells. This inhibitory effect of *ALOX15* shRNA was further enhanced by the pan-metalloprotease inhibitor GM6001 (Figure 5). Knocking in of *ALOX12* into MCF7/*ALOX15*⁻ cells (Supplemental Figure 7) fully reestablished their CCID-forming capacity in the spheroid assay (Figure 5).

Reduced metastatic capacity of ALOX15-deficient tumor cells. We used MCF7 cells with transgene expression of VEGFC (MCF7/VEGFC cells) (38, 39) to induce metastasis formation in vivo. Both

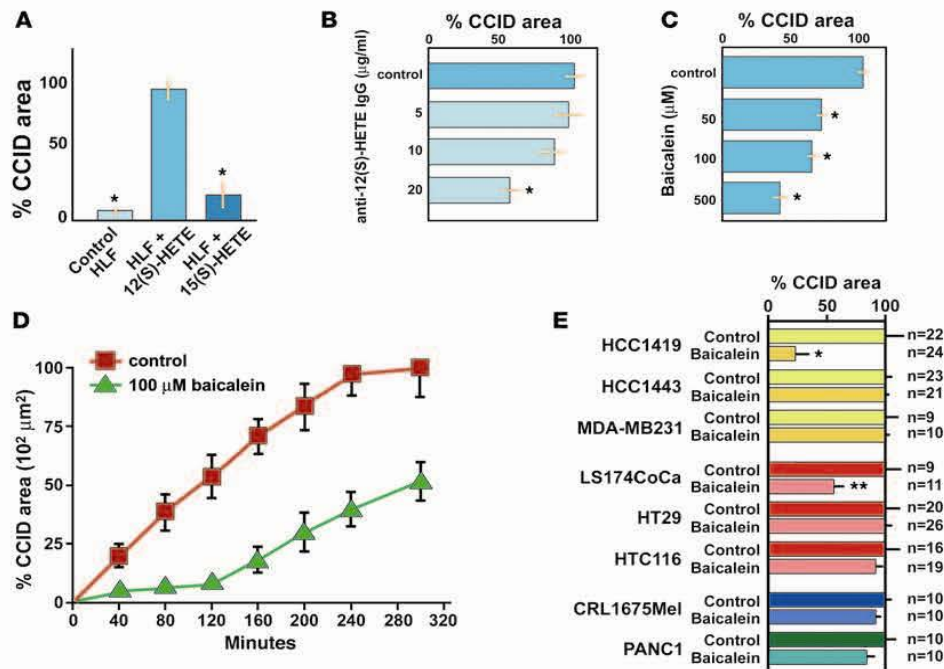


Figure 3
 12(S)-HETE causes CCIDs in lymphatic endothelial cell monolayers. (A) CCID area in lymphatic endothelial cell monolayers induced by HLF cell spheroids that were presoaked with synthetic 12(S)-HETE ($n = 11$), 15(S)-HETE ($n = 12$), or solvent alone (control; $n = 21$). 12(S)-HETE induced approximately 20 times larger CCIDs than controls ($*P < 0.0001$) after 4 hours of incubation. (B) Antibody against 12(S)-HETE reduces the CCID area by approximately 50% ($*P = 0.0020$). (C) The ALOX inhibitor baicalein, a traditional Asian anti-cancer drug, reduces CCID area in a dose-dependent fashion, with the highest dose of 500 μM ($n = 11$) causing reduction to 38% ($*P < 0.0001$) of controls ($n = 20$). (D) Time-course incubation over 4 hours with 100 μM baicalein in the media results in approximately 90% reduction of CCID size in the first 2 hours and a gradual increase in CCID formation to more than 50% after 4 hours. (E) Spheroids made of the mammary carcinoma cell lines HCC1419, HCC1443, and MDA-MB231 form spheroids that induce CCIDs in lymphatic monolayers, but only HCC1419 cell-mediated CCID formation is sensitive to 100 μM baicalein (inhibition of 78.2%; $*P = 0.0008$). Similarly, spheroids formed from colorectal carcinoma cell lines LS174CoCa, HT29, and HTC116 form CCIDs, but only LS174CoCa are baicalein sensitive (inhibition of 53.3%; $**P = 0.0168$). A melanoma (CRL1675MeI) and a pancreatic carcinoma cell line (PANC1) formed CCIDs in monolayers of lymphatic endothelial cells, but were insensitive (i.e., statistically not significant) to baicalein. All data are presented as mean \pm SEM.

VEGFC-overexpressing and unmodified MCF7 cells expressed *ALOX15* and formed CCIDs of similar size in lymphatic monolayers (Supplemental Figure 8). Stable transfection with luciferase (MCF7/*VEGFC/luc*) did not interfere with the expression of other transgenes (data not shown). MCF7/*VEGFC/ALOX15/luc* or control MCF7/*VEGFC/luc* cells that contained scrambled shRNA were injected orthotopically into mammary fat pads of SCID mice. After 32 days, tumors had formed in 100% of animals injected with control MCF7 cells, but only in 50% with MCF7/*VEGFC/ALOX15*-cells, presumably due to a less receptive microenvironment at the sites of injection, which showed minimal inflammatory infiltration in all cases. However, once established, the xenograft tumors of all MCF7/*VEGFC* cell variants showed similar growth rates, tumor cell turnover, weights, and intratumoral lymphatic vascular densities (Figure 6). At 32 days, 60% of animals in the control groups, but none of the mice bearing MCF7/*ALOX15*-xenograft tumors, had developed regional lymph node metastases (Figure 6). Sixty-three days after injection, we found lymph node metastases in 100% of control mice, but only in 5% of the MCF7/*ALOX15*-group. At this end point, the

weight of all primary xenograft tumors was similar, and the expression of *VEGFC* transgene and the *ALOX15* shRNA knockdown were unaltered (Figure 6). In xenograft tumors induced by cells of the *ALOX15*-expressing control groups, podoplanin⁺ and LYVE1⁺ intratumoral lymphatic vessels had formed that were distended and focally obliterated by tumor emboli at 32 days after injection (38, 39). In contrast, tumors composed of MCF7/*VEGFC/15LOX*-cells developed collapsed intratumoral lymphatic vessels that were devoid of embolic tumor cells (Figure 6). These *in vivo* results support the concept that *ALOX15*-driven production of 12(S)-HETE is required for formation of lymph node metastases, by facilitating the entry of tumor cells into intrametastatic lymphatic vessels.

ALOX15 and 12(S)-HETE in human metastases. The relevance of our experimental findings for the formation of human postsentinel lymph node metastases was underscored by immunohistochemical localization of 12(S)-HETE and of *ALOX15* in metastatic carcinoma cells in sentinel lymph nodes (Figure 7). This was extended and confirmed by further analysis of tissue arrays containing cores of primary tumors and their corresponding sentinel metastases from

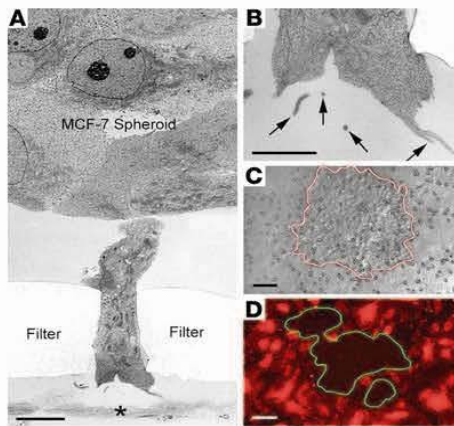


Figure 4

MCF7 tumor cell induced CCID formation in lymphatic monolayers from the abluminal side in Transwell inserts. MCF7 cell spheroids were placed onto the upper side of a filter that was covered by an LEC monolayer on its lower side so that the spheroids were separated from the lymphatic endothelial cells by the filter membrane. Coincubation was performed for 12 hours. **(A)** Low-power electron micrograph of a spheroid extending a "finger" through a filter pore. The LEC monolayer at the basal aspect of the filter shows only extracellular material and debris (*). **(B)** Higher magnification of the tip of the spheroid's extension, showing microvillar or vesicular (arrow) membrane structures, resembling shedding microparticles. **(C)** A spreading spheroid of MCF7 cells (outlined in red) on the upper face of the Transwell membrane. **(D)** At the opposite basal (abluminal) side of the Transwell membrane, a CCID (outlined in green) is formed in the monolayer of lymphatic endothelial cells (tagged red) precisely corresponding to the MCF7 spheroid on the luminal side. Scale bars: 1 μm (**A**); 0.2 μm (**B**); 50 μm (**C** and **D**).

13 patients with ductal carcinomas. These samples were precisely matched for staging pT1c and pN1a. Scoring of immunostaining for ALOX15 (Figure 7) provided evidence for a link between enzyme expression in lymph node metastases and the time of metastasis-free survival, and thus clinical outcome. A similar trend was also observed for the expression of ALOX12 (Supplemental Figure 9).

Discussion

The number of axillary lymph nodes that host metastases of mammary carcinomas is of predictive clinical significance. In this study, we have gained insights into the potential cellular and molecular events involved in metastatic tumor progression from the sentinel to the postsentinel axillary lymph nodes in human mammary carcinomas. This process involves premetastatic conditioning of axillary lymph nodes, invasion of tumor cells into the interconnecting lymphatic vessels, and eventually intranodal tumor cell arrest and proliferation.

Tumors programmed for lymph node metastasis have acquired a specific strategy for premetastatic adaptation of their regional lymph nodes (40, 41), which prominently involves expansion of lymph node sinus and transformation of their lining cells into lymphatic endothelia. This reaction is a stereotypic response to diverse stimuli that range from chemokines and growth factors to lymph congestion by mechanical obliteration of efferent lymphatic vessels (42, 43). However, it is of importance for formation of lymph node metastases and is referred to as *premetastatic lymph node lymphangiogenesis* (41). Moreover, lymphatic vessels develop *de novo* within the lymph node's metastatic colony and are frequently embolized by tumor cells that phenotypically correspond to cells of the metastasis and not to those in the primary tumors. Intrametastatic lymphangiogenesis occurs in all cases with postsentinel metastasis, and it is also present when the tumor is restricted to the sentinel lymph node. However, only when tumor cells have invaded and embolized the intrametastatic lymphatics do they spread to further lymph nodes downstream, as documented by a 100% correlation of embolization with postsentinel lymph node metastasis, which also applies to further tumor spreading from postsentinel metastases into more distal axillary lymph nodes. This also implies that the intrametastatic lymphatics are connected to the lymph node's efferent lymphatic vessels and is in line with recent experimental evidence (44). Collectively, these results indicate that tumor cell invasion of intrametastatic lymphatic vessels is crucial for lymphatic metastatic tumor dissemination.

These results raise the question of how the tumor cells get access into the intrametastatic lymphatic vasculature. Several pathways of tumor invasion into lymphatic vessels have been observed for different experimental and human tumors (45). One variant implies single tumor cell penetration between or even through endothelial cells, possibly also involving tumor cell epithelial-mesenchymal transition (21, 46, 47). In this investigation, we provide evidence for another pathway for mammary carcinomas similar to that previously described (45), which involves bulk invasion of metastatic tumor cells through large discontinuities of the lymphatic vessel wall. This pathway matches with recent experimental results obtained by *in vivo* microscopy in which xenografted mammary carcinoma cells spontaneously form mobile cohesive groups that preferentially invade into lymphatic vessels (24).

To gain insights into the mechanisms underlying lymphatic bulk invasion, we have adapted a reductionistic *in vitro* assay (25, 26) that mimics some features of the *in vivo* situation. In this system, tumor cell spheroids corresponded to invasive tumor aggregates *in vivo*, and in lieu of intrametastatic lymphatic vessels, we used monolayers of dermal lymphatic endothelial cells. This choice of endothelial cells was justified because a panel of typical lymphatic genes, including PROX1 and podoplanin, was expressed equally in both normal dermal and intrametastatic lymphatic endothelial cells. In contrast, we have noted that MCF7 cells altered their gene expression program upon spheroid formation and that this includes overexpression of the 12(S)-HETE-producing enzyme ALOX15. The human gene project has revealed 2 ALOX isoforms, ALOX15 and ALOX15B. ALOX15B produces 15(S)-HETE only, and there is no evidence that it plays a role in breast cancer pathology (48, 49). In contrast, ALOX15 also generates 12(S)-HETE, which is of relevance for various cancers, including mammary carcinomas (50).

12(S)-HETE was previously shown to increase malignant behavior of some tumors and to reduce it in others (51), and to increase endothelial cell motility and retraction of human umbilical cord endothelial cells (52). This has prompted us to investigate the role of 12(S)-HETE in our *in vitro* surrogate system of tumor bulk invasion. Our results show that 12(S)-HETE released by MCF7 tumor spheroids induced CCIDs that were formed by centrifugal migration of lymphatic endothelial cells just beneath spheroids. It is possible that this local restriction of endothelial cell mobility could be due to the hydrophobicity

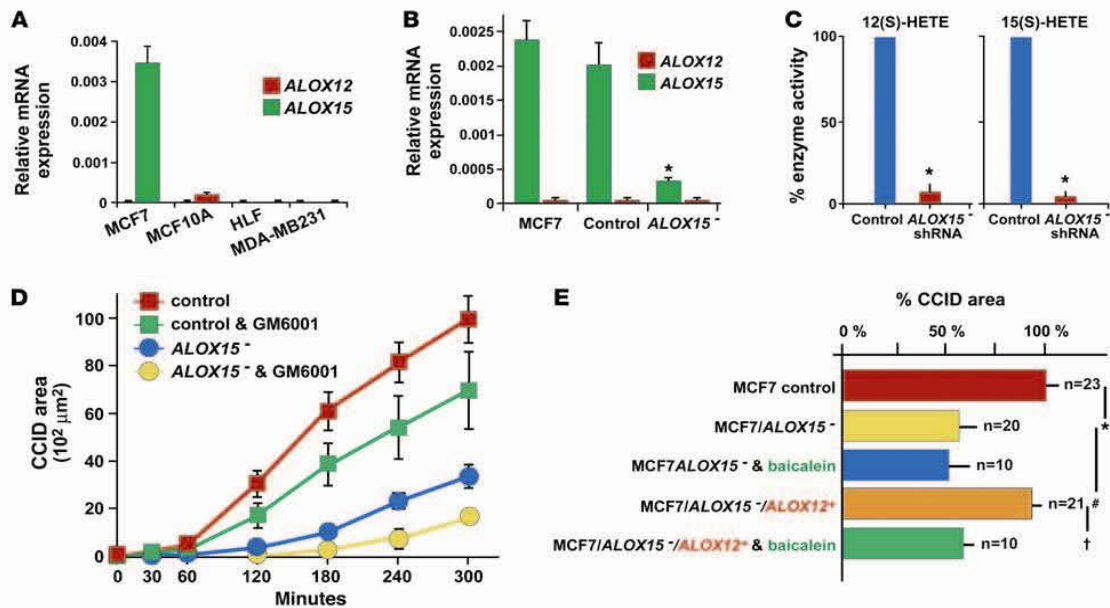


Figure 5 shRNA-mediated knockdown and rescue of lipoxygenase in MCF7 cells. (A) The expression of mRNAs of *ALOX15* and *ALOX12* was determined by real-time PCR in MCF7 and MDA-MB231 mammary carcinoma cells and in controls (noncancerous breast epithelial cells MCF-10A and HLFs). MCF7 cells express only *ALOX15* mRNA, but not *ALOX12* mRNA, whereas all other cells fail to produce any of the tested *ALOXs*. (B) mRNA levels of *ALOX15* were determined in unmodified MCF7 cells, in control MCF7 cells transfected with scrambled shRNA, and in MCF7/*ALOX15*⁻ cells. Knockdown of *ALOX15* reduced the expression of *ALOX15* mRNA significantly ($*P = 0.0009$ compared with vector control) when compared with unmodified or control transfected MCF7 cells. (C) Production of 12(S)-HETE and 15(S)-HETE, the arachidonic acid metabolites of *ALOX15*, is reduced by more than 90% in MCF7/*ALOX15*⁻ cells when compared with control MCF7 cells that were transfected with scrambled shRNA ($*P > 0.0001$). (D) shRNA-mediated knockdown of *ALOX15* in MCF7 cells (blue line) causes a size reduction similar to that of baicalein in CCID (compare to Figure 3D). This is further aggravated by coincubation with 20 μM of the pan-metalloprotease inhibitor GM6001 (yellow line), which had a similar effect (green line) on controls (MCF7 cells transfected with scrambled shRNA, red line). (E) Reconstitution of CCID-forming activity of MCF7/*ALOX15*⁻ cells by transfection with *ALOX12*. MCF7 spheroid-induced CCID formation is analyzed in the presence or absence of 100 μM baicalein. There is a significant difference in CCID size between MCF7/control versus MCF7/*ALOX15*⁻ spheroids ($*P = 0.0017$), MCF7/*ALOX15*⁻ versus MCF7/*ALOX15*⁻/*ALOX12*⁺ spheroids ($*P = 0.0249$), and MCF7/*ALOX15*⁻/*ALOX12*⁺ spheroids \pm baicalein treatment ($\dagger P = 0.0331$). All data are presented as mean \pm SEM.

of 12(S)-HETE that could be released in poorly diffusing membrane microvesicles above its critical micellar concentration (53). However, the actual concentration of 12(S)-HETE in the micromilieu at the spheroid tumor endothelial interface remains to be determined (54). 12(S)-HETE was not toxic for lymphatic endothelial cells, and accordingly, we failed to encounter apoptotic endothelial cells in association with CCIDs. The significance of 12(S)-HETE was confirmed by blocking of CCID formation by a specific antibody or by shRNA-mediated knockdown of the producing enzyme *ALOX15*. The ability to cause CCIDs was restored by knocking in of *ALOX12*, which also produces 12(S)-HETE and is not expressed in MCF7 cells. 15(S)-HETE, the alternative arachidonic acid metabolite produced by *ALOX15*, was ineffective. CCID formation was further supported by metalloproteases that loosen the meshwork of VE-cadherin at interendothelial junctions and matrix attachment (36, 37). Taken together, our *in vitro* findings suggested a hitherto unknown dominant role for *ALOX15* and its product 12(S)-HETE in tumor cell-lymphatic endothelial cell interaction. When we extrapolate these *in vitro* findings to the vascular

defects we have observed at sites of tumor cell bulk invasion, it is possible that induction of lymphatic endothelial migration and focal disruption of interendothelial adhesion (e.g., by destabilization of VE-cadherin) could contribute to focal openings in the vascular wall.

Intriguingly, blood endothelial cells were much less sensitive to the migration-inducing effect of 12(S)-HETE than lymphatics. It remains to be determined whether or not this is due to differences in receptor- or nonreceptor-mediated effects. So far, several proteins have been implicated in binding of 12(S)-HETE; however, a definitive universal receptor or receptors are still elusive. We have screened for the expression of 2 putative 12(S)-HETE membrane protein receptors – the leukotriene B₄ receptor (55) and the orphan receptor GPR31 (56) (data not shown) – and failed to detect expression differences between blood and lymphatic endothelial cells. Thus, our results show that 12(S)-HETE preferentially caused CCID formation in lymphatic endothelial monolayers, either by direct interaction with so-far elusive lymphatic receptor or receptors, or indirectly, via currently unidentified intermediaries.

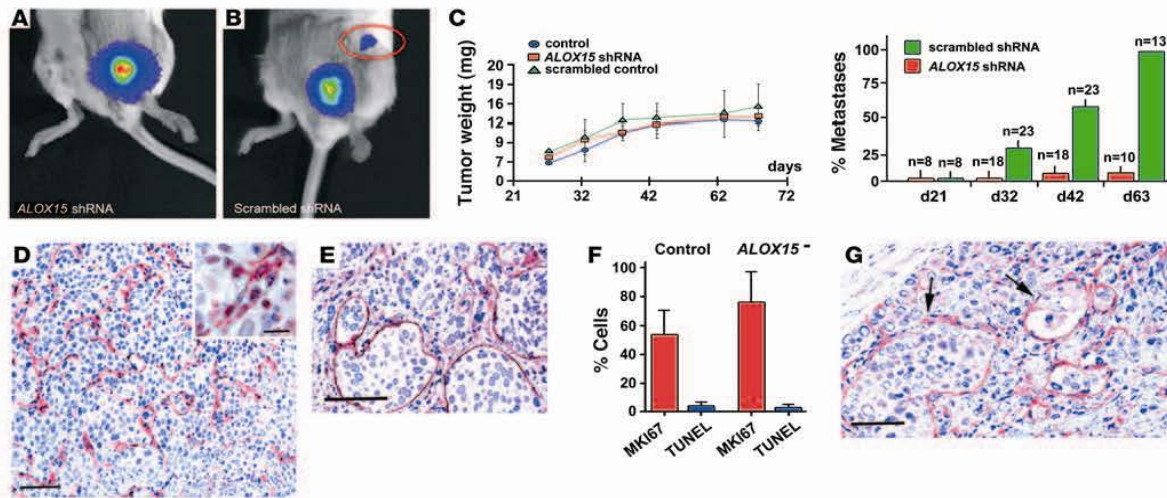


Figure 6

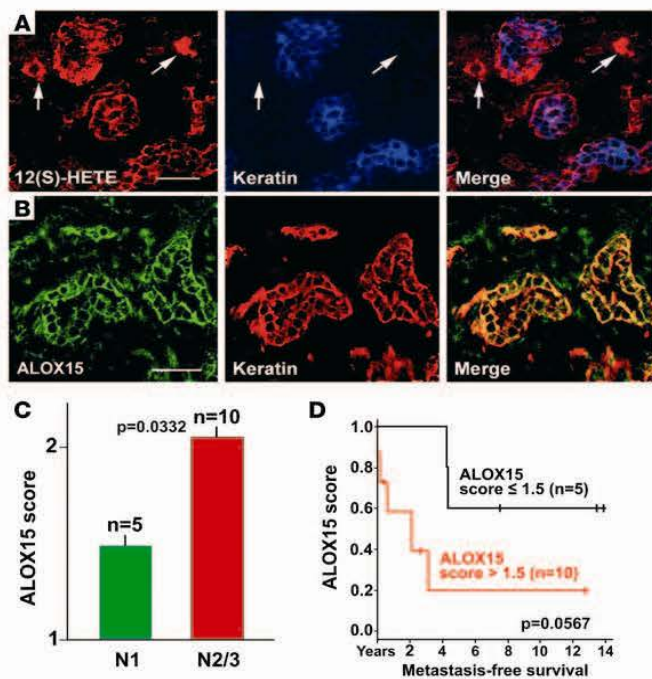
Xenograft tumors induced by *ALOX15* shRNA knockdown cells and control MCF7/VEGFC cells expressing luciferase as reporter. **(A)** Bioluminescence image of a xenograft tumor induced by cells that lack *ALOX15* after injection into the fifth mammary fat pad failed to develop lymph node metastases after 32 days. **(B)** Image of a xenograft tumor induced by control MCF7/VEGFC cells that were transfected with scrambled shRNA and expressed *ALOX15*, showing a regional lymph node metastasis (red circle). **(C, left panel)** The sizes and growth rates of all xenograft tumors, irrespective of the nature of the inoculated tumor cells (MCF7/VEGFC, or MCF7/VEGFC cells transfected with scrambled or *ALOX15* shRNA) were similar. **(C, right panel)** Time course of metastasis formation of xenograft tumors induced by MCF7/VEGFC cells transfected with *ALOX15* shRNA (red) or with control scrambled shRNA (green) showing that *ALOX15*-deficient MCF7/VEGFC were incompetent of metastasis formation. **(D)** Representative picture of a xenograft tumor (same as depicted in **A**). The tumor cells fail to invade into the collapsed intratumoral podoplanin⁺ lymphatic vessels (red). Insert, tumor embolus-free intratumoral lymphatic vessel with a narrow lumen. **(E and G)** Xenograft tumor of the control group (same as in **B**) showing massive tumor intravasation into dilated lymphatic vessels (arrows) that were immunostained for LYVE1 **(E)** or podoplanin **(G)**. **(F)** Growth rates of xenograft tumor MCF7/VEGFC and MCF7/VEGFC/*ALOX15*⁻ cells were determined by labeling for MKI67 (Ki-67) or by the TUNEL assay. Image analysis revealed a higher (but not significant) MKI67 positivity in *ALOX15*⁻ tumors compared with control tumors. The rate of apoptosis was similar in both primary tumor types. *n* = 6. Total number of counted nuclei was greater than 2000. Scale bars: 70 μ m (**D, E, and G**); 20 μ m (inset). All data are presented as mean \pm SEM.

Our results apply primarily to ductal mammary carcinomas that are represented in vitro by MCF7 and HCC1419 cells derived from estrogen receptor-positive ductal carcinomas of the luminal subtype (57). However, only 50% of the lobular mammary carcinomas followed this pattern of tumor spreading. Baicalein-insensitive CCIDs were formed by MDA-MB321 and HCC1443 mammary carcinoma cells that are derived from estrogen receptor-negative ductal carcinomas of the basal subtype and lack ALOXs. This is in contrast to our findings in human tumors and could be due to changes induced by in vitro culturing. Furthermore, the CCID assay suggested that tumors derived from other organs apparently use LOX-independent mechanisms. These include most colorectal carcinomas, melanomas, and a pancreatic cancer. Thus, there is no universal mechanism by which different types of tumors form and propagate lymph node metastases. They apparently also have at their disposal *ALOX15*-independent mechanisms to enter lymphatic vessels and do not use bulk but rather single-cell invasion, with or without epithelial-mesenchymal transition, possibly depending on TGF- β (24).

These results required verification in a tumor xenograft model that mimics the key findings in sentinel lymph node metastases, i.e., formation of intratumoral lymphatic vessels, bulk invasion of tumor cells, lymphatic embolization, and formation of lymph node metastases. A suitable model for this in vivo proof of principle was found in mouse xenograft tumors produced

by human mammary carcinoma MCF7 cells that transgenically overexpress VEGFC (38, 39). This transforms MCF7 cells from nonmetastatic into highly metastatic, with intratumoral lymphangiogenesis, lymph vessel invasion, and embolization, i.e., analogous to human sentinel lymph node metastases. Moreover, we found that MCF7 cells express only a single lipoxygenase, *ALOX15*, and are thus ideally suited for studying the contribution of this enzyme to CCID. shRNA-induced knockdown of *ALOX15* efficiently repressed formation of lymph node metastases. Intratumoral lymphatic vessels were induced both in the control and the *ALOX15* knockdown xenografted tumors. However, in *ALOX15*-deficient tumors, the lymphatics were collapsed and empty and tumor cells failed to invade and form emboli, in striking contrast to *ALOX15*-expressing and 12(S)-HETE-producing control MCF7 cells. However, we cannot exclude the possibility that the absence of LOX products alters the lymphatic endothelial phenotype to make it less permissive to tumor cell invasion in general.

Here we have brought together 3 correlative observations, i.e., the embolization and invasion of mammary carcinoma cells into intrametastatic lymphatics in human tissues, the 12(S)-HETE-driven formation of CCIDs in vitro, and the important role of the 12(S)-HETE-producing enzyme, *ALOX15*, for lymph node metastasis formation in mouse xenograft models.

**Figure 7**

12(S)-HETE and ALOX15 in human sentinel metastases. (A) Localization of 12(S)-HETE (red) in the mammary carcinoma cells in a representative sentinel lymph node of a patient with postsentinel lymph node metastasis (total examined: $n = 12$). 12(S)-HETE colocalizes with tumor cell keratin (blue and merge) and is also expressed by nontumor, presumably inflammatory cells (arrows). (B) The 12(S)-HETE-producing enzyme ALOX15 shows a localization similar to that of its product (ALOX15: green; keratin: red). (C) Results of the tissue array scoring of the immunostaining for ALOX15 in the tumor cells of the sentinel metastasis in 15 cases of ductal carcinoma. In 5 cases without postsentinel metastases, the score is lower (N1, green column) than in 10 cases with postsentinel spreading (N2/3, red column). (D) Metastasis-free survival correlates inversely with the expression of ALOX15 in the tumor cells of the sentinel lymph nodes ($P = 0.0507$). Scale bars: 50 μm . All data are presented as mean \pm SEM.

Taken together, these complementary results favor the hypothesis that 12(S)-HETE-mediated CCID formation is a central event for accession of mammary carcinoma cells into the lymphatic vasculature in sentinels and thus furthers tumor spreading into postsentinel lymph nodes (Supplemental Figure 10).

Do these potential mechanisms of intrametastatic lymphatic invasion also apply to human patients? Our results suggest that this is feasible. Metastatic tumor cells in sentinel lymph nodes of human mammary carcinomas express all the key players, ALOX12, ALOX15, and 12(S)-HETE. In feasibility studies using tissue microarrays of a relatively small number of carefully matched human samples, we found that the abundance of ALOXs is inversely correlated with metastasis-free survival. Pharmacological ALOX inhibition has previously been recognized as antimetastatic and proapoptotic (58, 59) therapy for mammary and other carcinoma cells. Here we show the CCID-reducing efficiency of the ALOX inhibitor baicalein (34), a polyflavone isolated from the roots of *Scutellaria baicalensis* and still applied in traditional Asian medicine. Thus, our findings could hold the potential that inhibition of ALOX interferes with lymphatic dissemination of ductal mammary carcinomas. Formal clinical studies are required to determine whether or not ALOXs in mammary carcinomas can be used as biomarkers and potential therapeutic targets.

Methods

Selection of cases and tissue samples. Use of human tissue samples and experimental mouse models was approved by the Ethical Committee of the Medical University of Vienna (Approval EK-Nr 270/2006) in compliance with Austrian legislation. We have selected 104 archival cases of mammary carcinomas, classified as NOS, with 69 cases of ductal and 35 of lobular subtype. The patients had not received preoperative neoadjuvant

therapy. The primary tumors were matched by their diameters ($pT1c$, $1-2 \pm 0.6$ cm), availability of the sentinel, and, when clinically indicated, also postsentinel axillary lymph nodes. Further inclusion criteria were similar sizes of sentinel lymph node metastases ($pN1a$, > 2 mm) and documented follow-up periods of 55 months after surgery. The tumor grading is listed in Table 1. The tumors were also subclassified by immunohistochemistry as luminal, basal, or ERBB2 enriched (22). Sentinel lymph nodes were free of tumors (stage $pN0$, $n = 16$) (11), or metastasis was restricted to the sentinel lymph node only ($pN1a$, $n = 56$), or also involved additional postsentinel axillary lymph nodes ($pN2$ or 3, $n = 32$). All tumors were analyzed for the expression of estrogen and progesterone receptors, the overexpression of ERBB2, and in some cases also for keratins, CD133, CD44, and aldehyde dehydrogenase (60, 61). As controls, naive nontumor-associated lymph nodes were used that were removed during carotid angioplasty or abdominal surgery ($n = 16$). These nonactivated lymph nodes were devoid of capsular fibrosis, intranodal scars, or activation of germinal centres.

Immunohistochemistry. 4- μm -thick freshly prepared sections from archival paraffin blocks for immunolabeling were processed as described previously (62) using rabbit anti-human podoplanin IgG (5 $\mu\text{g/ml}$) or with a monoclonal mouse IgG (Bender Med Systems BMS 1105; 1 $\mu\text{g/ml}$), and anti-human PROX1 rabbit IgG (AngioBio). Some sections were also incubated after podoplanin labeling with monoclonal mouse anti-Ki67 IgG (MIB-1) or anti-human LYVE1 rabbit IgG (DAKO). Rabbit antibodies to 12(S)-HETE (Assay Designs), with less than 2.5% cross-reactivity with 12(R)-HETE and less than 0.3% with 15(S)- and 5(S)-HETE, and ALOX12 and ALOX15 (Abcam) were used on cryostat sections of unfixed primary carcinomas and their sentinel metastases ($n = 12$). For immunofluorescence, we used appropriate secondary antibodies labeled with Alexa Fluor 488, Alexa Fluor 594, or Alexa Fluor 633 (Molecular Probes). Double-labeling experiments were controlled



by omitting the primary antibodies or by replacement with irrelevant antibodies raised in the same species or of the same mouse IgG subtype. The densities of lymphatic vessels were determined in duplicate by 3 independent observers on unmarked histological sections. We counted the number of lymphatic vessel profiles in at least 30 microscopic fields for each slide, using an objective lens with $\times 25$ magnification. Inter- and intra-observer variations resulted in a “background noise” of 1 vessel per field, and only counts above this threshold were entered into the evaluation. Statistical significance was determined by the *t* test, using the Prism 4 software package (GraphPad). Production and composition of tissue microarrays were performed as described (63). We have carefully selected 15 cases of ductal carcinomas with the identical stages pT1c, pN1a ($n = 10$), and pT1c, pN2/3 ($n = 5$).

Isolation and characterization of human dermal lymphatic endothelial cells. Human lymphatic endothelial cells and blood vessel endothelial cells were prepared from commercial (C-12260; PromoCell) or freshly prepared dermal microvascular endothelial cells by sorting with anti-podoplanin and anti-CD31 IgG using Dynabeads (M-280; Dynal 11203) or FACS (FaxStar), as described (64). Also, telomerase “immortalized” lymphatic endothelial cells were used (27). No differences in the expression of other proteins previously thought to distinguish lymphatic vessels outside and within tumors (biglycan, endoglin, CD34, VE-cadherin) were found (Supplemental Figure 4C).

Determination of 12(S)-HETE. 12(S)-HETE and 15(S)-HETE were determined by a reverse-phase high-performance liquid chromatography method (RP-HPLC), as described (65).

Spheroid preparation. Cell spheroids were prepared as described in preliminary experiments (25, 26). Briefly, MCF7 cells were grown in McCoy 5A medium containing 10% fetal calf serum and 1% penicillin/streptomycin (Gibco-BRL; Invitrogen). Noncancerous MCF-10A breast epithelial cells were grown in MEGM medium (CC-3150; Clonetic Bullet Kit) supplemented with bovine pituitary extract, human epithelial growth factor, hydrocortisone, insulin, 1% penicillin/streptomycin, and 10 μ M isotretinoin. Normal HLFs were grown in nonessential amino acid media containing 10% fetal calf serum and 1% penicillin/streptomycin and 1% nonessential amino acids.

Low-density real-time PCR arrays. Template cDNAs prepared from total RNA of MCF7 cells grown as monolayer or spheroid were characterized in triplicates using the Human Extracellular Matrix and Adhesion Molecules PCR Array (SABiosciences) and the RT2 SYBR Green/Fluorescein qPCR Master Mix (SABiosciences) on the Chromo4 PCR System (Bio-Rad), following the manufacturer’s instructions. The resulting Ct values were analyzed by using the RT2 Profiler PCR Array Data Analysis Template v3.2 (SABiosciences). Genes not included on the low-density real-time array were analyzed by using the following FAM probes obtained from Applied Biosystems: *VEGFA* Hs00173626_m1, *ALOX15* Hs00609608_m1, *ALOX12* Hs00167524_m1, and *ALOX12B* Hs00153961_m1.

MCF-7 spheroid/LEC monolayer cocultivation. In all experiments, telomerase-“immortalized” lymphatic endothelial cells (27) or freshly prepared lymphatic endothelial cells (64) (maximal 6 passages) were used, with identical results. Lymphatic endothelial cells were seeded in EGM2MV medium on 24-well plates and allowed to grow to confluence. Then, the lymphatic endothelial cells (LECs) monolayers were stained with Cytotracker green (2 μ g/ml, C2925; Molecular Probes) or Hoechst 33258 (5 μ g/ml, H1398; Sigma-Aldrich) at 37 °C for 90 minutes. Into each well, 10 MCF7 spheroids were transferred. During the cocultivation period, frames were taken at 15-minute intervals with an inverse fluorescence microscope (Zeiss Axio-phot) and composed to a time-lapse video. Some preparations were examined in a Zeiss confocal fluorescence microscope.

Transwell culture. Primary or telomerase-immortalized lymphatic endothelial cells were grown on the lower surface of Transwell inserts (membrane diameter 6.5 mm; pore size 8 μ m, precoated with 10 μ g/ml fibronectin; Costar) until confluent. Then lymphatic endothelial cells were stained with Cytotracker as described above, and tumor cell spheroids were placed onto the upper surface. Cocultivation was performed for 24 hours, with fluorescence microscopic control of the LEC monolayer every 180 minutes.

Analysis of CCID formation. Areas of LEC monolayers beneath spheroids were photographed in an Axiovert (Zeiss) fluorescence microscope, using the FITC filter to visualize Cytotracker-stained (green) lymphatic endothelial cells, and the area of CCIDs was measured using Axiovision software (Zeiss).

shRNA knockdown of ALOX15. Lentiviral particles containing shRNA targeting the human *ALOX15* mRNA (SHCLNV-NM_001140) and controls with nonsense shRNA (SHC002V) were obtained from Sigma-Aldrich. MCF7 cells that transgenically overexpress *VEGFC* (38) were seeded onto 24-well plates, and transduced with 2e5 TU in 250 μ l MEM containing 10% FCS and 8 μ g polybrene/ml by spin infection at 1500 g at 32 °C for 90 minutes. After incubation for 12 hours, the cells were reseeded onto 100-mm culture plates and selected with 1 μ g/ml puromycin for 1 week. Single cell colonies were tested for knockdown efficiency by real-time PCR, normalizing gene expression to the housekeeping gene *GAPDH*.

Knockin of ALOX12 cDNA. N-terminal V5-tag was fused to the *ALOX12* full-length cDNA. The fusion was constructed by PCR (5’ primer: TCAGATCCGCTAGCGGGCGCCATGGGTAAGCCTATCCCTAACCCCTCCTCGGTCTCGATTCTACGGGCGCTACCGCATCCGCGTGGCCA, 3’ primer: GGTGGCGCGCCGCTCAGATGGTGACACTGTTCTCTATGCAGCTGGG) using standard PCR conditions and an *ALOX12*-containing expression plasmid (gift from Brigitte Marian, Cancer Research Institute, Vienna, Austria) as template. The primer pair contained 5’ Nhe-I and 3’ Not-I linkers and the PCR product was directly subcloned into pTag-CFP-N (Evrogen) by replacing CFP with the tagged fusion construct. The resulting vector DNA was controlled by sequencing and proper expression of the target gene by Western blotting with a V5-tag antibody (Invitrogen) using total lysates of transfected cells.

Xenograft tumors. For xenografting, 10⁷ MCF7 cells or their derivatives were dispersed in 30 μ l PBS and injected orthotopically into the fat pads of the fifth mammary glands of 8-week-old female SCID mice (Harlan Animal Research Laboratory). 60-day slow-release pellets containing 0.72 mg of 17 β -estradiol (Innovative Research of America) were implanted 48 hours previously. Primary tumor growth and formation of metastases were monitored at 10-day intervals by noninvasive bioluminescence imaging using a highly sensitive CCD camera (IVIS 100; Caliper Life Sciences). 150 μ g D-luciferin/g of body weight (firefly, potassium salt; Caliper Life Sciences) was injected intraperitoneally. Bioluminescence signals were acquired 18 minutes after application, and normalized signals (photons/sec/cm²/sr) were evaluated and quantified using Living Image Software (Caliper Life Sciences); the tumor weight was calculated from a calibration curve. The experiment was terminated after 63 days, and primary tumors and lymph node metastases were processed for anti-podoplanin immunohistochemistry or for mRNA determination of *VEGFC*, *ALOX12*, and *ALOX15*, shRNAs, and luciferase. Paraffin sections of formalin-fixed tissues were labeled by the TUNEL assay (Chemicon), MKI67 (KI-67, Novo Castra NCL-Ki67p), and cytokeratin (DAKO Z0622). Fluorescence microscopy was performed on an Axio-phot microscope equipped with an AxioCam Colour camera (Zeiss) at a standard magnification of 250. Images were analyzed using ImageJ software package 1.42q (Wayne Rasband, NIH; <http://rsb.info.nih.gov/ij>).



Statistics. We have used a 2-tailed *t* test for statistical analysis of the experimental data. $P < 0.05$ was considered significant. All data are presented as mean \pm SEM. The human correlative data were expressed by Kaplan-Meier statistics.

Acknowledgments

This work was supported in part by European Community project LSHG-CT-2004-503573 (Lymphangiogenomics) (to D. Kerjaschki and K. Alitalo); a research fund from the Keyaki-kai Medical Corporation, Tokyo, Japan (to H. Nosaka); by the GenAU project Drug Action by Genomic Networks (DRANGON) (to V. Sexl); by Fonds für Innovative und Interdisziplinäre Krebsforschung der Gemeinde Wien (to G. Krupitza); and by the Austrian Breast and Colorectal Cancer Study Group (ABCSG) (to M. Gnant and M. Rudas). We thank A. Rees for reading the manuscript and A. Jaeger for help with the graphic work.

Received for publication August 13, 2010, and accepted in revised form February 2, 2011.

Address correspondence to: Dontscho Kerjaschki, Clinical Department of Pathology, Allgemeines Krankenhaus Wien, Medical University of Vienna; Waehringer Guertel 18-20, A 1090 Vienna, Austria. Phone: 431.40400.5176; Fax: 431.40400.5193; E-mail: dontscho.kerjaschki@meduniwien.ac.at.

Gregor Bartel's present address is: Department of Internal Medicine III, Medical University of Vienna, Vienna, Austria.

Veronika Sexl's present address is: Department of Pharmacology, Veterinary Medical University, Vienna, Austria.

Hitonari Nosaka's present address is: Department of Internal Medicine, Teikyo University, Tokyo, Japan.

Monika Hämmerle's present address is: Department of Pathology, University of Heidelberg, Heidelberg, Germany.

Helmut Dolznig's present address is: Department of Medical Genetics, Medical University of Vienna, Vienna, Austria.

- Fidler IJ. The pathogenesis of cancer metastasis: the "seed-and-soil" hypothesis revisited. *Nat Rev Cancer*. 2003;3(6):453-458.
- Psaila B, Lyden D. The metastatic niche: adapting the foreign soil. *Nat Rev Cancer*. 2009;9(4):285-293.
- Metha P. Potential role of platelets in the pathogenesis of tumor metastasis. *Blood*. 1984;63(1):55-63.
- Tammela T, Alitalo K. Lymphangiogenesis: Molecular mechanisms and future promise. *Cell*. 2010;140(4):460-476.
- Byles J, et al. Tumor cells disseminate early, but immunosurveillance limits metastatic outgrowth, in a mouse model of melanoma. *J Clin Invest*. 2010;120(6):2030-2039.
- Müller-Hermelink N, et al. TNFR1 signaling and IFN-gamma signaling determine whether T-cells induce tumor dormancy or promote multistage carcinogenesis. *Cancer Cell*. 2008;13(6):507-518.
- Tait CR, Dodwell D, Horgan K. Do metastases metastasize? *J Pathol*. 2004;203(1):515-518.
- Norton L, Massagué J. Is cancer a disease of self-seeding? *Nat Med*. 2006;12(8):875-878.
- Ben-Porath I, et al. An embryonic stem cell-like gene expression signature in poorly differentiated aggressive human tumors. *Nat Genet*. 2008;40(5):499-507.
- Carlson RW, et al. Breast cancer. Clinical practice guidelines in oncology. *J Natl Compr Canc Netw*. 2009;7(2):122-192.
- Sobin LH, Gospodarowicz MK, Wittekind C, eds. *TNM Classification of Malignant Tumours (UICC International Union Against Cancer)*. New York, New York, USA: Wiley-Blackwell; 2009.
- Britton TB, Solanki CK, Pinder SE, Mortimer PS, Peters AM, Purushotham AD. Lymphatic drainage pathways of the breast and the upper limb. *Nucl Med Commun*. 2009;30(6):427-430.
- Van den Eynden G, et al. Increased sentinel lymph node lymphangiogenesis is associated with non-sentinel axillary lymph node involvement in breast cancer patients with a positive sentinel node. *Clin Cancer Res*. 2007;13(18 pt 1):5391-5397.
- Breiteneder-Geleff S, et al. Angiosarcomas express mixed endothelial phenotypes of blood and lymphatic capillaries: podoplanin as a specific marker for lymphatic endothelium. *Am J Pathol*. 1999;154(2):385-394.
- Banerji S, et al. LYVE1, a new homologue of the CD44 glycoprotein, is a lymph-specific receptor for hyaluronan. *J Cell Biol*. 1999;144(4):789-801.
- Wigle JT, Oliver G. Prox1 function is required for the development of the murine lymphatic system. *Cell*. 1999;98(6):769-778.
- Marinho VF, Metzke K, Sanches FS, Rocha GF, Gobbi H. Lymph vascular invasion in invasive mammary carcinomas identified by the endothelial lymphatic marker D2-40 is associated with other indicators of poor prognosis. *BMC Cancer*. 2008;8:64.
- Van den Eynden GG, et al. Induction of lymphangiogenesis in and around axillary lymph node metastases of patients with breast cancer. *Br J Cancer*. 2006;95(10):1362-1366.
- Hirakawa S, Kodama S, Kunstfeld R, Kajiji K, Brown LF, Detmar M. VEGFA induces tumor and sentinel lymph node lymphangiogenesis and promotes lymphatic metastasis. *J Exp Med*. 2005;201(7):1089-1099.
- Schoppmann SF, et al. Tumor-associated macrophages express lymphatic endothelial growth factors and are related to peritumoral lymphangiogenesis. *Am J Pathol*. 2002;161(3):947-956.
- Hirakawa S, et al. Nodal lymphangiogenesis and metastasis: Role of tumor-induced lymphatic vessel activation in extramammary Paget's disease. *Am J Pathol*. 2009;175(5):2235-2248.
- Sotiriou C, et al. Breast cancer classification and prognosis based on gene expression profiles from a population-based study. *Proc Natl Acad Sci U S A*. 2003;100(18):10393-10398.
- Bertucci F, et al. Lobular and ductal carcinomas of the breast have distinct genomic and expression profiles. *Oncogene*. 2008;27(40):5359-5372.
- Giampieri S, Manning C, Hooper S, Jones L, Hill CS, Sahai E. Localized and reversible TGFbeta signalling switches breast cancer cells from cohesive to single cell motility. *Nat Cell Biol*. 2009;11(11):1287-1296.
- Offner FA, et al. Interaction of human malignant melanoma tumor spheroids with endothelium and reconstituted basement membrane: modulation by RGDS. *Int J Cancer*. 1993;54(3):506-512.
- Madlener S, et al. Multifactorial anticancer effects of digalloyl-resveratrol encompass apoptosis, cell cycle arrest, and inhibition of lymphendothelial gap formation in vitro. *Br J Cancer*. 2010;102(9):1361-1370.
- Schoppmann SF, et al. Telomerase-immortalized lymphatic and blood vessel endothelial cells are functionally stable and retain their lineage specificity. *Microcirculation*. 2004;11(3):261-269.
- Matsumura F, Hartschorne DJ. Myosin phosphatase target subunit F: Many roles in cell function. *Biochem Biophys Res Commun*. 2008;369(1):149-156.
- Hultén LM, et al. 15-Lipoxygenase-2 is expressed in macrophages in human carotid plaques and regulated by hypoxia-inducible factor-1alpha. *Eur J Clin Invest*. 2010;40(1):11-17.
- Funk CD. The molecular biology of mammalian lipoxygenases and the quest for eicosanoid functions using lipoxygenase-deficient mice. *Biochim Biophys Acta*. 1996;1304(1):65-84.
- Subbarayan V, et al. Inverse relationship between 15-lipoxygenase-2 and PPAR-gamma gene expression in normal epithelia compared with tumor epithelia. *Neoplasia*. 2005;7(3):280-293.
- Honn KV, et al. Tumor cell-derived 12(S)-hydroxyeicosatetraenoic acid induces microvascular endothelial cell retraction. *Cancer Res*. 1994;54(2):565-574.
- Funk CD. Lipoxygenase pathways as mediators of early inflammatory events in atherosclerosis. *Arterioscler Thromb Vasc Biol*. 2006;26(6):1204-1206.
- Li-Weber M. New therapeutic aspects of flavones: the anticancer properties of Scutellaria and its main active constituents Wogonin, Baicalin and Baicalin. *Cancer Treat Rev*. 2009;35(1):57-68.
- González-Núñez D, Claria J, Rivera F, Poch E. Increased levels of 12(S)-HETE in patients with essential hypertension. *Hypertension*. 2001;37(2):334-338.
- Deryugina EI, Quigley JP. Matrix metalloproteinases and tumor metastasis. *Cancer Metastasis Rev*. 2006;25(1):9-34.
- Baker AH, Edwards DR, Murphy G. Metalloproteinase inhibitors: biological actions and therapeutic opportunities. *J Cell Sci*. 2002;115(pt 19):3719-3727.
- Karpanen T, et al. Vascular endothelial growth factor C promotes tumor lymphangiogenesis and intralymphatic tumor growth. *Cancer Res*. 2001;61(5):1786-1790.
- He Y, et al. Vascular endothelial cell growth factor receptor 3-mediated activation of lymphatic endothelium is crucial for tumor cell entry and spread via lymphatic vessels. *Cancer Res*. 2005;65(11):4739-4746.
- Ran S, Volk L, Hall K, Plister MJ. Lymphangiogenesis and lymphatic metastasis in breast cancer. *Pathophysiology*. 2010;17(4):229-251.
- Mumprecht V, Detmar M. Lymphangiogenesis and cancer metastasis. *J Cell Mol Med*. 2009;13(8A):1405-1416.
- Steinmann G, Földi E, Földi M, Rácz P, Lennert K. Morphologic findings in lymph nodes after occlusion of their efferent lymphatic vessels and veins. *Lab Invest*. 2009;47(1):43-50.
- Angeli V, et al. B cell-driven lymphangiogenesis



- in inflamed lymph nodes enhances dendritic cell mobilization. *Immunity*. 2006;24(2):203-215.
44. Harrell MI, Iritani BM, Ruddell A. Tumor-induced sentinel lymph node lymphangiogenesis and increased lymph flow precede melanoma metastasis. *Am J Pathol*. 2007;170(2):774-786.
 45. Carr I. Lymphatic metastasis. *Cancer Metastasis Rev*. 1983;2(3):307-317.
 46. Azzali G. Tumor cell transendothelial passage in the absorbing lymphatic vessel of transgenic adenocarcinoma mouse prostate. *Am J Pathol*. 2007;170(1):334-346.
 47. Yang J, et al. Twist, a master regulator of morphogenesis, plays an essential role in tumor metastasis. *Cell*. 2004;117(7):927-939.
 48. Tang DG, Bhatia B, Tang S, Schneider-Broussard R. 15-lipoxygenase 2 (15-LOX2) is a functional tumor suppressor that regulates human prostate epithelial cell differentiation, senescence and growth (size). *Prostaglandins Other Lipid Mediat*. 2007;82(1-4):135-146.
 49. Brash AR, Boeglin WE, Chang MS. Discovery of a second 15S-lipoxygenase on humans. *Proc Natl Acad Sci U S A*. 1997;94(12):6148-6152.
 50. Jiang WG, Douglas-Jones A, Mansell RE. Levels of expression of lipoxygenases and cyclooxygenase 2 in human breast cancer. *Prostaglandins Leukot Essent Fatty Acids*. 2003;69(4):275-281.
 51. Bhattacharya S, Mathew G, Jayne DG, Pelengaris S, Khan M. 15-lipoxygenase-1 in colorectal cancer: a review. *Tumour Biol*. 2009;30(4):185-199.
 52. Honn KV, et al. Enhanced endothelial cell retraction mediated by 12(S)-HETE: a proposed mechanism for the role of platelets in tumor cell metastasis. *Exp Cell Res*. 1994;210(1):1-9.
 53. Uchida K, Sakon M, Ariyoshi H, Nakamori S, Tokunaga M, Monden M. Cancer cells cause vascular endothelial cell (vEC) retraction via 12(S)HETE secretion; the possible role of cancer cell derived microparticle. *Ann Surg Oncol*. 2007;14(2):862-868.
 54. Moreno JJ. New aspects of the role of hydroxyeicosatetraenoic acids in cell growth and cancer development. *Biochem Pharmacol*. 2009;77(1):1-10.
 55. Kim GY, Lee JW, Cho SH, Seo JM, Kim JH. Role of the low-affinity leukotriene B4 receptor BLT2 in VEGF-induced angiogenesis. *Arterioscler Thromb Vasc Biol*. 2009;29(6):915-920.
 56. Guo Y, Nie D, Honn KV. Cloning and identification of a G-protein coupled receptor for 12(S)-HETE. *Proc Amer Assoc Cancer Res*. 2004;45:2746.
 57. Neve RM, et al. A collection of breast cancer cell lines for the study of functionally distinct cancer subtypes. *Cancer Cell*. 2006;10(6):515-527.
 58. Umezawa K. Inhibition of experimental metastasis by enzyme inhibitors from microorganisms and plants. *Adv Enzyme Regul*. 1996;36:267-81.
 59. Tong WG, Ding XZ, Adrian TB. The mechanisms of lipoxygenase inhibitor-induced apoptosis in human breast cancer cells. *Biochem Biophys Res Commun*. 2002;296(4):942-948.
 60. Russo J, et al. The concept of stem cell in the mammary gland and its implication in morphogenesis, cancer and prevention. *Front Biosci*. 2006;11:151-172.
 61. Charafé-Jauffret E, Monville F, Ginestier C, Dontu G, Birnbaum D, Wicha MS. Cancer stem cells in breast: current opinion and future challenges. *Pathobiology*. 2008;75(2):75-84.
 62. Wick N, et al. Lymphatic precollectors contain a novel, specialized subpopulation of podoplanin low, CCL27-expressing lymphatic endothelial cells. *Am J Pathol*. 2008;173(4):1202-1209.
 63. Vinatzer U, et al. Expression of HER2 and the coamplified genes GRB7 and MLN64 in human breast cancer: quantitative real-time reverse transcription-PCR as a diagnostic alternative to immunohistochemistry and fluorescence in situ hybridization. *Clin Cancer Res*. 2005;11(23):8348-8357.
 64. Kriehuber B, et al. Isolation and characterization of dermal lymphatic and blood endothelial cells reveal stable and functionally specialized cell lineages. *J Exp Med*. 2001;194(6):797-808.
 65. Werz O, Steinhilber D. Selenium-dependent peroxidases suppress 5-lipoxygenase activity in B-lymphocytes and immature myeloid cells. The presence of peroxidase-insensitive 5-lipoxygenase activity in differentiated myeloid cells. *Eur J Biochem*. 1996;242(1):90-97.

3.3 Conditional STAT1 ablation reveals the importance of interferon signaling for innate and adaptive immunity to *Listeria monocytogenes* infection.

Manuscript published in PLoS Pathog. 2012 Jun;8(6):e1002763. Epub 2012 Jun 14.

Elisabeth Kernbauer¹, Verena Maier¹, Dagmar Stoiber^{2,3}, Birgit Strobl⁴, **Christine Schneckenleithner**⁵, Veronika Sexl⁵, Ursula Reichart⁶, Boris Reizis⁷, Ulrich Kalinke⁸, Amanda Jamieson¹, Mathias Müller⁴, Thomas Decker^{1*}

¹ Max F. Perutz Laboratories, University of Vienna, Vienna, Austria, ² Ludwig Boltzmann Institute for Cancer Research (LBI-CR), Vienna, Austria, ³ Institute of Pharmacology, Centre for Physiology and Pharmacology, Medical University of Vienna, Vienna, Austria, ⁴ Institute of Animal Breeding and Genetics, University of Veterinary Medicine Vienna, Vienna, Austria, ⁵ Institute of Pharmacology and Toxicology, University of Veterinary Medicine Vienna, Vienna, Austria, ⁶ Biomodels Austria, University of Veterinary Medicine Vienna, Vienna, Austria, ⁷ Department of Microbiology and Immunology, Columbia University Medical Center, New York, New York, United States of America, ⁸ Twincore, Center for Experimental and Clinical Infection Research, Hannover, Germany

My contribution: Designed research, performed experiments.

I performed the adoptive transfer experiments (Fig1. and page 2). The purpose of this experiment was to define the contribution of STAT1 in the hematopoietic versus non-hematopoietic cell compartment in the protection to *Listeria monocytogenes* infections. Wild type and *Stat1*^{-/-} mice were lethally irradiated and reconstituted with bone marrow of the reciprocal genotype. To allow an accurate discrimination between donor and receptor, the Ly5.1/Ly5.2 system was used. Mice were checked for efficient engraftment and subsequently subjected to intraperitoneal infections with sublethal doses of *Listeria monocytogenes*. The following experiments on determining the bacterial burdens in different organs were carried out by Elisabeth Kernbauer.

Conditional Stat1 Ablation Reveals the Importance of Interferon Signaling for Immunity to *Listeria monocytogenes* Infection

Elisabeth Kernbauer¹, Verena Maier¹, Dagmar Stoiber^{2,3}, Birgit Strobl⁴, Christine Schneckenleithner⁵, Veronika Sexl⁵, Ursula Reichart⁶, Boris Reizis⁷, Ulrich Kalinke⁸, Amanda Jamieson¹, Mathias Müller⁴, Thomas Decker^{1*}

1 Max F. Perutz Laboratories, University of Vienna, Vienna, Austria, **2** Ludwig Boltzmann Institute for Cancer Research (LBI-CR), Vienna, Austria, **3** Institute of Pharmacology, Centre for Physiology and Pharmacology, Medical University of Vienna, Vienna, Austria, **4** Institute of Animal Breeding and Genetics, University of Veterinary Medicine Vienna, Vienna, Austria, **5** Institute of Pharmacology and Toxicology, University of Veterinary Medicine Vienna, Vienna, Austria, **6** Biomodels Austria, University of Veterinary Medicine Vienna, Vienna, Austria, **7** Department of Microbiology and Immunology, Columbia University Medical Center, New York, New York, United States of America, **8** Twincore, Center for Experimental and Clinical Infection Research, Hannover, Germany

Abstract

Signal transducer and activator of transcription 1 (Stat1) is a key player in responses to interferons (IFN). Mutations of Stat1 cause severe immune deficiencies in humans and mice. Here we investigate the importance of Stat1 signaling for the innate and secondary immune response to the intracellular bacterial pathogen *Listeria monocytogenes* (Lm). Cell type-restricted ablation of the Stat1 gene in naïve animals revealed unique roles in three cell types: macrophage Stat1 signaling protected against lethal Lm infection, whereas Stat1 ablation in dendritic cells (DC) did not affect survival. T lymphocyte Stat1 reduced survival. Type I IFN (IFN-I) signaling in T lymphocytes reportedly weakens innate resistance to Lm. Surprisingly, the effect of Stat1 signaling was much more pronounced, indicating a contribution of Stat1 to pathways other than the IFN-I pathway. In stark contrast, Stat1 activity in both DC and T cells contributed positively to secondary immune responses against Lm in immunized animals, while macrophage Stat1 was dispensable. Our findings provide the first genetic evidence that Stat1 signaling in different cell types produces antagonistic effects on innate protection against Lm that are obscured in mice with complete Stat1 deficiency. They further demonstrate a drastic change in the cell type-dependent Stat1 requirement for memory responses to Lm infection.

Citation: Kernbauer E, Maier V, Stoiber D, Strobl B, Schneckenleithner C, et al. (2012) Conditional Stat1 Ablation Reveals the Importance of Interferon Signaling for Immunity to *Listeria monocytogenes* Infection. PLoS Pathog 8(6): e1002763. doi:10.1371/journal.ppat.1002763

Editor: Dana J. Philpott, University of Toronto, Canada

Received: January 10, 2012; **Accepted:** May 2, 2012; **Published:** June 14, 2012

Copyright: © 2012 Kernbauer et al. This is an open-access article distributed under the terms of the Creative Commons Attribution License, which permits unrestricted use, distribution, and reproduction in any medium, provided the original author and source are credited.

Funding: This work was supported by grants from the Austrian Science Fund (SFB-F28) to TD, MM, BS, AJ and VS, and from the Austrian Genome Research Programme GEN-AU II and III (Austromouse) to MM. The funders had no role in study design, data collection and analysis, decision to publish, or preparation of the manuscript.

Competing Interests: The authors have declared that no competing interests exist.

* E-mail: thomas.decker@univie.ac.at

Introduction

Signal transducer and activator of transcription (Stat1) is a central mediator of interferon responses in the immune system. Signals from type I (IFN α /IFN β ; IFN-I), type II (IFN γ ; IFN-II) and type III (IFN λ , IFN-III) interferons employ receptor-associated Janus kinases (Jaks) to activate Stats by tyrosine phosphorylation [1,2]. Gene transcription is induced and leads to a range of cellular changes, including anti-viral properties, growth inhibition, apoptosis and differentiation. Depending on the cellular context Stat1 can act as either a tumour-suppressor or promote oncogenesis [3,4,5]. The central character of Stat1 in signal transduction by the IFN receptors results from the importance of Stat1 homodimers for transcriptional regulation by IFN γ . Moreover, Stat1 forms the ISGF3 complex together with Stat2 and interferon regulatory factor 9 (Irf9). ISGF3 is the main player in transcriptional responses to both IFN-I and IFN-III. Consistent with its central role, Stat1 deficiency in mice recapitulates the lack of IFN-I, IFN-III and IFN γ responses and leads to high susceptibility to viral and bacterial

infections [6,7,8]. The critical importance of Stat1 for resistance to infection is emphasized by mutations of the Stat1 gene in humans. Patients with various degrees of Stat1 loss-of-function present clinically with recurrent and often lethal mycobacterial and viral infections [9,10,11].

Listeria monocytogenes (Lm) is the causative agent of human listeriosis and a serious threat for the health of immunocompromised individuals. It is also a well-studied model organism to analyse cell-mediated immunity to intracellular pathogens. Innate protection critically depends on the activities of the cytokines interleukin (IL) 12 and IFN γ [12,13]. This most likely reflects NK cell activation, IFN γ production and subsequent clearance of the bacteria by activated macrophages. Sterile immunity and immunological memory result from the development of CD8⁺ T cells [14,15]. Stat1-deficient mice succumb to Lm during the early, innate phase of infection, strongly suggesting a dominant role for Stat1 in IFN γ -mediated macrophage activation [7]. As even very low numbers of Lm, even if attenuated, rapidly kill Stat1^{-/-} mice it is difficult to study attributes of the innate response. For example,

Author Summary

Signal transducer and activator of transcription 1 (Stat1) is an indispensable component of the cellular response to interferons (IFN) during immune reactions to pathogens. Stat1 deficiency leads to severe immune defects in humans and mice. The sensitivity of animals with complete Stat1 ablation to microbial pathogens prevented determining its contribution to various effector systems of the immune response. By way of tissue-restricted Stat1 ablation we now decipher the impact of Stat1 signaling in different cell populations on the innate and adaptive immune response to the intracellular pathogen *Listeria monocytogenes*. Our data highlight the importance of and requirement for IFN γ -activated macrophages for clearance of the pathogen during early phases of infection, and show a yet unanticipated detrimental role for T cell Stat1. During secondary responses the picture changes and Stat1 in T cells is crucial for proper clearance of *L. monocytogenes*. Likewise, Stat1 signaling in dendritic cells plays a fundamental role for adaptive immunity to *L. monocytogenes*. Exploring the local response to *L. monocytogenes* infection we reveal a role of Stat1 in shaping the cellular composition of inflammatory infiltrates. Furthermore, Stat1 deficiency in dendritic cells increases the proliferation of regulatory T cells, an effect likely to dampen the antibacterial response.

Lm replicates in a variety of non-hematopoietic cell types such as epithelial cells or hepatocytes and the contribution of Stat1 to bacterial clearance in these cell types is not known. Moreover, the impact of Stat1 on the generation of adaptive immunity and immunological memory is unclear [16,17,18,19,20]. In this regard the potential role of both IFN-I and IFN γ in the maturation and activation of dendritic cells [21,22,23] and the impact of both IFN types on the development of effector and memory CTL is of particular interest. Moreover, it has not been possible to investigate a potential contribution of macrophage activation to Lm clearance in secondary immune responses of mice lacking Stat1 in all tissues.

Further interest in cell type-specific Stat1 activities derives from the opposing effects of IFN γ and IFN-I on innate resistance to Lm. IFN γ -deficient mice show a similar susceptibility as Stat1 $^{-/-}$ mice [24]. By contrast IFN-I receptor (Ifnar) deficient mice are protected from lethal Lm infections [25,26,27]. Suppression of protective innate immunity by IFN-I was suggested to result from increased T lymphocyte apoptosis and subsequent IL10-mediated immunosuppression [28]. Furthermore, infection of macrophages and DCs with Lm causes IFN-I dependent downregulation of the IFN γ -receptor, hence unresponsiveness to IFN γ [29]. IFN-I also sensitizes infected macrophages *in vitro* to die from infection with Lm [30,31].

To overcome the limitations posed by the exquisite sensitivity of Stat1 $^{-/-}$ mice to infections with Lm or other pathogens we generated mice with floxed Stat1 alleles. Here we report that cell type-restricted Stat1 ablation reveals a striking dichotomy of immunological effects. Macrophage Stat1 produces protective innate immunity whereas the opposite is true for T lymphocytes. In secondary immune responses to Lm T lymphocyte and dendritic cell Stat1 signaling becomes protective, but Stat1 in macrophages does not contribute to clearance of bacteria.

Results

STAT1 in the hematopoietic compartment is crucial for host protection to *Listeria monocytogenes* infection

To decipher the importance of Stat1 signaling for protective immunity to Lm in the hematopoietic and non-hematopoietic cell

compartments we conducted adoptive transfer experiments. WT and Stat1 $^{-/-}$ mice were lethally irradiated and bone marrow of either Stat1 $^{-/-}$ or WT background was implanted in these mice. After 8 weeks the chimerism was examined in blood, spleen and liver showing an efficient implantation of the transferred bone marrow (supplemental figure S1). Bone marrow-chimeric mice were subjected to intraperitoneal infections with sublethal doses of Lm and 72 hrs later the bacterial burden in spleen and liver was determined (figure 1A, 1B). Compared to WT mice reconstituted with WT bone marrow, mice lacking Stat1 in non-hematopoietic cells showed a minor reduction of bacterial clearance, hence minor contribution of non-hematopoietic Stat1 to innate resistance. This suggests that hepatocytes, although representing an important niche for Lm multiplication [32,33], are not protected by Stat1 signaling. By contrast mice lacking Stat1 in bone marrow-derived cells displayed a clear loss of resistance.

In addition to pathogen clearance we tested the impact of Stat1 deficiency on the systemic cytokine response. WT mice which received Stat1 $^{-/-}$ bone marrow responded to infection with a systemic cytokine storm, i.e. elevated serum levels of almost all measured cytokines and chemokines (IL6, IL22, TNF α , MCP1, IL10, Rantes, IP10 and MCP3; figure 1C). This is likely to reflect the increase in bacterial burden, hence a higher intensity of the innate response. Intriguingly however, the highest levels of IL12p70 were determined in the group of Stat1 $^{-/-}$ mice that received protective WT bone marrow and had very similar bacterial loads as WT mice. This suggests that Stat1 of non-hematopoietic cells participates in the negative regulation of IL12 synthesis. In line with increased IL12, IFN γ production was elevated compared to WT. Likewise IFN γ was increased in mice with Stat1 $^{-/-}$ bone marrow although IL12 levels were normal. Therefore, IL12 and IFN γ levels are not strictly correlated. In this situation IFN γ synthesis is most likely part of the cytokine storm as a consequence of high bacterial burden.

Stat1 signaling in myeloid cells is essential, whereas Stat1 in T cells reduces innate resistance to *Listeria monocytogenes* infection

To further study the contribution of individual immunocompetent cells for the innate phase of Lm infection we analysed resistance to lethal infection and bacterial clearance after tissue-restricted Stat1 ablation. To determine the importance of Stat1 signaling in myeloid cells we used LysMCreStat1 $^{fl/fl}$ mice, which delete predominantly in macrophages and neutrophils [34,35]. These mice display a significantly reduced ability to clear even a low dose of Lm from spleen and liver (figure 2A, 2B) and hence succumbed to infection, whereas all WT mice survived the intraperitoneal infection (figure 2C).

To test the involvement of Stat1 to the immune response to Lm in other cell types of the immune system, mice with Stat1 deficiency in CD11c-positive cells, predominantly dendritic cells, but also subpopulations of NK cells and alveolar macrophages, were generated (CD11cCreStat1 $^{fl/fl}$, figure S2); [36,37]. Mice lacking Stat1 in T cells were obtained by crossing Stat1 $^{fl/fl}$ to LckCre mice (LckCreStat1 $^{fl/fl}$; figure S2). DC- and T cell- deleted mouse strains were subjected to a sublethal dose of Lm by intraperitoneal injection and bacterial loads in spleen and liver were monitored for the next three days (figure S3A, S3B). These mice did not show elevated numbers of Lm in spleen and liver at day three (figure 2D, 2E) or a significantly altered susceptibility to sublethal infection (2C).

Intravenous infection with Lm lead to the same outcome as intraperitoneal infection. Three different doses of Lm, ranging from sublethal to lethal referred to WT mice, were chosen to

A

R

Cell Type Restricted Antibacterial Stat1 Activity

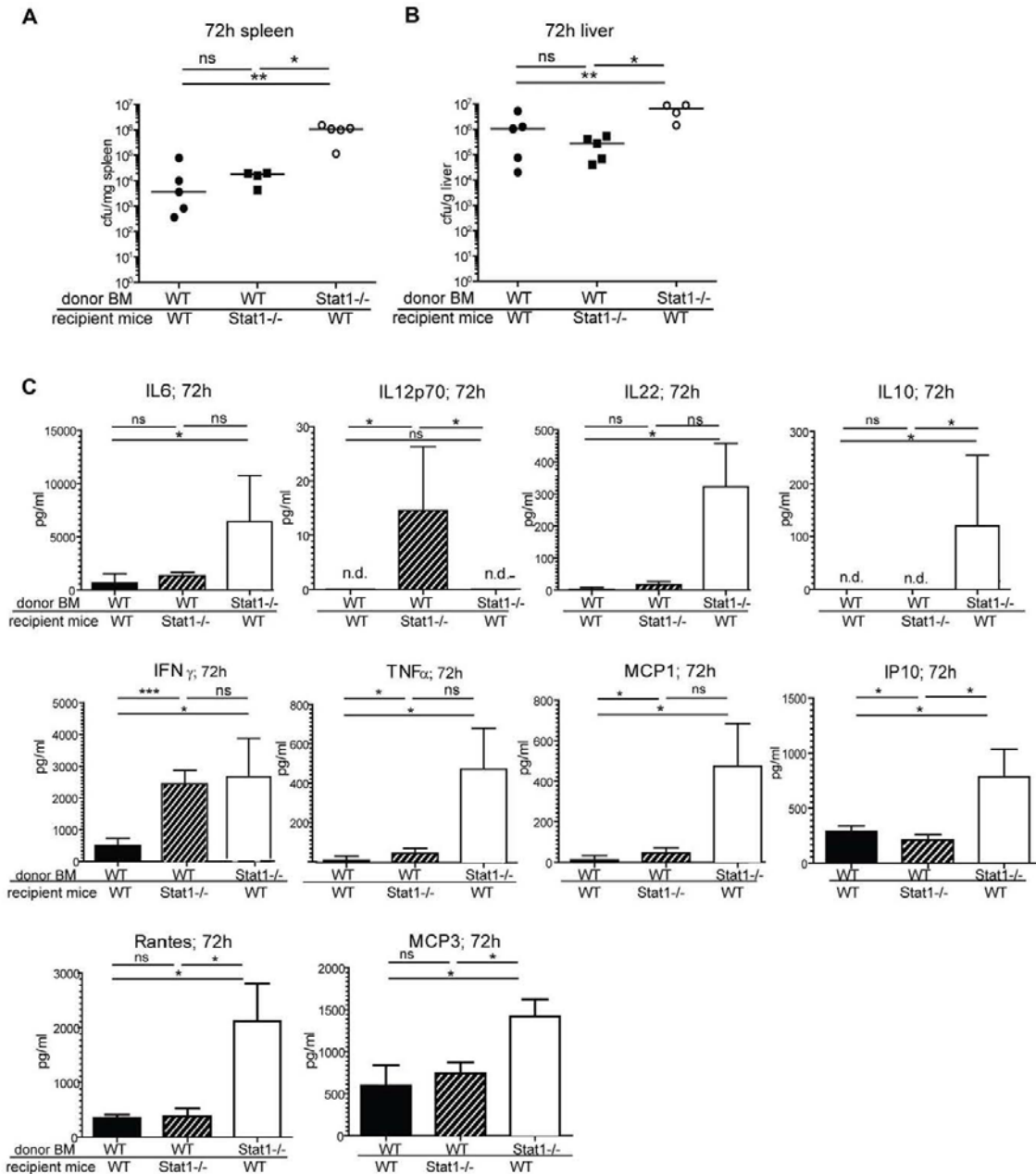


Figure 1. Role of STAT1 in the hematopoietic compartment. C57BL/6N (WT) and Stat1^{-/-} mice were lethally irradiated and bone marrow of the respective donor mice was transferred into recipient mice. After engraftment mice were infected i.p. with 1×10^5 Lm and the bacterial load of spleen (1A) and liver (1B) was determined and medians were calculated (n=5). Statistical significance was determined using the Mann-Whitney Test. Serum of infected mice (n=5) was collected and cytokines (IL6, IL12p70, IL22, IL10, IFN γ , TNF α , MCP1, IP10, Rantes, MCP3) were determined (1C). Means and standard deviations are shown. doi:10.1371/journal.ppat.1002763.g001

determine the response of the Stat1-ablated mice (figure 2F H). Increased sensitivity to infection was seen when myeloid cells lacked Stat1, whereas CD11cCreStat1^{fl/fl} animals behaved similar

to WT. Strikingly, LckCreStat1^{fl/fl} mice displayed increased resistance to high infectious doses. This consequence of T cell specific Stat1 ablation was similarly observed following intraper-

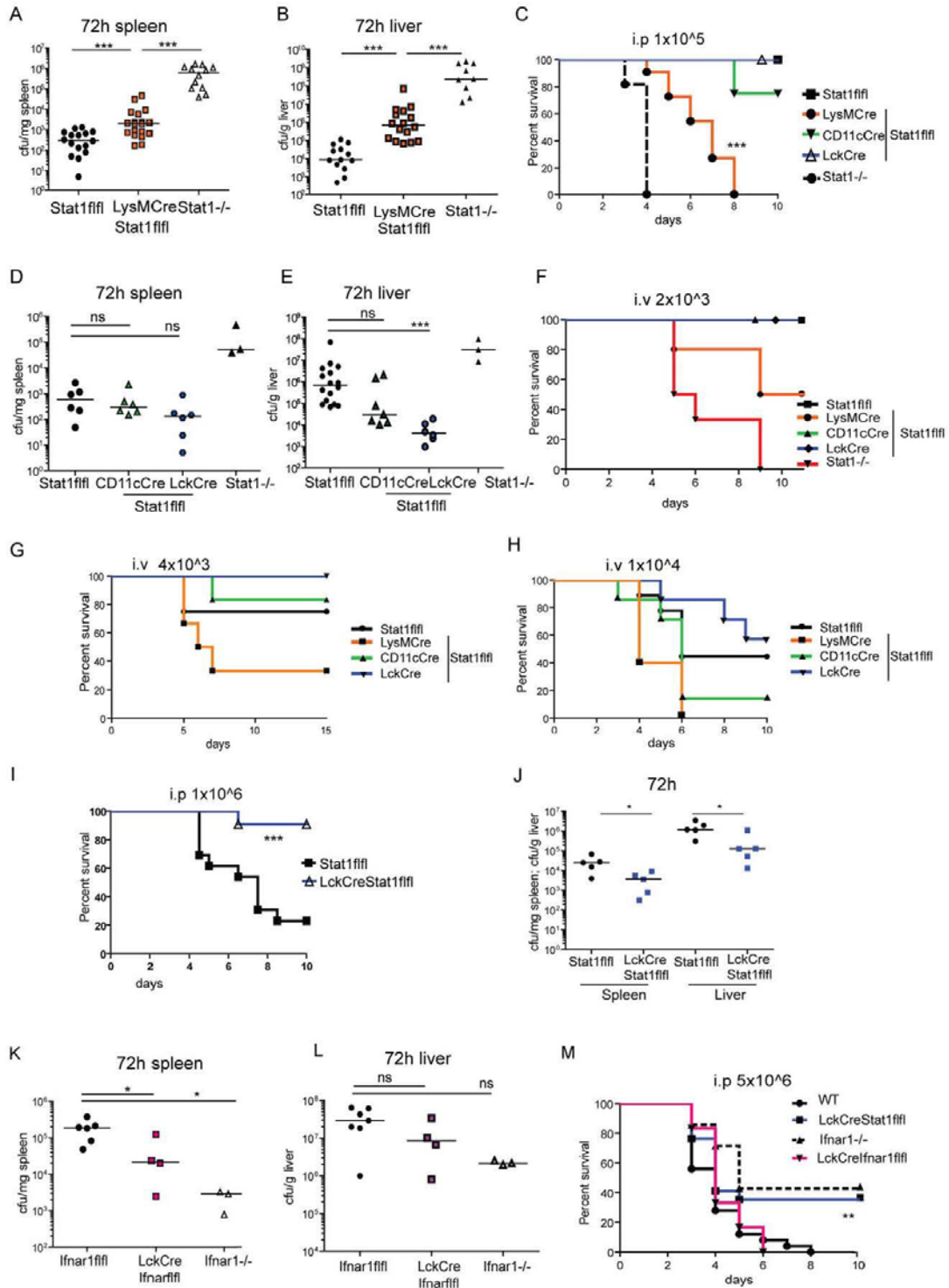


Figure 2. Bacterial load and survival in mice with cell-type specific Stat1 ablation. Stat1^{fl/fl}, Stat1^{-/-} and LysMCreStat1^{fl/fl} mice were infected for 72 h with 1×10^5 Lm i.p. and bacterial load of spleen (A) and liver (B) was determined after 72 h or survival was monitored over 10 days (n = 11–14) (C). Stat1^{fl/fl}, Stat1^{-/-}, CD11cCreStat1^{fl/fl} and LckCreStat1^{fl/fl} mice were infected with 1×10^5 Lm i.p. and bacterial load was determined after 72 h in spleen (D) or liver (E). The survival of i.v. infected animals was monitored over 10 days with different doses of Lm; 2×10^3 (F); 4×10^3 (G), 1×10^4 (H). Stat1^{fl/fl} and LckCreStat1^{fl/fl} mice were infected with 1×10^6 Lm and survival was monitored over 10 days (n = 11–13) (I). LckCreStat1^{fl/fl} and control mice (J) and LckCreIrfnar1^{fl/fl} and respective control mice (K; L) were infected with 1×10^6 Lm and the CFU of spleen and liver was determined after 72 h. Survival was monitored for 10 days (n = 6–15) after infection with 5×10^6 Lm i.p. (M). Representative results of at least two independent experiments are shown.
doi:10.1371/journal.ppat.1002763.g002

itoneal infection with a higher than LD50 inoculum of Lm. Lack of activity of T cell Stat1 resulted in both increased survival of the animals and an enhanced clearance of the bacteria from spleen and liver (figure 2I, 2J).

IFN-I signaling in T cells was previously shown to reduce the clearance of Lm upon infection in the spleen [26]. To examine whether the enhanced survival in LckCreStat1^{fl/fl} mice was due to a lack of IFN-I signaling, we analysed the bacterial load and survival in mice with IFN-I receptor deficiency in T cells (LckCreIrfnar1^{fl/fl}). We noted a significantly lower number of splenic Lm in LckCreIrfnar1^{fl/fl} mice compared to WT mice at high doses of infection, whereas the number of bacteria in the liver was not significantly reduced (figure 2K, 2L). Mice with complete Irfnar1 deficiency showed a clearly better ability to contain Lm infection than mice lacking Irfnar1 only in T cells. The increased ability of LckCreIrfnar1^{fl/fl} mice to clear bacteria in the spleen did not result in a higher rate of survival compared to WT mice, whereas complete Irfnar1 deficiency did (figure 2M). This result suggests that the increase in resistance produced by the absence of T cell Stat1 cannot be entirely explained on the basis of the lack of IFN-I signaling in T cells.

Stat1's contribution to splenocyte apoptosis reflects IFN-I signalling

TUNEL staining of spleen cells two days after i.p. infection with Lm produced the expected large number of apoptotic cells in WT mice [26], which was strongly reduced in both LckCreStat1^{fl/fl} and LckCreIrfnar1^{fl/fl} mice (figure 3). Since the decrease in cell apoptosis resulting from either Stat1 or Irfnar1 ablation was highly similar, the additional protection of LckCreStat1^{fl/fl} mice from Lm infection is not due to a lesser rate of infection-induced apoptosis in Stat1-deficient T cells.

To further clarify the difference of LckCreStat1^{fl/fl} and LckCreIrfnar1^{fl/fl} we isolated splenocytes of these genotypes and appropriate controls (WT, Stat1^{-/-}, Irfnar1^{-/-}) and infected them *in vitro* for two days with Lm at MOI 10. Subsequently we analysed the supernatant of these cultures for T cell cytokines. Stat1 deficiency in T cells lead to increased production of IL4 and IL17 and a clear suppression of IFN γ . In contrast, Irfnar1 deficiency in T cells did not decrease production of the signature cytokines under study, but increased the amounts of IFN γ , IL17 and IL10. The data indicate a Th population-independent negative regulation of T cell activation by IFN-I and demonstrate the strong influence of Stat1 on the generation of Th1 cells through its target gene T-bet [38] (figure S4). Thus, Irfnar or Stat1 ablation in T cells impact differently on the generation and function of Th cell populations *in vitro*.

Systemic cytokine levels in mice with cell specific Stat1 ablation after *Listeria monocytogenes* infection

Examination of systemic cytokine/chemokine levels demonstrated that mice lacking myeloid Stat1 signaling show increased levels of IL6, IL12p70, MCP1, MCP3, IL22, MIP1 β , Rantes and IFN γ in their serum, similar to but not as dramatic as complete

Stat1 deficiency (figure 4). As these mice have strongly elevated numbers of pathogens in their organs the increase in inflammatory cytokines may again reflect an increased activity of the innate immune system. Alternatively, increased cytokine production could also result from the loss of Stat1-mediated gene repression as reported for IL6 [39]. The function of Stat1 as both a transcriptional activator and repressor is well documented [40]. Both functions require binding to GAS sequences [41], but the detailed mechanisms are not understood.

Stat1 signaling in CD11c⁺ cells had a very selective impact on the levels of systemic cytokines, showing elevated levels of MCP1 compared to WT mice but interestingly, lower amounts of IL12p70. By contrast, higher levels of IL12p70 were detected in the serum of mice lacking Stat1 signaling in T cells, despite an equal bacterial load. The levels of TNF α and IL10 were too low to be detectable at this dose of infection.

Organ damage in mice with cell type-restricted ablation of Stat1 signaling after *Listeria monocytogenes* infection

Spleens (figure 5A) and livers (figure 5B) of infected animals with conditional Stat1 gene ablation were analysed using H&E staining to determine the severity of inflammation two days post-infection. In keeping with the loss of innate resistance, mice lacking Stat1 in myeloid cells showed a severe pathology of the spleen with increased lymphocyte depletion [42]. In the liver the radius of the inflammatory infiltrate area, classified as microabscess [43], correlated with the increase of bacteria found in this organ (figure 5B, 5C). In addition, the numbers of micro-abscesses correlated with bacterial burden, as lack of Stat1 in myeloid cells increased the area of infiltrates in the liver. Whereas CD11c⁺ cell-specific ablation of Stat1 led to significantly bigger areas of infiltrates compared to WT (figure 5C), the amount of infiltrates (figure 5D) and bacteria in the liver was not significantly enhanced compared to WT (figure 2E). Mice with T cell-restricted Stat1 gene deletion showed smaller infiltrate areas compared to the WT, again reflecting the protection of these mice from infection.

Liver failure may significantly contribute to the lethality of Lm infection [44]. To assess liver damage, we measured the amount of circulating amino aspartate transferase (AST), an enzyme released from damaged hepatocytes and readily measurable in serum samples [45] (figure 5E). LysMCreStat1^{fl/fl} mice displayed strongly elevated levels of AST, indicating massive liver damage. No significant differences in AST were found in all other animals/genotypes compared to WT animals.

In addition to organ damage we examined the immune status of Stat1-ablated mice by analysing the composition of blood leukocytes. Mice lacking Stat1 in T cells had the highest numbers of circulating immune cells in their blood 72 h after infection (figure 5F, 5G, 5H). This is consistent with the notion that the reduced number of Lm in organs, coupled with reduced numbers of apoptotic cells led to a diminished recruitment of blood leukocytes. Additionally this result may indicate a defect in Stat1 regulated synthesis of T cell-derived chemokines.

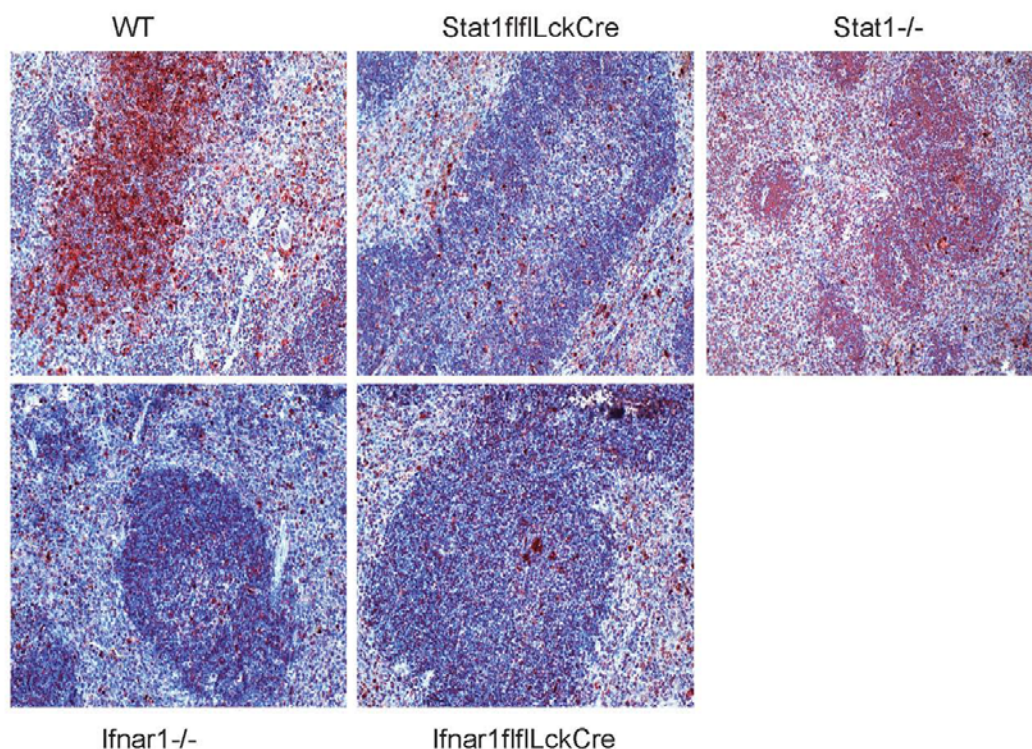


Figure 3. Apoptotic cell death in the spleen. WT, LckCreStat1fl/fl, LckCreIfnar1fl/fl, Ifnar1^{-/-} and Stat1^{-/-} were infected with 1×10^6 Lm and spleens were isolated 48 h after infection. TUNEL positive cells are visible in dark red; hematoxyline counterstaining indicates the structure of the spleen (3).

doi:10.1371/journal.ppat.1002763.g003

STAT1 signaling regulates cellular influx to local sites of inflammation

The results shown in figures 1 and 2 emphasize the importance of Stat1 mediated macrophage activation. In spite of this, mice completely devoid of Stat1 cleared Lm less well than LysMCreStat1fl/fl animals. This result could be explained by incomplete ablation of the Stat1 gene in macrophages although our recent inspection of macrophages demonstrates deletion with very high efficiency [35]. Alternatively or additionally, therefore, the difference between LysMCreStat1fl/fl and Stat1^{-/-} mice may reflect shaping of the innate immune response by Stat1 signaling in several different leukocyte populations. In our infection model the peritoneum is the site of immediate exposure of innate cells to the bacterial pathogen that initiates a local inflammatory response. To determine the degree to which cell type-specific Stat1 signaling determines this local immune response, we first analyzed the local chemokine/cytokine milieu in the peritoneal cavity over the course of the first three days of infection (figure S6). The most striking differences between genotypes were observed at day 2 (figure 6A). Absence of Stat1 in myeloid cells increased MIP1 α MCP1 and Rantes amounts at day two and three compared to WT. MCP1 and Rantes were decreased upon CD11c-Cre-mediated Stat1 ablation at day two, but the levels of these chemokines recovered and exceeded WT levels at day three. T cell-specific Stat1 ablation lead to a decrease in Rantes levels at day two after infection, at day three the amount of the tested chemokines reached WT level. Examination of the pro- and anti-inflammatory cytokine gene

expression patterns of adherent peritoneal macrophages isolated from infected mice indicated a small but significant role of myeloid cell Stat1 in the negative regulation of IL12 (figure 6B). Remarkably, Stat1 signaling in T cells was required for full IL12p40 expression. In keeping with the aforementioned negative regulation by Stat1 a more profound effect was noted with regard to IL6 production that was markedly upregulated upon STAT1 deficiency in either myeloid cells or the CD11c⁺ population. The CD11cCreStat1fl/fl genotype was unique in producing an adherent cell population with reduced IL10 production. Together with the systemic analyses shown in figure 1 and 2 our data suggest that peritoneal macrophages are major producers of IL6 and IL12. Lack of Stat1 signaling in CD11c⁺ dendritic cells or inflammatory monocytes may stimulate macrophages to produce excess amounts of IL6 and decreased amounts of IL10.

To determine whether the altered peritoneal chemokine/cytokine levels changed the cell recruitment, we isolated peritoneal exudate cells two days after intraperitoneal Lm infection and analysed the cell composition by Wright-Giemsa-stained cytopins and flow cytometry (figure 6C E). Myeloid cells together constitute >95% of the peritoneal exudates in WT mice. In animals lacking Stat1 in DC reduced numbers of leukocytes were recruited, however neutrophils were increased at the expense of macrophages (figures 6C E). Thus, Stat1 signaling in CD11c⁺ DC regulates monocyte/macrophage migration to the inflamed peritoneum. Mice with myeloid Stat1 ablation showed an increased influx of total peritoneal leukocytes with a similar

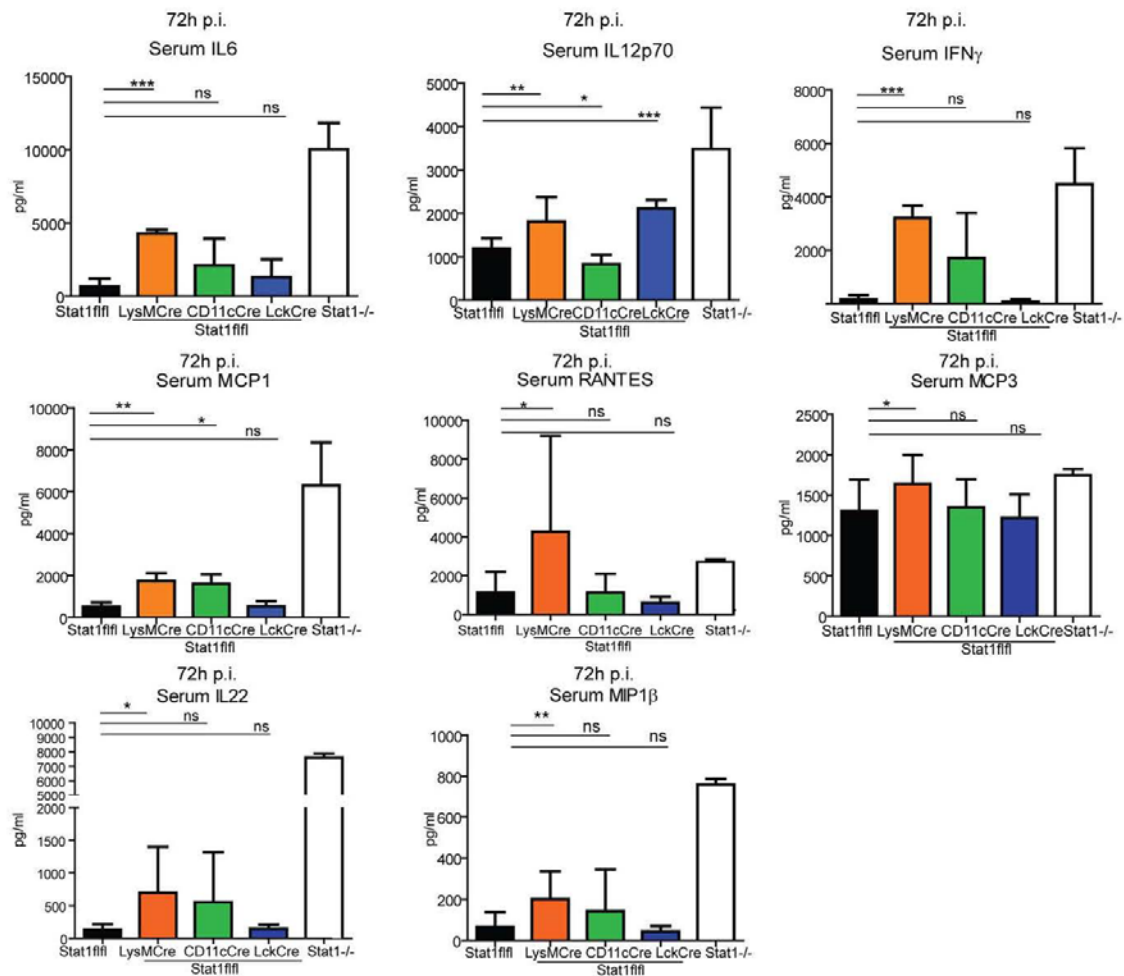


Figure 4. Analysis of serum cytokines in mice with cell-type specific Stat1 ablation 72 hrs after infection with Lm. Mice with Stat1 ablation in different cell compartments were infected with 1×10^5 Lm and serum was collected over the course of three days after infection. Indicated cytokines (MCP1, IL6, IFN γ , IL12p70, MCP3, Rantes, MIP1 β , IL22) were analysed (4). Mean values of cumulative data out of two experiments (n = 8) are depicted with standard deviations. Significant differences are indicated using asterisks. doi:10.1371/journal.ppat.1002763.g004

tendency to reduce monocytes/macrophages and increase neutrophils. Finally, the absence of Stat1 signaling in T cells caused a strong increase in the amount of immune cells travelling to the peritoneum without altering their composition.

Together the data characterizing the peritoneal inflammatory response suggest a profound impact of Stat1 in different cell types on the cytokine milieu and on leukocyte composition. This may explain in part why myeloid cell-restricted Stat1 ablation does not fully reproduce the loss of bacterial clearance observed upon complete Stat1 gene deletion.

Stat1 expression in DC and T cells regulates adaptive immunity to *Listeria monocytogenes*

To analyse the impact of Stat1 signaling in different cell populations on establishing adaptive immunity against Lm, we applied an immunisation and challenge protocol to the respective conditional knockout mice. Under these conditions mice lacking

Stat1 signaling in T cells failed to clear Lm from the spleen (figure 7A). Accordingly, an increased percentage of LckCreStat1fl/fl mice succumbed to infection compared to WT mice (figure 7B). Immunized mice lacking Stat1 in CD11c+ cells showed a slight impairment in clearing splenic Lm, yet the impact on survival was almost as pronounced as in mice lacking Stat1 in T cells. Myeloid Stat1 did not contribute to the establishment of adaptive immunity to Lm as bacterial clearance after immunisation was as strong as in WT mice.

Overall systemic cytokine levels were generally lower than those found after infection of naive mice. Stat1 deficiency in CD11c+ cells caused a selective reduction of systemic IFN γ that may contribute to the reduced ability to raise adaptive immunity to Lm (figure 7C). The levels of IFN γ in mice lacking Stat1 signaling in T cells were equally high as in naive mice. Given the reduced ability of Stat1 $^{-/-}$ T cells to generate the Th1 lineage [38] (figure S4) this may reflect IFN γ production by cells other than Th1 or,

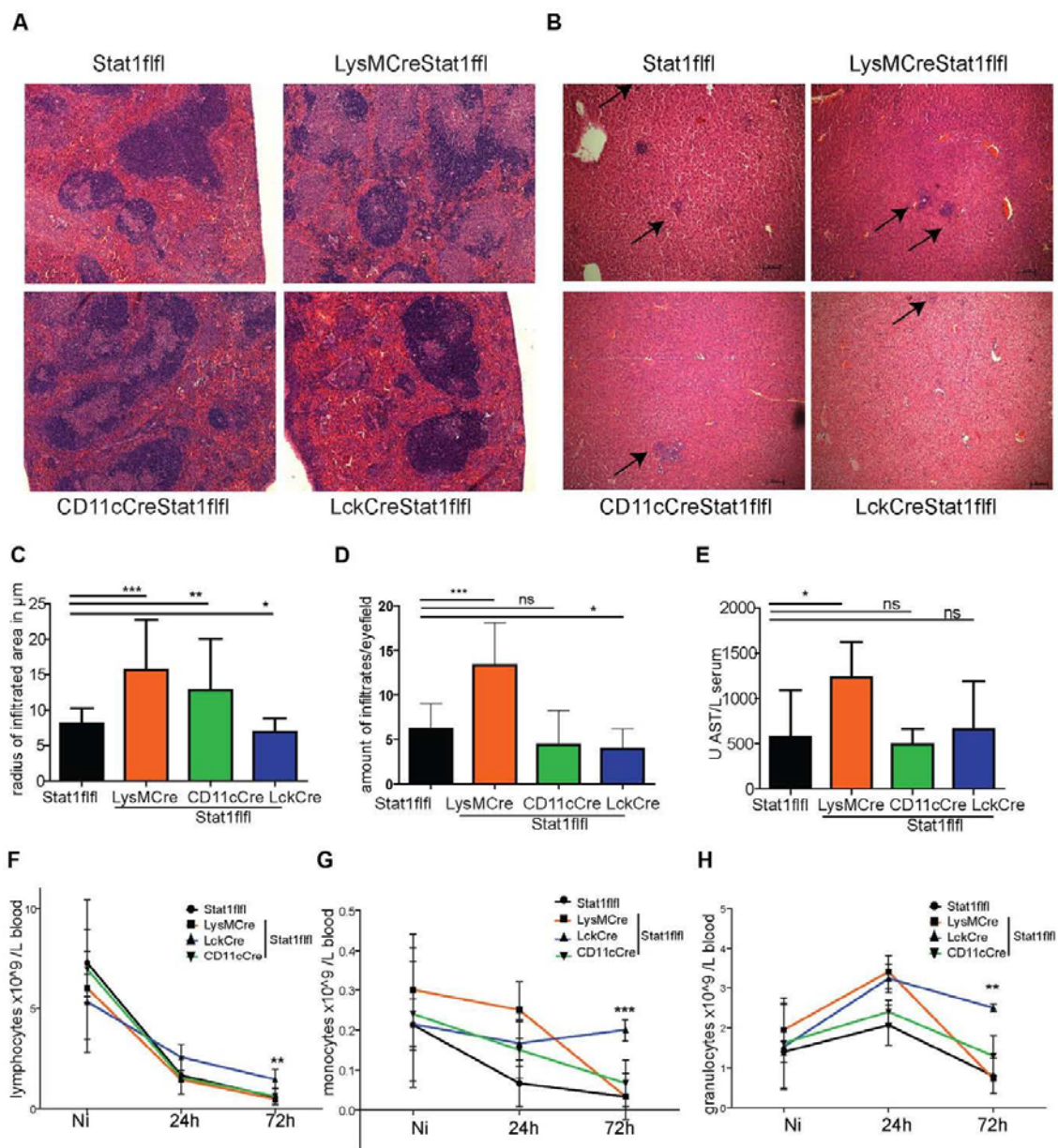


Figure 5. Organ damage and blood cell populations after 72 h of infection. Spleen (5A) and liver (5B) sections of animals infected with Lm for 72 hrs were stained with H&E, arrows point to infiltrates in the liver. The amount of infiltrates and the radius of the infiltrated area was measured in μm of three individual mice in three microscopic fields ($10\times$) using the Zeiss AxioVision LE software and depicted in (5C, 5D). One representative picture is shown. Amino aspartate transferase levels were analysed in the serum of indicated mice ($n = 6$) infected with Lm for 72 h (5E). Numbers of lymphocytes (5F), monocytes (5G) and granulocytes (5H) were determined in blood samples of uninfected mice (Ni) or of mice after infection for 24 hrs or 72 hrs ($n = 3-6$) using a vet haematology counter. Data from two independent experiments are shown and statistical significances are indicated with asterisks where applicable.
doi:10.1371/journal.ppat.1002763.g005

alternatively, low numbers of Th1 cells developing in absence of Stat1 may produce higher IFN γ amounts due to the lack of the negative regulation Stat1 imposes on the IFN γ gene [46].

To further analyse the immunisation defects in CD11cCreStat1^{fl/fl} mice, we investigated T cell responses after immunisation. Proliferation of splenic CD3⁺ T cells showed no significant

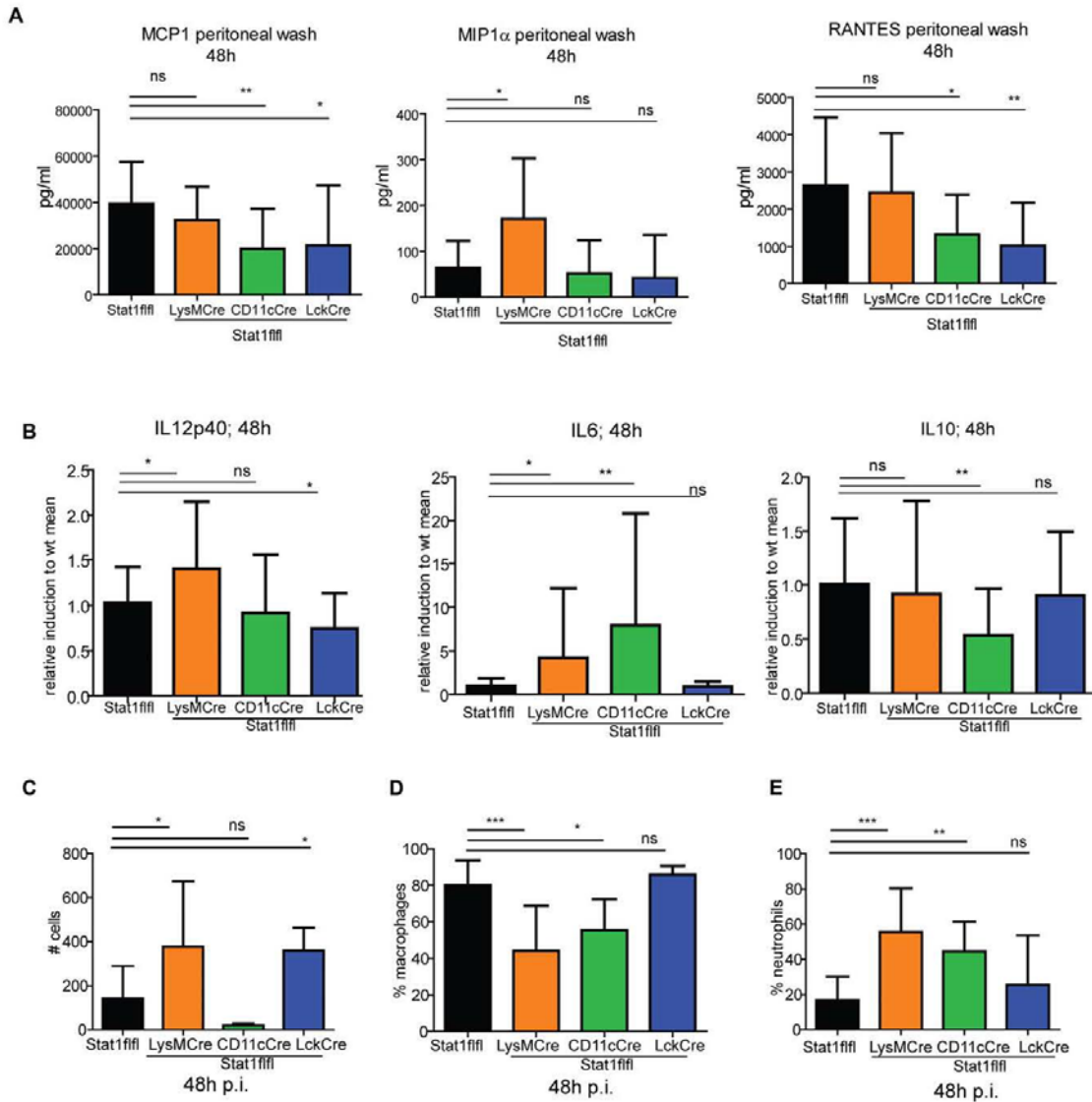


Figure 6. Peritoneal inflammation 48 hrs after infection. Chemokines (MCP1, Mip1 α , Rantes) were determined in the peritoneal lavage fluid of mice (n = 6) after 48 hrs of infection (6A). Peritoneal exudate cells were isolated 48 h after i.p. infection with 1×10^6 Lm, adherent cells were enriched and RNA prepared and subjected to qPCR for IL12p40, IL6 and IL10 (6B). Data from 3–5 experiments (n = 10–15) are pooled and means with standard deviation are shown. 48 h after i.p. infection peritoneal exudate cells were isolated and cytopins stained with Wright-Giemsa solution. The amount of cells (6C), the percentage of macrophages (6D) and the percentage of neutrophils (6E) were counted and depicted (n = 9). doi:10.1371/journal.ppat.1002763.g006

differences (figure 8A). However, examination of the Treg population (CD4+Foxp3+) revealed an enhanced proliferative response in the spleens of mice with CD11c+-restricted Stat1 ablation (figure 8B). As regulatory T cells represent only a minor percentage of total splenic T cells it is not surprising that the difference in proliferation went unnoticed when analyzed in the context of total CD3+ T cell cells. The data suggest a contribution of DC Stat1 to the control of proliferation of a small proportion of antigen-specific Treg.

Discussion

Studies in gene-modified mice and with cells from human patients suffering from recurrent infectious disease have unequivocally established the central importance of Stat1 for the establishment of protective innate immunity to viral and nonviral pathogens [6,7,47]. This includes Lm, the bacterial pathogen studied here. Conditional gene targeting allowed us to examine whether there is a uniform immunological impact of Stat1 across

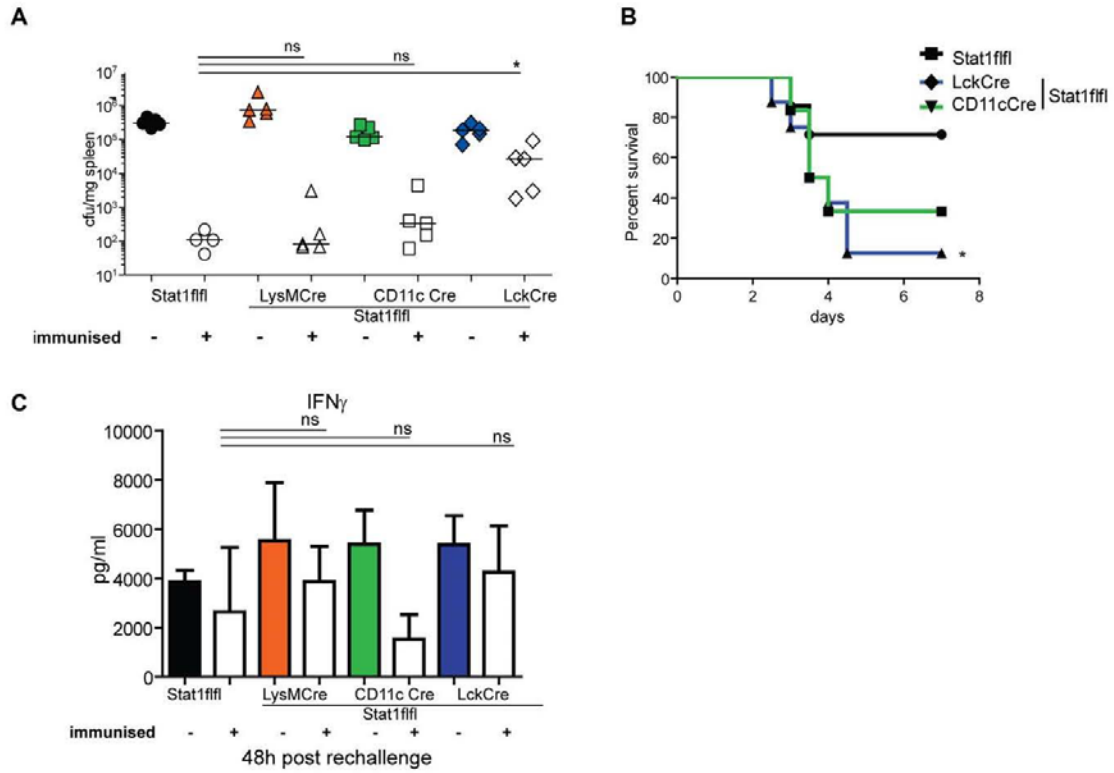


Figure 7. Adaptive immunity to *Listeria monocytogenes* in mice with tissue-restricted Stat1 ablation. Immunised and naïve mice were infected i.v. with 1×10^5 Lm and bacterial load was determined 48 h after infection ($n=4-5$) (7A) or survival of 7 mice of each genotype was monitored (7B). Serum of immunised and naïve mice was analysed for the presence of IFN γ (7C). One representative result of at least two independently performed experiments is shown ($n=4-5$). doi:10.1371/journal.ppat.1002763.g007

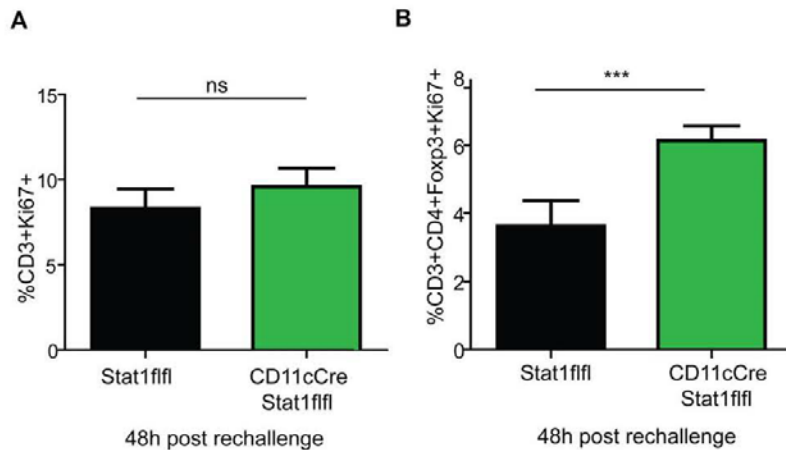


Figure 8. Dendritic cell Stat1 regulates adaptive immunity. Splenocytes of immunised and rechallenged Stat1fl/fl and CD11cCreStat1fl/fl mice were isolated and evaluated for proliferating CD3+ cells (8A) and Tregs (CD3+, CD4+, FoxP3+, Ki67+) (8B). Means and standard deviations of one representative experiment out of two independently performed experiments are shown with 5 mice per group. doi:10.1371/journal.ppat.1002763.g008

different cell types. Furthermore, we were able to investigate the importance of Stat1 signaling in the same cell types for the development of acquired antibacterial immunity.

Clearance of intracellular bacterial pathogens is caused either by a microbicidal effector mechanism of the infected cell or indirectly through CD8+ T cell-mediated cytotoxicity. *Lm* infects a variety of different cell types *in vitro*, either by active invasion or phagocytosis [48,49]. In infected mice the pathogen replicates in both hematopoietic cells, predominantly macrophages, and non-hematopoietic cells amongst which the hepatocytes form a major niche [32,33]. To our surprise Stat1 signaling provides non-hematopoietic cells with little effector potential, posing the question how *Listeria* are killed in these cell compartments particularly before the influx of antigen-specific CTL. One possibility is the death of infected hepatocytes and the subsequent phagocytosis of the cell contents including bacterial cargo by phagocytic cells of the innate immune system [32]. Subsequent sterile clearance most likely requires the development of CTL and active lysis of infected cells [50,51,52]. The importance of clearing *Lm* in the liver is underscored by our findings that the death of mice with different Stat1 genotypes correlated well with the inflammatory infiltrate in this organ and with the hepatotoxicity caused by infection.

LysMCre mediated gene deletion occurs predominantly in macrophages and granulocytes [34]. A recent report shows that the contribution of neutrophils to the immune response against *Lm* is surprisingly small [53] and, given the short half life of granulocytes, Stat1-dependent transcriptional response to IFN is unlikely to enhance their microbicidal activity. Therefore our data are consistent with the previous notion that IFN γ and Stat1 cause macrophage activation and that activated macrophages represent a dominant innate anti-listericidal effector mechanism of the innate immune response [54,55]. Indeed, our data reveal the essential role of this cell type for clearance of *Lm*. That said the clearance deficit of mice lacking macrophage Stat1 was significantly lower than that of Stat1 $^{-/-}$ mice. In this regard inspection of the local immune reaction elicited by intraperitoneal infection with *Lm* showed that besides macrophages T cells and particularly CD11c+ cells shape the inflammatory environment by regulating chemokine production and cell influx. CD11c+ cells in this situation are likely to represent inflammatory DC that arise from inflammatory monocytes [56]. Although lack of Stat1 signaling in non-hematopoietic cells or DC does not per se affect survival and clearance of infection, it may synergize with the Stat1 deficiencies of other cell types to produce the more severe outcome of the complete Stat1 knockout. Increased *Lm* replication in Stat1 $^{-/-}$ compared to LysMCreStat1 $^{fl/fl}$ mice caused a more severe cytokine storm that is likely to be one cause of their accelerated death.

While the amount of serum cytokines generally followed the severity of infection in different Stat1 genotypes, IL12 was the exception because it was strongly increased in mice with Stat1-deficiency outside the hematopoietic compartment that were able to cope with infection nearly as well as WT mice. This finding reveals negative regulation of IL12 synthesis by a non-hematopoietic cell. IL10 is a negative regulator of IL12 production [57] and its synthesis can be suppressed by IFN γ [58]. However, IL10 is considered to be a product of hematopoietic cells [59]. The nature of the suppressive cell type and the mechanism of IL12 suppression will require further investigation.

The exacerbation of infection by Stat1 in T lymphocytes is particularly intriguing. Unanue and colleagues demonstrated the T cell response to IFN-I as a mechanism underlying their adverse effect [26,28]. While our data confirm that the IFN-I response of T

cells indeed reduces bacterial clearance, *Ifnar1*-deficiency in this cell type alone does not reproduce the consequences of the complete *Ifnar1* knockout and it does not cause the robust effect of T cell-specific Stat1 deletion. Hence, T cells indeed inhibit protective innate immunity to *Lm*, but the effect of Stat1 goes beyond IFN-I signaling. Furthermore, additional cell compartments must contribute to the suppressive effect of IFN-I, as suggested by the comparison between infected *Ifnar1 $^{-/-}$ and *LckCreIfnar1* $^{fl/fl}$ mice. At present we do not fully understand how Stat1 signaling in T cells reduces innate immunity to *Lm*. Clearly, it increases apoptosis of splenic cells, and the comparison to *Ifnar1*-ablated cells suggests this results from the activity of type I interferons. However, T cell Stat1-mediated loss of innate protection goes beyond IFN-I effects on splenocyte apoptosis. In line with the results shown in figure S4, skewed CD4+ T cell differentiation causing a reduction of IFN γ -producing Th1 cells and a concomitant increase in Th2 and Th17 cells may be a contributing factor. Importantly, *Ifnar1* deficiency in T cells increases IFN γ production when *Lm* antigens are presented by wt APC *in vitro*. At present we do not know whether T cell differentiation is a decisive factor within the first three days of infection in mice. Systemic cytokine profiles of *LckCreStat1* $^{fl/fl}$ animals showed little change with respect to WT mice in this period. Systemic IL10 levels were below the detection limit, leading us to assume that reduced clearance does not result from global immunosuppression. In addition, bacterial multiplication might be enhanced by the reported suppressive activity of IFN-I on IFN γ receptor expression [29].*

Infection of immunized mice with *Lm* caused a drastic change in the consequences of Stat1 signaling in cell types of the immune system. Most importantly Stat1 activity in T cells was now required for protective immunity. Antigen-specific CTL are critical effectors for adaptive immunity to *Lm* [15,52]. Our data provide the first genetic proof that Stat1 signaling in both T cells and DC is required for acquired resistance, in addition to showing that IFN γ -activated macrophages are dispensable once memory lymphocytes have been produced. The essential stimulus for Stat1 signaling in T cells is unclear. IFN-I appear to be dispensable for both CD4+ and CD8+ T cell development during *Lm* infection [60,61]. Furthermore, a study analyzing CTL development in IFN γ -deficient animals infected with very low numbers of *Lm* shows that IFN γ is not essential for protective CTL-mediated immunity [51]. Possibly IFN γ contributes to protective CTL memory when infection occurs with a high infectious dose. Therefore, Stat1 may increase the efficacy of memory CD8+ T cell responses.

Defective Stat1 signaling in CD11c+ DC also reduced protection by the adaptive immune system upon secondary challenge with *Lm*. This is consistent with our recent finding that immunization with Stat1 $^{-/-}$ DC caused a strongly diminished CTL response to Ova peptide [62] and with reports by others that Stat1 $^{-/-}$ DC fail to elicit protective immunity to *Leishmania major* [63]. IFN-I and Stat1 reportedly support DC maturation and activation [64,65]. Data in the literature thus suggest a defect of Stat1-deficient DC to present antigen to T cells. In line with this IFN-I were reported to stimulate the ability of DC to cross-present antigen [23]. In our experiments the lack of DC Stat1 affected survival of mice more than splenic clearance of bacteria, which argues against a general defect in generating effector CTL. Moreover, activation of both CD4+ and CD8+ T cells to the levels found with wt cells occurred *in vitro* when Stat1 $^{-/-}$ DC were used as antigen presenters (Figure S5). In a mouse model of graft versus host disease Ma and colleagues noted an increased proliferation of FoxP3+ regulatory T cells upon transfer of

Stat1^{-/-} splenocytes into irradiated hosts [66]. Prompted by this finding we tested whether Stat1 deficiency in DC might similarly cause increased Treg proliferation in *Listeria*-infected mice. Indeed we noted that the proportion of proliferating FoxP3⁺ cells was about two-fold higher in spleens from infected mice with a CD11cCreStat1^{fl/fl} genotype. It is therefore possible that an increased number of antigen-specific regulatory T cells suppresses effector T cells and thus reduces the immune response to *Lm*.

In summary, cell type-restricted ablation reveals a fascinating complexity of Stat1's regulatory power for the development of both innate and adaptive immune responses to *Lm*.

Materials and Methods

Mice and bacteria

Animal experiments were discussed and approved by the University of Veterinary Medicine Vienna institutional ethics committee and carried out in accordance with protocols approved by the Austrian law (BMWF-68.205/0204-C/GT/2007; BMWF-68.205/0210-II/10b/2009, BMWF-68.205/0243-II/3b/2011). Bacteria were prepared for infection as described previously [67]. For infection, *Lm* LO28 were washed with PBS and injected intraperitoneally (i.p) or intravenously (i.v) of 8- to 10-week-old sex and age matched C57BL/6N (WT), Stat1^{fl/fl} (B6.129P2-Stat1^{tmBiat}; [35]), LysMCre Stat1^{fl/fl} (B6.129P2-Lyz2^{tm1(Cre)Flv}/J-Stat1^{tmBiat}; [34]), CD11cCre Stat1^{fl/fl} (B6.Cg-Tg(CD11c-Cre)-Stat1^{tmBiat} [68]), LckCre Stat1^{fl/fl} (B6.129P2-Tg(LckCre)-Stat1^{tmBiat} LckCre [69]), *Ifnar1*^{-/-} (B6.129P2-*Ifnar1*^{tm1}) [70], *Stat4*^{-/-} (B6.129P2-Stat1^{tm1}), *Ifnar1*^{fl/fl}LckCre (B6.129P2-*Ifnar1*^{tm1}-Tg (LckCre) [71] mice at the respective dose. The infectious dose was controlled by plating serial dilutions on Oxford agar plates. The survival of mice was monitored for 10 days, and data were displayed as Kaplan-Meier plots. For determination of bacterial loads of liver and spleen mice were killed at the indicated time points. The respective organs were isolated and homogenized in PBS. Serial dilutions of the homogenates were plated on BHI plates and incubated at 37°C for 24 h. For immunisation mice were injected i.p with 1 × 10⁶ attenuated *Listeria* (Δ ActA). After 2–3 weeks mice were infected i.v with 1 × 10⁵ *Lm*.

Cytokine analysis

For cytokine analysis mice were bled via the retro-orbital sinuses and serum was collected and stored at -80°C. Using the FlowCytomix system (ebioscience) concentrations of indicated cytokines (IFN γ , IL6, IL10, IL12p70, Mcp1, Mcp3, Rantes, GM-CSF, Mip1 α , Mip1 β , IP10, IL22, TNF α) in 25 μ l of serum were measured.

Peritoneal exudate cell isolation

For isolation of peritoneal macrophages mice were infected for 48 h with 5 × 10⁶ LO28 i.p. Mice were sacrificed, the peritoneum was flushed with two times 10 ml of DMEM and cells were harvested by centrifugation and plated on 6 well plates. After 2 h adherent cells were washed with PBS and RNA was prepared for Real Time PCR analysis. The composition of total peritoneal exudate cells was examined using Wright-Giemsa staining of cytospins. Composition of adherent cells were analysed by flowcytometric analysis (F4/80-APC, CD11b-PE, CD3-FITC (BD biosciences), Ly6C-PerCP (ebioscience)). Chemokines and cytokines were measured using the FlowCytomix system after flushing the peritoneum with 1 ml of DMEM.

RNA isolation, cDNA synthesis and Real Time PCR

RNA was isolated using the Nucleospin II kit (Macherey and Nagel) according to protocol. Reverse transcription was accom-

plished using RevertAid (Fermentas). The Real Time PCRs were run on an Eppendorf cyclor. After correction for the housekeeping gene *Gapdh*, every sample was calculated to the mean of WT mRNA levels. The following primer sequences were used (all 5'-3'): IL6: for TAGTCCTTCCTACCCCAATTTCC; rev TTG-GTCCTTAGCCACTCCTTC; IL10: for GGTTGCCAAGCC-TTATCGGA; rev ACCTGCTCCACTGCCTTGCT; IL12p40: for TGGTTTGCCATCGTTTTGCTG; rev ACAGGTGAGG-TTCACTGTTTCT; GAPDH: for CATGGCCTTCCGTGT-TCTA; rev GGGGACGTCAGATCCA.

Flowcytometric analysis

Spleens were isolated after indicated timepoints and single cell suspensions were prepared using a 80 μ m cell strainer. After red blood cell lysis cells were stained for CD3-PE, CD4-FITC, CD8-APC, CD11b-PerCP, Gr1-PE, FOXP3-APC, Ki67-PerCP (all BD bioscience). For intracellular staining cells were fixed and permeabilised using the FoxP3 staining kit (ebioscience)

Histology

Mouse organs were fixed with 4% paraformaldehyde overnight, paraffin embedded and 4 μ m sections were prepared using a microtome. Hematoxyline and eosin staining (H&E) were performed using standard protocols. The radius of the infiltrate was measured using the Zeiss Axioplan software. For TUNEL staining, sections of spleens were stained using the TUNEL-POD kit (Roche) according to protocol. Additionally, sections were blocked for endogenous peroxidase activity in methanol with H₂O₂ and after proteinase K treatment blocked with 5% normal goat serum to reduce background staining. TUNEL enzyme and POD conversion was applied as described, and AEC+ high sensitivity chromogen (Dako) was used as a HRP substrate. Subsequently, sections were counterstained with hematoxyline.

AST measurement

Aspartate amino transferase concentrations were measured in mouse serum using a COBASc11 analyzer (Roche).

Adoptive transfer

WT (Ly5.1 and C57BL/6) and Stat1^{-/-} animals were lethally irradiated with 8,2 Gy for 17 minutes and engrafted with 5 × 10⁶ bone marrow cells of respective genotypes by i.v injection. After 6 weeks engraftment was analysed in blood, spleen and liver by flow cytometry using the antibodies Ly5.1-FITC, Ly5.2-PE, CD11b-PerCP (BD biosciences).

Blood lymphocyte population

Mice were bled via the retro-orbital sinuses in tubes coated with EDTA and the cellular composition was measured using a vet haematology analyzer V sight (A. Menarini diagnostics).

Statistical analysis

Bacterial loads of organs were compared using the Mann-Whitney test; mRNA expression data and cytokines levels were analysed with the Students t test. For both the GraphPad Software was used. Asterisks describe the significances as follows: * p \leq 0,05; **p \leq 0,01; ***p \leq 0,001

Supporting Information

Figure S1 Bone marrow chimerism and blood lineage analysis. Percentage of Ly5.1 positive leukocytes in the blood and Ly5.1+ and CD11b+ cells in spleen and liver. For bone

marrow Ly5.2 positive cells are shown due to a large proportion of Ly5.1 and Ly5.2 negative cells. Percentages of positive cells are indicated in the figure (S1). Representative plots of a Stat1^{-/-} mouse reconstituted with WT (Ly5.1) bone marrow are shown. (EPS)

Figure S2 Deletion efficiency of CD11c and LckCre in splenic DC and T cells. Splenic dendritic cells (S2a) and splenic T cells (S2b) were isolated, respectively, from CD11cCreStat1^{fl/fl}, LckCreStat1^{fl/fl}, and control mice (S2b) and subjected to Western blot analysis for Stat1N and pan-erk. (EPS)

Figure S3 Time course of bacterial burden in mice with cell type-restricted Stat1 ablation. Stat1-ablated and control mice were infected i.p. with 1×10^6 Lm and bacterial load of spleen (S3A) and liver (S3B) over the course of three days was determined. Medians of cumulative data from 2–3 experiments are depicted. (EPS)

Figure S4 In vitro infection of splenocyte cultures. Splenocytes were isolated from WT, Irfar1^{-/-}, Stat1^{-/-}, LckCreStat1^{fl/fl} and LckCreIrfar1^{fl/fl} mice and infected *in vitro* with Lm at a MOI of 10. 48 h after infection the supernatant was harvested and analysed for IFN γ , IL4, IL17 and IL10. Means of cumulative data of two individual experiments are shown with standard deviations. (EPS)

Figure S5 Time course of serum cytokines after Lm infection. The respective Stat1 ablated animals were infected with 1×10^6 Lm and respective cytokines were measured in 25 μ l of serum at day 1, 2 and 3 after infection. Means of cumulative

data from 2–3 experiments are shown with standard deviation. Significances are indicated with asterisks. (EPS)

Figure S6 Time course of peritoneal chemokines after Lm infection. The peritoneum of mice infected for 48 h with 1×10^6 Lm was flushed with 1 ml of DMEM. Chemokines were measured in 25 μ l of the peritoneal wash. The means of cumulative data from 2 experiments are shown with standard deviation. (EPS)

Figure S7 Stat1^{-/-} dendritic cells can stimulate T cell proliferation. WT mice were immunised with Δ ActA Lm and splenic T cells were isolated from these animals 2–3 weeks later. Splenic dendritic cells were isolated from WT and CD11cCreStat1^{fl/fl} animals, pulsed over night with heat-killed Listeria (HKL) and admixed to the CFSE labelled T cells at different ratios. Unstimulated, CFSE labelled T cells were used as a control. Dilution of T cell CFSE was determined 8 days after stimulation. Means of percent divided (CFSElo) CD8⁺ T cells and CD4⁺ T cells are depicted of one representative experiment out of three. (EPS)

Text S1 Supplemental methods. (DOC)

Author Contributions

Conceived and designed the experiments: VS MM TD EK AJ DS BS. Performed the experiments: EK VM CS UR. Analyzed the data: EK TD MM VS. Contributed reagents/materials/analysis tools: UK BR. Wrote the paper: EK TD AJ.

References

- Borden EC, Sen GC, Uze G, Silverman RH, Ransohoff RM, et al. (2007) Interferons at age 50: past, current and future impact on biomedicine. *Nat Rev Drug Discov* 6: 975–990.
- Stark GR, Kerr IM, Williams BR, Silverman RH, Schreiber RD (1998) How cells respond to interferons. *Annu Rev Biochem* 67: 227–264.
- Kaplan DH, Shankaran V, Dighe AS, Stockert E, Aguet M, et al. (1996) Demonstration of an interferon gamma-dependent tumor surveillance system in immunocompetent mice. *Proc Natl Acad Sci U S A* 95: 7556–7561.
- Kovacic B, Stoiber D, Moriggi R, Weisz E, Ott RG, et al. (2006) STAT1 acts as a tumor promoter for leukemia development. *Cancer Cell* 10: 77–87.
- Schneckenleithner C, Bago-Horvath Z, Dolznig H, Neugebauer N, Kollmann K, et al. (2011) Putting the brakes on mammary tumorigenesis: Loss of STAT1 predisposes to intraepithelial neoplasias. *Oncotarget* 2: 1043–1054.
- Durbin JE, Hackenmiller R, Simon MC, Levy DE (1996) Targeted disruption of the mouse Stat1 gene results in compromised innate immunity to viral disease. *Cell* 84: 443–450.
- Meraz MA, White JM, Sheehan KC, Bach EA, Rodig SJ, et al. (1996) Targeted disruption of the Stat1 gene in mice reveals unexpected physiologic specificity in the JAK-STAT signaling pathway. *Cell* 84: 431–442.
- Levy DE, Darnell JE, Jr. (2002) Stats: transcriptional control and biological impact. *Nat Rev Mol Cell Biol* 3: 651–662.
- Chappier A, Kong XF, Boisson-Dupuis S, Jouanguy E, Averbuch D, et al. (2009) A partial form of recessive STAT1 deficiency in humans. *J Clin Invest* 119: 1502–1514.
- Kristensen IA, Veirum JE, Møller BK, Christiansen M (2011) Novel STAT1 alleles in a patient with impaired resistance to mycobacteria. *J Clin Immunol* 31: 265–271.
- Zhang SY, Boisson-Dupuis S, Chappier A, Yang K, Bustamante J, et al. (2008) Inborn errors of interferon (IFN)-mediated immunity in humans: insights into the respective roles of IFN- α /beta, IFN- γ , and IFN- λ in host defense. *Immunol Rev* 226: 29–40.
- Hsieh CS, Macatonia SE, Tripp CS, Wolf SF, O'Garra A, et al. (1993) Development of TH1 CD4⁺ T cells through IL-12 produced by Listeria-induced macrophages. *Science* 260: 547–549.
- Lu B, Ebensperger C, Dembic Z, Wang Y, Kvatsyuk M, et al. (1998) Targeted disruption of the interferon-gamma receptor 2 gene results in severe immune defects in mice. *Proc Natl Acad Sci U S A* 95: 8233–8238.
- Kaufmann SH (1993) Immunity to intracellular bacteria. *Annu Rev Immunol* 11: 129–163.
- Pamer EG (2004) Immune responses to Listeria monocytogenes. *Nat Rev Immunol* 4: 812–823.
- Badovinac VP, Harry JT (2000) Adaptive immunity and enhanced CD8⁺ T cell response to Listeria monocytogenes in the absence of perforin and IFN- γ . *J Immunol* 164: 6444–6452.
- Durbin JE, Fernandez-Sesma A, Lee CK, Rao TD, Frey AB, et al. (2000) Type I IFN modulates innate and specific antiviral immunity. *J Immunol* 164: 4220–4228.
- Fallarino F, Gajewski TF (1999) Cutting edge: differentiation of antitumor CTL *in vivo* requires host expression of Stat1. *J Immunol* 163: 4109–4113.
- Gil MP, Salomon R, Louten J, Biron CA (2006) Modulation of STAT1 protein levels: a mechanism shaping CD8 T-cell responses *in vivo*. *Blood* 107: 987–993.
- Messingham KA, Badovinac VP, Jabbari A, Harty JT (2007) A role for IFN- γ from antigen-specific CD8⁺ T cells in protective immunity to Listeria monocytogenes. *J Immunol* 179: 2457–2466.
- Akbar SM, Kajino K, Tanimoto K, Yamamura K, Onji M, et al. (1999) Unique features of dendritic cells in IFN- γ transgenic mice: relevance to cancer development and therapeutic implications. *Biochem Biophys Res Commun* 259: 294–299.
- Banyer JL, Halliday DG, Thomson SA, Hamilton NH (2003) Combinations of IFN- γ and IL-4 induce distinct profiles of dendritic cell-associated immunoregulatory properties. *Genes Immun* 4: 427–440.
- Le Bon A, Etchart N, Rossmann C, Ashton M, Hou S, et al. (2003) Cross-priming of CD8⁺ T cells stimulated by virus-induced type I interferon. *Nat Immunol* 4: 1009–1015.
- Huang S, Hendriks W, Althage A, Hemmi S, Bluethmann H, et al. (1993) Immune response in mice that lack the interferon-gamma receptor. *Science* 259: 1742–1745.
- Auerbuch V, Brockstedt DG, Meyer-Morse N, O'Riordan M, Porunou DA (2004) Mice lacking the type I interferon receptor are resistant to Listeria monocytogenes. *J Exp Med* 200: 527–533.
- Carrero JA, Calderon B, Unanue ER (2004) Type I interferon sensitizes lymphocytes to apoptosis and reduces resistance to Listeria infection. *J Exp Med* 200: 535–540.
- O'Connell RM, Saha SK, Vaidya SA, Bruhn KW, Miranda GA, et al. (2004) Type I interferon production enhances susceptibility to Listeria monocytogenes infection. *J Exp Med* 200: 437–445.
- Carrero JA, Calderon B, Unanue ER (2006) Lymphocytes are detrimental during the early innate immune response against Listeria monocytogenes. *J Exp Med* 203: 933–940.

29. Rayamajhi M, Humann J, Penheiter K, Andreasen K, Lenz LL (2010) Induction of IFN- α enables *Listeria monocytogenes* to suppress macrophage activation by IFN- γ . *J Exp Med* 207: 327–337.
30. Stockinger S, Materna T, Stoiber D, Bayr L, Steinborn R, et al. (2002) Production of type I IFN sensitizes macrophages to cell death induced by *Listeria monocytogenes*. *J Immunol* 169: 6522–6529.
31. Zwaferink H, Stockinger S, Hazemi P, Lemmens-Gruber R, Decker T (2008) IFN- β increases listeriolysin O-induced membrane permeabilization and death of macrophages. *J Immunol* 180: 4116–4123.
32. Rogers HW, Gallery MP, Deck B, Unanue ER (1996) *Listeria monocytogenes* induces apoptosis of infected hepatocytes. *J Immunol* 156: 679–684.
33. Gregory SH, Sagnimeni AJ, Wing EJ (1997) Internalin B promotes the replication of *Listeria monocytogenes* in mouse hepatocytes. *Infect Immun* 65: 5137–5141.
34. Clausen BE, Burkhardt C, Reith W, Renkawitz R, Forster I (1999) Conditional gene targeting in macrophages and granulocytes using *LysMcre* mice. *Transgenic Res* 8: 265–277.
35. Wallner B, Leitner NR, Vieinascher RM, Kernbauer E, Kolbe T, et al. (2012) Generation of mice with a conditional Stat1 null allele. *Transgenic Res* 21: 217–224.
36. Homann D, Jahreis A, Wolfe T, Hughes A, Coon B, et al. (2002) CD40L blockade prevents autoimmune diabetes by induction of bitypic NK/DC regulatory cells. *Immunity* 16: 403–415.
37. Jakubick C, Tacke F, Llodra J, van Rooijen N, Randolph GJ (2006) Modulation of dendritic cell trafficking to and from the airways. *J Immunol* 176: 3578–3584.
38. Szabo SJ, Sullivan BM, Peng SL, Glimcher LH (2003) Molecular mechanisms regulating Th1 immune responses. *Annu Rev Immunol* 21: 713–758.
39. Kimura A, Naka T, Nakahama T, Chinen I, Masuda K, et al. (2009) Aryl hydrocarbon receptor in combination with Stat1 regulates LPS-induced inflammatory responses. *J Exp Med* 206: 2027–2035.
40. Ramana CV, Gü MP, Han Y, Ransohoff RM, Schreiber RD, et al. (2001) Stat1-independent regulation of gene expression in response to IFN- γ . *Proc Natl Acad Sci U S A* 98: 6674–6679.
41. Ramana CV, Grammatikakis N, Chernov M, Nguyen H, Goh KC, et al. (2000) Regulation of c-myc expression by IFN- γ through Stat1-dependent and -independent pathways. *EMBO J* 19: 263–272.
42. Mandel TE, Cheers C (1980) Resistance and susceptibility of mice to bacterial infection: histopathology of listeriosis in resistant and susceptible strains. *Infect Immun* 30: 851–861.
43. Dancygier H (2010) Bacterial Liver Abscess and Other Bacterial Infections. In: Dancygier H, ed. *Clinical Hepatology* Springer, Berlin Heidelberg, pp 831–842.
44. Sasaki T, Mieno M, Udono H, Yamaguchi K, Usui T, et al. (1990) Roles of CD4⁺ and CD8⁺ cells, and the effect of administration of recombinant murine interferon gamma in listerial infection. *J Exp Med* 171: 1141–1154.
45. Ozer J, Ratner M, Shaw M, Bailey W, Schomaker S (2008) The current state of serum biomarkers of hepatotoxicity. *Toxicology* 245: 194–205.
46. Nguyen KB, Watford WT, Salomon R, Hofmann SR, Pien GC, et al. (2002) Critical role for STAT4 activation by type I interferons in the interferon- γ response to viral infection. *Science* 297: 2063–2066.
47. Chappier A, Boisson-Dupuis S, Jouanguy E, Vogt G, Feinberg J, et al. (2006) Novel STAT1 alleles in otherwise healthy patients with mycobacterial disease. *PLoS Genet* 2: e131.
48. Portnoy DA, Auerbuch V, Glomski JJ (2002) The cell biology of *Listeria monocytogenes* infection: the intersection of bacterial pathogenesis and cell-mediated immunity. *J Cell Biol* 158: 409–414.
49. Hamon M, Bieme H, Cossart P (2006) *Listeria monocytogenes*: a multifaceted model. *Nat Rev Microbiol* 4: 423–434.
50. Gregory SH, Liu CC (2000) CD8⁺ T-cell-mediated response to *Listeria monocytogenes* taken up in the liver and replicating within hepatocytes. *Immunol Rev* 174: 112–122.
51. Harty JT, Bevan MJ (1995) Specific immunity to *Listeria monocytogenes* in the absence of IFN- γ . *Immunity* 3: 109–117.
52. Lara-Tejero M, Pamer EG (2004) T cell responses to *Listeria monocytogenes*. *Curr Opin Microbiol* 7: 45–50.
53. Shi C, Hohl TM, Leiner I, Equinda MJ, Fan X, et al. (2011) Ly6G⁺ Neutrophils Are Dispensable for Defense against Systemic *Listeria monocytogenes* Infection. *J Immunol* 187: 5293–5298.
54. Mackaness GB (1962) Cellular resistance to infection. *J Exp Med* 116: 381–406.
55. Shaughnessy LM, Swanson JA (2007) The role of the activated macrophage in clearing *Listeria monocytogenes* infection. *Front Biosci* 12: 2683–2692.
56. Shi C, Pamer EG (2011) Monocyte recruitment during infection and inflammation. *Nat Rev Immunol* 11: 762–774.
57. Zhou L, Nazarian AA, Smale ST (2004) Interleukin-10 inhibits interleukin-12 p40 gene transcription by targeting a late event in the activation pathway. *Mol Cell Biol* 24: 2385–2396.
58. Hu X, Paik PK, Chen J, Yarinina A, Kockeritz L, et al. (2006) IFN- γ suppresses IL-10 production and synergizes with TLR2 by regulating GSK3 and CREB/AP-1 proteins. *Immunity* 24: 563–574.
59. Saraiva M, O'Garra A (2010) The regulation of IL-10 production by immune cells. *Nat Rev Immunol* 10: 170–181.
60. Havenar-Daughton C, Kolumam GA, Murali-Krishna K (2006) Cutting Edge: The direct action of type I IFN on CD4 T cells is critical for sustaining clonal expansion in response to a viral but not a bacterial infection. *J Immunol* 176: 3315–3319.
61. Thompson LJ, Kolumam GA, Thomas S, Murali-Krishna K (2006) Innate inflammatory signals induced by various pathogens differentially dictate the IFN- γ dependence of CD8 T cells for clonal expansion and memory formation. *J Immunol* 177: 1746–1754.
62. Pilz A, Kratky W, Stockinger S, Simma O, Kalinke U, et al. (2009) Dendritic cells require STAT-1 phosphorylated at its transactivating domain for the induction of peptide-specific CTL. *J Immunol* 183: 2286–2293.
63. Johnson LM, Scott P (2007) STAT1 expression in dendritic cells, but not T cells, is required for immunity to *Leishmania major*. *J Immunol* 178: 7259–7266.
64. Jackson SH, Yu CR, Mahdi RM, Ehong S, Egwuagu CE (2004) Dendritic cell maturation requires STAT1 and is under feedback regulation by suppressors of cytokine signaling. *J Immunol* 172: 2307–2315.
65. Le Bon A, Schiavoni G, D'Agostino G, Gresser I, Belardelli F, et al. (2001) Type I interferons potently enhance humoral immunity and can promote isotype switching by stimulating dendritic cells in vivo. *Immunity* 14: 461–470.
66. Ma H, Lu C, Ziegler J, Liu A, Sepulveda A, et al. (2011) Absence of Stat1 in donor CD4 T cells promotes the expansion of Tregs and reduces graft-versus-host disease in mice. *J Clin Invest* 121: 2554–2569.
67. Stockinger S, Kastner R, Kernbauer E, Pilz A, Westermayer S, et al. (2009) Characterization of the interferon-producing cell in mice infected with *Listeria monocytogenes*. *PLoS Pathog* 5: e1000355.
68. Caton ML, Smith-Raska MR, Reizis B (2007) Notch-RBPJ signaling controls the homeostasis of CD8⁺ dendritic cells in the spleen. *J Exp Med* 204: 1653–1664.
69. Orban PC, Chui D, Marth JD (1992) Tissue- and site-specific DNA recombination in transgenic mice. *Proc Natl Acad Sci U S A* 89: 6861–6865.
70. Müller U, Steinhoff U, Reis LF, Hemmi S, Pavlovic J, et al. (1994) Functional role of type I and type II interferons in antiviral defense. *Science* 264: 1918–1921.
71. Kamphuis E, Junt T, Waibler Z, Forster R, Kalinke U (2006) Type I interferons directly regulate lymphocyte recirculation and cause transient blood lymphopenia. *Blood* 108: 3253–3261.

3.4 A new kinase-independent function of CDK6 links the cell cycle to tumour angiogenesis.

Manuscript under review in Nature Cell Biology.

Karoline Kollmann¹, Gerwin Heller^{2*}, **Christine Schneckenleithner**^{1*}, Wolfgang Warsch^{1*}, Ruth Scheicher¹, Rene G. Ott³, Markus Schäfer⁴, Sabine Fajmann¹, Ana-Iris Schiefer⁵, Ursula Reichart⁶, Matthias Mayerhofer⁷, Christoph Hoeller⁸, Sabine Zoechbauer-Mueller², Donscho Kerjaschki⁵, Lukas Kenner⁹, Gerald Hoefler¹⁰, Michael Freissmuth³, Richard Moriggl⁹, Meinrad Busslinger⁴, Marcos Malumbres¹¹ & Veronika Sexl¹

¹Institute of Pharmacology and Toxicology, University of Veterinary Medicine, Vienna, Austria; ²Clinical Division of Oncology, Department of Medicine I, Comprehensive Cancer Center, Medical University of Vienna, Vienna, Austria; ³Institute of Pharmacology, Center of Biomolecular Medicine and Pharmacology, Medical University of Vienna, Vienna, Austria; ⁴Research Institute of Molecular Pathology, Vienna Biocenter, Vienna, Austria; ⁵Department of Clinical Pathology, Medical University of Vienna, Vienna, Austria; ⁶Institute of Animal Breeding and Genetics, University of Veterinary Medicine Vienna, Vienna, Austria; ⁷Department of Laboratory Medicine, Medical University of Vienna, Austria; ⁸Department of Dermatology, Medical University of Vienna, Vienna, Austria; ⁹Ludwig Boltzmann Institute for Cancer Research, Vienna, Austria; ¹⁰Department of Pathology, Medical University of Graz, Graz, Austria; ¹¹Cell Division and Cancer Group, Molecular Oncology Programme, Centro Nacional de Investigaciones Oncológicas (CNIO), Madrid, Spain.

My contribution: Designed research, performed experiments, analyzed data.

I designed the cloning strategies and performed the cloning for the *pMSCV-cdk6-R31C-puro* construct (CDK6 mutant that fails to bind INK4 proteins) and the *pMSCV-cdk6-K43M-puro* construct (CDK6 kinase dead mutant). The constructs were used for several experiments throughout the whole study to delineate kinase-independent functions of CDK6 and display the specific regulation of p16^{INK4a} through CDK6 (Fig1. h-j; Fig3. a-i; Suppl. Fig3. b-d; Suppl Fig4. a-d, Suppl. Fig8. d). I also designed the cloning strategy and performed the cloning of the doxycycline inducible Tet-On CDK6-construct. I was further involved in establishing cell lines that induce the expression of CDK6 in response to doxycycline in a concentration-dependent manner. This was achieved by retroviral infection of *Cdk6*^{-/-} cell lines with the *pRevTet-On* regulatory plasmid and a GFP-expressing response plasmid (*pRevTRE-GFP*). Single cell clones were screened for clones with the highest doxycycline-dependent induction of GFP and the lowest background expression in the absence of doxycycline. Selected clones were then used for experiments with the CDK6-expressing response plasmid (*pRevTRE-tight-Cdk6*). The aim was to show that increasing levels of CDK6 expression do not induce apoptosis and to display that CDK6 regulates the expression of p16^{INK4a} and VEGF-A in a concentration dependent manner (Suppl. Fig1. e-h). I further established and conducted the shRNA knockdown of CDK6 in several human cell lines (Suppl. Fig11. a-i). The purpose of this experiment was to show that the regulatory effect of CDK6 on VEGF-A and p16^{INK4a} is also present in the human system.

A new kinase-independent function of CDK6 links the cell cycle to tumour angiogenesis

Karoline Kollmann¹, Gerwin Heller^{2*}, Christine Schneckenleithner^{1*}, Wolfgang Warsch^{1*}, Ruth Scheicher¹, Rene G. Ott³, Markus Schäfer⁴, Sabine Fajmann¹, Ana-Iris Schiefer⁵, Ursula Reichart⁶, Matthias Mayerhofer⁷, Christoph Hoeller⁸, Sabine Zoechbauer-Mueller², Donscho Kerjaschki⁵, Lukas Kenner⁹, Gerald Hoefler¹⁰, Michael Freissmuth³, Richard Moriggl⁹, Meinrad Busslinger⁴, Marcos Malumbres¹¹ & Veronika Sexl¹

¹Institute of Pharmacology and Toxicology, University of Veterinary Medicine, Vienna, Austria; ²Clinical Division of Oncology, Department of Medicine I, Comprehensive Cancer Center, Medical University of Vienna, Vienna, Austria; ³Institute of Pharmacology, Center of Biomolecular Medicine and Pharmacology, Medical University of Vienna, Vienna, Austria; ⁴Research Institute of Molecular Pathology, Vienna Biocenter, Vienna, Austria; ⁵Department of Clinical Pathology, Medical University of Vienna, Vienna, Austria; ⁶Institute of Animal Breeding and Genetics, University of Veterinary Medicine Vienna, Vienna, Austria; ⁷Department of Laboratory Medicine, Medical University of Vienna, Austria; ⁸Department of Dermatology, Medical University of Vienna, Vienna, Austria; ⁹Ludwig Boltzmann Institute for Cancer Research, Vienna, Austria; ¹⁰Department of Pathology, Medical University of Graz, Graz, Austria; ¹¹Cell Division and Cancer Group, Molecular Oncology Programme, Centro Nacional de Investigaciones Oncológicas (CNIO), Madrid, Spain.

*contributed equally

This work was supported by grants LS07-037 and LS07-019 from the WWTF and by the Austrian Science Foundation (FWF) via grants to VS (SFB F28 and P19723), LK and GH (FWF P18478) and GH (FWF SFB F3001).

Correspondence to: Veronika Sexl
Institute of Pharmacology and Toxicology
University of Veterinary Medicine, Vienna (VetmedUni)
Veterinaerplatz 1
A-1210 Vienna
Email: veronika.sexl@vetmeduni.ac.at
Fax: 0043-1-25077-2990
Tel: 0043-1-25077-2910

Total Word Count: 1810
Running Title: CDK6 and angiogenesis

Summary

Cell cycle alterations are common in cancer cells. The cell cycle kinase CDK6 - but not its close homologue CDK4 - is expressed at high levels in transformed lymphoid cells. We have studied the impact of deregulated CDK6 levels in a $p185^{BCR-ABL+}$ B-acute lymphoid leukaemia (B-ALL). We identified a novel, kinase-independent role for CDK6 as a transcriptional regulator. CDK6 acts in concert with c-JUN and STAT3 to induce the tumour suppressor $p16^{INK4a}$ and the pro-angiogenic factor VEGF-A. Our model implies that high CDK6 expression initially suppresses proliferation by up-regulating $p16^{INK4a}$, thereby providing an internal safeguard. Studies of human B- and T-cell lymphomas confirm the inverse relationship between CDK6 and $p16^{INK4a}$. Further validation comes from a murine T-cell lymphoma model driven by NPM-ALK. Only in the absence of $p16^{INK4a}$ is CDK6 able to reach its full potential in tumour promotion. In addition, CDK6 is part of a transcriptional complex that regulates VEGF-A. CDK6 thus uses two independent mechanisms to drive transcription: it interacts with STAT3 and D-type cyclins to regulate $p16^{INK4a}$ and cooperates with the AP-1 transcription factor c-JUN to regulate VEGF-A. The finding that CDK6 connects cell-cycle progression to tumour angiogenesis confirms CDK6's central role in hematopoietic malignancies and explains the selection pressure to up-regulate CDK6 and to silence $p16^{INK4a}$. As CDK6 is a major target for anti-cancer drug development, future therapeutic strategies should consider the potential involvement of the protein's kinase-independent functions in transcriptional regulation.

Enhanced CDK6 protein expression has been documented in human and murine lymphoma and leukaemia¹⁻⁸. CDK6 is required for AKT-induced thymoma formation and BCR-ABL-driven ALL in murine models^{1,9}. To investigate the consequences of increasing CDK6 expression in B-lymphoid leukaemia/lymphoma we generated stable $p185^{BCR-ABL}$ -transformed pro B-cell lines. These were infected with either a pMSCV-puro ($Cdk6^{+/+}$) or a pMSCV-Cdk6-puro based retrovirus ($Cdk6^{+/+}+Cdk6$). In contrast to our expectations $Cdk6^{+/+}+Cdk6$ cells displayed a strong reduction of proliferation (as confirmed by three different experimental techniques, see Supplementary Fig.1a-d). Moreover, cells with high CDK6 levels formed fewer and smaller colonies in growth factor-free methylcellulose (Fig. 1a). We did not find any increase in apoptosis or senescence on inducing CDK6 expression (Supplementary Fig. 1e-h). Consistently with their *in vitro* phenotype, $Cdk6^{+/+}+Cdk6$ cells gave rise to subcutaneous lymphoma-like tumours or leukaemia with increased latency (Fig.

1b and Supplementary Fig. 1i). We confirmed the reduced proliferation of *Cdk6*^{+/+}+*Cdk6* cells by staining tumour sections for the proliferation marker Ki-67 (Supplementary Fig. 1j and k). To investigate the underlying mechanism we examined the expression of several genes known to be important for cell-cycle control. Elevated CDK6 expression was consistently accompanied by high levels of the cell-cycle inhibitor and tumour suppressor p16^{INK4a}, while expression of other members of the INK4 family (p15^{INK4b}, p18^{INK4c}, p19^{INK4d}) and of p19^{ARF} remained unchanged (Fig. 1c and Supplementary Fig. 2a). These findings were recapitulated in murine embryonic fibroblasts (MEFs) that had not yet undergone senescence (Supplementary Fig. 2b). The up-regulation of p16^{INK4a} is not caused by increased protein stability as it persisted upon treatment with the proteasome inhibitor bortezomib (Supplementary Fig. 2c). High CDK4 expression in *p185*^{BCR-ABL} leukemic cells did not change p16^{INK4a} expression and proliferation, nor was any change in tumour growth observed (Supplementary Fig. 2d-g).

Enforced expression of CDK6 led to a pronounced increase in levels of *p16*^{INK4a} mRNA and pre-mRNA (Fig. 1d and Supplementary Fig. 3a). Chromatin immunoprecipitation (ChIP) experiments revealed that CDK6 binds specifically to the *p16*^{INK4a} promoter, while no binding to the *p19*^{ARF} promoter was detected (Fig. 1e). These findings define CDK6 as part of a transcriptional complex that regulates the tumour suppressor p16^{INK4a}. In line with this finding we detected the loss of the inhibitory histone mark H3K27me3, which controls p16^{INK4a} expression (Fig. 1f)^{10,11}. Consistently, the level of H3K36me3 is significantly increased: this marker parallels transcriptional activity (Fig. 1g).

To investigate whether CDK6 exerts its action on the promoter by phosphorylation (of an unknown substrate), we tested whether the CDK6 mutant CDK6K43M (in which the kinase domain is inactivated)¹² could up-regulate p16^{INK4a}. p185^{BCR-ABL}-transformed *Cdk6*^{-/-} and wild-type cells were infected with a *pMSCV-puro* based retrovirus containing Cdk6K43M, to generate stable cell lines (Fig. 1h and Supplementary Fig. 4a). Surprisingly, up-regulation of p16^{INK4a} mRNA and protein is kinase-independent (Fig. 1h and Supplementary Fig. 3b, 4a and 4b) and expression of the mutant *Cdk6K43M* reduces cell growth (Supplementary Fig. 3c and 4c). These experiments indicated the existence of a novel, kinase-independent function of CDK6 as a transcriptional regulator of the tumour suppressor p16^{INK4a}.

To examine whether p16^{INK4a} expression accounts for the growth inhibition caused by CDK6, we expressed CDK6 in p185^{BCR-ABL}-transformed cells deficient for p16^{INK4a}/p19^{ARF}. We did not observe any growth inhibitory effects or reduction of leukaemogenesis (Fig. 1i and 1j). In addition, we reconstituted p185^{BCR-ABL}-transformed *Cdk6*^{-/-} and wild-type cells with a

pMSCV-puro based retrovirus containing Cdk6R31C, a CDK6 mutant that cannot bind INK4 proteins (Supplementary Fig. 3d and 4d)¹³. Despite the presence of high p16^{INK4a} levels, the growth inhibitory effect of CDK6 was not mimicked by Cdk6R31C (Supplementary Fig. 3b-d, 4-d). These experiments confirm that the tumour-suppressing effect of high CDK6 expression results from a negative feedback loop mediated by p16^{INK4a}.

Our model makes a testable prediction: high CDK6 expression in a lymphoid tumour confers a growth advantage only if p16^{INK4a} expression is disrupted. Support for the prediction comes from an analysis of patient samples. Levels of CDK6 and p16^{INK4a} protein were analysed in two human tissue arrays, one for B-cell malignancies and one for T-cell malignancies. Figure 2a compiles 3 samples of the tissue array consisting of 16 different cases of B-cell lymphoma as well as a control lymph node. In all cases we found high levels of CDK6 expression accompanied by reduced or undetectable expression of p16^{INK4a}. The tissue array for T-cell malignancies consisted of 28 cases of anaplastic large cell lymphoma (ALCL), among which 17 carried the NPM-ALK fusion kinase (Fig. 2b and 2c). As ALCL cells diffusely infiltrate affected lymph nodes we employed CD30 staining to define the malignant cells. We found an inverse relationship between CDK6 and p16^{INK4a} in all samples (Chi-square test, $\chi^2 = 11.603$, $p \sim 0.02$). The majority of cases had high CDK6 expression and no or scarcely detectable expression of p16^{INK4a}. However, 4 of 11 NPM-ALK-negative tumours displayed the opposite phenotype: they had high p16^{INK4a} levels but lacked immunoreactivity against CDK6 antibodies (Fig. 2c). The correlation was verified by HistoQuestTM-assisted analysis (Supplementary Fig. 5a and 5b) (TissueGnostics GmbH, Vienna, Austria). The array experiments revealed an inverse relationship between p16^{INK4a} and CDK6 expression in human B- and T-cell lymphomas, which was confirmed by immunofluorescence staining (Supplementary Fig. 5c). The importance of CDK6 for NPM-ALK-driven tumorigenesis was verified using NPM-ALK transgenic mice. CDK6 deficiency significantly prolonged disease latency and NPM-ALK⁺ *Cdk6*^{-/-} cells showed reduced proliferation *in vitro* (Fig. 2d and Supplementary Fig. 5d). Lymphoma cell lines obtained from diseased wild-type mice showed consistently elevated CDK6 expression accompanied by loss of p16^{INK4a} expression due to methylation of CpG islands on the p16^{INK4a} promoter (Fig. 2e and Supplementary Fig. 5e). Importantly, the expression levels of CDK6 in human and the (over-expressed) levels in transformed murine cells were comparable (Fig. 2f and 2g and Supplementary Fig. 5f).

Detailed analysis of eight human ALCL samples indicated that tumour cells expressing high levels of CDK6 showed an enhanced density of blood vessels (Supplementary Fig. 6a and 6b). As tumour angiogenesis is frequently driven by ligands of the vascular endothelial

growth factor (VEGF) receptor, we investigated the levels of the most prominent growth factor VEGF-A. The investigation of ten human hematopoietic cell lines and human control lymphocytes indicated a positive correlation between *VEGF-A* and *CDK6* but not *CDK4* mRNA expression levels (Supplementary Fig. 6c and 6d). *CDK6*'s role in tumour angiogenesis was tested directly by experiments in which NPM-ALK⁺ *Cdk6*^{-/-} cell lines were subcutaneously injected into mice. *Cdk6*^{-/-} tumours evolved significantly later and displayed severely reduced blood vessel formation and *Vegf-A* expression (Supplementary Fig. 7a-c).

To investigate the mechanism of *CDK6*-regulated angiogenesis, we reconstituted *CDK6*-deficient p185^{BCR-ABL}-transformed cells with wild-type *CDK6*, *CDK6K43M* or *CDK6R31C*. Several independently derived cell lines were injected subcutaneously into mice and the ability to stimulate angiogenesis as well as VEGF-A protein levels was found to correlate with *CDK6* expression (Fig. 3a-d). To confirm the pro-angiogenic effect of *CDK6*, we added the cell supernatant to murine endothelial cells. Supernatant from cells expressing *CDK6* - either wild-type or mutant - was capable of significantly stimulating endothelial cell proliferation, migration and sprouting (Fig. 3e-h). *CDK6* induced expression of *Vegf-A* pre-mRNA, mRNA and protein, irrespective of the mutant used (Fig. 3i and Supplementary Fig. 8a and 8b). Similar observations were made in p185^{BCR-ABL}-transformed wild-type cells after enforced expression of *CDK6* but not of *CDK4* (Supplementary Fig. 8a-d and 9a-c). That regulation of VEGF-A is independent of *CDK6* (and *CDK4*) kinase activity was confirmed by treating wild-type cell lines with the *CDK6/CDK4* inhibitor PD033299, which was found to reduce proliferation but not to affect *Vegf-A* mRNA levels (Fig. 3j and 3k).

Enforced expression of VEGF-A in *Cdk6*^{-/-} cells restored the size of subcutaneous p185^{BCR-ABL}⁺ tumours. The increased size could not be attributed to an increase in cell proliferation (Supplementary Fig. 10a-c). Conversely, reduction of *CDK6* protein in the human hematopoietic cell lines Mac2a and Sudhl1 by shRNA-mediated knockdown was accompanied by decreased VEGF-A expression (Supplementary Fig. 11a-f). No effect of *CDK6* knockdown on VEGF-A was observed in the human kidney cell line HEK293T (Supplementary Fig. 11g-i). In total, *CDK6* was found to have a transcriptional regulatory effect on *Vegf-A* in 7/14 human and murine cell lines, especially in hematopoietic cells and in non-transformed fibroblasts (Supplementary Table 1).

ChIP assays verified *CDK6*'s role in the regulation of *Vegf-A* and *p16^{INK4a}* transcription (Fig. 4a, 4b and Supplementary Fig. 12a). Increased *CDK6*-induced *Vegf-A* transcription was reflected by a significant increase in H3K36 trimethylation, while changes in other histone marks did not reach significant levels (Supplementary Fig. 12b and 12c).

Co-immunoprecipitation experiments revealed that CDK6 is found in a complex with the proto-oncogene STAT3 and the AP-1 transcription factor c-JUN (Fig. 4c and 4d). To test whether the transcriptional activity of CDK6 depends on these proteins we used p185^{BCR/ABL}-transformed cell lines lacking either c-JUN or STAT3. CDK6 was capable of inducing *Vegf-A* expression in the absence of STAT3 but not of c-JUN (Fig. 4e and 4f). In contrast, induction of *p16^{INK4a}* by CDK6 required the presence of STAT3 (Fig. 4g and 4h). The findings were confirmed by luciferase assays (Supplementary Fig. 13a and 13b) and ChIP/Re-ChIP studies (Fig. 4i and Supplementary Fig. 13c and 13d). Recent studies have demonstrated that D-type cyclins possess transcriptional activity¹⁴. ChIP experiments confirmed that CyclinD2 is present at the *p16^{INK4a}* promoter (Supplementary Fig. 13e) and consistently CDK6 failed to induce *p16^{INK4a}* transcription in MEFs deficient for Cyclin D1, D2 and D3 (Fig. 4j and 4k). The ability to induce *Vegf-A* transcription was unaffected by deletion of these cyclins (Fig. 4l, 4m and Supplementary Fig. 13f). In summary, our data show that CDK6 regulates transcription in at least two ways – either in cooperation with STAT3 and D-type cyclins or together with the AP-1 transcription factor c-JUN (Fig. 4n).

p16^{INK4a} regulation can be regarded as a safeguard that needs to be overcome for full transformation by oncogenic CDK6. Accordingly, malignancies of the B- or T- lymphoid lineage frequently display loss of *p16^{INK4a}* due to deletion, mutation or methylation¹⁵⁻²². We predict that in such cases enhanced CDK6 protein levels drive both cell-cycle progression and angiogenesis. The finding that CDK6 is able to induce transcription of growth factors such as *Vegf-A* provides a possible explanation why this protein is consistently up-regulated in leukaemia and lymphoma. Although tumour growth depends on angiogenesis, to date there have been few indications of factors involved in the regulation of both processes and the mechanism underlying their interdependence has remained elusive. As CDK6 promotes tumour growth while simultaneously guaranteeing the supply of oxygen and energy to the rapidly growing tumour, it enables tumours to proliferate extremely efficiently. CDK6 already represents a promising target for anti-cancer drugs. In the light of our findings, it is important that drug design take into account the novel, kinase-independent function of the CDK6 protein.

Materials and methods

Mice

All mice were on a C57BL/6 background. *Cdk6*^{-/-} ²³, *INK4a/ARF*^{-/-24}, *NPM-ALK*^{tg25}, *Nu/Nu* and *Rag2*^{-/-} mice ²⁶ were described previously. Animal experiments were performed in accordance with protocols approved by the Animal Welfare Committee (MUW).

Cell culture, infection of foetal liver cells and expression vectors

Tissue culture conditions, virus preparation, infections establishment of cell-lines and colony forming assays were performed as described previously ^{9,27-29}. Expression vectors employed: *pMSCV-puro*, *pMSCV-Cdk6-puro*, *pMSCV-Cdk6R31C-puro* ¹³, *pMSCV-Cdk6K43M-puro* ¹², *pMSCV-Cdk4-puro*, *pMSCV-JunB-puro* and *pMSCV-cJun-puro*. *cJun*^{ΔΔ} and *Stat3*^{ΔΔ} p185^{BCR/ABL}-transformed cell lines as well as Cyclin D1/2/3^{-/-} MEFs were described previously ^{9,30,31}.

Transplantation of tumour cells into *Rag2*^{-/-} and *Nu/Nu* mice

Tail vein injection as well as subcutaneous injection was performed as described previously ⁹.

Monolayer wounding assay

1 x 10⁵ murine endothelial cells (mECs) were seeded in endothelial cell growth medium (RPMI containing 10% FCS mixed 1:1 with Epithelial Cell Growth Medium MV (PromoCell)). After 24 hours medium was removed and a scratch through the monolayer was made. Afterwards cells were washed 2 times with PBS and covered with different supernatants.

For supernatant production a defined cell number of different cell lines was incubated in medium for 24 hours. Supernatant was collected and filtered to avoid leukaemic cells.

After 2 and 24h incubation of the mECs with the supernatant pictures of the scratch were taken under a microscope (Nikon, Eclipse TS100; 10x) using a digital camera (Nikon, Coolpix P5000; Zoom F2.7). To analyse migration differences the percentage of open area of the scratch was measured with the TScratch software.

Spheroid sprouting assay

mECs were suspended in 80% endothelial cell growth medium (RPMI containing 10% FCS mixed 1:1 with Epithelial Cell Growth Medium MV (PromoCell) and 20% methylcellulose

(Sigma) and seeded as drops (800 cells/30 μ L) in non-adherent dishes. The dishes were incubated upside down as hanging drops for 24 h. Under these conditions, all suspended cells contribute to the formation of a single spheroid per drop of defined size and cell number (800 cells/spheroid). Afterwards, spheroids were harvested and seeded in methylcellulose and supernatant (preparation as described in ‘monolayer wounding assay’) of the leukaemic cells was added. After 24h incubation the cumulative length of the sprouts that had grown out of each spheroid was measured with ImageJ software.

³[H]-thymidine incorporation and flow cytometric analysis

³[H]-thymidine incorporation and cell cycle analysis were performed as previously described ⁹.

Protein analysis and Immunoblotting

Cell lysates and Immunoblotting was performed as described previously ⁹. The used antibodies are shown in Supplementary Table 2.

Co-Immunoprecipitation: 1000 μ g of cell lysates were incubated with 2 μ g of antibody (Supplementary Table 2) on a rotating wheel at 4°C over night, followed by 1/2 hour of incubation in presence of equilibrated protein A sepharose beads on rotating wheel at 4°C. After washing 4x the mixture was centrifugated and SDS loading buffer was added. Heating the samples for 5 min. on 95°C separated beads and proteins. Reaction mixtures were run on a SDS polyacrylamide gel.

ELISA

VEGF Quantikine ELISA Kit (R&D Systems) was used according to manufacturer’s recommendation.

RNA-isolation and qPCR analysis

RNA was isolated using TriZol (Invitrogen). First-strand cDNA-synthesis and PCR-amplification were performed using a reverse transcriptase–polymerase chain reaction (RT-PCR) kit (GeneAmp RNAPCRkit; Applied Biosystems) according to the manufacturer. qPCR was performed on an Eppendorf RealPlex cycler using RealMasterMix (Eppendorf) and SYBR Green as described ³². Primer pairs used in this study are shown in Supplementary Table 3. Each experiment was performed in triplicate and results normalized by comparison to *rplpO* mRNA expression.

Chromatin Immunoprecipitation (ChIP) and Re-ChIP Assays

ChIP assays were performed using the Chromatin immunoprecipitation Assay Kit (Upstate Biotechnology) according to the manufacturer's protocol. In brief,

5×10^6 cells were treated with 1% formaldehyde for 10 minutes and lysed subsequently. Chromatin was sheared to 200-1000 bp fragments using Bioruptor™ (Diagenode). The antibodies used are shown in Supplementary Table 1. Irrelevant IgG (10µg) was used as a control. Immunoprecipitated DNA was Phenol-Chlorophorm extracted, ethanol precipitated and dissolved in 30µl TE buffer. 2µL of recovered DNA were used for subsequent PCR analyses. Primer sequences for *p16^{INK4a}*, *ARF* and *Vegf-A* promoter and PCR conditions were used as reported previously^{33,34}. PCR products were separated on a 2% agarose gel stained with GelRed™ (Biotium). Primer sequences for histonmark analysis are shown in Supplementary Table 3.

For Re-ChIP experiments, 1×10^8 cells were lysed and chromatin was sonicated as described above. After immunoprecipitation with the first antibody protein-DNA complexes were eluted from protein A agarose beads by incubation for 30 min at 37°C in 50 µl of elution buffer (1X TE, 15% DTT and protease inhibitors). The second immunoprecipitation was performed as described above.

Statistical Analysis

Data are reported as mean values \pm SEM. Biochemical experiments were performed in triplicates and a minimum of three independent experiments were evaluated. Differences were assessed for statistical significance by an unpaired two-tailed *t* test, by the log rank test (for Kaplan-Meier plots) or by the χ^2 -square test (for contingency tables).

References

- 1 Hu, M. G. *et al.* A requirement for cyclin-dependent kinase 6 in thymocyte development and tumorigenesis. *Cancer Res* **69**, 810-818 (2009).
- 2 Zhao, J. J. *et al.* microRNA expression profile and identification of miR-29 as a prognostic marker and pathogenetic factor by targeting CDK6 in mantle cell lymphoma. *Blood* **115**, 2630-2639 (2010).
- 3 Agirre, X. *et al.* Epigenetic silencing of the tumor suppressor microRNA Hsa-miR-124a regulates CDK6 expression and confers a poor prognosis in acute lymphoblastic leukemia. *Cancer Res* **69**, 4443-4453 (2009).
- 4 Hayette, S. *et al.* In B-cell chronic lymphocytic leukemias, 7q21 translocations lead to overexpression of the CDK6 gene. *Blood* **102**, 1549-1550 (2003).
- 5 Chen, D. *et al.* Clinicopathologic features of CDK6 translocation-associated B-cell lymphoproliferative disorders. *Am J Surg Pathol* **33**, 720-729 (2009).
- 6 Brito-Babapulle, V. *et al.* Translocation t(2;7)(p12;q21-22) with dysregulation of the CDK6 gene mapping to 7q21-22 in a non-Hodgkin's lymphoma with leukemia. *Haematologica* **87**, 357-362 (2002).
- 7 Nagel, S. *et al.* Amplification at 7q22 targets cyclin-dependent kinase 6 in T-cell lymphoma. *Leukemia* **22**, 387-392 (2008).
- 8 Chilosi, M. *et al.* Differential expression of cyclin-dependent kinase 6 in cortical thymocytes and T-cell lymphoblastic lymphoma/leukemia. *Am J Pathol* **152**, 209-217 (1998).
- 9 Kollmann, K. *et al.* c-JUN promotes BCR-ABL-induced lymphoid leukemia by inhibiting methylation of the 5' region of Cdk6. *Blood* **117**:4065-4075(2011).
- 10 Agger, K. *et al.* The H3K27me3 demethylase JMJD3 contributes to the activation of the INK4A-ARF locus in response to oncogene- and stress-induced senescence. *Genes Dev.* 2009;23:1171–1176.
- 11 Barradas, M. *et al.* Histone demethylase JMJD3 contributes to epigenetic control of INK4a/ARF by oncogenic RAS. *Genes Dev.* 2009;23:1177–1182.
- 12 Zacharek, S. J., Xiong, Y. & Shumway, S. D. Negative regulation of TSC1-TSC2 by mammalian D-type cyclins. *Cancer Res* **65**, 11354-11360 (2005).
- 13 Gossel, M. J., Baker, G. L. & Hinds, P. W. cdk6 can shorten G(1) phase dependent upon the N-terminal INK4 interaction domain. *J Biol Chem* **274**, 29960-29967 (1999).
- 14 Despouy, G. *et al.* Cyclin D3 is a cofactor of retinoic acid receptors, modulating their activity in the presence of cellular retinoic acid-binding protein II. *J. Biol. Chem.* 278:6355-6362 (2003).
- 15 Malumbres, M. & Barbacid, M. To cycle or not to cycle: a critical decision in cancer. *Nat Rev Cancer* **1**, 222-231 (2001).
- 16 Nobori, T. *et al.* Deletions of the cyclin-dependent kinase-4 inhibitor gene in multiple human cancers. *Nature* **368**, 753-756, doi:10.1038/368753a0 (1994).
- 17 Hebert, J., Cayuela, J. M., Berkeley, J. & Sigaux, F. Candidate tumor-suppressor genes MTS1 (p16INK4A) and MTS2 (p15INK4B) display frequent homozygous deletions in primary cells from T- but not from B-cell lineage acute lymphoblastic leukemias. *Blood* **84**, 4038-4044 (1994).
- 18 Fizzotti, M. *et al.* Detection of homozygous deletions of the cyclin-dependent kinase 4 inhibitor (p16) gene in acute lymphoblastic leukemia and association with adverse prognostic features. *Blood* **85**, 2685-2690 (1995).
- 19 Kees, U. R., Burton, P. R., Lu, C. & Baker, D. L. Homozygous deletion of the p16/MTS1 gene in pediatric acute lymphoblastic leukemia is associated with unfavorable clinical outcome. *Blood* **89**, 4161-4166 (1997).
- 20 Ruas, M. & Peters, G. The p16INK4a/CDKN2A tumor suppressor and its relatives.

-
- Biochim Biophys Acta* **1378**, F115-177, doi:S0304-419X(98)00017-1 [pii] (1998).
- 21 Hennessy, B. T., Garcia-Manero, G., Kantarjian, H. M. & Giles, F. J. DNA methylation in haematological malignancies: the role of decitabine. *Expert Opin Investig Drugs* **12**, 1985-1993, doi:10.1517/13543784.12.12.1985 (2003).
- 22 Hackanson, B., Guo, Y. & Lubbert, M. The silence of the genes: epigenetic disturbances in haematopoietic malignancies. *Expert Opin Ther Targets* **9**, 45-61, doi:ETT090103 [pii]10.1517/14728222.9.1.45 (2005).
- 23 Malumbres, M. *et al.* Mammalian cells cycle without the D-type cyclin-dependent kinases Cdk4 and Cdk6. *Cell* **118**, 493-504 (2004).
- 24 Serrano, M., *et al.* Role of the INK4a locus in tumor suppression and cell mortality. *Cell* **85**(1):27-37(1996).
- 25 Chiarle, R., *et al.* NPM-ALK transgenic mice spontaneously develop T-cell lymphomas and plasma cell tumors. *Blood* **101**(5): 1919-1927(2003).
- 26 Shinkai, Y. *et al.* RAG-2-deficient mice lack mature lymphocytes owing to inability to initiate V(D)J rearrangement. *Cell* **68**, 855-867 (1992).
- 27 Ott, R. G. *et al.* JunB is a gatekeeper for B-lymphoid leukemia. *Oncogene* **26**, 4863-4871 (2007).
- 28 Sexl, V. *et al.* Stat5a/b contribute to interleukin 7-induced B-cell precursor expansion, but abl- and bcr/abl-induced transformation are independent of stat5. *Blood* **96**, 2277-2283 (2000).
- 29 Szremska, A. P. *et al.* JunB inhibits proliferation and transformation in B-lymphoid cells. *Blood* **102**, 4159-4165 (2003).
- 30 Hoelbl, A. *et al.* Stat5 is indispensable for the maintenance of bcr/abl-positive leukaemia. *EMBO Mol Med.* Mar;2(3):98-110(2010).
- 31 Kozar, K. *et al.* Mouse Development and Cell Proliferation in the Absence of D-Cyclins. *Cell* **118**p.p.477-491 (2004).
- 32 Kerényi, M. A. *et al.* Stat5 regulates cellular iron uptake of erythroid cells via IRP-2 and TfR-1. *Blood* **112**, 3878-3888, doi:blood-2008-02-138339 [pii]10.1182/blood-2008-02-138339 (2008).
- 33 Gonzalez, S. *et al.* Oncogenic activity of Cdc6 through repression of the INK4/ARF locus. *Nature* **440**, 702-706 (2006).
- 34 Ray, B. K., Shakya, A. & Ray, A. Vascular endothelial growth factor expression in arthritic joint is regulated by SAF-1 transcription factor. *J Immunol* **178**, 1774-1782, doi:178/3/1774 [pii] (2007).

Acknowledgements

We thank Gabriele Schöppel for taking excellent care of the mice. We are grateful to Michaela Schlederer for helping us with the T-cell lymphoma tissue array and immunohistochemistry. We are grateful to Graham Tebb and Mathias Mueller for scientific discussions. We should like to thank Manuel Serrano as well as Peter Sicinski for providing important tools including luciferase constructs and CyclinD1/2/3 deficient MEFs.

Author Contributions

K.K., G.H., C.S., W.W., R.S., R.G.O., M.S., S.F., A.S., U.R., M.M., C.H., S.Z.M., D.K., L.K., G.H., M.F., R.M., M.B., M.M. and V.S. designed and performed research and analysed data; M.M. provided vital new reagents and analytic tools; K.K., W.W. and V.S. wrote the paper.

Author Information

Information on reprints and permissions is available at www.nature.com/reprints.

Correspondence and requests for materials should be addressed to Veronika Sendl (veronika.sendl@vetmeduni.ac.at)

Conflict of interest disclosure: The authors declare no competing financial interests.

Figure legends

Figure 1: Enforced expression of CDK6 unmasks its tumour suppressing activities by regulating p16^{INK4a} expression

- a) Colony-forming assays were performed by seeding *p185^{BCR-ABL}*-transformed *Cdk6^{+/+}* (expressing a *pMSCV-puro* based retrovirus) or *Cdk6^{+/+}+Cdk6* (expressing a *pMSCV-Cdk6-puro* based retrovirus) cells in growth factor-free methylcellulose. Left side: representative set of pictures of both genotypes is given. Right side: Number of colonies per dish counted after five days of incubation (n = 4/genotype; p = 0.023)
- b) Kaplan Meier blot of *Nu/Nu* mice injected subcutaneously with *Cdk6^{+/+}* or *Cdk6^{+/+}+Cdk6* cells (n = 4 cell lines/genotype; n = 4 mice/cell line; mean survival: 16.5 (*Cdk6^{+/+}*) vs. 27 (*Cdk6^{+/+}+Cdk6*) days; p = 0.002).
- c) Immunoblot for CDK6 and p16^{INK4a} of three individually derived *Cdk6^{+/+}* cell lines with (+Cdk6) or without (w/o vector, empty vector) enforced CDK6 expression.
- d) *p16^{INK4a}* mRNA levels of *Cdk6^{+/+}* and *Cdk6^{+/+}+Cdk6* cells were analysed by qPCR (n = 6; p = 0.03).
- e) ChIP assays were performed using *Cdk6^{+/+}+Cdk6* and *Cdk6^{-/-}* cells. Protein-DNA complexes were immunoprecipitated using an anti-CDK6-antibody and analysed by PCR for the presence of *p16^{INK4a}* promoter sequence. As specificity control the presence of *ARF* promoter sequence was analysed. One representative experiment out of three is depicted.
- f) Promoter ChIP assays were performed using *Cdk6^{+/+}*, *Cdk6^{+/+}+Cdk6* and *Cdk6^{-/-}* cells. Protein-DNA complexes were immunoprecipitated using antibodies specific for the indicated histone modification. ChIP and input DNA were analysed by qPCR for the presence of a *p16^{INK4a}* promoter sequence (region 1 in Figure g). The relative enrichment of the histone modification was determined by dividing the percentage of precipitated DNA of the *p16^{INK4a}* promoter sequence (ChIP/input) by the percentage of precipitated DNA of a positive control region (ChIP/input). A *Tbp* promoter region was used as positive control for H3K9ac, H3K4me2 and H3K4me3 and a *Neurog1* promoter region was used for H3K27me3. The mean and S.E.M. of two independent experiments is shown.
- g) H3K36me3 ChIP assays were performed using *Cdk6^{+/+}* and *Cdk6^{+/+}+Cdk6* cells. Protein-DNA complexes were immunoprecipitated using an antibody specific for H3K36me3. ChIP and input DNA were analysed by qPCR for the presence of *p16^{INK4a}* sequences depicted in the lower panel [black rectangles; middle of the amplicon relative to the TSS (arrow symbol marked +1) of *p16^{INK4a}*: 1 -169 bp, 2 +538 bp, 3 +2278 bp, 4 +4312 bp]. The relative enrichment of the histone modification was determined by dividing the percentage of

precipitated DNA of the given $p16^{INK4a}$ region (ChIP/input) by the percentage of precipitated DNA of a *Gapdh* gene region (ChIP/input). The mean and S.E.M. of two independent experiments is shown.

h) Immunoblot for CDK6 and $p16^{INK4a}$ of $Cdk6^{+/+}$, $Cdk6^{+/+}+Cdk6$ and $Cdk6^{+/+}+Cdk6K43M$ cells.

i) $^3\text{[H]}$ -thymidine incorporation of $Cdk6^{+/+}$, $INK4a/ARF^{-/-}$, $INK4a/ARF^{-/-}+Cdk6$ and $INK4a/ARF^{-/-}+Cdk6R31C$ $p185^{\text{BCR-ABL}}$ -transformed cells ($n = 3$; $Cdk6^{+/+}$ vs.: $INK4a/ARF^{-/-}$, $p = 0.002$; $INK4a/ARF^{-/-}+Cdk6$, $p = 0.001$; $INK4a/ARF^{-/-}+Cdk6R31C$, $p = 0.005$).

j) Kaplan Meier blot of *Rag2*^{-/-} mice intravenously transplanted with $Cdk6^{+/+}$, $INK4a/ARF^{-/-}$, $INK4a/ARF^{-/-}+Cdk6$ and $INK4a/ARF^{-/-}+Cdk6R31C$ cells ($n = 3$ cell lines/genotype; mean survival: 18 ($Cdk6^{+/+}$), 15 ($INK4a/ARF^{-/-}$), 15 ($INK4a/ARF^{-/-}+Cdk6$) and 15.5 ($INK4a/ARF^{-/-}+Cdk6R31C$) days; $p = 0.02$).

Figure 2: Inverse relation between CDK6 and $p16^{INK4a}$ expression in human lymphomas

a) Immunohistochemical stainings of a B-cell lymphoma tissue array including 16 lymphoma samples and two control lymph nodes for CDK6 and $p16^{INK4a}$. Representative examples including different types of B-cell lymphoma, a diffuse large B-cell lymphoma (patient #A) and two follicular lymphoma (patient #B and #C) and one control lymph node (left panel) are depicted. Original magnification 20x.

b, c) The expression of CD30, CDK6 and $p16^{INK4a}$ was analysed for **(b)** 17 *NPM-ALK* positive and **(c)** 11 *NPM-ALK* negative lymphoma cases by immunohistochemistry. Representative cases for *NPM-ALK* positive (patient #D and #E) and *NPM-ALK* negative (patient #F and #G) cases are depicted. Original magnification 20x.

d) $Cdk6^{+/+}$, $Cdk6^{+/-}$ and $Cdk6^{-/-}$ mice crossed with *NPM-ALK* transgenic mice developed a T-cell lymphoma after several weeks ($n \geq 8$; mean survival 120 ($Cdk6^{+/+}$), 143.5 ($Cdk6^{+/-}$) and 212 ($Cdk6^{-/-}$) days; $p = 0.001$).

e) Immunoblot for CDK6 and $p16^{INK4a}$ of *NPM-ALK*-transformed $Cdk6^{+/+}$ and $Cdk6^{-/-}$ cells.

f) Immunoblot for CDK6 of murine $Cdk6^{+/+}$ and $Cdk6^{+/+}+Cdk6$ $p185^{\text{BCR-ABL}}$ -transformed cells as well as human B-lymphoid leukemic cell lines (RL-7, REH, Ramos).

g) Immunoblot for CDK6 of murine $Cdk6^{+/+}$ *NPM-ALK*-transformed cells as well as human T-lymphoid leukemic cell lines (Mac2a, HPB-ALL, Sudh11, CCRF).

Figure 3: CDK6 regulates *Vegf-A* expression and angiogenesis

a, b, c, d *Cdk6*^{+/+}, *Cdk6*^{-/-}, *Cdk6*^{-/-}+*Cdk6*, *Cdk6*^{-/-}+*Cdk6R31C* or *Cdk6*^{-/-}+*Cdk6K43M* p185^{BCR-ABL}-transformed cells were injected subcutaneously (sc) into *Nu/Nu* mice (n = 3 cell lines/genotype; n ≥ 6 tumors/genotype). **(a)** Immunofluorescence staining for CD31 (red) was performed to analyze blood vessel formation in the tumours. Original magnification 20x. Representative cases of each genotype are depicted. **(b)** Quantitative assessment (HistoQuest™) of the blood vessels of the subcutaneous tumours (n ≥ 4 tumours of three independent cell lines; *Cdk6*^{-/-} vs.: *Cdk6*^{+/+}; p = 0.001; *Cdk6*^{-/-}+*Cdk6*: p < 0.0001; *Cdk6*^{-/-}+*Cdk6R31C*: p = 0.0002; *Cdk6*^{-/-}+*Cdk6 K43M*: p < 0.0001). **(c)** Tumour weight was detected after eight days (*Cdk6*^{-/-} vs.: *Cdk6*^{+/+}; p = 0.003; *Cdk6*^{-/-}+*Cdk6R31C*: p = 0.0001). **(d)** *Ex vivo* VEGF-A protein levels (pg/mL) of the tumours were analysed by an ELISA experiment (n = 3).

e, f Murine endothelial cell (mEC) spheroids were cultured in methylcellulose with 20% supernatant derived from indicated cells for 24 h. **(e)** Quantitative analysis of the relative sprout length was measured with ImageJ software (n ≥ 3; *Cdk6*^{-/-} vs.: *Cdk6*^{+/+}, p = 0,042; *Cdk6*^{-/-}+*Cdk6*, p = 0.002; *Cdk6*^{-/-}+*Cdk6R31C*, p = 0.009; *Cdk6*^{-/-}+*Cdk6K43M*, p = 0.038). **(f)** One representative set of pictures is given.

g, h A monolayer wounding assay was performed to analyse migration of mECs incubated with supernatant derived from indicated cells. After 2 and 24 h pictures were taken and mEC migration quantified (% open area after 24h) by the TScratch Software. **(g)** (n ≥ 5; *Cdk6*^{-/-} vs.: *Cdk6*^{+/+}, p = 0.0007; *Cdk6*^{-/-}+*Cdk6*, p = 0.0014; *Cdk6*^{-/-}+*Cdk6R31C*, p = 0.0092; *Cdk6*^{-/-}+*Cdk6K43M*, p = 0.0009). **(h)** One representative set of pictures is given.

i Relative *Vegf-A* mRNA levels of indicated cells were analysed by qPCR. The fold change compared to *Cdk6*^{-/-} *Vegf-A* mRNA level is shown (n ≥ 4; *Cdk6*^{-/-} vs.: *Cdk6*^{-/-}+*Cdk6*: p < 0.0001; *Cdk6*^{-/-}+*Cdk6R31C*: p = 0.03; *Cdk6*^{-/-}+*Cdk6K43M*: p = 0.004).

j Dose-response curve of *Cdk6*^{+/+} p185^{BCR-ABL}-transformed cells treated 24 h with the CDK6/4 inhibitor PD 0332991 (n = 3).

k *Vegf-A* mRNA levels of *Cdk6*^{+/+} p185^{BCR-ABL}-transformed cells (n = 3) treated 24 h with 0, 30, 100, 300 and 1000 nM PD 0332991 were analysed by qPCR. The fold change compared to untreated *Vegf-A* mRNA levels is shown.

Figure 4: Transcriptional interaction partners of CDK6

a, b ChIP assays were performed on **(a)** *Cdk6*^{-/-} and *Cdk6*^{-/-} cells expressing an HA-tagged CDK6 using different amounts of an anti-HA-antibody (5 µg, 10µg or 15 µg) as well as on **(b)** *Cdk6*^{-/-} and *Cdk6*^{+/+}+*Cdk6* cells using an anti-CDK6-antibody. PCR for the presence of

Vegf-A promoter sequence was performed. IgG and no-antibody controls were included. One representative experiment out of three is depicted.

c) An anti-STAT3 co-immunoprecipitation (co-IP) was done with *Stat3^{Δ/Δ}*, *Cdk6^{-/-}*, *Cdk6^{+/+}* and *Cdk6^{+/+}+Cdk6* cell extracts and immunoblotted with anti-STAT3- and anti-CDK6-antibodies.

d) An anti-cJUN co-IP was done with *cJun^{Δ/Δ}*, *Cdk6^{-/-}*, *Cdk6^{+/+}* and *Cdk6^{+/+}+Cdk6* cell extracts and immunoblotted with anti-cJUN- and anti-CDK6-antibodies.

e, f) *Vegf-A* mRNA levels of **(e)** *cJun^{Δ/Δ}* vs. *cJun^{Δ/Δ}+Cdk6* and **(f)** *Stat3^{Δ/Δ}* vs. *Stat3^{Δ/Δ}+Cdk6* p185^{BCR-ABL}-transformed cells were analysed by qPCR (n ≥ 3; *Stat3^{Δ/Δ}* vs. *Stat3^{Δ/Δ}+Cdk6*: p = 0.025).

g, h) *p16^{INK4a}* mRNA levels of **(g)** *cJun^{Δ/Δ}* vs. *cJun^{Δ/Δ}+Cdk6* and **(h)** *Stat3^{Δ/Δ}* vs. *Stat3^{Δ/Δ}+Cdk6* p185^{BCR-ABL}-transformed cells were analysed by qPCR (n ≥ 3; *cJun^{Δ/Δ}* vs. *cJun^{Δ/Δ}+Cdk6*: p = 0.008).

i) A potential interaction between CDK6 and cJUN or STAT3 was analyzed in *Cdk6^{+/+}+Cdk6* cells by ChIP-Re-ChIP experiments at the promoter regions of *Vegf-A* and *p16^{INK4a}*. *Cdk6^{-/-}*, *cJun^{Δ/Δ}* and *Stat3^{Δ/Δ}* cells were used as controls as well as IgG and no-antibody controls were included. Antibodies used for ChIP (1st AB) and Re-ChIP (2nd AB) are shown on the right side of the panel.

j, k) *Vegf-A* and **(l, m)** *p16^{INK4a}* mRNA levels of Cyclin D1/2/3^{-/-} MEFs vs. Cyclin D1/2/3^{-/-} MEFs enforced expressing CDK6 as well as Cyclin D1/2/3^{+/+} MEFs vs. Cyclin D1/2/3^{+/+} MEFs enforced expressing CDK6 were analysed by qPCR.

n) Schematic representation of the kinase dependent, as well as the non-canonical kinase-independent functions of CDK6.

Figure 1

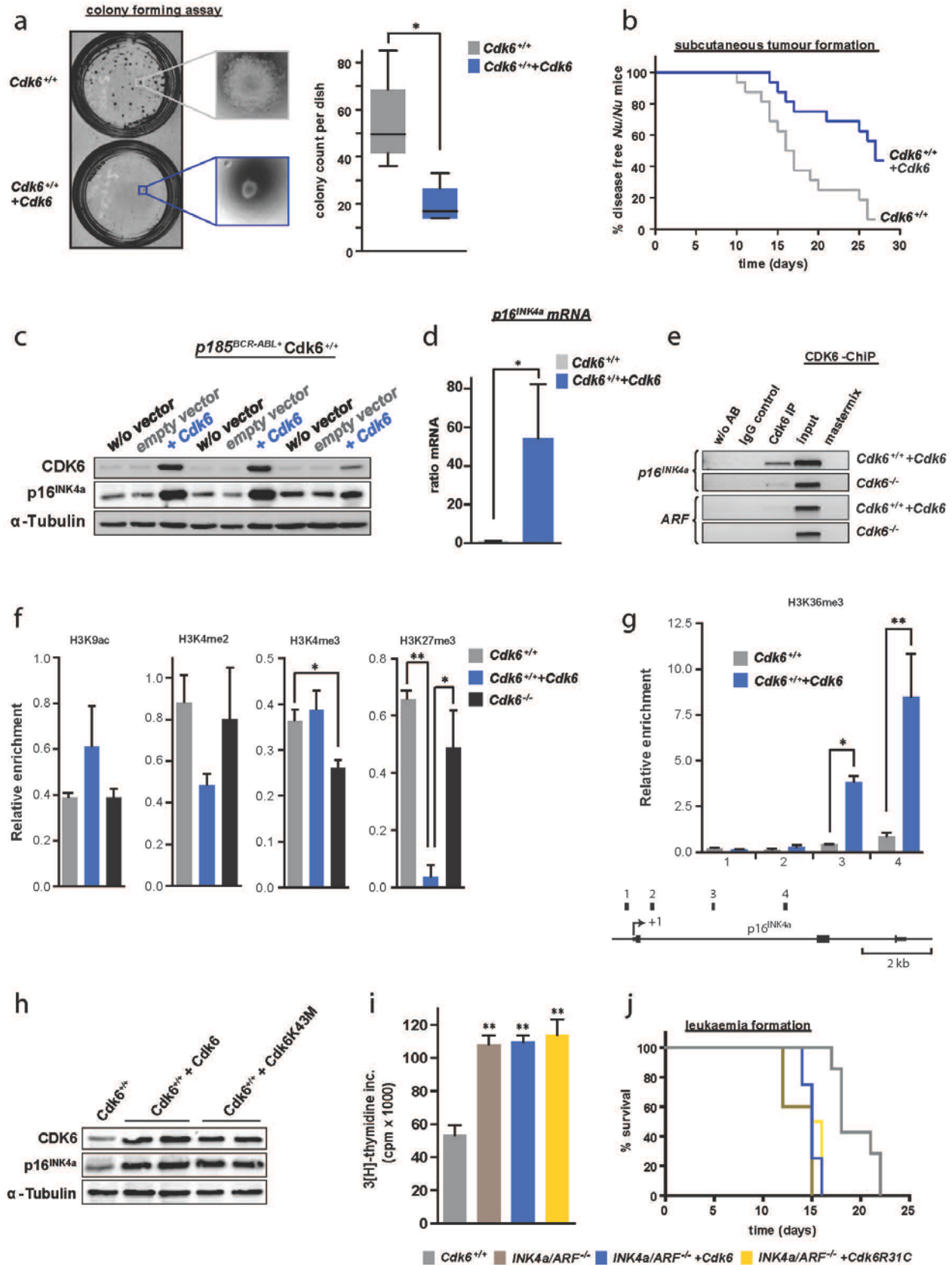


Figure 2

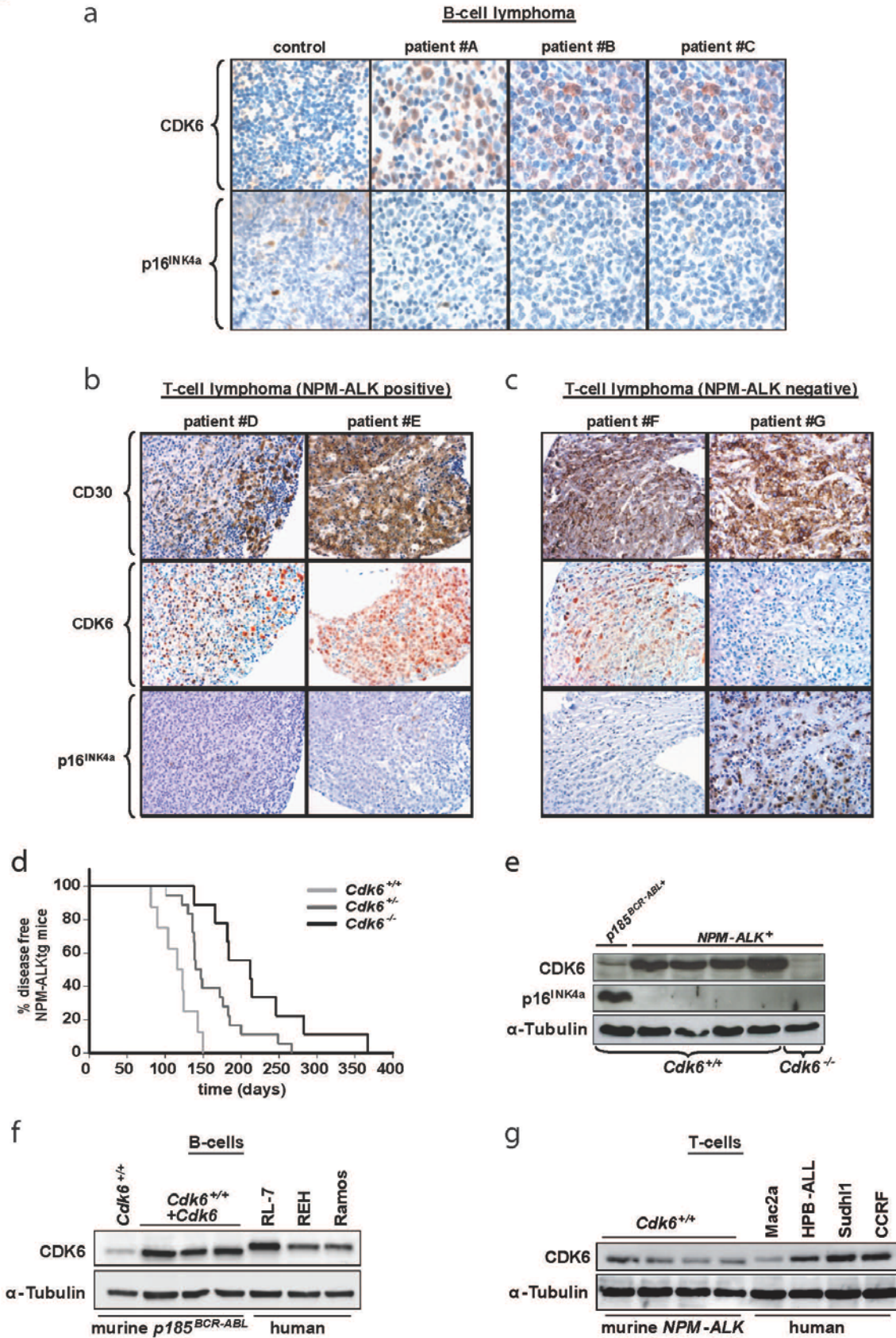


Figure 3

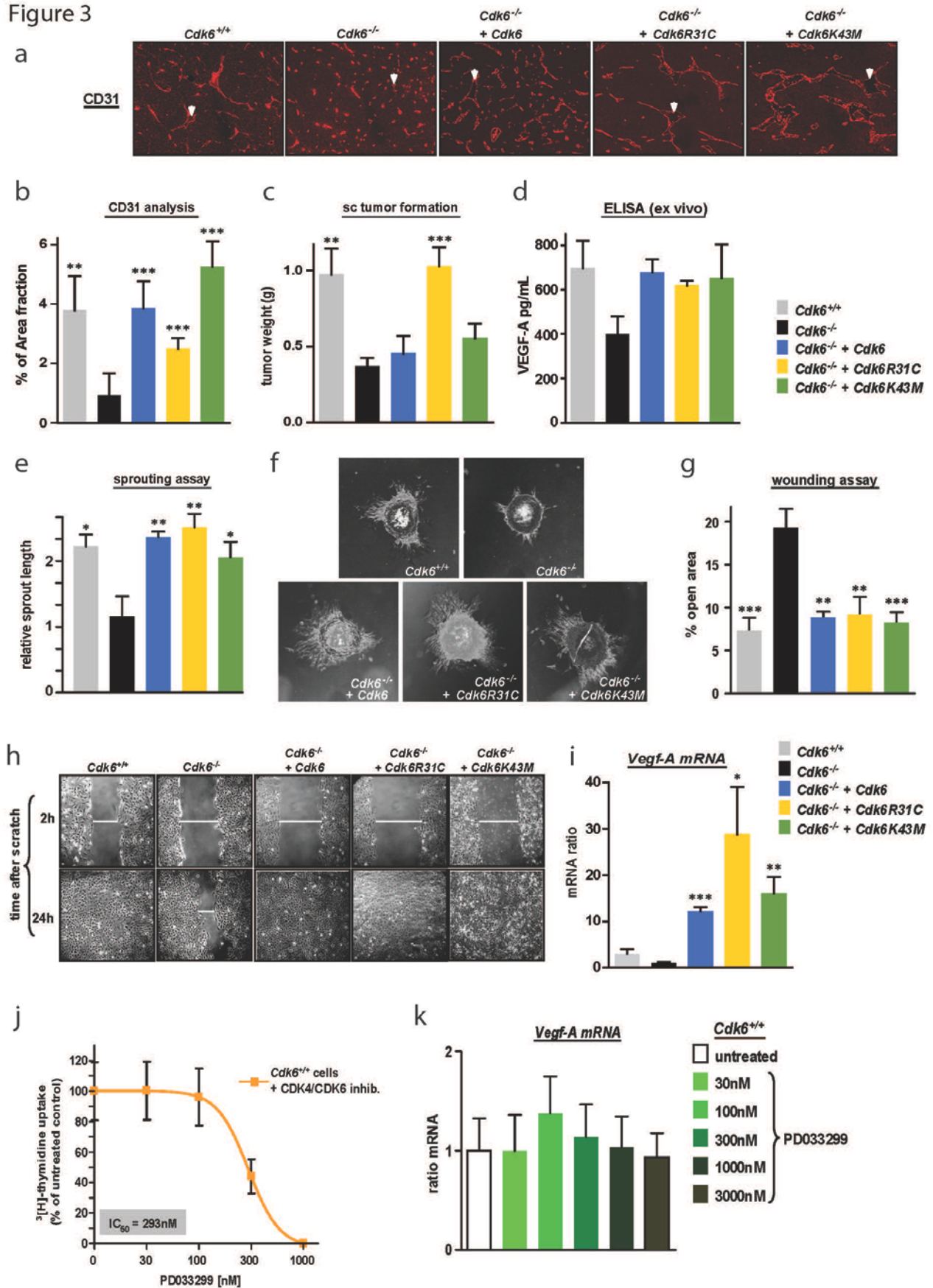
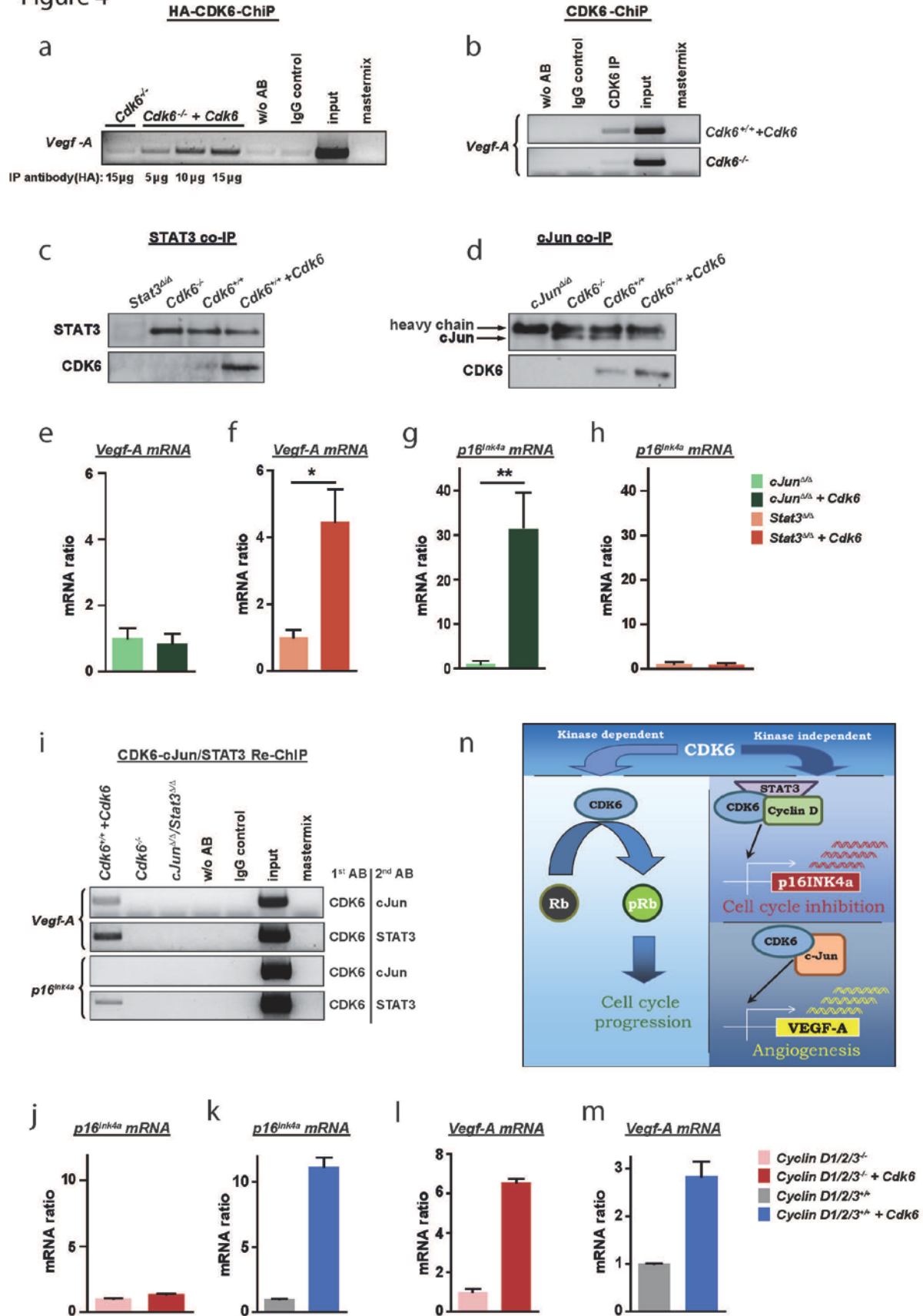
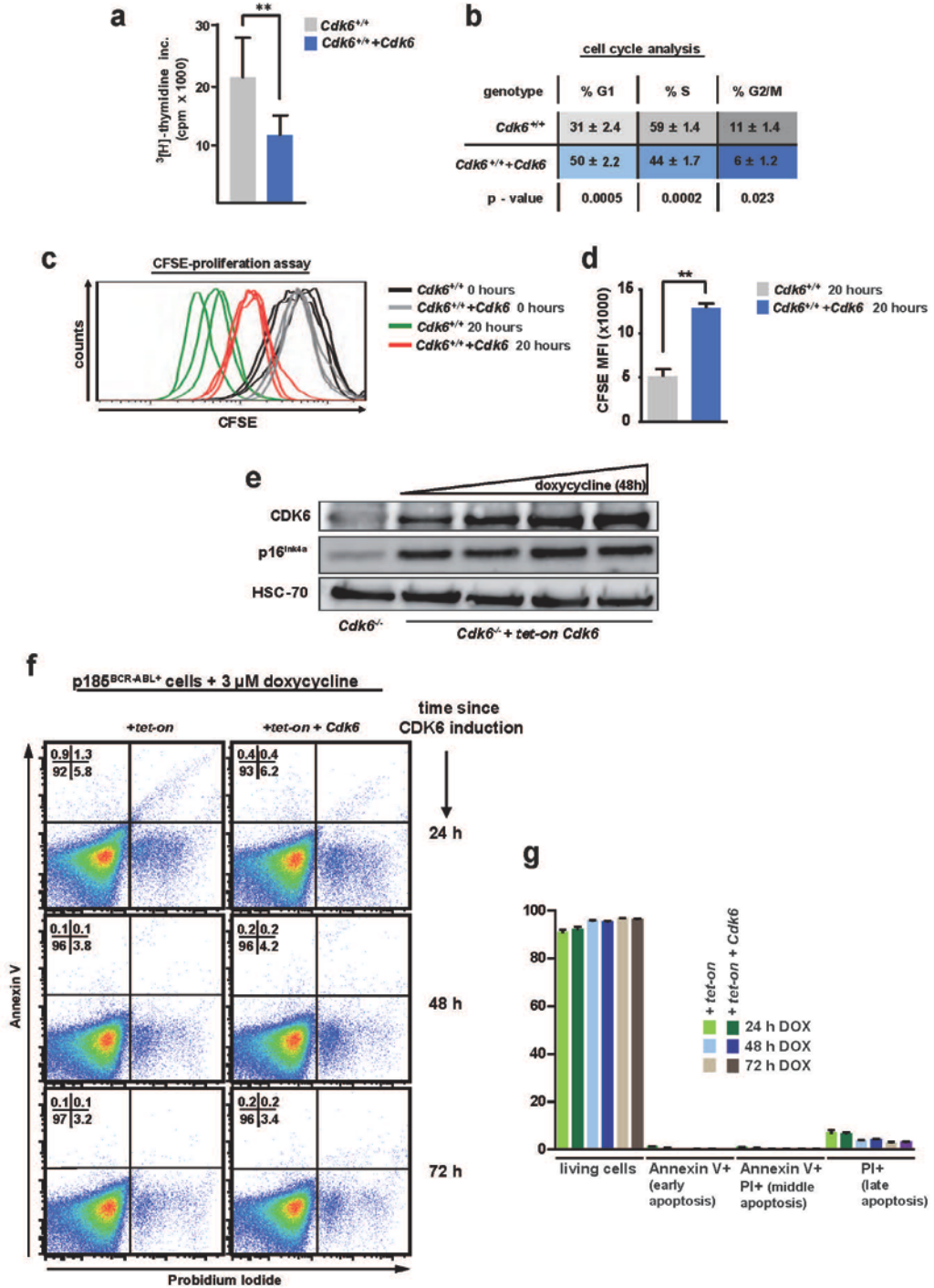


Figure 4

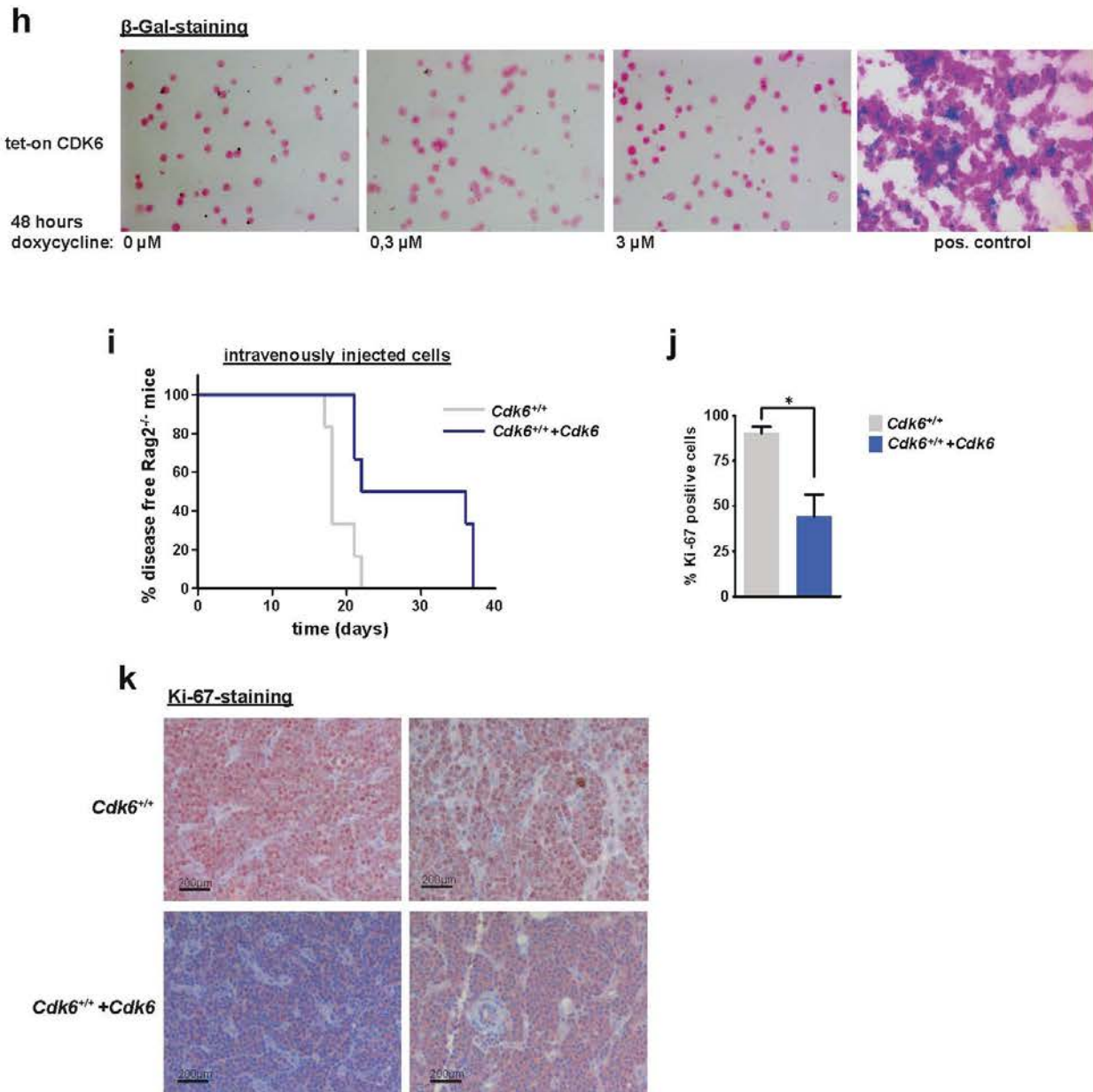


Suppl. Figure 1



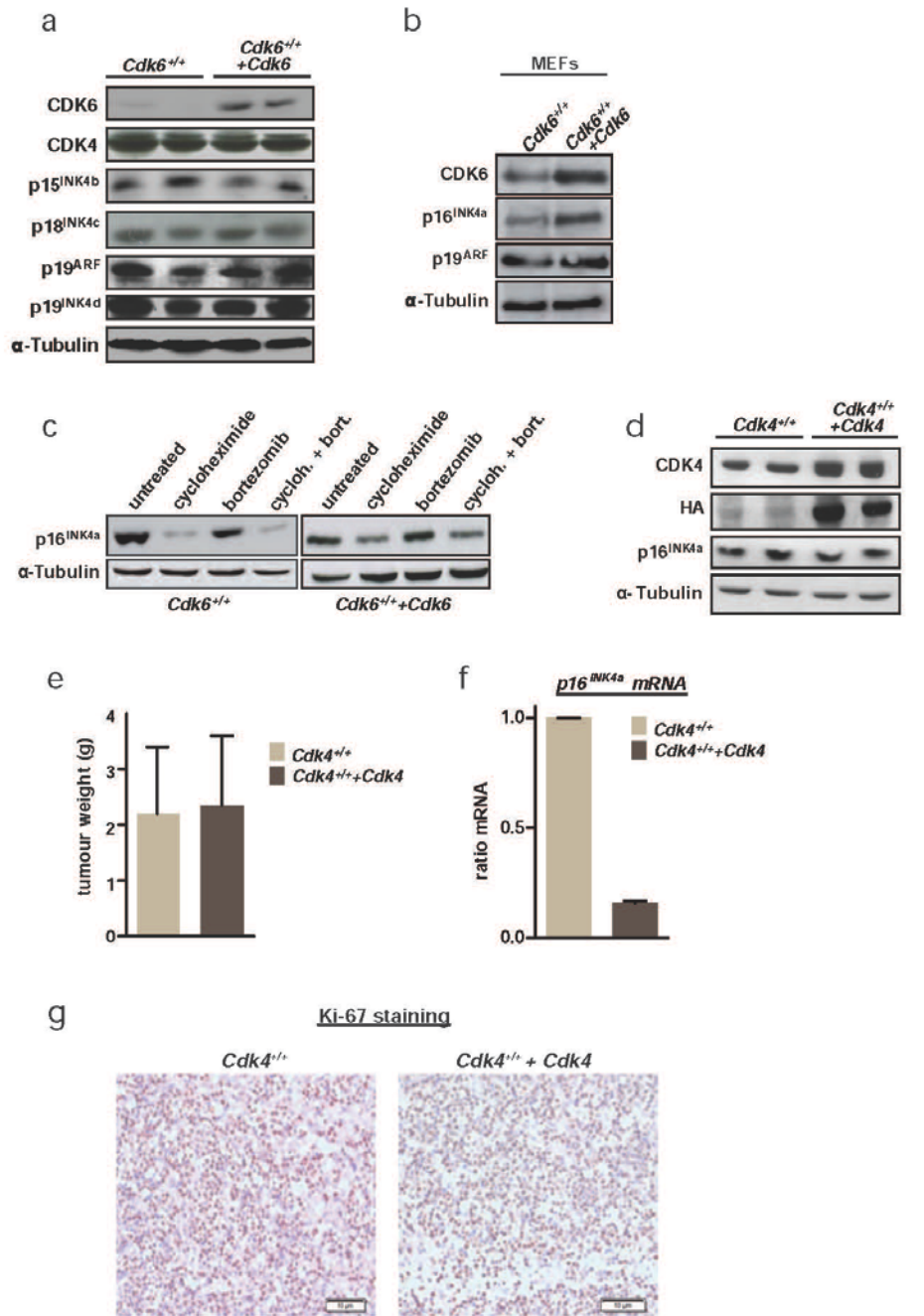
a) ³[H]-thymidine incorporation of *Cdk6*^{+/+} and *Cdk6*^{+/+} + *Cdk6* p185^{BCR-ABL}-transformed cells (n = 4; p = 0.009). **b**) Cell cycle profiles of *Cdk6*^{+/+} and *Cdk6*^{+/+} + *Cdk6* cells were determined by FACS (n = 3). **c, d**) Proliferation assay of *Cdk6*^{+/+} and *Cdk6*^{+/+} + *Cdk6* cells via CFSE dilution staining over a period of 20 h. **e**) Histogram overlay is shown. **d**) Mean fluorescence intensity (MFI) was analyzed after 20 h (n = 3; p = 0.001). **e**) Immunoblot for CDK6 and p16^{INK4a} of *Cdk6*^{-/-} cells expressing a doxycycline inducible *tet-on Cdk6* vector (*Cdk6*^{-/-} + *tet-on Cdk6*). 1. lane: *Cdk6*^{-/-} cells; 2.-5. lane: *Cdk6*^{-/-} + *tet-on Cdk6* cells 48 h after treatment with doxycycline (0, 0.3, 1, 3 μM). **f, g**) Apoptosis stain of *Cdk6*^{-/-} + *tet-on Cdk6* cells 24-72h after 3μM doxycycline (DOX) treatment. Propidium iodide (PI)- annexin V+ cells, early apoptosis; PI+annexin V+ cells, middle apoptosis; PI+annexin V- cells, late apoptosis. **f**) Percentages of each apoptotic stage are in the corner of each blot. **g**) Bar graphs represent the indicated stages of apoptosis.

Suppl. Figure 1



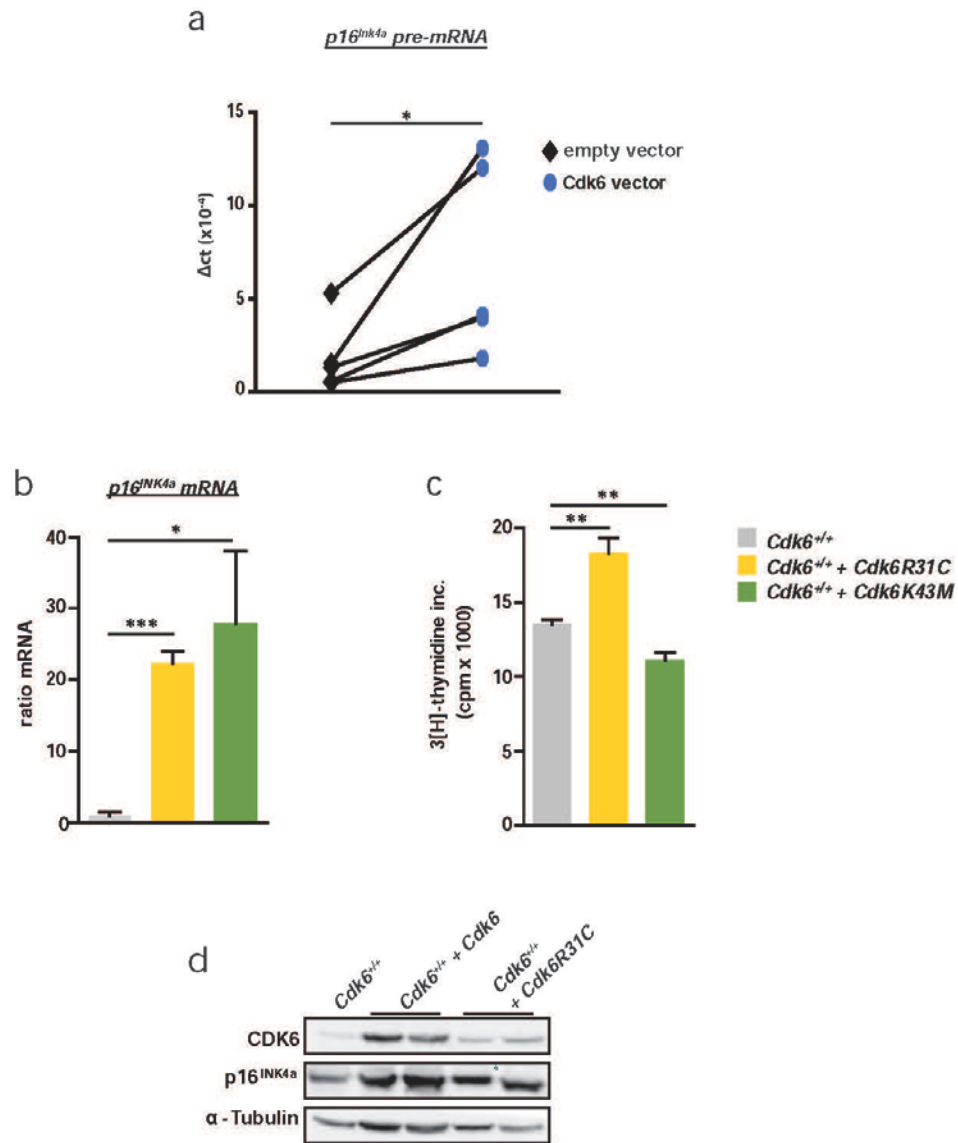
h) Senescence β -Galactosidase (β -Gal) -staining of *Cdk6*^{-/-}+*tet-on Cdk6* cells 48 h after treatment with doxycycline (0, 0.3, 3 μ M).
i) Kaplan Meier plot of Rag2^{-/-} mice transplanted with *Cdk6*^{+/+} or *Cdk6*^{+/+}+*Cdk6* cells (n = 3 cell lines/genotype, n = 6 mice/genotype; mean survival: 18 (*Cdk6*^{+/+}) and 29 (*Cdk6*^{+/+}+*Cdk6*) days; p = 0.014).
j, k) Immunohistochemical stainings for the proliferation marker Ki -67 of *Cdk6*^{+/+} (n = 4) and *Cdk6*^{+/+}+*Cdk6* (n = 9) tumours were quantified by HistoQuest™ software. **(j)** Bar graphs depict percentage of Ki -67 positive tumour cells (p = 0.029). **(k)** A representative set of pictures is given. Original magnification 20x.

Suppl. Figure 2



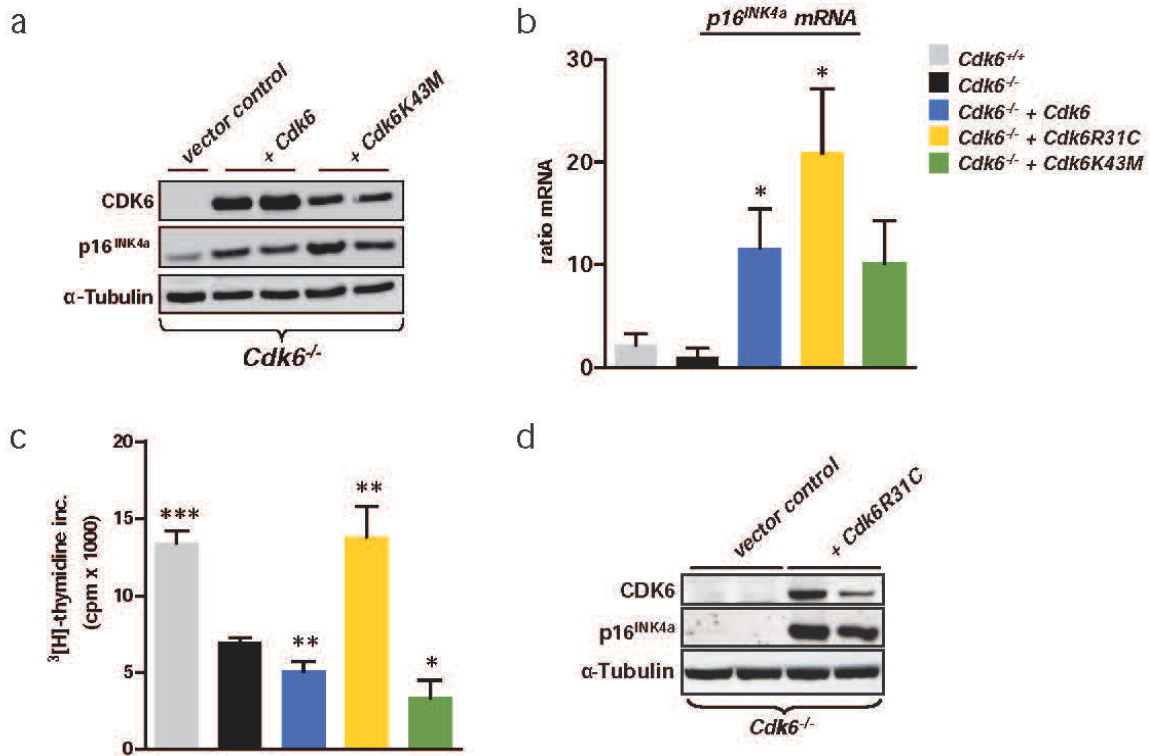
- a) Immunoblot for CDK6, CDK4, p15^{INK4b}, p18^{INK4c}, p19^{INK4d} and p19^{ARF} of *Cdk6*^{+/+} and *Cdk6*^{+/+}+*Cdk6* cells.
- b) Immunoblot for CDK6, p16^{INK4a} and p19^{ARF} of MEFs infected with either a *pMSCV-puro* (*Cdk6*^{+/+}) or a *pMSCV-Cdk6-puro* (*Cdk6*^{+/+}+*Cdk6*) based retrovirus.
- c) Immunoblot for p16^{INK4a} of *Cdk6*^{+/+} and *Cdk6*^{+/+}+*Cdk6* cells after treatment with cycloheximide (an inhibitor of protein biosynthesis), bortezomib (a proteasome inhibitor) or a combination of both for four hours.
- d) Immunoblot for CDK4, HA and p16^{INK4a} in p185^{BCR-ABL}-transformed wild type cells infected with either a *pMSCV-puro* (*Cdk4*^{+/+}) or a *pMSCV-Cdk4HA-puro* (*Cdk4*^{+/+}+*Cdk4*) based retrovirus.
- e) *Cdk4*^{+/+} and *Cdk4*^{+/+}+*Cdk4* cells were injected subcutaneously into *Nu/Nu* mice. Tumour weight was measured after eight days (n = 2 cell lines/genotype; n = 3 mice/genotype; p = 0.94).
- f) p16^{INK4a} mRNA levels of *Cdk4*^{+/+} and *Cdk4*^{+/+}+*Cdk4* cells were analysed by qPCR (n = 2).
- g) Immunohistochemical stainings for the proliferation marker Ki-67 of *Cdk4*^{+/+} and *Cdk4*^{+/+}+*Cdk4* cells. Original magnification 20x. A representative set of pictures is given.

Suppl. Figure 3



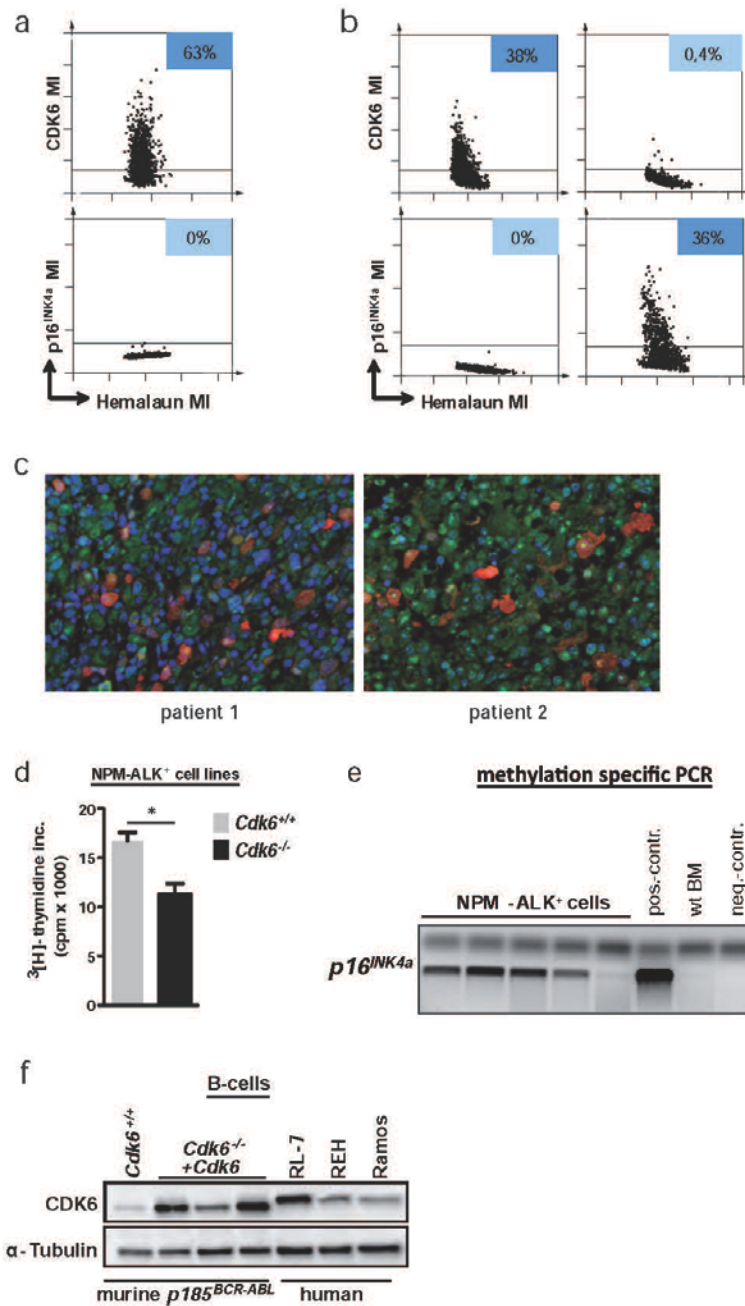
- a)** *p16^{INK4a}* pre-mRNA levels of *Cdk6^{+/+}* and *Cdk6^{+/+} + Cdk6* as well as *Cdk6^{-/-}* and *Cdk6^{-/-} + Cdk6* were analyzed (n = 5, p = 0.048). Elevated pre-mRNA levels support our concept of a transcriptional regulation by CDK6. This experiment excludes that the observed effect originate uniquely from an increased mRNA stability.
- b)** *p16^{INK4a}* mRNA levels of *Cdk6^{+/+}*, *Cdk6^{+/+} + Cdk6R31C* and *Cdk6^{+/+} + Cdk6K43M* cells were analysed by qPCR (n ≥ 3; *Cdk6^{+/+}* vs: *Cdk6^{+/+} + Cdk6R31C*, p < 0.0001; *Cdk6^{+/+} + Cdk6K43M*, p = 0.025).
- c)** ³[H]-thymidine incorporation of *Cdk6^{+/+}*, *Cdk6^{+/+} + Cdk6R31C* and *Cdk6^{+/+} + Cdk6K43M* cells (n ≥ 3; *Cdk6^{+/+}* vs: *Cdk6^{+/+} + Cdk6R31C*, p = 0.002; *Cdk6^{+/+} + Cdk6K43M*, p = 0.006).
- d)** Immunoblot for CDK6 and p16^{INK4a} of *Cdk6^{+/+}*, *Cdk6^{+/+} + Cdk6* and *Cdk6^{+/+} + Cdk6R31C* cells.

Suppl. Figure 4



- a)** Immunoblot for CDK6 and p16^{INK4a} of Cdk6^{-/-}, Cdk6^{-/-}+Cdk6 and Cdk6^{-/-}+Cdk6K43M cells.
- b)** p16^{INK4a} mRNA levels of Cdk6^{+/+}, Cdk6^{-/-}, Cdk6^{-/-}+Cdk6 and Cdk6^{-/-}+Cdk6R31C and Cdk6^{-/-}+Cdk6K43M cells were analysed by qPCR (n ≥ 4; Cdk6^{-/-} vs: Cdk6^{+/+}+Cdk6, p = 0.036; Cdk6^{+/+}+Cdk6R31C, p = 0.02).
- c)** ³[H]-thymidine incorporation of Cdk6^{+/+}, Cdk6^{-/-}, Cdk6^{-/-}+Cdk6, Cdk6^{-/-}+Cdk6R31C and Cdk6^{-/-}+Cdk6K43M cells was measured (n ≥ 3; Cdk6^{-/-} vs.: Cdk6^{+/+}: p < 0.0001; Cdk6^{-/-}+Cdk6: p = 0.008; Cdk6^{-/-}+Cdk6R31C: p = 0.005).
- d)** Immunoblot for CDK6 and p16^{INK4a} of Cdk6^{-/-} and Cdk6^{-/-}+Cdk6R31C cells.

Suppl. Figure 5



a, b) The immunohistochemical sections of **(a)** 17 *NPM-ALK* positive lymphomas and **(b)** 11 *NPM-ALK* negative lymphomas were quantified by the HistoQuest™ software. Scattergrams show the percentage of cells positive for CDK6 or p16^{INK4a} of all samples (MI = Mean Intensity).

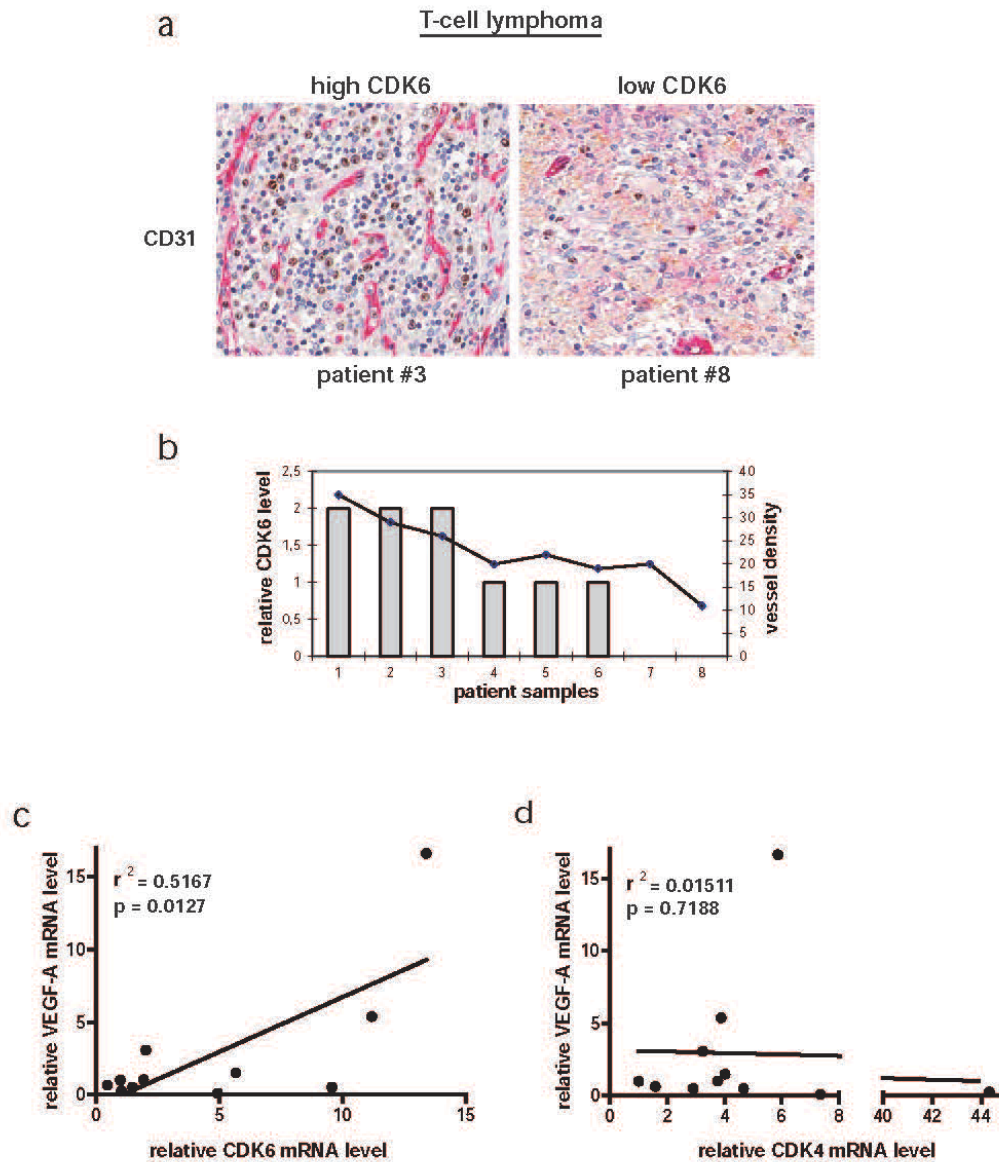
c) Double immunofluorescence stainings on 8 human ALCL whole tissue sections were performed for co-localization studies; stainings illustrated an inverse relation between CDK6 (green) and p16^{INK4a} (red), with tumour cells being either positive for CDK6 or p16^{INK4a}. Original magnification 20x. Representative cases are depicted.

d) ³[H]-thymidine incorporation of *NPM-ALK*-transformed *Cdk6*^{+/+} and *Cdk6*^{-/-} cells (n ≥ 3; p = 0.009).

e) Hypermethylation in *NPM-ALK*-transformed cells as detected by methylation specific PCR. The visible PCR product indicates the presence of methylated alleles. Abbreviations: wt BM, bone marrow of a healthy mouse; pos.-Ctrl (control for methylated samples); neg.-Ctrl (control for unmethylated samples).

f) Immunoblot for CDK6 of murine *Cdk6*^{+/+} and *Cdk6*^{-/-}+*Cdk6* p185^{BCR-ABL}-transformed cells as well as human B-lymphoid leukemic cell lines (RL-7, REH, Ramos).

Suppl. Figure 6

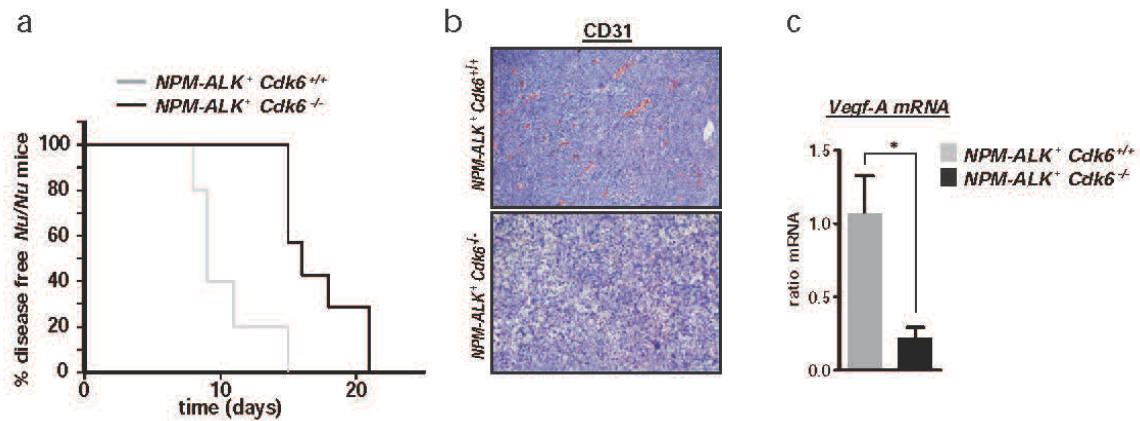


a) The expression of CD31 was analysed of eight human ALCL whole tissue sections by immunohistochemistry. Original magnification 200x. A high CDK6 expressing case (left panel, patient #3) and a low CDK6 expressing case (right panel, patient #8) are depicted.

b) Statistical analysis of vessel density of CD31 immunohistochemical stainings of eight human ALCL whole tissue sections (two of them depicted in panel a). Two independent observers noticed a higher vessel density in human ALCL with high CDK6 expression compared to human ALCL with low or lacking CDK6 levels. CD31 stained lumen were counted within a hotspot in an area of $0,25 \text{ mm}^2$ at a magnification of 200x. Counting results confirmed the increase in vessels in T-cell lymphoma cases with high CDK6 expression.

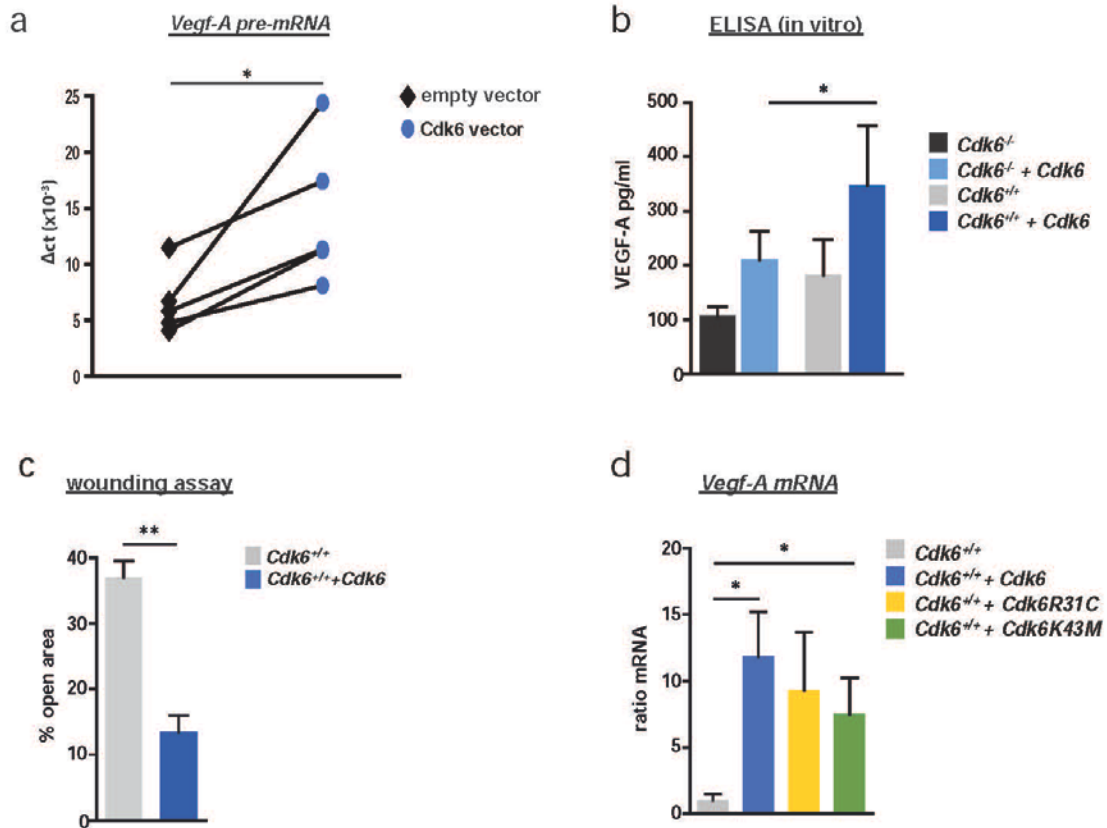
c, d) Human **(c)** *CDK6* or **(d)** *CDK4* as well as *VEGF-A* mRNA levels of several human cell lines (Mac2A, Sudh11, CCRF, HPB-ALL, K562, Reh, RL-7, Ramos, Jurkat, Molt4 and control lymphocytes) were analysed by qPCR. The correlation between *CDK6* and *VEGF-A* as well as *CDK4* and *VEGF-A* is depicted in a x,y plot.

Suppl. Figure 7



- a) Kaplan Meier plot of *Nu/Nu* mice subcutaneously injected with *Cdk6^{+/+}* and *Cdk6^{-/-}* NPM-ALK-transformed cells (n = 2 cell lines/genotype; n = 6 mice/genotype; mean survival: 9 (*Cdk6^{+/+}*) and 16 (*Cdk6^{-/-}*); p = 0.003).
- b) Immunohistochemical staining for CD31 (red) was performed in *Cdk6^{+/+}* and *Cdk6^{-/-}* NPM-ALK⁺ subcutaneous tumours to analyze blood vessel formation. Original magnification 20x. Representative cases of each genotype are depicted.
- c) *Vegf-A* mRNA levels of *Cdk6^{+/+}* and *Cdk6^{-/-}* NPM-ALK-transformed cells were quantified by qPCR (n = 3; p = 0.036).

Suppl. Figure 8



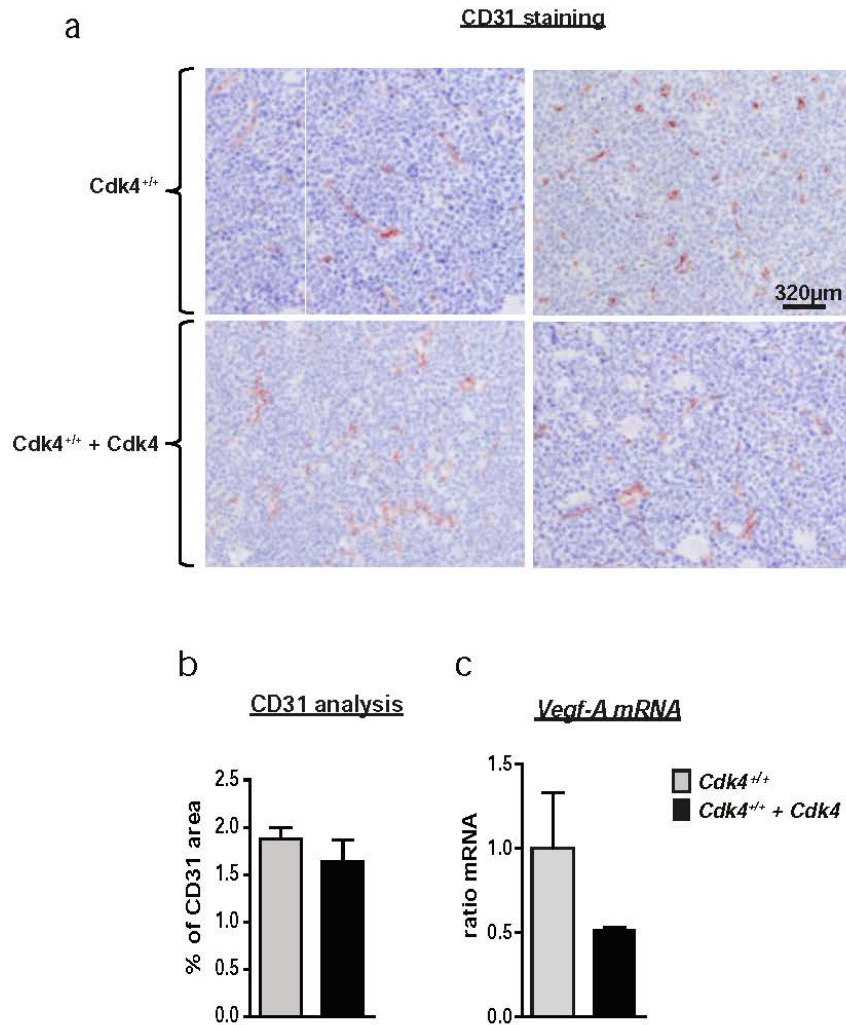
a) *Vegf-a* pre-mRNA levels of *Cdk6^{+/+}* and *Cdk6^{+/+}+Cdk6* as well as of *Cdk6^{-/-}* and *Cdk6^{-/-}+Cdk6* cells were analyzed (n = 5, p = 0.035). Elevated pre-mRNA levels support our concept of a transcriptional regulation by CDK6. This experiment excludes that the observed effect originate uniquely from an increased mRNA stability.

b) VEGF-A protein (pg/mL) levels in the supernatant of *Cdk6^{-/-}* and *Cdk6^{-/-}+Cdk6* as well as of *Cdk6^{+/+}* and *Cdk6^{+/+}+Cdk6* cells were analyzed by ELISA (n = 3).

c) A monolayer wounding assay was performed to analyse migration of mEC s incubated with the supernatant derived from *Cdk6^{+/+}* and *Cdk6^{+/+}+Cdk6* cells. After 2 and 24 hours pictures were taken and mEC migration quantified (% open area after 24h) by the TScratch Software (n = 3; *Cdk6^{+/+}* vs. *Cdk6^{+/+}+Cdk6*, p = 0.0007).

d) *VegfA* mRNA levels of *Cdk6^{+/+}* and *Cdk6^{+/+}+Cdk6*, *Cdk6^{+/+}+Cdk6R31C* and *Cdk6^{+/+}+Cdk6K43M* cells analysed by qPCR . The fold change compared to *Cdk6^{+/+}* *VegfA* mRNA level is shown (n ≥ 3; *Cdk6^{+/+}* vs.: *Cdk6^{+/+}+Cdk6*: p = 0.02; *Cdk6^{+/+}+Cdk6R31C*: p = 0.06; *Cdk6^{+/+}+Cdk6K43M*: p = 0.04).

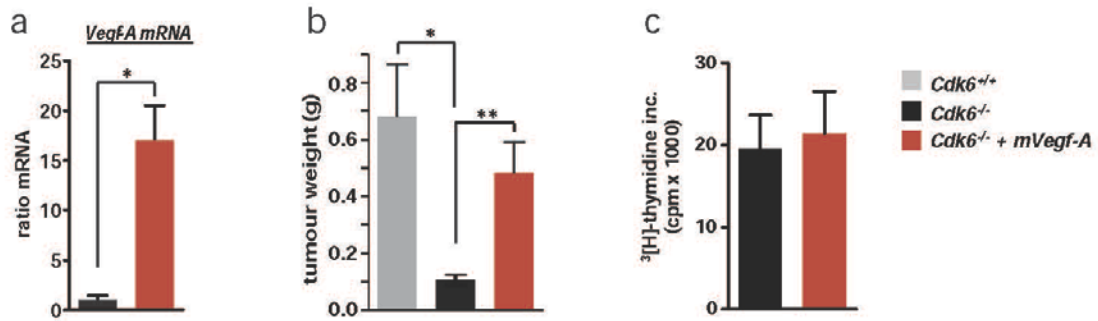
Suppl. Figure 9



a, b) *Cdk4*^{+/+} and *Cdk4*^{+/+} + *Cdk4* p185^{BCR-ABL}-transformed cells were injected subcutaneously into *Nu/Nu* mice (n = 2 cell lines/genotype; n ≥ 4 tumors/genotype). **(a)** Immunofluorescence staining for CD31 (red) was performed to analyze blood vessel formation in the tumours. Original magnification 20x. Representative cases of each genotype are depicted. **(b)** Quantitative assessment (HistoQuest™) of the blood vessels of the subcutaneous tumours (n = 3).

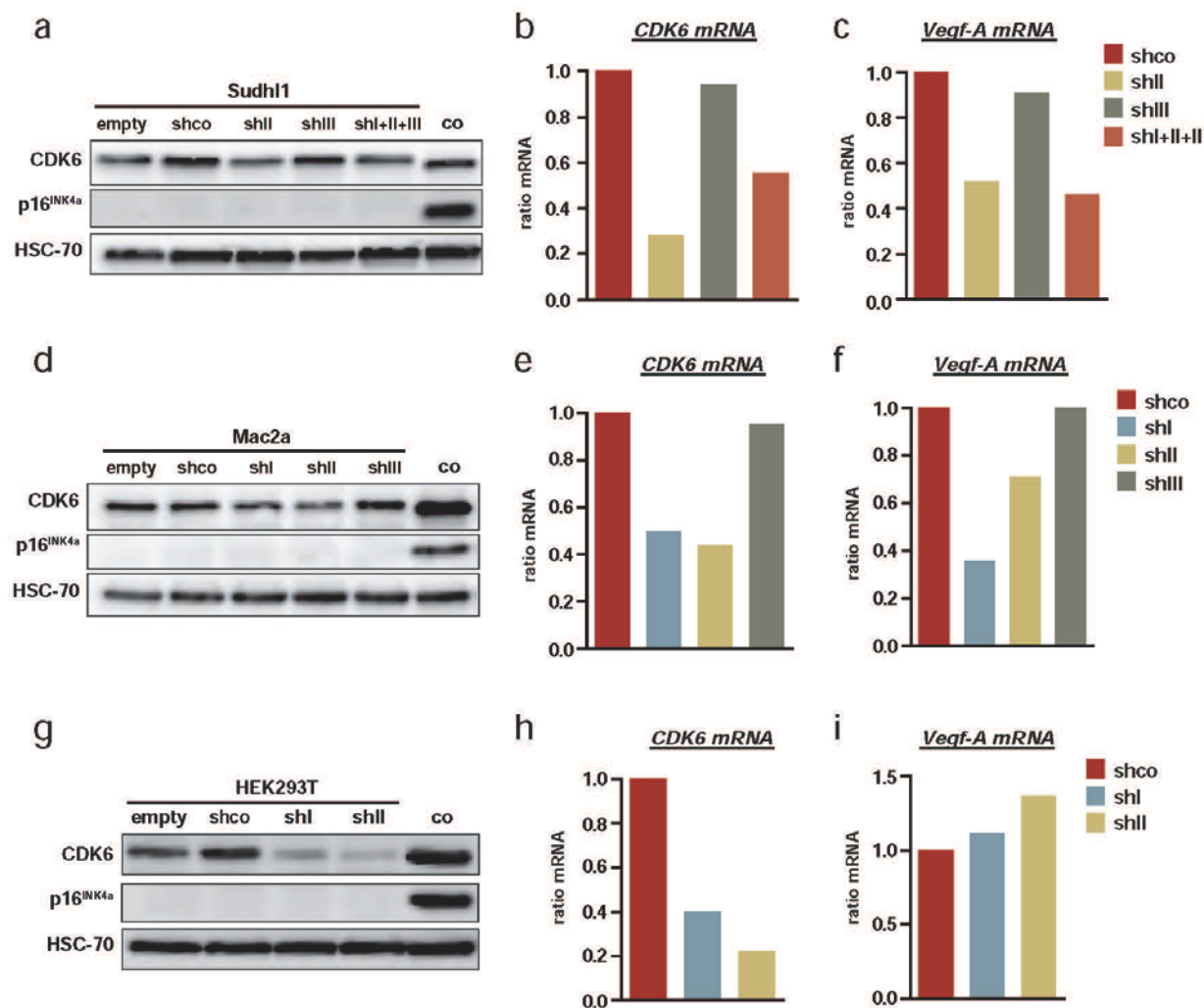
c) *Vegf-A* mRNA levels of *Cdk4*^{+/+} and *Cdk4*^{+/+} + *Cdk4* cells analysed by qPCR (n = 2).

Suppl. Figure 10



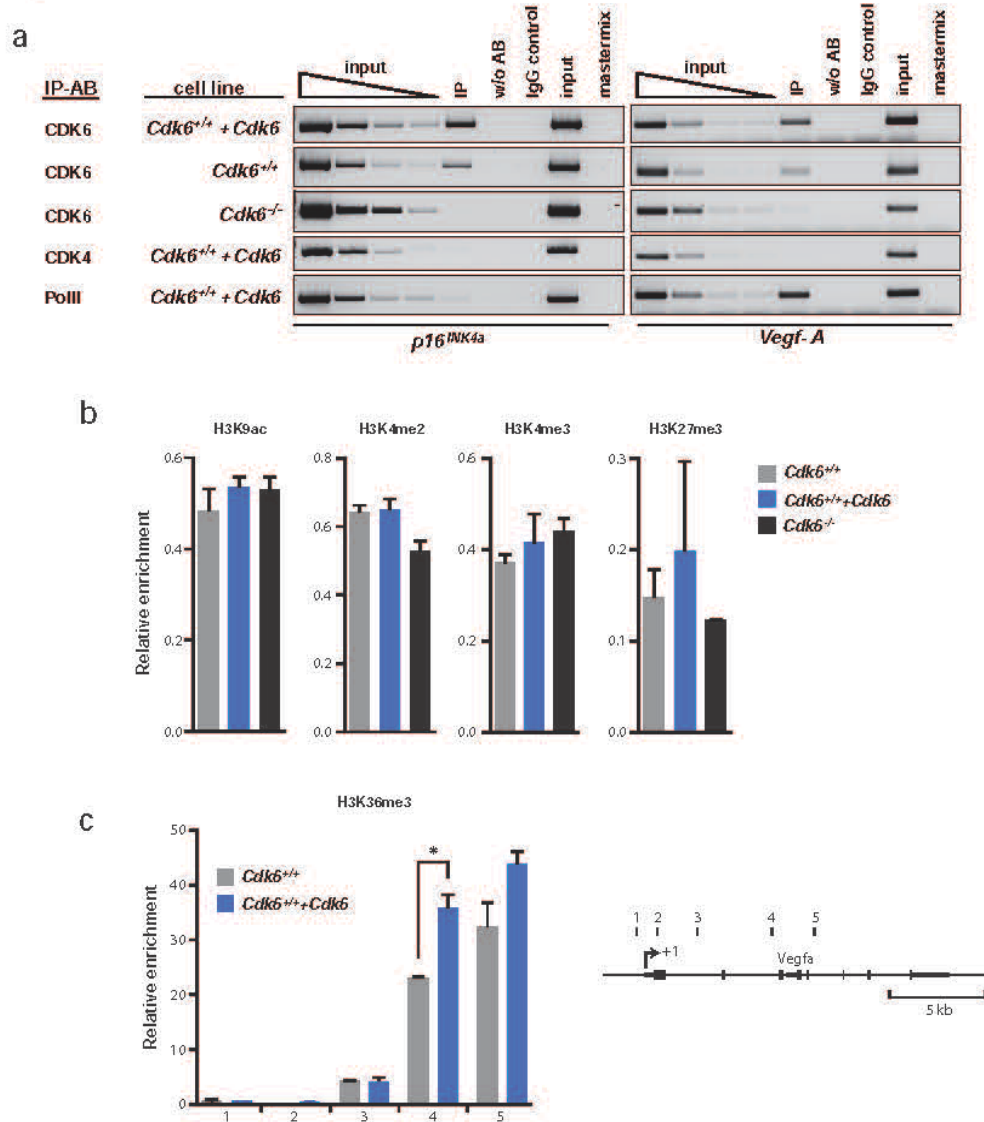
- a) *VegfA* mRNA levels of *Cdk6*^{-/-} p185^{BCR-ABL}-transformed cells and the cells overexpressing mVEGF -A were quantified by qPCR (n = 3; p = 0.01).
- b) *Cdk6*^{+/+}, *Cdk6*^{-/-} and *Cdk6*^{-/-}+mVegf-A cells were injected subcutaneously into *Nu/Nu* mice. Tumour weights of diseased mice were analysed after eight days (n = 3 cell lines/genotype; n = 5 mice/genotype; *Cdk6*^{+/+} vs. *Cdk6*^{-/-}: p = 0.015 and *Cdk6*^{-/-} vs. *Cdk6*^{-/-}+mVegf-A: p = 0.009).
- c) ³[H]-thymidine incorporation of *Cdk6*^{-/-} and *Cdk6*^{-/-}+mVegf-A cells (n = 3; p = 0.8).

Suppl. Figure 11



- a)** Immunoblot for CDK6 and p16^{INK4a} of the human cell line Sudhl1 expressing one or a combination of three different shRNA CDK6 knockdown constructs or the shRNA control construct.
- b, c)** *CDK6* and *VEGF-A* mRNA levels of the shRNA transfected human cell line Sudhl1 (shown in panel **a**) quantified by qPCR.
- d)** Immunoblot for CDK6 and p16^{INK4a} of the human cell line Mac2a expressing one of three different shRNA CDK6 knockdown constructs or the shRNA control construct.
- e, f)** *CDK6* and *VEGF-A* mRNA levels of the shRNA transfected human cell line Mac2a (shown in panel **d**) quantified by qPCR.
- g)** Immunoblot for CDK6 and p16^{INK4a} of the human cell line HEK293T expressing one of two different shRNA CDK6 knockdown constructs or the shRNA control construct.
- h, i)** *CDK6* and *VEGF-A* mRNA levels of the shRNA transfected human cell line HEK293T (shown in panel **g**) quantified by qPCR.

Suppl. Figure 12

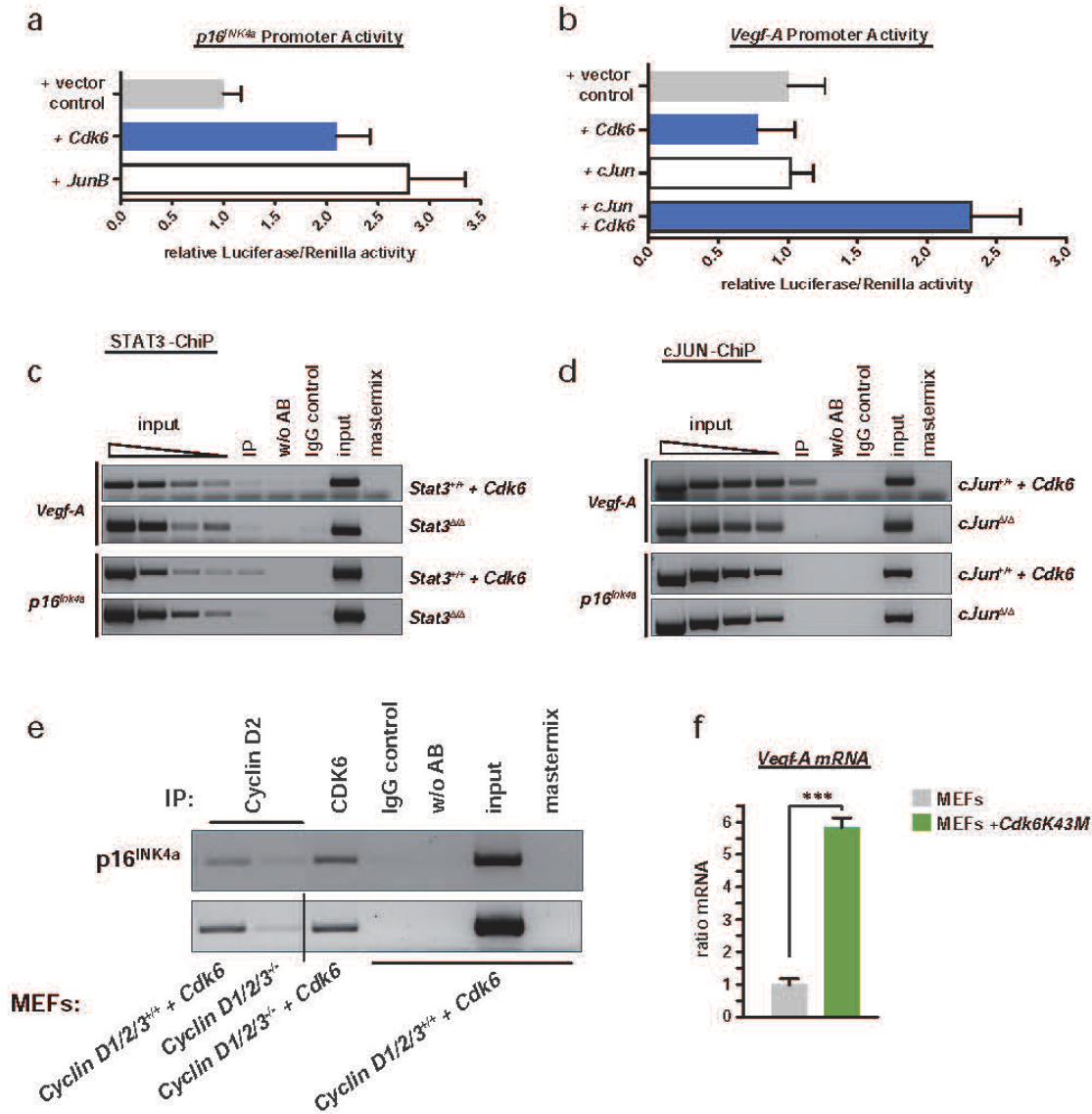


a) ChIP assays were performed using *Cdk6*^{+/+} + *Cdk6*, *Cdk6*^{+/+} and *Cdk6*^{-/-} cells. Protein-DNA complexes were immunoprecipitated using an anti -CDK6, anti -CDK4 or anti -PoIII-antibody and analysed by PCR for the presence of *p16*^{INK4a} or *VegfA* promoter sequence. One representative experiment out of three is depicted.

b) Promoter ChIP assays were performed using *Cdk6*^{+/+}, *Cdk6*^{+/+} + *Cdk6* and *Cdk6*^{-/-} cells. Protein-DNA complexes were immunoprecipitated using antibodies specific for the indicated histone modification. ChIP and input DNA were analysed by qPCR for the presence of a *VegfA* promoter sequence (region 1 in Supplementary Figure 11c). The relative enrichment of the histone modification was determined by dividing the percentage of precipitated DNA of the *VegfA* promoter region (ChIP/input) by the percentage of precipitated DNA at a positive control region (ChIP/input). A *Tbp* promoter region was used as positive control for H3K9ac, H3K4me2 and H3K4me3 and a *Neurog1* promoter region was used for H3K27me3. The mean + S.E.M. of two independent experiments is shown.

c) H3K36me3 ChIP assays were performed using *Cdk6*^{+/+} and *Cdk6*^{high} cells. Protein-DNA complexes were immunoprecipitated using an antibody specific for H3K36me3. ChIP and input DNA were analysed by qPCR for the presence of *VegfA* sequences depicted in the lower panel [black rectangles; middle of the amplicon relative to the TSS (arrow symbol marked +1) of *VegfA*: 1 -386 bp, 2 +693 bp, 3 +2710 bp, 4 +6461 bp, 5 +8621 bp]. The relative enrichment of the histone modification was determined by dividing the percentage of precipitated DNA of the given *VegfA* region (ChIP/input) by the percentage of precipitated DNA of a *Gapdh* gene region (ChIP/input). The mean + S.E.M. of two independent experiments is shown.

Suppl. Figure 13



a) Luciferase reporter assay was performed in HEK293T cells. Cells were co-transfected with 0.4 μ g of the *p16^{INK4a}* promoter reporter construct together with 0.4 μ g of empty plasmid (*pMSCV-puro*) or plasmid expressing CDK6 (*pMSCV-Cdk6-puro*) or JUNB (*pMSCV-JunB-puro*) and 0.04 μ g of a Renilla -expressing vector. Experiments were performed in triplicates and repeated three times.

b) Luciferase reporter assay was performed in HEK293T cells. Cells were co-transfected with 0.4 μ g of the *VegfA* promoter reporter construct together with 0.4 μ g of empty plasmid (*pMSCV-puro*) or plasmid expressing CDK6 (*pMSCV-Cdk6-puro*) or /and cJUN (*pMSCV-cJun-puro*) and 0.04 μ g of a Renilla -expressing vector. Experiments were performed in triplicates and repeated three times.

c, d, e) ChIP assays were performed using **(c)** *Stat3^{+/+}+Cdk6* and *Stat3^{ΔΔ}* cells. Protein-DNA complexes were immunoprecipitated using an anti-STAT3-antibody and analysed by PCR for the presence of *VegfA* or *p16^{INK4a}* promoter sequence **(d)** *cJun^{+/+}+Cdk6* and *cJun^{ΔΔ}* cells. Protein-DNA complexes were immunoprecipitated using an anti-cJUN-antibody and analysed by PCR for the presence of *VegfA* or *p16^{INK4a}* promoter sequence **(e)** *CyclinD1/2/3^{+/+}+Cdk6* and *CyclinD1/2/3^{-/-}* cells. Protein-DNA complexes were immunoprecipitated using an anti-CYCLIN D2 or CDK6-antibody and analysed by PCR for the presence of *p16^{INK4a}* promoter sequence. Two representative experiments are depicted.

f) *VegfA* mRNA levels of MEFs infected with either a *pMSCV-puro* or a *pMSCV Cdk6K43M* based retrovirus were quantified by qPCR.

Supplementary Table 1

| origin | species | cell line | Vegf-a mRNA ratio | p16 ^{INK4a} mRNA ratio | proliferation |
|-----------------|---------|--------------------------|-------------------|---------------------------------|---------------|
| epithelial | human | HEK | 0.3 | - | → |
| | | Panc-1 | 0.1 | - | → |
| | | DLD-1 | 0.3 | - | ↑ |
| melanom | mouse | B16-F10 | 0.1 | - | ↑ |
| | human | Mac2a | 1.2 | - | → |
| haemato-poietic | mouse | p185 ^{BCR-ABL+} | 11.9 | 54.2 | ↓ |
| | | NPM-ALK+ | 6.2 | - | ↑ |
| | | RAW2 | 7.7 | 5.8 | ↓ |
| | | RMA-S | 0.8 | - | ↑ |
| | | RN2 | 7.0 | 3.6 | ↓ |
| liver | mouse | HEPA-1 | 19.8 | - | → |
| | | IHSC | 0.7 | - | ↑ |
| non-transformed | mouse | MEFs | 2.8 | 11.1 | ↓ |
| | | NIH3T3 | 3.5 | - | ↑ |

Fold increase of *Vegf-a* and *p16^{INK4a}* mRNA of murine and human cell lines overexpressing murine or human CDK6, respectively. Arrows indicate changes in proliferation compared to control cells. (-: not detectable; Arrows: % change of cells in S phase upon enforced expression of CDK6; ↑: ≥ 5% increase; ↓: ≥ 5% decrease; →: changes < 5%).

Supplementary table 2: Antibodies used in the study

| Antibodies used for histonmark analysation: | |
|--|------------------------|
| H3K9ac | Millipore, 07-352 |
| H3K4me2 | Millipore, 07-030 |
| H3K4me3 | Diagenode, pAb-003-050 |
| H3K27me3 | Millipore, 07-449 |
| H3K36me3 | Cell Signaling, 4909 |

| Antibodies used for Chip experiments: | |
|--|-----------------------|
| CDK6 | Santa Cruz, sc-177 |
| HA | Abcam, ab9110 |
| CDK4 | Santa Cruz, sc-260 |
| STAT3 | Cell Signalling, 9132 |
| c-JUN | Santa Cruz, sc-1694x |
| PolII | Santa Cruz, sc-899 |
| CyclinD2 | Santa Cruz, sc-593 |

| Antibodies used for immunoblot and co-immunoprecipitation experiments: | |
|---|----------------------------|
| CDK6 | Santa Cruz, C8343 |
| α -Tubulin | Sigma Aldrich Inc., T-9026 |
| CDK4 | Santa Cruz, sc-260 |
| STAT3 | Cell Signalling, 9132 |
| c-JUN | Santa Cruz, sc-1694x |
| HA | Abcam, ab9110 |
| p15 ^{INK4b} | Santa Cruz, sc-612 |
| p16 ^{INK4a} | Santa Cruz, sc-1207 |
| p18 ^{INK4c} | Santa Cruz, sc-865 |
| p19 ^{INK4d} | Santa Cruz, sc-1063 |
| p19 ^{ARF} | Abcam Inc., Ab80 |
| Gapdh | Cell Signalling, 2119 |

Supplementary table 3: Primer used in the study

| Primer (5' - 3') used for histonmark analyzation: | | |
|--|-----------------|---|
| mouse | <i>Cdkn2a_1</i> | AACACCCCTGAAAACACTGC TCCTGAACCCCTGCATCTCTT |
| mouse | <i>Cdkn2a_2</i> | AGGAGTCCTGGCCCTAGAAA TATGCACAGGCTCTGGAATG |
| mouse | <i>Cdkn2a_3</i> | TGGCAATGTGTGCAAGACT TCCTCCTCCTCTCCTGTTGA |
| mouse | <i>Cdkn2a_4</i> | CCTCAGGGATGACCTGTGTT GAATGCTTGCCTGGTGTTTT |
| mouse | <i>Vegfa_1</i> | GGCAGGGACGTATGAGGATA GCATGCATGTGTGTGTGTGT |
| mouse | <i>Vegfa_2</i> | CCAACTTCTGGGCTCTTCTC GCTAGCACTTCTCCAGCTC |
| mouse | <i>Vegfa_3</i> | GCCACAGTGTGACCTCAGA CTTTGAACCCCTTCCCAGAT |
| mouse | <i>Vegfa_4</i> | GGGATGAATGGTGGTGTTTC CTCCCCATGTTCCCCTAA |
| mouse | <i>Vegfa_5</i> | CACAGCAGAGTGCAGGAGAG CACAGTCACCACCCAACAAG |
| mouse | <i>Tbp</i> | AAAGGGGAGGAGCCAGTAAG TGTGTAGCCCCGACTTTCTT |
| mouse | <i>Neurog1</i> | CAATCTTGGTGAGCTTGGTG GAGGCTCTGCTGCACTCC |
| mouse | <i>Gapdh</i> | TGAAGCAGGCATCTGAGGG CGAAGGTGGAAGAGTGGGAG |

| Primer (5' - 3') used for qPCR analysis: | | |
|---|-------------------------------------|---|
| mouse | <i>p16^{INK4a}</i> | GTGTGCATGACGTGCGGG GCAGTTCGAATCTGCACCGTAG |
| mouse | <i>Vegf-A</i> | GCACAGCAGATGTGAATGCAG CGCTCTGAACAAGGCTCACA |
| mouse | <i>Cdk6</i> | GCTTCGTGGCTCTGAAGCGCG TGGTTTCTGTGGGTACGCCGG |
| mouse | <i>rplpO</i> | TTCATTGTGGGAGCAGAC CAGCAGTTTCTCCAGAGC |
| mouse | <i>pre-mRNA p16^{INK4a}</i> | GGGTGCTCTTTGTGTTCGCG GCTTTTGGACCAACTATGC |
| mouse | <i>pre-mRNA Vegf-A</i> | TCCCTCTACAG ATCATGCGG CCTGAGTGTGAAGCTCTGG |
| human | <i>Cdk6</i> | GGACGTGATTGGACTCCC AAGTATGGGTGAGACAGGG |
| human | <i>Cdk4</i> | GCTGACTTTTAACCCACACA AAAGATTGCCCTCTCAGTGT |
| human | <i>Vegf-A</i> | GTCGGGCCTCCGAAACCATG CGTGATGATTCTGCCCTCCTCCTTC |
| human | <i>rplpO</i> | GGCGACCTGGAAGTCCAAC CCATCAGCACCACAGCCTTC |

Supplementary Information

Material and Methods

Generation of p185^{BCR-ABL}-transformed *Cdk6*^{-/-} cells with inducible expression of CDK6

To generate cell lines with doxycycline-inducible expression of CDK6, p185^{BCR-ABL}-transformed *Cdk6*^{-/-} cells were retrovirally transduced with pRevTet-On (Clontech) and selected with puromycin (2 µg/ml). To test for doxycycline-inducible gene expression, *Cdk6*^{-/-}-tet-on cells were transduced with the pRevTRE vector (Clontech) containing a GFP cDNA and selected by growing in hygromycin (400 µg/ml). Single cell clones were generated by FACS sorting and screened for clones with the highest doxycycline-dependent induction of GFP and the lowest background expression. These *Cdk6*^{-/-}-tet-on cells were then transduced with the pRevTRE-tight vector (Clontech) containing CDK6 cDNA and selected by growing in hygromycin (400 µg/ml). Expression of CDK6 was induced by addition of doxycycline (0.3-10 µg/ml)¹.

FACS analysis

Cells were analyzed by a BD FACS-Canto II FACS device and BD FACS Diva software (Beckton Dickinson). To evaluate the onset of apoptosis, 5 x 10⁶ cells were stained with propidium iodide and an APC-conjugated antibody to annexinV (BD Bioscience) and analyzed using a FACS device. For evaluation of proliferation rate, 5 x 10⁶ cells were stained with CFSE using the CellTrace CFSE Proliferation Kit (Invitrogen) and CFSE-MFI was measured over 20 h. Cell cycle profiles were obtained by staining 5 x 10⁶ cells with propidium iodide (50 µg ml⁻¹) in hypotonic lysis solution (0.1% (w/v) sodium citrate, 0.1% (v/v) Triton X-100, 100 µg ml⁻¹ RNase) and incubated at 37 °C for 30 min before measurement via FACS.

Senescence β-Galactosidase-staining

Senescence β-Galactosidase-staining Kit (Cell Signaling, #9860) was used according to manufacturer's recommendation.

Protein analysis and Immunoblotting

Cell lysates and Immunoblotting was performed as described previously¹¹. The used antibodies are shown in Supplementary Table 1.

Treatment with bortezomib and cycloheximide: 5×10^6 cells were seeded in either 10nM bortezomib, 1 μ M cycloheximide or a combination of these drugs. After 4h incubation immunoblot analysis was performed.

Immunohistochemistry

The B-lymphoid tissue array was obtained from the Institute of Pathology, University Hospital Graz. The T-lymphoid tissue array was obtained from the Department of Clinical Pathology, University of Vienna and was established using samples from patients with anaplastic large cell lymphoma (NPM-ALK positive and NPM-ALK negative). Samples were obtained after informed consent in compliance with the Declaration of Helsinki.

Tissue array technology was applied to compare samples using antibodies against CDK6 (sc-177, Santa Cruz Biotechnology), CD30 (Ber-H2, 0751, DakoCytomation), p16^{INK4a} (9511, CINtec® p16^{INK4a} Histology Kit, mtm laboratories AG), Ki-67 (Novocastra Laboratories, Newcastle, UK) and murine CD31 (Dianova, Hamburg, Germany) and using the ABC kit (Vector Laboratories) (AEC for CDK6 and DAB for p16, CD30) according to the manufacturers' recommendations. The Ki-67 signal was visualized with 3-amino-9-ethylcarbazole (ID laboratories, London, CDN) followed by a counterstaining with hematoxylin. Samples were rated positive for the individual antibodies when the staining intensity of the tumour cells was consistently higher than that of the surrounding untransformed cells. Normal lymph nodes were used as controls.

Human CD31 immunohistochemistry was performed on whole tissue sections. CD31 (JC70A, Dako)–ABC kit: AEC according to the manufacturers recommendations.

Immunofluorescence staining for blood vessels was performed using an antibody against murine CD31 (DIA310, Dianova) and as fluorochrome Alexa Fluor® 594 (A11007, Molecular Probes).

Image Acquisition and Protein Quantification *in vivo*

Samples were analysed with a Zeiss AxioImager Z1 microscope system with CCD camera and an automated acquisition system TissueFAXS™ (TissueGnostics GmbH). The percentages of Ki-67-, CDK6-, p16^{INKa}- or CD30-positive cells were depicted as scattergrams. Pictures were digitalized, analysed and quantified. Statistical analysis was performed using HistoQuest™ software (TissueGnostics GmbH).

Vessel density of human tissue samples: Vessel density was assessed by two independent observers. CD31 immunostained sections were scanned (Aperio technologies).

Hot spots of vessel density were determined at low magnification (40x). Each CD31-stained lumen within this hot spot was counted at a magnification of 200x in an area of 0, 25 mm² by two independent pathologists. Vessel density was prescribed as mean values of counting results.

Immunofluorescence Analysis

IF- Analyses were performed on whole tissue sections of 8 human ALCL cases. Tissue sections were deparaffinized, antigen retrieval was carried out by steamer in TE-buffer. Non specific binding sites were saturated by goatserum for 15 minutes at room temperature. The primary antibodies CDK6 (1: 50 dilution; Sigma-Aldrich, AB-13, SAB4300595) and p16^{INK4a} (9511, CINtec® p16^{INK4a} Histology Kit, mtm laboratories AG) were incubated at 4° C overnight. After washing the primary antibodies were detected with appropriate secondary antibodies 1 hour at room temperature (Alexa Flour 488 goat anti rabbit, 1: 500 for CDK6; Alexa Flour 594 goat anti mouse, 1:500 for p16^{INK4a}). After immunostaining the sections were incubated with 4', 6-diamidino-2 phenylindole (DAPI).

Stainings for CDK6 und p16^{INK4a} were scored semiquantitatively as negative (-: <10% positive tumour cells, weak positive (+: 10-30% positive tumour cells or weakly positive tumour cells) and positive (+: >30% positive tumour cells).

Methylation-specific PCR (MSP)

Genomic DNA was sodium bisulfite treated using Epiect bisulfite kit (Qiagen) according to the manufacturer's instructions. The following primer sequences were used: MSP-f, 5'-TGGTTATACGATTGGGCGATTGG-3' and MSP-r, 5'-CGCACGTCATACACAGACCCTA-3'. Annealing temperatures of MSP primers were 62°C and 58°C, respectively. PCR products were separated on a 2% agarose gel stained with GelRedTM (Biotium).

shRNA knockdown of CDK6

For the knockdown of CDK6, a set of 3 different pGIPZ lentiviral particles containing short hairpin RNAs targeting human CDK6 (I: V3LHS_112906, II: V3LHS_636830, III: V3LHS_404081) were purchased from Open Biosystems (Huntsville, AL, USA). pGIPZ viral particles containing a validated non-silencing shRNA (RHS4348) were used as control. Mac2a and SUDHL1 cells were infected with lentiviral particles at a MOI of 20. Briefly, Mac2a and SUDHL1 cells were transduced by spin infection (800 x g, 30 minutes, 32 °C) in

the presence of 7 µg/ml polybrene (Sigma-Aldrich) and selected with 2 µg/ml puromycin (Invivogen/Eubio) for 10 days. Cells were also checked for their GFP-expression. The knockdown of CDK6 was confirmed by immunoblotting and qPCR.

Luciferase reporter assay

Calcium phosphate transfection of 293T cells: 1×10^6 cells were seeded per well in a 6-well plate one day before transfection in DMEM complete. On the next day HeBS (Hepes buffered saline) buffer and CaCl_2 were thawed at room temperature. For each transfection aliquots of 71µL HeBS buffer were prepared. 1.5µg of expression vector, 1.5µg of the luciferase construct and 0.15µg of a constitutively expressed SV40-*Renilla* luciferase plasmid was added to 62µL distilled water and 9µL CaCl_2 . This mixture was added dropwise to the HeBS buffer, gently mixed and incubated for 3min. at room temperature. The DNA precipitate was added dropwise to the cells and incubated for 24-48h. SV40-*Renilla* luciferase plasmid (Promega) was used as an internal control. The dual luciferase reporter assay system (Promega) was employed to measure luciferase activity. Positive reporter firefly luciferase values were normalized to constitutively expressed renilla luciferase and a negative reporter fold change of 1.

Supplementary Reference:

1. Mayerhofer, M. *et al.* Unique effects of KIT D816V in BaF3 cells: induction of cluster formation, histamine synthesis, and early mast cell differentiation antigens. *Journal of immunology (Baltimore, Md. : 1950)* **180**, 5466-76 (2008).

DISCUSSION

The successful treatment of breast cancer patients requires reliable prognostic and predictive markers that allow appropriate therapy design. Therefore it is of great importance to define candidate genes that serve as stable predictors and help to estimate treatment responses and outcome. The transcription factor STAT1 has recently gained attention in the field of breast cancer research and is discussed as an independent prognostic marker. High expression of tyrosine phosphorylated and thus activated STAT1 protein in human breast cancer patients correlates positively with disease outcome and relapse-free survival ¹. However, the exact function of STAT1 in mammary tumorigenesis and how STAT1 confers this positive effect had not been clarified. Using STAT1-deficient mice, I showed for the first time that the absence of STAT1 suffices to significantly enhance the incidence of spontaneous mammary tumor development. Moreover, my studies revealed a dual function of STAT1 in suppressing mammary tumor formation: on the one hand STAT1 sustains efficient CTL dependent tumor surveillance and is required for full-fledged T cell cytotoxicity; on the other hand STAT1 regulates cell proliferation in the mammary epithelial cells themselves and acts as key factor controlling growth.

Three related studies were performed in the laboratories of R. Schreiber ², L. Hennighausen ³ and A. Koromilas ⁴ all investigating the role of STAT1 in mammary tumor formation. In **Table I** and **Table II** the distinct study designs and outcomes of each individual report - including mine ⁵ - are summarized. Despite the use of different experimental conditions all studies reached similar conclusions and confirmed the tumor suppressing role of STAT1 in mammary tumorigenesis. Klover *et al.* (Hennighausen laboratory) reported on the generation of a novel floxed allele of *Stat1*; the selective STAT1 deletion in the mammary epithelium was achieved by crossing *Stat1^{fl/fl}* mice to *MMTV-neu-IRES-cre* and used to study ErbB2/neu-induced tumor formation in virgin mice. Although first tumors were detectable in both groups 36 weeks after birth, the overall disease latency was significantly enhanced in “STAT1-deleter” mice being 49.4 weeks compared to 62.4 weeks in STAT1-expressing animals. In this experimental system all cells of the

tumor microenvironment do express STAT1; the tumor suppressing role of STAT1 is thereby unequivocally linked to a cell intrinsic function of STAT1 within the mammary epithelium.

Similarly, Raven *et al.* (Koromilas laboratory) employed ErbB2/neu as an oncogene to drive tumor formation. They showed that ErbB2 induces phosphorylation of STAT1 on tyrosine 701 (Y701) and serine 727 (S727). When they used purified bacterial lysates, ErbB2 directly phosphorylated STAT1 on Y701 *in vitro*. Whether this is actually the case in cells remains to be determined. Raven *et al.* excluded that these effects are mediated by JAK kinases or by Src family members using signal interceptors. The ErbB2-induced phosphorylation of STAT1 does not promote tumor formation but appears to serve as an internal safeguard counteracting transformation. ErbB2-transformed MEFs lacking both p53 and STAT1 formed large tumors upon transplantation into SCID mice; this tumor growth is significantly suppressed by the expression of wild type STAT1. Interestingly, the tumor suppressing effect is independent of STAT1 activation as STAT1-Y701F as well as STAT1-S727A exerted comparable effects to wild type STAT1.

Raven *et al.* also observed a clear tumor suppressing effect of STAT1 when they exposed STAT1-deficient animals to ErbB2/neu-driven tumor formation. Both, virgin as well as parous females developed mammary tumors significantly faster in the absence of STAT1 when compared to wild type controls. No differences in histological appearances were detected between *Stat1*^{-/-} and wild type tumors irrespective whether they were derived from virgin or parous mice. When cells obtained from these tumors were further orthotopically transplanted into wild type and *Stat1*^{-/-} mice, a clear effect of the microenvironment became visible. The transplantation of *Stat1*^{-/-} cells induced a significantly larger tumor growth in *Stat1*^{-/-} mice than in wild type mice. Notably, no significant enhancement in tumor growth was observed when *Stat1*^{+/+} tumor cells were orthotopically injected which may point at a STAT1-dependent interaction between the tumor and the microenvironment. It is currently hard to interpret the data based on the low numbers of individual tumors investigated in this interesting experimental setting.

Further evidence for a key role of STAT1 in the tumor microenvironment was obtained in the study of Chan *et al.* (Schreiber laboratory) as well as from my own data. Chan reported on the selective down-regulation of STAT1 protein in a large cohort of patients using immunohistochemistry in tumor biopsies. The down-regulation was most prominent in the tumor cells themselves and lower when compared to the surrounding stroma and infiltrating lymphocytes. The expression of STAT1 in the tumor stroma and the infiltrating lymphocytes may

explain why many researchers do find high STAT1 expression in breast cancer samples if they use methods that do not allow dissection of tumor stroma and the tumor cells themselves such as western blotting or microarrays of total tumors. There is increasing evidence highlighting the key role of the microenvironment for tumor development. Thus, it is necessary to perform single-cell resolution analysis in order to assign protein expression to a distinct cellular compartment. The availability of conditional knockout mouse strains and Cre mouse lines that allow the deletion of genes in distinct cellular subtypes will provide further insights.

Similar to my study, Chan used spontaneous mammary tumor development to evaluate the impact of STAT1 *in vivo* and confirmed my findings. In her mouse cohort the tumor incidence in *Stat1*^{-/-} animals was even higher and exceeded 90% in the parous mice compared to 55% in my cohort. While I never observed tumors in virgin mice, Chan also reported on a tumor incidence of 65% in virgin animals. Slight differences were also found in the receptor expression of the tumors in both studies; whereas the tumors in Chan's study displayed an estrogen receptor alpha (ER α)⁺ phenotype and closely resembled human progesterone receptor (PR)⁺/ER α ⁺ tumors of the luminal subtype, "my" *Stat1*^{-/-} tumors were only in 50% ER α ⁺. One can only speculate on the underlying differences. One major difference is the background of the animals; while I was using BALB/c animals, Chan investigated 129S6/SvEv mice which are prone to develop mammary tumors ⁶. It should also be mentioned that two different knockout mouse model for STAT1 do exist which were both presented to the scientific community in 1996. The group around D. Levy's laboratory deleted exon 7-10 which resulted in the complete loss of the STAT1 protein ⁷. In contrast, Schreiber's lab targeted exon 1-3 which resulted in the appearance of an N-terminally truncated protein ⁸. I used the "Levy-mouse model" for my studies, whereas Chan initially worked with mice expressing the truncated version (the "Schreiber-mice"). During the course of her work she confirmed her findings by using the complete "Levy-knockout mouse". This rules out that the N-terminus of STAT1 plays a major role - a consideration which is not a far-fetched as the experience with STAT5 deficient mouse models had revealed considerable activity of an N-terminally truncated protein even when expressed at low level ^{9,10}. While complete STAT5 knockout mice display perinatal lethality ¹¹, mice carrying an N-terminally truncated version of STAT5 are viable with minor phenotypes ^{9,10}. One can also not exclude that the difference in mouse housing affects mammary tumor development which is known to be influenced by nutrition. Moreover, recent evidence has shown that the gut microbiota may alter phenotypes occurring in transgenic mouse strains ¹². Therefore, I can also not exclude that

different microbiota contribute to the alterations in outcome between the study of Chan *et al.* and my own data.

Both studies, Chan and my own work, report on the enhanced appearance of mammary intraepithelial neoplasias (MINs) in *Stat1*^{-/-} animals. These alterations represent precancerous lesions and have the potential to develop into carcinomas. MINs are considered to result from an increased proliferative rate and the decreased capability to undergo apoptosis of the mammary epithelial cells. STAT1 has been implicated in both processes; on the one hand STAT1 is an important regulator of cell growth and inhibits cell proliferation e.g. downstream of interferons. Among the STAT1-dependent target genes are important cell cycle regulators such as the cell cycle inhibitor proteins p27^{Kip1} and p21^{WAF1/cip1}. Most importantly, the group of Koromilas has recently shown that the STAT1-p27 axis controls Ras-dependent transformation and proliferation^{13,14}. Both, p21^{WAF1/cip1} and p27^{Kip1} deficient mice are tumor prone; mice lacking p21^{WAF1/cip1} or p27^{Kip1} show increased frequencies of intestinal tumors in *Apc* mutant mice¹⁵⁻¹⁷. Other STAT1 target genes involved in cell cycle regulation are D-type cyclins as well as CDK4¹⁸. The significance of cyclinD/CDK4 complexes for mammary cancer development has recently come into the focus of attention and is currently a matter of debate in the field^{19,20}. On the other hand, STAT1 also regulates apoptosis as demonstrated in numerous reports. STAT1 was shown to regulate the expression of several caspases as well as of Fas and Fas ligand²¹. Accordingly, Chan *et al.* were capable to induce apoptosis in STAT1-deficient breast cancer cell lines solely by the enforced expression of STAT1. Apoptosis induction required active STAT1 as only wild type but not STAT1-Y701F was capable to induced cell death. This opposes the findings by Raven *et al.* where tumor suppression did not rely on tyrosine phosphorylation and was also observed upon the expression of STAT1-Y701F. It has to be mentioned that Chan *et al.* performed annexin V stainings to unequivocally determine apoptosis, whereas Raven investigated tumor growth as read-out system and did not further dissect the underlying mechanisms. The reduced tumor growth may be related to altered apoptosis but as well to a reduced cell proliferation which has not been clarified. Moreover, the study of Raven *et al.* employed *p53*^{-/-}*Stat1*^{-/-} MEFs transformed with the *ErbB2/neu*-oncogene to monitor tumor growth upon transplantations in SCID mice whereas Chan *et al.* used *Stat1*^{-/-} mammary tumor cells. Different cell types may certainly act in a different manner. Moreover, p53 has been reported to interact with STAT1, again representing a considerable difference in experimental models. It will be of great significance to decipher the molecular mechanism underlying the tumor suppressive effect of STAT1 in different experimental models. The interaction of p53 and

STAT1 and its relevance for mammary cancer needs to be unraveled, as both p53 and Stat1 have prognostic and/or therapeutic relevance in human breast cancer^{1,22}. In this regard it should also be noted that an interaction between STAT1 and BRCA1 has been reported which underscores the importance of studying STAT1 in human mammary tumors²³.

I failed to detect any obvious signs of cell death or apoptosis in our experimental system. In contrast, I was clearly able to observe enhanced proliferation *in vivo* in both, non-tumorigenic and tumorigenic mammary epithelial cells. Further confirmation for a key role of STAT1 to regulate mammary epithelial cell growth came from my 3D culture studies. Jechlinger *et al.* developed the 3D culture system to study the effects of Kras(G12D) and MYC on the ability of mammary epithelial cells to form structured and polarized mammospheres²⁴. I used this novel and innovative technique to compare the formation of mammospheres derived from primary mammary epithelial cells of STAT1-deficient versus wild type virgin mice. The first steps of MIN formation were recapitulated in *Stat1*^{-/-} mammospheres; *Stat1*^{-/-} cells formed spheres with significantly thicker epithelial layers, displayed increased proliferation rates and in some cases started to fill the lumen of the acini. Therefore, I consider the 3D cultures system by Jechlinger *et al.* as an exciting novel tool to test the probability of primary epithelial cells to undergo MIN formation and may serve as valuable screening system.

My data also suggest that the STAT1 downstream transcription factor IRF1 mediates the growth inhibitory effects of STAT1 in mammary epithelial cells. This assumption is supported by several lines of evidence. First, I found a significant down-regulation of IRF1 in STAT1-deficient mammary tumors. This result may be anticipated as STAT1 does regulate the expression of IRF1. Importantly, I found structural similarities in *Stat1*^{-/-} and *Irf1*^{-/-} mammary tissue when analyzing mammary gland whole mounts of 7 week old virgin mice. In both cases the density of ductal structures was enhanced when compared to wild type controls indicative of the increased proliferative capacity. Accordingly, when exposing *Irf1*^{-/-} mammary epithelial cells to 3D cultures, I recapitulated the alteration seen in *Stat1*^{-/-} mammospheres. Lastly, *in vivo*-BrdU incorporation experiments confirmed the overlap of phenotypes between STAT1 and IRF1 in mammary epithelial cells and revealed increased proliferative capacities of both *Stat1*^{-/-} and *Irf1*^{-/-} mammary epithelial cells. It is thus attractive to speculate that at least the effects of STAT1 on cell cycle control are mediated via IRF1. The importance of IRF1 is further supported by observation in human patients suffering from breast cancer; IRF1 is frequently heterozygous in tumor tissue²⁵ and high-grade ductal carcinomas *in situ* or node-positive invasive ductal cancers

express less IRF1 than normal tissue²⁶. Tissue microarrays confirmed the finding that IRF1 is down-regulated in high grade breast cancer²⁷. However, information on the expression levels of STAT1 is unfortunately missing in these studies; no parallel analysis of STAT1 has been done. It is thus not clear whether down-regulation of IRF1 correlates with loss of STAT1 or occurs irrespective whether STAT1 is expressed at regular levels. It is attractive to speculate that the loss of IRF1 occurs independently of alterations in STAT1 expression and suffices to trigger tumorigenesis. Support for this concept comes from observations in cell lines; the enforced expression of IRF1 may inhibit cell proliferation and suffices to induce apoptosis in mammary cell lines²⁸. It is currently unclear under which conditions STAT1/IRF1 block proliferation and when they induce apoptosis. In my hands, STAT1/IRF1-deficiency resulted in increased proliferative capacities of mammary epithelial cells. Though, I can also not exclude the possibility that the 3D culture system is not perfectly suited to detect alterations in apoptosis but rather proliferation.

One open question that still remains to be determined is the influence of STAT1 in already established tumors. It will be interesting to explore whether deletion of STAT1 in established tumors has the potency to modulate tumorigenesis. The fact that I found a mosaic expression in human (observation unpublished) and murine mammary tumors for STAT1 favors this possibility. The lack of STAT1 in wild type tumors was focal and restricted to certain areas of the tumors indicating that the tumor cell do down-regulate STAT1 after tumor induction. The loss of STAT1 appears to be advantageous as huge homogenous patches of the tumor lacked STAT1. The availability and use of inducible conditional knockout mouse models will ultimately address this issue.

Conditional mouse models will also be crucial in dissecting the contribution of individual cell types to STAT1 mediated tumor suppression. Besides the effects of STAT1 in the mammary epithelial cells themselves, there is a clear-cut effect of the microenvironment. Raven *et al.* were the first who described - using orthotopic transplantation of tumor cells - that mammary tumors develop significantly faster in a *Stat1*^{-/-} microenvironment when compared to a wild type host. Interestingly, in his experimental setting the effect was only detectable when he transplanted STAT1-deficient tumors. Only minor effects were observed upon the transplantation of wild type tumors. I reached a similar conclusion - albeit with an entirely different system. I transplanted untransformed mammary gland tissue from 3 weeks old *Stat1*^{-/-} and control animals into the cleared fat pad of both *Stat1*^{-/-} and wild type recipients and monitored tumor incidence and tumor latency. In this setting and in line with the findings of Raven, mammary tumor

development occurred at the highest rate upon transplantation of *Stat1*^{-/-} mammary cells into *Stat1*^{-/-} recipients. The transplantation of *Stat1*^{-/-} cells into wild type mice significantly reduced tumor incidence and increased disease latency. This indicates that STAT1 controls both, tumor onset as well as growth of a once established malignancy. Wild type mammary tumors also evolved, with a slightly higher incidence in *Stat1*^{-/-} mice compared to wild-type animals again supporting a role for the tumor microenvironment. Further evidence came from the finding that tumor growth was significantly faster in a *Stat1*^{-/-} microenvironment. As I detected a prominent infiltration of lymphoid cells within the mammary tumors, I concentrated on the influence of cytotoxic T lymphocytes (CTLs) and NK cells. Both cell types represent major components of the tumor microenvironment and the tumor surveillance system. Of note, this is also the case in human breast cancers which frequently display dense infiltrations of lymphoid cells; further, high numbers of tumor-infiltrating CD8⁺ T lymphocytes in invasive breast cancer have been correlated with a better prognosis²⁹. Immunohistochemical analysis of the tumors identified the infiltrates as primarily of T lymphoid origin. To test their impact, I made use of *Rag2*^{-/-} mice which lack mature lymphoid cells but do express functional NK cells. The transplantation of four individually derived mammary tumor cell lines confirmed the dominating role of cytotoxic T cells in mammary tumor surveillance. Tumor growth was significantly enhanced in *Rag2*^{-/-} mice irrespective whether the tumor cells did express STAT1 or not. A comparable increased tumor growth was observed in *Stat1*^{-/-} mice which lack fully functional cytotoxic T cells as well as NK cells. The removal of *Stat1*^{-/-} defective T cells by crossing *Stat1*^{-/-} to *Rag2*^{-/-} mice did not change tumor progression. These findings underscore the importance of STAT1 for CTL dependent tumor surveillance. The loss of STAT1 suffices to completely abrogate CTL-dependent immune control as no further enhancement of the *Stat1*^{-/-}-phenotype was obtained by complete removal of the T cell compartment in *Rag2*^{-/-}/*Stat1*^{-/-} mice.

Therefore, it is clearly of advantage for a breast tumor if the controlling CTLs express no or low levels of STAT1. Patients with STAT1 mutations do exist and have been described³⁰. However, these patients suffer from severe recurrent infections and most of them die at young age which does not allow to draw any conclusions or statements on tumor development. However, there is one interesting report in a murine model: mice which had been transplanted with a mammary tumor cell line displayed a time dependent down-regulation of STAT1 in the T lymphoid compartment³¹. It is tempting to propose that the tumor may somehow induce the down-regulation of STAT1 in order to facilitate its own proliferation and escape immune control. Tumor cells frequently display alterations that help them to escape immune control. Down-

regulation of interferon receptors has been described in many tumor types³². Interferons are considered as major players in tumor surveillance with STAT1 being a key transcription factor mediating IFN-induced effects. Nevertheless, the effects of STAT1 on mammary tumor development may not simply reflect the inability to react on interferons and are beyond the control of interferon only. STAT1 has been shown to suppress Ras-mediated transformation independent of IFNs by up-regulating p27^{Kip1}^{13,14}. The mechanisms, how STAT1 regulates growth control of mammary epithelial cells and whether this occurs IFN-dependent or independent has not been addressed in my study and still needs further investigation.

Several recent studies investigated the role of STAT1 in the context of mammary tumor formation and the evidence is compelling: it is safe to conclude that loss of STAT1 not only represents a predictive factor that correlates with disease outcome, but represents a true mammary tumor suppressor. All studies on STAT1's role in mammary tumorigenesis – including mine – demonstrated the crucial role of STAT1 in the tumor initiating phase. It will be interesting to determine if and how STAT1 influences the progression of an already established breast cancer using inducible and conditional STAT1 mouse models.

Table I. Recent publications on the topic “Stat1 acts as suppressor of mammary tumorigenesis in murine model systems”- Different experimental setups and outcomes are summarized.

| Ref. | Mouse genotype (STAT1 exons deleted) | Mouse background | oncogenic driver | parous / virgin | Earliest tumor onset [weeks] (Stat1 ^{-/-} /wt) | median tumor onset [weeks] (Stat1 ^{-/-} /wt) | % tumor bearer (Stat1 ^{-/-} /wt) |
|---|--|-------------------|------------------|-----------------|---|---|---|
| Klover, P.J. et al. ³ | Stat1 ^{fl/fl} x MMTV-neu-IRES-cre (1-3) | 129SvEv | MMTV-neu | virgin | 36/36 | 49/62 | 100%/100% |
| Raven, J.F. et al. ⁴ | Stat1 ^{-/-} (7-10) | BALB/c | MMTV-neu | virgin | 29/43 | 42/49 | 100%/100% |
| | Stat1 ^{-/-} (7-10) | BALB/c | MMTV-neu | parous | 21/22 | 27/33 | 100%/100% |
| Schneckenleithner, C. et al. ⁵ | Stat1 ^{-/-} (7-10) | BALB/c | none | virgin | no tumors | no tumors | 0%/0% |
| | Stat1 ^{-/-} (7-10) | BALB/c | none | parous | 37/53 | 54/70 | 55%/10% |
| Chan, S.R. et al. ² | Stat1 ^{-/-} (1-3) | 129SvEv | none | virgin | 49/no tumors | 104/no tumors | 65%/0% |
| | Stat1 ^{-/-} (1-3) | 129SvEv | none | parous | 50/no data | 64/no data | 99%/no data |
| | Stat1 ^{-/-} (7-10) | mixed 129SvEv/BL6 | none | virgin | 40/no data | 65/no data | 65%/no data |

Table II. Recent publications on the topic “Stat1 acts as suppressor of mammary tumorigenesis in murine model systems”- Different experimental setups and outcomes are summarized.

| Ref. | Method used to test STAT1's ... in suppressing mammary tumor formation | | | additional notes |
|---|---|--|---|--|
| | cell-intrinsic contribution | immunological contribution | phosphorylation status | |
| Klover, P.J. et al. ³ | mammary gland specific deletion of STAT1 | no data | / | no tumors in parous <i>Stat1^{fl/fl}</i> x <i>MMTV-cre</i> mice after 15 month (numbers of pregnancies unknown) |
| Raven, J.F. et al. ⁴ | xenografts of <i>p53^{-/-}/Stat1^{-/-}-Neu</i> MEFs reconstituted with STAT1; orthotopic injection of <i>Stat1^{-/-}</i> and wt mammary tumor cells in <i>Stat1^{-/-}</i> and wt mice | orthotopic injection of <i>Stat1^{-/-}</i> and wt mammary tumor cells in <i>Stat1^{-/-}</i> and wt mice | xenografts of <i>p53^{-/-}/Stat1^{-/-}-Neu</i> MEFs reconstituted with STAT1 Y701F/S727A: tumor suppressive function independent of P-Y701 and P-S727 | no tumors in <i>Stat1^{-/-}</i> mice (gestation/latency unknown) |
| Schnecke nleithner, C. et al. ⁵ | orthotopic mammary gland transplanations, 3D cultures of mammary epithelial cells | orthotopic mammary gland transplantations, orthotopic injection of mammary tumor cell lines in wt, <i>Stat1^{-/-}</i> , <i>Rag2^{-/-}</i> , <i>Stat1^{-/-} Rag2^{-/-}</i> mice | / | MIN formation in <i>Stat1^{-/-}</i> mice; heterogeneous immunohistology of <i>Stat1^{-/-}</i> tumors (50% ER α ⁺ /50% ER α ⁻) |
| Chan, S.R. et al. ² | re-expression of STAT1 in <i>Stat1^{-/-}</i> mammary tumor cell lines | no data | re-expression of STAT1 Y701F/S727A in <i>Stat1^{-/-}</i> mammary tumor cell lines: tumor suppressive function dependent of P-Y701, independent of P-S727 | MIN formation in <i>Stat1^{-/-}</i> mice; > 90% of <i>Stat1^{-/-}</i> tumors ER α ⁺ , luminal subtype |

Additional thoughts - Why does pregnancy induce mammary tumorigenesis?

During my thesis, I was frequently confronted with the question: “Why do only multiparous mice develop mammary cancer in your study, and not nulliparous ones? I always thought that pregnancy offers a certain protection against breast cancer?” One might only speculate to address this issue:

Already in the 1700s, reports on childless nuns associated nulliparity with an increased likelihood to develop breast cancer ³³. Subsequently, numerous studies associated an early first pregnancy (younger than 25) and a high number of full-term pregnancies to a protective effect, compared with nulliparous women and women with a late first pregnancy (after 30 years). The underlying mechanism mediating this protective effect towards breast cancer development remained

speculative and has not been unraveled yet. Changes that occur during pregnancy and lactation include a complex morphological, physiological and molecular remodelling of the mammary gland tissue. Recent evidence points at an increase in DNA repair capability of the mammary epithelium after pregnancy and involution. Parity induces a distinct “genomic signature” that is clearly distinct from the gene pattern found in nulliparous mammary glands. The transcription of genes controlling differentiation and programmed cell death is enhanced³⁴. Apparently, protection only occurs if the pregnancy and involution have been completed prior to the exposure of any damaging agent such as carcinogen exposure, radiation, smoking, etc. This explains why only pregnancies at early age do have a protective effect.

Despite the overall reduced breast cancer risk in parous females, there is the consensus that each gestation temporarily increases the probability to develop breast cancer. After each full-term pregnancy, the breast cancer risk is transiently increased³⁵. This may be explained two-fold: in mouse models, Wagner *et al.* described a distinct parity-induced mammary epithelial cell population that accumulates during pregnancy without undergoing apoptosis during involution³⁶. These cells display features of multipotent progenitors such as self-renewal and have the capability to contribute to ductal and alveolar morphogenesis. Moreover, these parity-induced mammary epithelial cells represent cellular targets for MMTV-neu-induced mammary tumorigenesis³⁷. In line, MMTV-neu-induced tumor formation is significantly enhanced in pregnant mice and ablation of parity-induced mammary epithelial cells reduces the risk for tumor formation. Beside this distinct cell population the microenvironment of an involuting mammary gland has been discussed to contribute to tumor formation. Involution is associated with inflammation and wound healing which are discussed to drive tumorigenesis in many types of tumors³⁸. However, the role in the mammary gland is unclear and matter of a vivid debate.

References

1. Widschwendter, A. *et al.* Prognostic significance of signal transducer and activator of transcription 1 activation in breast cancer. *Clinical cancer research : an official journal of the American Association for Cancer Research* **8**, 3065–74 (2002).
2. Chan, S. R. *et al.* STAT1-deficient mice spontaneously develop estrogen receptor alpha-positive luminal mammary carcinomas. *Breast cancer research : BCR* **14**, R16 (2012).
3. Klover, P. J. *et al.* Loss of STAT1 from mouse mammary epithelium results in an increased Neu-induced tumor burden. *Neoplasia (New York, N.Y.)* **12**, 899–905 (2010).
4. Raven, J. F. *et al.* Stat1 is a suppressor of ErbB2/Neu-mediated cellular transformation and mouse mammary gland tumor formation. *Cell cycle (Georgetown, Tex.)* **10**, 794–804 (2011).
5. Schneckenleithner, C. *et al.* Putting the brakes on mammary tumorigenesis : Loss of STAT1 predisposes to intraepithelial neoplasias ABSTRACT : **2**, 1043–1054 (2011).
6. Shankaran, V. *et al.* IFN γ and lymphocytes prevent primary tumour development and shape tumour immunogenicity. *Nature* **410**, 1107–11 (2001).
7. Durbin, J. E., Hackenmiller, R., Simon, M. C. & Levy, D. E. Targeted disruption of the mouse Stat1 gene results in compromised innate immunity to viral disease. *Cell* **84**, 443–50 (1996).
8. Meraz, M. A. *et al.* Targeted disruption of the Stat1 gene in mice reveals unexpected physiologic specificity in the JAK-STAT signaling pathway. *Cell* **84**, 431–42 (1996).
9. Teglund, S. *et al.* Stat5a and Stat5b Proteins Have Essential and Nonessential, or Redundant, Roles in Cytokine Responses. *Cell* **93**, 841–850 (1998).
10. Sexl, V. *et al.* Stat5a/b contribute to interleukin 7-induced B-cell precursor expansion, but abl- and bcr/abl-induced transformation are independent of stat5. *Blood* **96**, 2277–83 (2000).
11. Cui, Y. *et al.* Inactivation of Stat5 in mouse mammary epithelium during pregnancy reveals distinct functions in cell proliferation, survival, and differentiation. *Molecular and cellular biology* **24**, 8037–47 (2004).
12. Bleich, A. & Hansen, A. K. Time to include the gut microbiota in the hygienic standardisation of laboratory rodents. *Comparative immunology, microbiology and infectious diseases* **35**, 81–92 (2012).
13. Wang, S., Raven, J. F. & Koromilas, A. E. STAT1 represses Skp2 gene transcription to promote p27Kip1 stabilization in Ras-transformed cells. *Molecular cancer research : MCR* **8**, 798–805 (2010).
14. Wang, S., Raven, J. F., Durbin, J. E. & Koromilas, A. E. Stat1 phosphorylation determines Ras oncogenicity by regulating p27 kip1. *PloS one* **3**, e3476 (2008).

-
15. Yang, W. C. *et al.* Targeted Inactivation of the p21WAF1/cip1 Gene Enhances Apc-initiated Tumor Formation and the Tumor-promoting Activity of a Western-Style High-Risk Diet by Altering Cell Maturation in the Intestinal Mucosa. *Cancer Res.* **61**, 565–569 (2001).
 16. Yang, W., Bancroft, L., Nicholas, C., Lozonshi, I. & Augenlicht, L. H. Targeted inactivation of p27kip1 is sufficient for large and small intestinal tumorigenesis in the mouse, which can be augmented by a Western-style high-risk diet. *Cancer research* **63**, 4990–6 (2003).
 17. Philipp-Staheli, J. *et al.* Pathway-specific tumor suppression. Reduction of p27 accelerates gastrointestinal tumorigenesis in Apc mutant mice, but not in Smad3 mutant mice. *Cancer cell* **1**, 355–68 (2002).
 18. Dimco, G., Knight, R. A., Latchman, D. S. & Stephanou, A. STAT1 interacts directly with cyclin D1/Cdk4 and mediates cell cycle arrest. *Cell cycle (Georgetown, Tex.)* **9**, 4638–49 (2010).
 19. Yu, Q. *et al.* Requirement for CDK4 kinase function in breast cancer. *Cancer cell* **9**, 23–32 (2006).
 20. Landis, M. W., Pawlyk, B. S., Li, T., Sicinski, P. & Hinds, P. W. Cyclin D1-dependent kinase activity in murine development and mammary tumorigenesis. *Cancer cell* **9**, 13–22 (2006).
 21. Kim, H. S. & Lee, M.-S. STAT1 as a key modulator of cell death. *Cellular signalling* **19**, 454–65 (2007).
 22. Dookeran, K. A. *et al.* Race and the prognostic influence of p53 in women with breast cancer. *Annals of surgical oncology* **19**, 2334–44 (2012).
 23. Ouchi, T., Lee, S. W., Ouchi, M., Aaronson, S. A. & Horvath, C. M. Collaboration of signal transducer and activator of transcription 1 (STAT1) and BRCA1 in differential regulation of IFN-gamma target genes. *Proceedings of the National Academy of Sciences of the United States of America* **97**, 5208–13 (2000).
 24. Jechlinger, M., Podsypanina, K. & Varmus, H. Regulation of transgenes in three-dimensional cultures of primary mouse mammary cells demonstrates oncogene dependence and identifies cells that survive deinduction. *Genes & development* **23**, 1677–88 (2009).
 25. Cavalli, L. R., Riggins, R. B., Wang, A., Clarke, R. & Haddad, B. R. Frequent loss of heterozygosity at the interferon regulatory factor-1 gene locus in breast cancer. *Breast cancer research and treatment* **121**, 227–31 (2010).
 26. Doherty, G. M., Boucher, L., Sorenson, K. & Lowney, J. Interferon regulatory factor expression in human breast cancer. *Annals of surgery* **233**, 623–9 (2001).
 27. Connett, J. M., Badri, L., Giordano, T. J., Connett, W. C. & Doherty, G. M. Interferon regulatory factor 1 (IRF-1) and IRF-2 expression in breast cancer tissue microarrays. *Journal of interferon & cytokine research : the official journal of the International Society for Interferon and Cytokine Research* **25**, 587–94 (2005).
 28. Kim, P. K. M. *et al.* IRF-1 expression induces apoptosis and inhibits tumor growth in mouse mammary cancer cells in vitro and in vivo. *Oncogene* **23**, 1125–35 (2004).

-
29. Mahmoud, S., Lee, A., Ellis, I. & Green, A. CD8(+) T lymphocytes infiltrating breast cancer: A promising new prognostic marker? *Oncoimmunology* **1**, 364–365 (2012).
 30. Averbuch, D., Chapgier, A., Boisson-Dupuis, S., Casanova, J.-L. & Engelhard, D. The clinical spectrum of patients with deficiency of Signal Transducer and Activator of Transcription-1. *The Pediatric infectious disease journal* **30**, 352–5 (2011).
 31. Handel-Fernandez, M. E., Ilkovitch, D., Iragavarapu-Charyulu, V., Herbert, L. M. & Lopez, D. M. Decreased levels of both Stat1 and Stat3 in T lymphocytes from mice bearing mammary tumors. *Anticancer research* **29**, 2051–8 (2009).
 32. Dunn, G. P., Koebel, C. M. & Schreiber, R. D. Interferons, immunity and cancer immunoediting. *Nature reviews. Immunology* **6**, 836–48 (2006).
 33. Mustacchi, P. Ramazzini and Rigoni-Stern on parity and breast cancer. Clinical impression and statistical corroboration. *Archives of internal medicine* **108**, 639–42 (1961).
 34. Russo, I. H. & Russo, J. Pregnancy-induced changes in breast cancer risk. *Journal of mammary gland biology and neoplasia* **16**, 221–33 (2011).
 35. Albrektsen, G., Heuch, I., Hansen, S. & Kvåle, G. Breast cancer risk by age at birth, time since birth and time intervals between births: exploring interaction effects. *British journal of cancer* **92**, 167–75 (2005).
 36. Wagner, K.-U. *et al.* An adjunct mammary epithelial cell population in parous females: its role in functional adaptation and tissue renewal. *Development (Cambridge, England)* **129**, 1377–86 (2002).
 37. Henry, M. D., Triplett, A. A., Oh, K. B., Smith, G. H. & Wagner, K.-U. Parity-induced mammary epithelial cells facilitate tumorigenesis in MMTV-neu transgenic mice. *Oncogene* **23**, 6980–5 (2004).
 38. Schedin, P. Pregnancy-associated breast cancer and metastasis. *Nature reviews. Cancer* **6**, 281–91 (2006).

ABBREVIATIONS

| | |
|--------------------|---|
| ATP | Adenosine triphosphate |
| BRCA1/2 | Breast cancer 1/2 |
| CTL | Cytotoxic T lymphocyte |
| DNA | Deoxyribonucleic acid |
| EGF | Epidermal growth factor |
| ER α | Estrogen receptor alpha |
| ET | Thrombocytopenia |
| GAS-site | Gamma-activated sequence-site |
| HER2 | Human epidermal growth factor receptor 2 |
| HP1 | Heterochromatin protein 1 |
| IFN α/β | Interferon alpha/beta |
| IFNAR1/2 | Interferon alpha receptor 1/2 |
| IFNGR1/2 | Interferon gamma receptor 1/2 |
| IGFBP | Insulin-like growth factor-binding protein |
| IL | Interleukin |
| IRF1/9 | Interferon regulatory factor 1/9 |
| ISG | Interferon-stimulated gene |
| ISGF3 complex | Interferon-stimulated gene factor 3 complex |
| ISRE | Interferon-stimulated response element |
| JAK | Janus kinase |
| LPS | Lipopolysaccharide |
| MAPK | Mitogen-activated protein kinases |

| | |
|------------|--|
| MCA | Methylcholanthrene |
| MIN | Mammary intraepithelial neoplasia |
| MMTV | Mouse mammary tumor virus |
| MPD | Myeloproliferative disorder |
| MRI | Magnetic resonance imaging |
| NK cell | Natural killer cell |
| NMU | <i>N</i> -nitroso- <i>N</i> -methylurea |
| NO | Nitric Oxide |
| SCID | Severe combined immune deficiency |
| PIAS | Protein inhibitors of activated STATs |
| PI3K | Phosphoinositide 3-Kinase |
| PR | Progesterone receptor |
| PTP | Protein tyrosine phosphatases |
| PV | Polycythemia vera |
| RANK | Receptor activator of nuclear factor-kappaB |
| RANKL | Receptor activator of nuclear factor-kappaB ligand |
| ROS | Reactive oxygen species |
| SH2 domain | Src-homology-2 domain |
| SOCS | Suppressor of cytokine signaling |
| STAT | Signal transducer and activator of transcription |
| S727F | Serine at amino acid position 727 mutated to Phenylalanine |
| TAD | Transactivation domain |
| TAg | Simian virus 40 large T antigen |
| Tyk2 | Tyrosine kinase |
| U-STAT | Unphosphorylated STAT |
| VEGF-A | Vascular endothelial growth factor-A |
| V617F | Valine at amino acid position 617 mutated to Phenylalanine |
| WAP | Whey acidic protein |
| Y701A | Tyrosine at amino acid position 701 mutated to Alanine |

CURRICULUM VITAE

Name: Christine Schneckenleithner
 Date of birth: 08.10.1981
 Place of birth: Salzburg
 Nationality: Austria
 Degree: Mag.rer.nat (Genetics/Microbiology)
 Current position: PhD Student
 Current address: University of Veterinary Medicine Vienna, Institute of Pharmacology and Toxicology, Veterinärplatz 1, 1210 Vienna, Austria
 Phone number: 0043-1-25077-2905
 Email-address: christine.schneckenleithner@vetmeduni.ac.at

Education

09/1992 - 06/2000 Wirtschaftskundliches Realgymnasium Salzburg
 10/2000 - 02/2001 Vienna University of Technology
 Field of study **Technical mathematics – Diploma studies**
 03/2001 - 05/2007 University of Vienna
 Field of study **Microbiology and Genetics – Diploma studies**
 Major subject Molecular Microbiology
 Minor subject 1 Microbial ecology
 Minor subject 2 Bioinformatics
 Diploma thesis Max F. Perutz Laboratories, Department of Microbiology and Immunobiology, Supervisor: Emmanuelle Charpentier
 “The mode of action of novel Pleuromutilin derivatives and the mode of resistance to these antibiotics in the human gram-positive pathogen *Staphylococcus aureus*”
 04/2008 – until now University of Vienna
 Field of study **Microbiology and Genetics – Doctoral studies**
 Doctoral thesis University of Veterinary Medicine Vienna, Institute for Pharmacology and Toxicology, Supervisor: Veronika Sexl
 “The role of STAT1 in mammary cancer and myeloid leukemia”

Work Experience

09/2007 – 03/2008 Medical University of Vienna, Department of Medical Genetics
(Research Associate)

International Experience

08/2005 - 12/2005 Study abroad (Erasmus) - Lund University, Sweden

Languages

- English (fluent)
- French (basic knowledge)
- Swedish (basic knowledge)

Selected Meetings

- 09/2012 22th Vetpharm-Symposium, Vienna, Austria. Oral Presentation: Putting the brakes on mammary tumorigenesis: Loss of STAT1 predisposes to intraepithelial neoplasias
- 06/2012 17th Congress of EHA. Amsterdam, The Netherlands. Oral Presentation: STAT1 deficient mice develop a myeloproliferative syndrome resembling human CML
- 10/2011 MFPL Joint Post Doc Retreat on Inflammation and Infection, Gols, Austria. Poster Presentation: Loss of STAT1 promotes mammary tumor development
- 09/2011 OEGMBT Annual Meeting 2011, Salzburg, Austria. Poster Presentation: Loss of STAT1 promotes mammary tumor development
- 06/2010 15th Congress of EHA, Barcelona, Spain. Poster Presentation: BCR-ABL induced transformation uncovers a critical role of c-Jun in VEGF regulation
- 06/2010 6th PhD Symposium MUW, Vienna, Austria. Poster Presentation: The role of STAT1 in myeloid leukemia
- 02/2010 FEBS-Special Meeting 2010 - JAK-STAT Signaling: from Basics to Disease, Vienna, Austria. Poster Presentation: The role of STAT1 in mammary tumor formation
- 06/2009 5th PhD Symposium MUW, Vienna, Austria. Poster Presentation: STAT1 in mammary cancer and leukemia

Scientific Publications

Schneckenleithner C, Bago-Horvath Z, Dolznig H, Neugebauer N, Kollmann K, Kolbe T, Decker T, Kerjaschki D, Wagner KU, Müller M, Stoiber D, Sexl V.

Putting the brakes on mammary tumorigenesis – Loss of STAT1 predisposes to intraepithelial neoplasias.

Published in Oncotarget 2011 Dec;2(12):1043-54.

Kernbauer E, Maier V, Stoiber D, Strobl B, **Schneckenleithner C**, Sexl V, Reichert U., Reizis B, Kalinke U, Jamieson A, Müller M, Decker T.

Conditional STAT1 ablation reveals the importance of interferon signaling for immunity to Listeria monocytogenes infection.

Manuscript published in PLoS Pathog. 2012 Jun;8(6):e1002763. Epub 2012 Jun 14.

Kerjaschki D, Bago-Horvath Z, Rudas M, Sexl V, **Schneckenleithner C**, Wolbank S, Bartel G, Krieger S, Kalt R, Hantusch B, Keller T, Nagy-Bojarszky K, Huttary N, Raab I, Lackner K, Krautgasser K, Schachner H, Kaserer K, Rezar S, Madlener S, Vonach C, Davidovits A, Nosaka H, Hämmerle M, Viola K, Dolznig H, Schreiber M, Nader A, Mikulits W, Gnant M, Hirakawa S, Detmar M, Alitalo K, Nijman S, Offner F, Maier TJ, Steinhilber D, Krupitza G.

Lipoxygenase mediates invasion of intrametastatic lymphatic vessels and propagates lymph node metastasis of human mammary carcinoma xenografts in mouse.

Published in J Clin Invest. 2011 May;121(5):2000-12. doi: 10.1172/JCI44751. Epub 2011 Apr 11.

Kollmann K, Heller G, Ott RG, Scheicher R, Zebedin-Brandl E, **Schneckenleithner C**, Simma O, Warsch W, Eckelhart E, Hoelbl A, Bilban M, Zöchbauer-Müller S, Malumbres M, Sexl V.

C-JUN promotes BCR-ABL induced lymphoid leukemia by inhibiting methylation of the CDK6 promoter.

Published in Blood. 2011 Apr 14;117(15):4065-75. Epub 2011 Feb 7.

Wieser R, Scheideler M, Hackl H, Engelmann M, **Schneckenleithner C**, Hiden K, Papak C, Trajanoski Z, Sill H, Fonatsch C.

microRNAs in acute myeloid leukemia: expression patterns, correlations with genetic and clinical parameters, and prognostic significance.

Published in Genes Chromosomes Cancer. 2010 Mar;49(3):193-203. Review.

Kollmann K, Heller G*, **Schneckenleithner C***, Warsch W*, Scheicher R, Ott R G, Schäfer M, Fajmann S, Schiefer AI, Reichert U, Mayerhofer M, Hoeller C, Zöchbauer-Mueller S, Kerjaschki D, Kenner L, Hoefler G, Freissmuth M, Moriggl R, Busslinger M, Malumbres M, Sexl V.

A new kinase-independent function of CDK6 links the cell cycle to tumour angiogenesis.

Manuscript under review in Nature Cell Biology.

Rommer A, Steinleitner K, Hackl H, **Schneckenleithner C**, Engelmann M, Scheideler M, Vlatkovic I, Vanura K, Kralovics R, Cerny-Reiterer S, Valent P, Sill H, Wieser R.

Primary microRNA 221/222 is a potential biomarker for acute myeloid leukemia.

Manuscript submitted in British Journal of Hematology.